MODELING AND OPTIMIZATION OF THE COOLING TOWER UNDER UNSATURATED OUTLET AIR CONDITIONS

A Thesis

by

XIE XIE

Submitted to the Office of Graduate and Professional Studies of
Texas A&M University
in partial fulfillment of the requirements for the degree of

MASTER OF SCIENCE

Chair of Committee,	David E. Claridge
Committee Members,	Charles H. Culp
	Michael B. Pate
Head of Department,	Andreas A. Polycarpou

August 2016

Major Subject: Mechanical Engineering

ABSTRACT

This thesis presents a comprehensive methodology for engineers and plant managers to use for optimizing the combined chiller power and cooling tower fan power for cooling systems without the traditional assumption that the exiting air is saturated. The most widely accepted and utilized classical models are the Merkel model and the Poppe model. However, the former is somewhat inaccurate and the latter has significant computational burdens. Thus, this work uses the Braun model supplemented with simple field measurements to provide an accurate procedure for optimizing combined cooling tower and chiller performance that is suitable for field use.

The effectiveness cooling tower model, developed by Braun (1988), is utilized to describe the cooling tower performance with supplemented with field measurements. The chiller model presented in the EnergyPlus Engineering Reference book based on the condenser entering temperature is applied. The models are coupled to determine the optimal operation for the cooling system. To optimize the system, correlations between the power consumption of chillers and cooling tower fans and approach temperatures are investigated and regressed. The performance curves based on these correlations can help to achieve a “near-optimal” operation over a range of operating conditions. By doing so, an optimized approach temperature and temperature range is given and evaluated at over a range of annual operating condition. The impact of the wet-bulb temperature is also explored. The procedure developed predicts that about 15% of the measured energy consumption of the chillers and cooling tower fans in the Connally Building chiller plant

at the Texas A&M University System would be saved if the optimal control in this study were applied to the 68 days across 12 months that were analyzed in this thesis.

DEDICATION

I dedicate my thesis to my family.

ACKNOWLEGEMENTS

I have to admit that this thesis was a big challenge for me. I wouldn't have done it without the support and encouragement from many people. First of all, I would like to express my sincere gratitude to Dr. David Claridge for guiding me as my committee chair. He is always there to give me effective guidance patiently and to help build my engineering thinking during my academic years. I would like to also thank Dr. Michael Pate and Dr. Charles Culp for their support throughout the research on my thesis as my committee members.

I want to extend my appreciation to Ms. Hala, Mr. Christopher Dieckert, and Mr. Jon King for sharing the data and helping me conduct the measurements smoothly. And thanks Energy Systems Laboratory for providing me metering instruments.

Thanks also go to my friends for making my time at Texas A&M University a great experience. Meng Fan, Linyan Wang, Jiajun Liao: Thanks for listening to me when I felt upset and giving me warm advices. Special thanks to Mr. Lei Wang for providing me lots of excellent ideas by sharing your engineering experience with me.

Thanks to my boyfriend Yuchen Zhao for standing by me and supporting me like always.

Finally, I am deeply grateful to my mother and father for their encouragement and love. Without their support, hardly can I pursue a master's degree in the alien land. They make it possible for me to make my dream come true.

NOMENCLATURE

Chapter II

c_{pa}	specific heat of water
c_{pw}	specific heat of water
h_d	mass transfer coefficient
h_a	enthalpy of moist air per mass of dry air
$h_{f,w}$	enthalpy of liquid water
h_{ma}	enthalpy of air
h_a	enthalpy of moist air per mass of dry air
$h_{f,w}$	enthalpy of liquid water
h_{ma}	enthalpy of air
h_{masw}	enthalpy of saturated air at the local bulk water temperature
h_v	enthalpy of the vapor
Le_f	the Lewis number
L_{fill}	unit length of fill
$\dot{m}_a$	air flowrate
$\dot{m}_w$	water flowrate
T_a	air temperature
T_w	water temperature
V_{fill}	unit volume of length dy of fill
w_a	air humidity ratio

w_{sw}	saturation air humidity ratio at the local bulk water temperature

Additional Subscripts

i	inlet conditions
o	outlet conditions

Chapter III

A_s	surface area of the cooling tower
A_V	surface area of water droplets per unit volume of cooling tower
C_{pm}	constant pressure specific heat of moist air
C_s	saturation specific heat
EBError	energy balance error
h_C	convection heat transfer coefficient
$h_{g,w}$	enthalpy of water vapor at the local temperature
$h_{s,w,e}$	effective saturation enthalpy
MBE	mean bias error
NTU	Number of Transfer Unit
$P_{Chiller}$	chiller input power
P_{fan}	fan power
PLR	part-load ratio
$Q_{Chiller}$	cooling capacity of the chiller
Q_{CT}	cooling capacity of the cooling tower ($Q_{CoolingTower}$)
RMSE	root mean square error

r_{WB}	heat of vaporization of water at wet-bulb temperature
T_{app}	approach temperature
T_{ref}	reference temperature
T_{WB}	wet-bulb temperature
V_T	total tower volume
W	water to air heat capacity rate ratio
$\omega_{s,w,e}$	effective saturation humidity ratio
ω_{WB}	humidity ratio of saturated air at wet-bulb temperature
X_O	Number of heat transfer units
θ_a	non-dimensional air temperature
θ_w	non-dimensional water temperature
ϵ_a	non-dimensional air humidity ratio
ϵ_w''	non-dimensional humidity ratio of saturated air at water temperature
ε_a	air-side effectiveness
ε_w	water-cooling efficiency

Chapter IV and Chapter V

COP	coefficient of performance
EIR	energy input to cooling output ratio
P_{ref}	reference chiller power
$\dot{Q}_{ref}$	reference cooling capacity

$\dot{Q}_{evap}$	chiller load
$T_{cond,e}$	entering condenser fluid temperature (also cooling tower exiting temperature)
$T_{cond,l}$	leaving condenser fluid temperature (also cooling tower exiting temperature)
$T_{cw,l}$	leaving chilled water temperature

TABLE OF CONTENTS

Page

LIST OF FIGURES

Page

LIST OF TABLES

Page

CHAPTER I

INTRODUCTION

1.1 Background

The heating and cooling demands are always considerable energy concerns in buildings and industry. Usually, there are central plants providing heating and cooling for building groups. Take Texas A&M University as an example. Based on the Texas A&M University Energy Management Report, the energy consumption is 211 kBtu per gross square foot and 4.98 trillion Btu in total in fiscal year 2014. The total annual cost is more than $75 million. Such a huge bill suggests that even a small relative decrease in the energy requirements of a plant can significantly reduce the operating costs. In the process of achieving the optimization, the plants' saving potential is usually evaluated and a higher efficiency mode can be realized. The potential for significant cost reduction and the higher-efficiency design and control practices for cooling systems, are the impetus for this project.

Typically, a centralized cooling plant consists of one or more chillers, cooling towers, and pumps to satisfy the cooling demands of one or more buildings. The system, with recirculating water, is basically a big heat and mass exchanger set. Figure 1.1 shows a simplified schematic of the typical water circuits for a tower-chiller-load combination. In the diagrammed case, the load is assumed to be air conditioning. For example, cool and relatively dry air is supplied to the zones where both the temperature and humidity rise due to sensible and latent gains from people, lights, equipment and other loads. The

chilled water pump (CHWP) circuit delivers water to the “load”. The chilled water then returns to the chiller where its load is transferred to the condenser water pump (CWP) circuit.

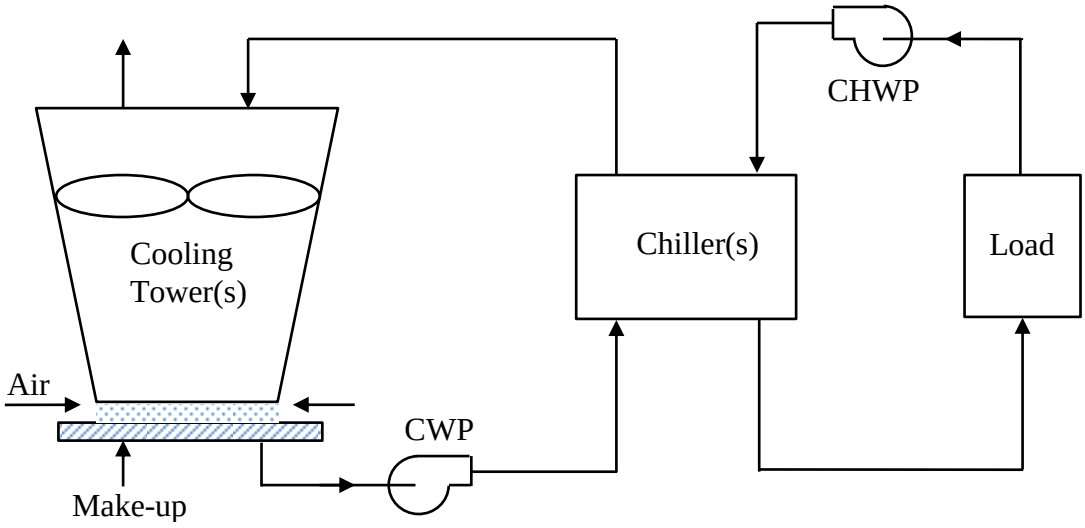

Figure 1.1 Simplified Schematic of Water Circuitry in a Typical Cooling System

A cooling tower is a vital component of Heating Ventilation and Air-Conditioning systems. They are also widely used in major industrial plants for the purpose of reducing the temperature of circulated cooling water with a view of maximizing its reusability and thus achieving improved overall efficiency. Cooling towers work on the principles of evaporative cooling and hence the cooled water temperature is limited by the wet bulb temperature of the cooling air.

The mass transfer and heat exchange processes in a cooling tower are quite complicated. There are several existing methods, such as the Merkel method and the Poppe method, which can model these complex processes and provide an estimate of the

performance of cooling towers. These methods, although widely studied and accepted by practitioners, have their own limits. The accuracy of the Merkel model is lowered due to simplifying assumptions used in its development to simplify the mathematical calculations. The Poppe method is difficult to use in practice because of its complexity. These limitations give rise to the need for a cooling tower model that is not only easily implementable in practice but also gives results with a high level of accuracy.

Usually, engineers are primarily interested in the water inlet and outlet temperatures of cooling towers and seek to reach a desired approach temperature. The outlet air conditions are neglected by nearly all cooling tower models. These actual exiting air conditions are necessary to better understand the tower performance. The water loss is also neglected in most models like the Merkel model. Modeling the water loss by evaporation and, the unsaturated outlet air condition would be a more accurate method to describe a cooling tower's performance. The laborious computational iterations of some models need to be simplified to improve the practical usability of the model. The Effectiveness Model developed by Braun (1988) to describe a cooling tower under specific conditions reduces the computational burden significantly and at the same time it is found to be highly accurate. This model can help determine the location of the optimal operation point and be used in the methodology to achieve this optimum.

This thesis will utilize the Braun model to reevaluate the performance characteristics of cooling towers with unsaturated exiting air. It will provide a recommendation for the energy consumption trade-off between the cooling tower fans

and the chillers with an aim to operate the entire cooling system at an optimal point and optimal range.

1.2 Purpose and Objectives

The heating and cooling demands are always considerable energy concerns in buildings and industry. The cooling towers, as a vital component in this system, have a major potential to save energy and money when they operate in the higher efficiency mode. The potential for cost reduction, as well as the higher-efficiency design and control practices for cooling systems, offers the impetus for this project.

There are some mature models for cooling towers such as the Merkel model and the Poppe model. They are widely studied and accepted by practitioners, but their limits have raised new questions in some cases when it comes to the practical application in the field. The Merkel model assumes a saturated outlet air condition and no water loss in the process, which underestimates the cooling capacity and hence gives less accurate results, although it does simplify the calculation significantly. The Poppe method is accurate enough to predict the outlet conditions for the cooling tower, but its requirement of super computers to solve the differential equations has set barriers for most practicing engineers. It is these limitations that have motivated the development of a cooling tower model that is not only easily implementable in practice but also gives results with high levels of accuracy.

This thesis will present the process of improving the performance of the cooling tower system with no assumption about the saturation of the exiting air, thus expanding

the horizons for the application of this methodology. The Effectiveness Model for the cooling towers developed by Braun (1988) is introduced and explored to achieve the above-mentioned goals. The most significant advantage of the Braun model is that the simplicity of the relationship between operating parameters offers great insights into their effects on the behavior of cooling towers. It can be applied to a wide operational range of a cooling tower. The general nature of the Braun model easily simplifies the testing of devices such as heat exchangers used to estimate the performance of cooling towers and reduces the number of measurements needed to obtain reliable data. The reduction in the number of required measurements significantly reduces the eventual error of the model. The Braun model combines the simplicity of models like that of Merkel and the high accuracy of models like that of Poppe and thus becomes a more desirable model for engineers to use in the field.

Braun's cooling tower model is one significant part of this thesis. This study will also review the performance curves of chillers and fans in order to analyze the performance of the entire cooling system. There are few practical methodologies in the existing literature concerning the procedure of evaluation and optimization for the entire cooling system, and hence there is a need for a simple but reliable methodology for field implementation. By combining the models for components included in the cooling system such as the cooling towers and chillers, we can easily estimate the optimal operating condition for a specific cooling system with only a few measurements. The methodology explored in this thesis involves field measurement of sufficient cooling tower performance data to determine the cooling tower NTU. This information is then

utilizedwith measured weather and load data and chiller performance curves to give field engineers a practical way to optimize the performance of the entire cooling system. With the Braun model and the analysis of measured data, we can describe the actual performance of a cooling system and predict its exiting air and water conditions in a simple but reliable way.

1.3 Organization of the Thesis

This thesis is divided into six chapters, including: 1) Introduction, 2) Literature Review, 3) Cooling Tower Model Development, 4) Chiller Model Development, 5) Methodologies for Optimal Control, 6) Conclusions and Discussion.

Chapter I presents an introduction to this study with a background, the purpose and objectives. Chapter II reviews the literature related to this study. It verifies the unsaturated outlet air condition, introduces some classical models and modified models and elaborates attempts for optimized cooling system operation. Chapter III and Chapter IV describe the considerations of comparing and selecting models for the cooling towers and chillers. Chapter V explains the methodology for optimal control with the selected model and performance curves. This chapter also discusses the optimized operation point and operation range under different wet-bulb temperatures and other weather conditions. Chapter VI summarizes this study, and discusses future research.

CHAPTER II

LITERATURE REVIEW

In this chapter, we first review the actual outlet air condition of the cooling tower which we use to explain the drawbacks of models such as that of Merkel and the advantages of the Braun model. The literature review then explores briefly several existing cooling tower models, including classical models developed by Merkel and Poppe. Attempts made by subsequent researchers to improve the performance of these cooling tower models are also discussed.

2.1 Outlet Air Conditions

Outlet air of the cooling tower is generally treated as saturated air in most models. During the process of heat and mass transfer in a cooling tower, the ambient air powered by a fan, goes through the fill from the bottom to the top of the tower in a counter clockwise flow. The air absorbs heat and moisture from water, with the absorbed moisture becoming vapor, which thus increases the relative humidity at the outlet. However, few cooling towers achieve the state of complete outlet air saturation.

Zheng et al. (2012) compared the total heat transfer rate, the outlet humidity ratio, and the outlet temperature of air under unsaturated and supersaturated conditions. They found that the difference in the total heat transfer rate between these two states of saturation was less than 0.1% if the inlet water temperature is fixed at 310K, while the inlet air temperature varies from 280K to 310K. The difference in outlet air conditions,

which includes the humidity ratio and the temperature, increases with increasing inlet air humidity ratio. They measured the status of outlet air at inlet air temperatures of only 280K, 290K, 300K and 310K, and thus it's hard to make a conclusion of air status at any other temperature. Based on these tests, they found that the outlet air conditions were unsaturated at inlet air temperature of 290K, 300K and 310 K and ambient RH varying from 8% to 97%. However, at an inlet air temperature of 280 K, the results showed that the outlet air conditions were all supersaturated for the specific cooling tower they investigated. The higher the inlet air temperature, the higher the saturation point and hence the more water vapor can be absorbed when the air gets saturated.

Kloppers and Kröger (2004) pointed out that it does not matter how much water vapor is present in the supersaturated air for a specific air enthalpy since the lines of constant air enthalpy in the supersaturated region are very close to vertical. In this case, the results calculated from supersaturated governing equations are fairly close to unsaturated ones. Thus the assumption that the air is unsaturated is also a very useful assumption to predict the total heat transfer rate of the cooling towers if the air is supersaturated.

2.2 Classical Methods and Models

There are several classical methods to model the performance of a cooling tower. We will now discuss some of them briefly.

The first practical theory and equation set was developed by Merkel in 1925. This theory is widely accepted for thermal evaluation of cooling towers and is still

widely used today. It relies on three critical assumptions to simplify the calculations involved. The assumptions are:

- the water loss by evaporation is negligible
- the air exiting the cooling tower is saturated
- the Lewis number, relating heat and mass transfer is unity

With all the assumptions taken into account, the Equations (2.1) and (2.2) for Merkel theory are obtained from mass and energy balances of control volumes shown in Figures 2.1 and 2.2.

$$\frac{dh_{ma}}{dy} = \frac{h_d V_{fill}}{m_a}(h_{masw} - h_{ma}) \tag{2.1}$$

$$\frac{dT_w}{dy} = \frac{m_a dh_{ma}}{m_w c_{pw} dy} \tag{2.2}$$

where h_{ma} is the enthalpy of air, h_{masw} is the enthalpy of saturated air at the local bulk water temperature, h_d is the mass transfer coefficient, and V_{fill} is the unit volume of length dy of fill.

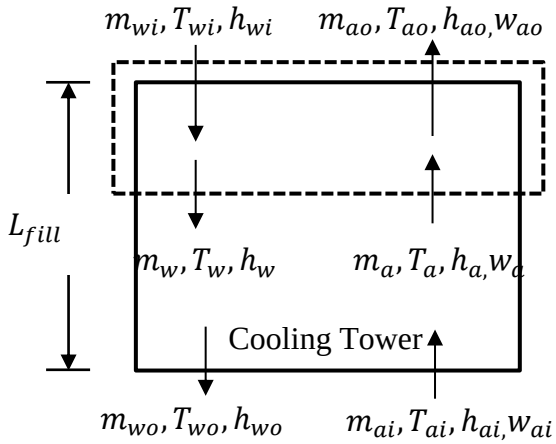

Figure 2.1 Schematic Diagram of a Counterflow Cooling Tower

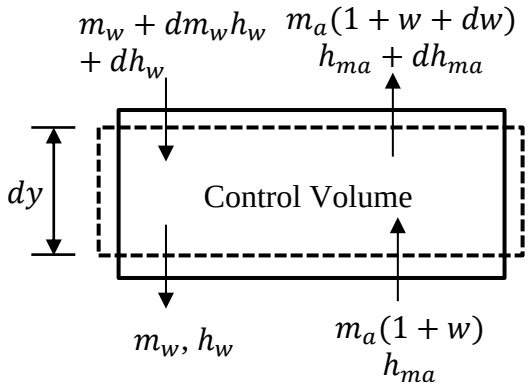

Figure 2.2 Control Volume of the Counterflow Fill

Because of the water lost by evaporation and the unsaturated outlet air condition, the Merkel model underestimates the cooling capacity. For this reason, the Merkel method cannot accurately represent the physics of the heat and mass transfer processes and so the predicted outlet air temperature and humidity could be significantly different from the actual observed values in certain cases. The underestimation of the tower capacity by the Merkel model and the deviation from observed performance gives rise to questions pertaining to the nature of air leaving the fill, and hence the optimal operation point of the cooling tower.

In the early 1970s, the Poppe method, without Merkel's simplifying assumptions, was developed by Poppe and Rögener. The Poppe method uses a more complex and accurate model for a cooling tower and predicts the outlet conditions better. It is based on a system of advanced differential equations. From Figures 2.1 and 2.2, governing equations for unsaturated air after some manipulation are:

$$\frac{dw}{dT_w} = \frac{c_{pw}(w_{sw}-w)m_w}{m_a} / [h_{sw} - h_{ma} + \left(Le_f - 1\right)\{h_{sw} - h_{ma} - (w_{sw} - w)h_v\} -$$

$$(w_{sw} - w)c_{pw}T_w] \quad (2.3)$$

$$\frac{dh_a}{dT_w} = \frac{c_{pw}m_w}{m_a}[1 + (w_{sw} - w)c_{pw}T_w / [h_{masw} - h_{ma} + \left(Le_f - 1\right)\{h_{masw} - h_{ma} -$$

$$(w_{sw} - w)h_v\} - (w_{sw} - w)c_{pw}T_w] \quad (2.4)$$

$$Le_f = \frac{h}{h_d c_{pa}} = 0.865^{\frac{2}{3}}(\frac{w_{sw}+0.622}{w+0.622} - 1)/\ln(\frac{w_{sw}+0.622}{w+0.622}) \quad (2.5)$$

where w_{sw} is the saturation humidity ratio of air evaluated at the local bulk water temperature and h_v is the enthalpy of the vapor (Kloppers and Kröger, 2005).

The Equations (2.3) to (2.5) of the Poppe method must be solved by an iterative procedure. This is a computationally laborious task requiring the help from super computers (Halasz, 1998). Despite its high accuracy, the Poppe method is seldom used in the field due to this computational burden.

2.3 Other Modified Models

The Merkel and Poppe methods are both accepted widely by researchers. However, because of their limitations stated above, there was need for models which would be both accurate and easy to implement in a field setting.

For the cooling tower models, one common traditional strategy is to utilize variable tower airflow to maintain a fixed supply temperature to the chiller condenser. Another “optimized” method of operation is to maintain a constant approach temperature (Braun, 1990). Braun indicated that the optimal supervisory control is primarily a function of two easily measured uncontrolled variables, which are the total chilled-water

cooling load and the ambient wet-bulb temperature. A modified non-dimensional model developed by Halasz (1998) transformed the complex system of differential equations to a pure non-dimensional form. According to Halasz, to obtain the simplest possible non-dimensional model, the Lewis number is assumed to be equal to 1 and the outlet air condition is not assumed to be saturated. Another popular cooling tower model was developed by Whillier (1976). He introduced a fundamental concept called the tower capacity factor, R, as a basis for correlation of test data and for predicting performance. His work also presented an optimal ratio of water flowrate to air flowrate for a certain set of outside conditions to minimize the average water temperature across the cooling tower.

For the chiller models, thermodynamic models of reciprocating chillers (Chua et al. 1996), centrifugal chillers (Gordon et al. 1995) and a "universal" thermodynamic model for chillers (Gordon and Ng 1995) are available. Several simpler models, including absorption chillers, combustion turbine chillers and electric chillers, are also introduced in the EnergyPlus Reference book.

There have been several attempts to optimize the operating methodology of a cooling system. Van (1985) utilized the condenser water flowrate and cooling tower fan speed as the control variables while Schwedler and Bradley (2001) used average water temperature to determine the capacity of the tower. Most of these attempts only optimized the operation of one component like the chiller or the cooling tower, instead of the whole system.

Several attempts have also been made to address the optimization of the entire cooling system as a whole with partial success. For instance, an optimum water flowrate was used to achieve the lowest possible average temperature of water when dissipating a specific amount of heat into a specific stream of air. Another discussion of optimal control was presented by Braun (1990). He argued for trade-offs in the power consumption of the chillers and the cooling tower fans and developed an algorithm, based upon an open-loop control equation, for the near-optimal control of the cooling system. He pointed out that the minimum total power occurs at a point where the rate of increase in the fan power with airflow is equal to the rate of decrease in the chiller power. The reset schedule of the optimal cooling tower condenser water leaving temperature was not discussed. Zhang et al. (2011) then introduced the optimization of the cooling tower condenser water leaving temperature using a component-based model. Their simulation results showed that the optimal cooling tower approach set-point reset schedule can be approximated with two straight lines, which can bring significant energy savings compared with the scenario with a constant cooling tower condenser water leaving temperature. However, currently, no single model in the published literature can represent all components in the cooling system (Graves, 2003).

Cortinovis et al. (2009) summarized some recommendations for optimal operation from their case studies. When there is an increase of thermal demand of the process without a simultaneous requirement of a lower water outlet temperature from the cooling tower, the optimal solution prescribes increasing the flowrate of circulating water through the system within a reasonable range, keeping the other operational

conditions constant. In situations when cooler water is needed to fulfill the process thermal demand, and it is sufficiently available, the most economical choice is to increase the air flowrate through the cooling tower. If the required temperature of the exiting water from the cooling tower must still be lower than the one achieved by the cooling tower and the air flowrate no longer can be raised, the methodology dictates the forced reduction of the water flowrate that enters the cooling tower.

2.4 Lewis Factor Influence

The Lewis factor is defined as the ratio of heat and mass transfer, playing an important role in cooling towers' modeling. It's a function of the humidity of the air in the boundary layer at the air-water interface. In the Merkel method, the Lewis factor is assumed equal to 1, while Poppe and Rögener use Equation (2.5) to express the Lewis factor. Kloppers and Kröger (2005) presented a comprehensive analysis for the influences of the Lewis factor.

The Lewis factor varies with change in atmospheric temperature and humidity. Kloppers and Kröger (2005) argued that the Lewis factor assumption of Merkel is not correct and that it is most likely in the range from 0.6 to 1.3.The higher the Lewis factor, the more heat is rejected from the tower, with a corresponding increase in outlet air temperature and a decrease in the outlet water temperature. Less water is evaporated with an increasing Lewis factor. At very high ambient temperatures, the results from the model are fairly close with different Lewis factors. However, as the inlet air temperature decreases, the results vary with the different Lewis factors. Thus at higher temperatures

(>26°C), it doesn't matter as much if the Lewis number specification is applied inconsistently (Kloppers and Kröger, 2005). Again, it is emphasized that the same specification of the Lewis factor must be applied to evaluate the performance characteristics of a certain fill material and subsequently to employ the same Lewis factor specification to predict the cooling tower performance.

The water temperature and heat rejected are within close tolerance for different Lewis factors. However, this trend is not observed for the evaporated water and the air outlet temperature. More water is evaporated for lower Lewis factors. This is because the Lewis factor is an indication of the relative rates of heat and mass transfer in an evaporative process.

CHAPTER III

COOLING TOWER MODEL DEVELOPMENT

This chapter describes and compares different cooling tower models, including the Merkel, Halasz, Braun and detailed models, with the derivation of the equation system and the application for a specific cooling tower. Among these models, the Halasz and Braun models abandon the assumption of saturated exiting air. In particular, the Braun model is selected for this thesis. Based on the Braun model and the measurements, regression will be carried out to obtain the NTU for a particular tower. The NTU, in turn, will be used as an input for Braun model to calculate the air flowrate.

3.1 General Mass and Energy Balances

There are two subsystems in cooling towers: air and water. The assumptions include a constant air flowrate, a steady-state energy balance condition and negligible heat transfer from the walls. A schematic of a counterflow cooling tower showing pertinent states and dimensions is given in Figure 3.1.

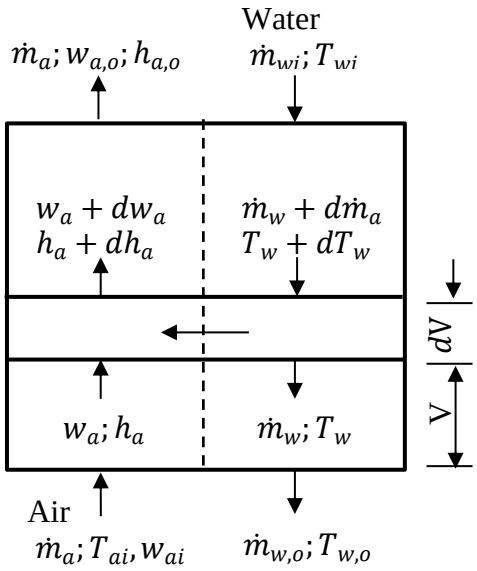

Figure 3.1 Directions of Water and Air in a Counterflow Cooling Tower

Within the incremental volume, *dV*, the relation between water and air enthalpies is shown in Equation (3.1). The incremental water loss, $d\dot{m}_w$, and water flowrate at any point within the tower, $\dot{m}_w$, are determined from steady-state water mass balance equations below:

$$\dot{m}_a dh_a = d\left(\dot{m}_w h_{f,w}\right) = \dot{m}_w h_{f,w} + h_{f,w} d\dot{m}_w \tag{3.1}$$

$$d\dot{m}_w = \dot{m}_a dw_a \tag{3.2}$$

$$\dot{m}_w = \dot{m}_{w,i} - \dot{m}_a(\omega_{a,o} - \omega_a) \tag{3.3}$$

where $\dot{m}_a$ is the mass flowrate of dry air, h_a is the enthalpy of moist air per unit mass of dry air, $\dot{m}_w$ is the mass flowrate of water, $h_{f,w}$ is the enthalpy of liquid water

and ω_a is the local air humidity ratio. Subscripts *i* and *o* represent inlet and outlet conditions respectively.

From Equations (3.1)-(3.3), the change in water temperature from the water inlet to the outlet is:

$$dT_w = \frac{dh_a - C_{pw}(T_w - T_{ref})dw_a}{[\frac{\dot{m}_{w,i}}{\dot{m}_a} - (\omega_{a,o} - \omega_a)]C_{pw}} \tag{3.4}$$

where T_w is the water temperature, T_{ref} is the reference temperature for zero enthalpy of liquid water, and C_{pw} is the constant pressure specific heat of liquid water.

For the air side, the enthalpy increase of the air stream equals the rate of energy transfer from the water droplets due to both heat and mass transfer:

$$\dot{m}_a dh_a = h_C A_V dV(T_w - T_a) + h_{g,w}\dot{m}_a d\omega_a \tag{3.5}$$

where h_C is the convection heat transfer coefficient, A_V is the surface area of water droplets per unit volume of cooling tower and $h_{g,w}$ is the enthalpy of water vapor at the local temperature.

The rate of mass transfer of water vapor to the air stream is:

$$\dot{m}_a dw_a = h_D A_V dV\left(\omega_{s,w} - \omega_a\right) \tag{3.6}$$

where h_D is the mass transfer coefficient and $\omega_{s,w}$ is the saturated air humidity ratio at the water temperature.

If the Lewis number definition ($Le = h_C/(h_D C_{pm})$) is used, the following equation is obtained from Equation (3.5):

$$\begin{aligned}\dot{m}_a dh_a &= h_D A_V dV\left[LeC_{pm}(T_w - T_a) + h_{g,w}\left(\omega_{s,w} - \omega_a\right)\right] \\ &= Leh_D A_V dV[\left(h_{s,w} - h_a\right) + h_{g,w}\left(\frac{1}{Le} - 1\right)\left(\omega_{s,w} - \omega_a\right)]\end{aligned} \tag{3.7}$$

where C_{pm} is the constant pressure specific heat of moist air and $h_{g,w}$ is the enthalpy of water vapor at the local water temperature. The overall number of transfer units for mass transfer is defined as

$$NTU = \frac{h_D A_V V_T}{\dot{m}_a} \tag{3.8}$$

where V_T is the total tower volume. Applying the NTU, Equations (3.6) and (3.7) can be reduced to:

$$\frac{dw_a}{dV} = -\frac{NTU}{V_T}(\omega_a - \omega_{s,w}) \tag{3.9}$$

$$\frac{dh_a}{dV} = -\frac{Le\ NTU}{V_T}[(h_a - h_{s,w}) + h_{g,w}\left(\frac{1}{Le} - 1\right)(\omega_a - \omega_{s,w}) \tag{3.10}$$

If the NTU, Lewis number and inlet conditions are given, the equations above can be solved numerically for air and water outlet conditions, including $w_{a,o}\ and\ T_{a,o}$, after an iteration process.

3.2 Halasz Non-Dimensional Model

Halasz (1998) developed a non-dimensional general mathematical model for the description of all types of evaporative cooling devices. This is a practical cooling tower model without a saturation assumption. This model transforms the complex system of differential equations to a pure non-dimensional form. By doing so, the parameters are greatly reduced; thus some obscure factors can also be evaluated. To obtain the simplest possible non-dimensional model, the Lewis number is assumed equal to 1.

Definitions of non-dimensional temperature and humidity ratios are:

$$\theta_a = \frac{T_a - T_{WB}}{T_{ai} - T_{WB}};\ \theta_w = \frac{T_w - T_{WB}}{T_{ai} - T_{WB}} \tag{3.11}$$

$$\epsilon_a = \frac{\omega_a - \omega_{WB}}{\omega_{WB} - \omega_{ai}};\ \epsilon''_w = \frac{\omega_{s,w} - \omega_{WB}}{\omega_{WB} - \omega_{ai}} \tag{3.12}$$

By introducing these parameters, a non-dimensional coordinate system (θ, ϵ) is established. And Equations (3.11) and (3.12) are related by the well-known equation:

$$T_{ai} - T_{WB} = \frac{h_d r_{WB}}{h_c}(w_{WB} - w_{ai}) \tag{3.13}$$

where $\omega_{s,w}$ and ω_{WB} is the humidity ratio of saturated air at bulk water temperature and wet-bulb temperature respectively, r_{WB} is the heat of vaporization of water at the wet-bulb temperature and h_c is the convective heat transfer coefficient.

Other non-dimensional coefficients are:

Number of heat transfer units: $$X_O = \frac{h_c A_s}{m_a c_{pa}} \tag{3.14}$$

Lewis factor: $$Le_f = \frac{h_d c_{pa}}{h_c} \tag{3.15}$$

Non-dimensional slope of the straight air saturation line *B*:

$$b = \frac{\omega_{s,w} - \omega_{WB}}{T_w - T_{WB}}, B = \frac{b r_{WB}}{c_{pa}} \tag{3.16}$$

Water to air heat capacity rate ratio: $$W = \frac{m_w c_w}{m_a c_{pa}} \tag{3.17}$$

A new combined non-dimensional parameter z can be defined:

$$\mathrm{z} = \frac{1+B}{W} \tag{3.18}$$

as the ratio of total heat capacity rate of the given mass flowrate of air along its saturation line to the heat capacity rate of the given water mass flowrate. A very simple formula for the water-cooling efficiency ε_w is obtained:

$$\varepsilon_w = \frac{T_{wi} - T_{wo}}{T_{wi} - T_{WB}} = 1 - \frac{\theta_{wo}}{\theta_{wi}} = z\frac{1 - e^{-(1-z)X_O}}{1 - ze^{-(1-z)X_O}} \tag{3.19}$$

Equation (3.16) gives us a plot of b versus T_w. Assume a value for T_{wo}, then the specific T_w for calculation can be simplified by the following equation:

$$T_w = \frac{T_{wi} - T_{wo}}{ln(\frac{T_{wi}}{T_{wo}})} \tag{3.20}$$

For measured data of T_{wi}, T_{WB}, T_{ai}, w_{ai} and designed m_a and m_w, values of b, B, z, ε_w W and T_{wo} can be calculated with energy balance equations. If the obtained T_{wo} has an error less than ±0.5% of the assumed T_{wo}, T_{wo} can be determined. This iteration process runs no more than 3 times for most cases, which is extremely simple for field use. The actual outlet air temperature and humidity can also be obtained from following equations:

$$T_{ao} = T_{WB} + [\frac{1}{z}(T_{wi} - T_{wo}) + (T_{ai} - T_{WB})e^{-X_O}] \tag{3.21}$$

$$w_{ao} = w_{WB} + (w_{WB} - w_{ai})[\frac{B}{z}\frac{T_{wi} - T_{wo}}{T_{ai} - T_{WB}} - e^{-X_O}] \tag{3.22}$$

If needed, the percentage of evaporated water is defined by Equation (3.23):

$$\frac{\Delta m_w}{m_w} = \frac{c_w(T_{ai} - T_{WB})}{r_{WB}}\frac{1+\epsilon_{ao}}{W} \tag{3.23}$$

Halasz (1998) pointed out that the outlet air enthalpy is computed fairly accurately with the non-dimensional model. Moreover, when the cooling range ($T_{wi} - T_{wo}$) is no greater than 10 °C, it gives a more accurate result than the Merkel method. However, the results of the non-dimensional model deviate from the detailed model, defined by Equation (3.4 – water temperature change), (3.9 - dw_a/dV through the tower) and (3.10 – dh_a/dV), by more than 10% in extreme conditions (with very minimum air flow, exceedingly large cooling range, or foggy outlet air condition). When the outlet temperature is too near to the water inlet temperature, this model yields no result. Since a

formula for the enthalpy of unsaturated air is used in deriving this model, error is inevitable. Overall, as far as the air outlet condition is concerned, the results of the non-dimensional model can be considered satisfactory in general. However, since the non-dimensional model can only describe the cooling towers performance accurately under moderate operating conditions, a better model is required.

3.3 Braun Effectiveness Model

The effectiveness model is a cooling tower model developed by Braun in 1988. It's a simple, yet mechanistic method for modeling the performance of cooling towers. This method doesn't assume saturated exiting air conditions as Merkel did. Consequently, the accuracy is more satisfactory, and it has significantly fewer computational requirements than the Poppe model. Compared to the Halasz model, the Braun model can be applied over a wider cooling temperature range.

In this section, the effectiveness model is developed by utilizing the assumption of a linearized saturated air enthalpy and a Lewis number of unity. The linearization was utilized earlier for cooling towers by Threlkeld (1970). This method can estimate the water loss in cooling towers and predict the exiting air conditions. After applying the assumptions, the equations for the cooling tower are reduced to:

$$\frac{dh_a}{dV} = -\frac{NTU}{V_T}\left(h_a - h_{s,w}\right) \tag{3.24}$$

$$\frac{dT_w}{dV} = \frac{\dot{m}_a\left(\frac{dh_a}{dV}\right)}{\dot{m}_w C_{pw}} \tag{3.25}$$

If a parameter, C_s, is introduced, then Equation (3.25) can be written as:

$$\frac{dh_{s,w}}{dV} = \frac{\dot{m}_a C_s (\frac{dh_a}{dV})}{\dot{m}_w C_{pw}} \tag{3.26}$$

where,

$$C_s = (\frac{dh_s}{dT})_{T=T_w} = \frac{h_{s,w,i} - h_{s,w,o}}{T_{w,i} - T_{w,o}} \tag{3.27}$$

C_s has the units of specific heat and will be termed the saturation specific heat. The linear relation between enthalpy and temperature differences helps to solve for the exiting conditions analytically. By selecting an appropriate average slope between the inlet and outlet water condition, an effectiveness relationship is derived in terms of C_s.

Another important parameter is air-side effectiveness, $\boldsymbol{\varepsilon_a}$, which is defined as the ratio of the actual heat transfer to the maximum possible air-side heat transfer if the exiting air stream were saturated at the temperature of the incoming water (i.e. $h_{a,o} = h_{s,w,i}$). Then the actual heat transfer is:

$$\dot{Q} = \varepsilon_a \dot{m}_a (h_{s,w,i} - h_{a,i}) \tag{3.28}$$

The effectiveness is calculated from:

$$\varepsilon_a = \frac{1 - exp(-NTU(1-m^*))}{1 - m^* exp(-NTU(1-m^*))} \tag{3.29}$$

where,

$$m^* = \frac{\dot{m}_a C_s}{\dot{m}_{w,i} C_{pw}} \tag{3.30}$$

The exiting air enthalpy and the water temperature are determined from overall energy balances on the flow streams.

$$h_{a,o} = h_{a,i} + \varepsilon_a \left(h_{s,w,i} - h_{a,i}\right) \tag{3.31}$$

$$T_{w,o} = \frac{\dot{m}_{w,i}(T_{w,i} - T_{ref}) C_{pw} - \dot{m}_a (h_{a,o} - h_{a,i})}{\dot{m}_{w,o} C_{pw}} \tag{3.32}$$

By integrating Equation (3.24) for a constant $h_{s,w}$, an effective saturation enthalpy is determined as:

$$h_{s,w,e} = h_{a,i} + \frac{h_{a,o} - h_{a,i}}{1 - exp(-NTU)} \tag{3.33}$$

The exiting humidity ratio could be calculated by numerically integrating Equation (3.9) over the tower volume. With assumption that the Lewis number is unity, integration of Equation (3.9) yields:

$$\omega_{a,o} = \omega_{s,w,e} + (\omega_{a,i} - \omega_{s,w,e}) exp(-NTU) \tag{3.34}$$

where the effective saturation humidity ratio, $\omega_{s,w,e}$, can be found from a psychrometric chart by using the value of $h_{s,w,e}$ under saturation condition.

The water loss is not neglected in the Braun model. The water flowrate exiting the cooling tower is usually 1% to 4% less than the entering flowrate. From an overall mass balance, the exiting water flowrate is:

$$\dot{m}_{w,o} = \dot{m}_{w,i} - \dot{m}_a(\omega_{a,o} - \omega_{a,i}) \tag{3.35}$$

By using these equations, the air outlet conditions and water loss rate all can be obtained.

3.4 Model Comparisons

To evaluate and compare the performance of the Halasz and Braun models, an accurate analysis defined by the numerical solution of Equations (3.4 – water temperature change), (3.9 - dw_a/dV through the tower) and (3.10 – dh_a/dV) and the Merkel analysis are applied as the criteria for the comparison. The Lewis number is assumed to be unity for both the Halasz and Braun models in this thesis.

Braun (1988) plotted the cooling tower air heat transfer effectiveness and water temperature effectiveness versus the NTU for different ratios of water flow to air flow and compared the outcomes of these four models. Braun's figures were also utilized in this work to verify the models performance and to also compare it with that of Halasz model.

Figure 3.2 shows the cooling tower air heat transfer effectiveness (ε_a) versus the NTU when the mass ratios of water to air flowrate are 0.5, 1 and 2 respectively. The operating condition is fixed at 70°F dry-bulb, 60°F wet-bulb and 90°F water inlet temperature. Overall, the Merkel, the Braun and the Halasz models all agree well with the detailed analysis for the conditions shown in Figure 3.2. The Merkel model slightly underpredicts the heat transfer effectiveness and the water evaporation rate because of the neglect of the water loss and a reduced mass transfer in the cooling tower but the error decreases for increasing ambient air temperatures. Braun pointed out that errors associated with the Braun model are primarily a result of the assumption of a linear saturation enthalpy relationship. The Halasz model also assumed a linear air saturation line, so similar errors exist for the Halasz model. The overestimation of the Halasz model is more distinct as the ratio of water to air decreases.

Figure 3.3 shows the cooling tower water temperature effectiveness (ε_w) under the same conditions as for Figure 3.2. The water temperature effectiveness is defined as the ratio of the temperature difference between the inlet and outlet water to the maximum possible temperature difference if the leaving water is at the entering air wet-bulb temperature. The Merkel model overstates the water temperature effectiveness

slightly due to the neglect of the water loss. The ε_w value predicted by the Halasz model is higher than the detailed analysis when the ratio of water to air is 0.5 and 1 but the gap decreases as the water-air ratio goes to 2.0. The Braun model gives results consistently closer to the detailed model for ε_w than the Merkel and Halasz models.

Based on the results in Figure 3.2 and Figure 3.3, the Braun model performs better than the Merkel and Halasz models when water loss and unsaturated conditions are present in the cooling tower. The Braun model offers a good compromise between simplicity, accuracy, and completeness.

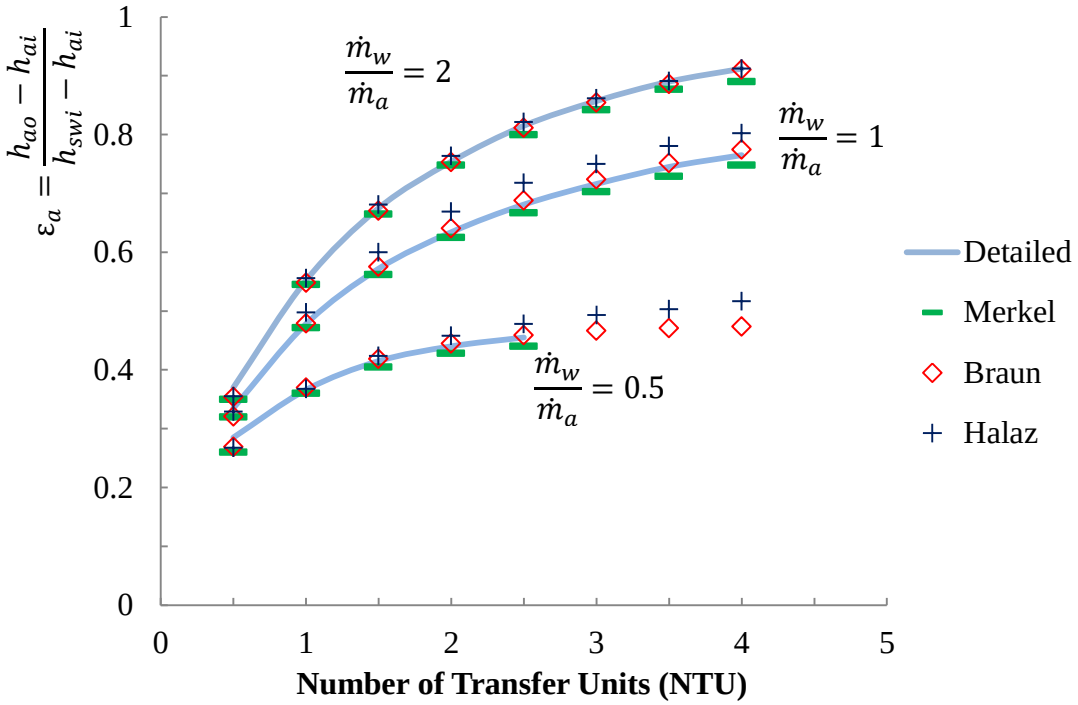

Figure 3.2 Air Heat Transfer Effectiveness Comparisons versus NTU

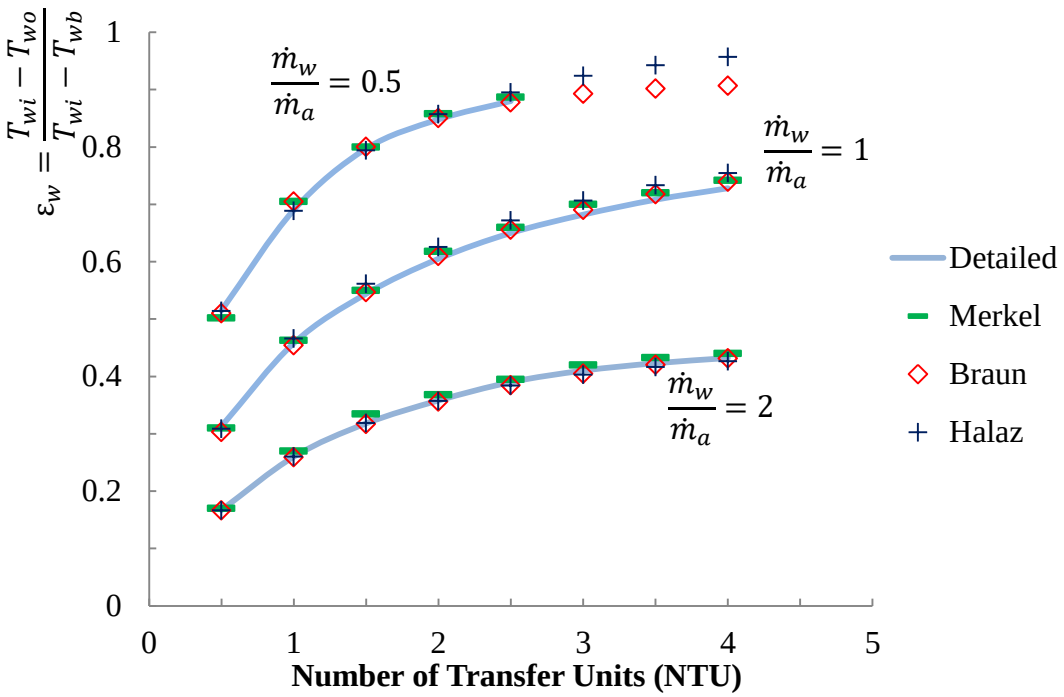

Figure 3.3 Water Temperature Effectiveness Comparisons versus NTU

3.5 Cooling Tower Operation

There are different methods to operate the cooling tower. For example, some cooling towers use approach temperatures as the feedback to control the fan, and some have setpoints to close or open the valves for the condensing water.

The two cooling towers at the Connally Building, on the campus of Texas A&M University that are analyzed in this thesis, are Ceramic Cooling Towers manufactured in Fort Worth, Texas. The model number is PL-144-6B, and serial number is PL1595-1207 6490. This tower has a reference capacity of 220 tons and a fan power of 15 hp. The design operating conditions at capacity of 220 tons are listed in Table 3.1. Figure 3.4 shows the general look of the cooling tower:

Table 3.1 Design Operating Conditions

Inputs	Water Flowrate (lb/min)	Dry-Bulb (°F)	Wet-Bulb (°F)	Water Inlet Temp (°F)	Water Outlet Temp (°F)
Value	6317	85	75	87	80

Figure 3.4 Test Facility Cooling Tower

Generally, this cooling system has two sets of cooling towers, chillers and pumps, which are shown schematically in Figure 3.5. Only one set is running at a time. Each cooling tower (CT) in this system is operated with the associated chiller. When chiller 1 is commanded on, then CT 1 will operate; this also works for CT 2 and chiller 2. The cooling tower basin water level is maintained by an adjustable water level set point, by providing domestic cold water (DCW) make-up with a DCW makeup valve. Water

enters both the cooling tower basins with the valve open. The basins are configured as two different cells but have an interlocked overflow function 4 ft above the bottom of the tower basin.

The cooling tower piping has the ability to deliver water to either the top of the cooling tower or directly to the basin, based on the condenser water temperatures and set points. If the condensing water temperature is below the set point, the pump valve will close and the condensing water will be delivered only to the top of the cooling tower.

Each cooling tower fan has a VFD. The operation of the fan is also based on the condenser water temperature and the set point. When the condenser water pump valve is open to the basin, the cooling tower fan is off. When the condenser water temperature ($T_{cond,e}$) is above the set point, the fan will operate between 20% and 100% speed for the sake of maintaining the set point.

The minimum possible condenser water temperature is the ambient wet-bulb temperature, which is not possible to achieve at any significant load. The design approach temperature for these cooling towers is 6 °F. The supply water temperature to the chiller doesn't go below 65 °F because of the installed by-pass valve. There is also an isolation valve that will shut water off completely when there is no need for the water cooling. If the fan is running at full speed, the water cannot be cooled any further. Figure 3.6 shows the measured data for the cooling range, which is defined as the difference between the inlet and outlet water temperatures, and the measured water flowrate of the cooling tower during calendar year 2015.

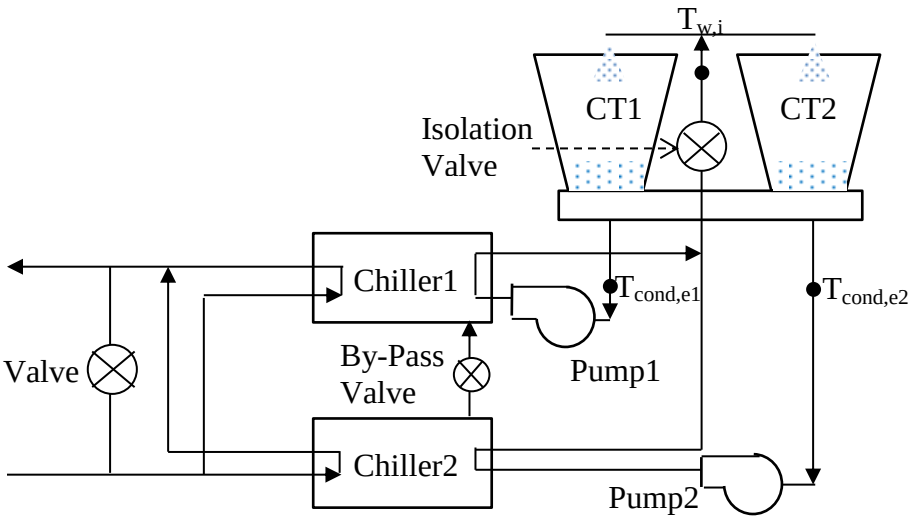

Figure 3.5 Schematic of the Cooling System at the Connally Building

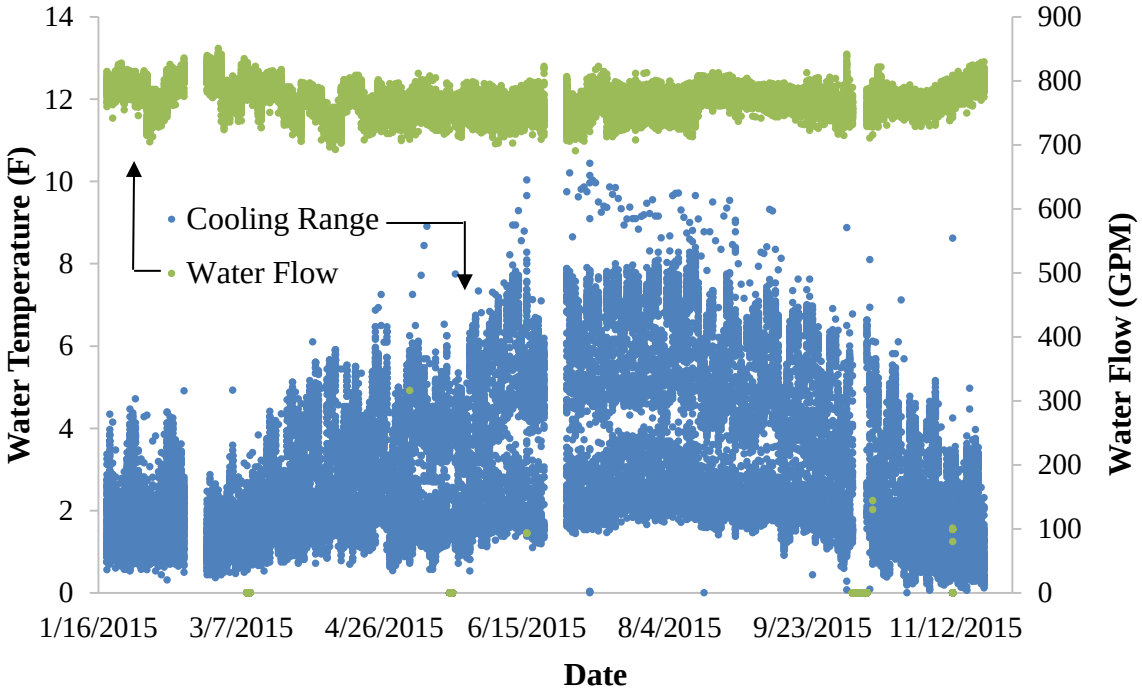

Figure 3.6 Cooling Range and Water Flowrate during Calendar Year 2015

3.6 Air Flowrate Distribution for the Fan

Cooling towers are also characterized by the air movement method. Mechanical-draft cooling towers rely on power-driven fans to draw or force the air through the tower. The fan's performance directly affects the performance of the cooling tower system. Achieving the optimized approach temperature for the cooling tower with the lowest electric power requirement is the main goal for the fan performance optimization. The fan models based on the regression with fan measurements and their performance curves can help determine the optimized operating condition combined with the chiller side.

3.6.1 Calibration for the Air Flowrate Meters

The instrument utilized to measure the air velocity in this thesis is the TSI VelociCalc® Air Velocity Meter Model 9555 Series with a range of 0 to 9999 ft/min and an accuracy of ±3% of reading or ±3 ft/min, whichever is greater.

To verify the credibility of the meters, a field calibration was performed. Two TSI meters (model 9555P0905005 and 9555P0732009) are put at a distance of 1 inch from each other at the exit of the cooling tower fan to measure the air velocity (ft/min) at the same time. The measurement samples are shown in Figure 3.7.

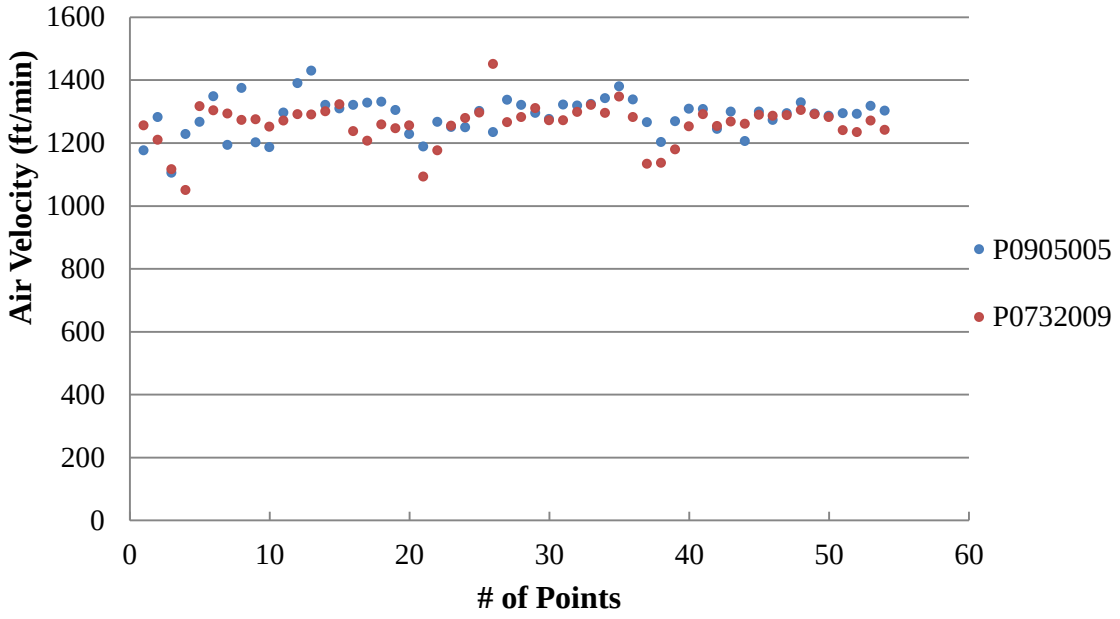

Figure 3.7 Comparison of Air Velocity Measurement for Two TSI Meters

To evaluate the degree of match between the two sets of measurements, three statistical metrics are used:

Firstly, the root mean square error (RMSE) is defined by following equation:

$$(\text{RMSE})^2 = \frac{\sum Residual_i{}^2}{N-2} \tag{3.36}$$

The second statistical metric used is the mean bias error (MBE):

$$(\text{MBE})^2 = \frac{\sum Residual_i}{N} \tag{3.37}$$

The third statistical metric is the combined error ($\text{ERROR}_{\text{TOT}}$) defined as:

$$ERROR_{TOT} = (RMSE_{TOT}^2 + MBE_{TOT}^2)^{1/2} \tag{3.38}$$

Together with the "max velocity residual", which is defined as the maximum velocity difference between the two meters, the values of the above-mentioned statistical

metrics are listed in Table 3.2 to analyze the degree of match between the two sets of air velocity measurements.

Table 3.2 Calibration Analysis of the TSI Meters

Max Velocity Residual (ft/min)	MBE (ft/min)	RMSE (ft/min)	$ERROR_{TOT}$ (ft/min)	$\frac{ERROR_{TOT}}{Mean}$
178	26.39	70.19	74.98	5.9%

The value of $\frac{ERROR_{TOT}}{Mean}$ is 5.9%, which was judged to indicate that the tested TSI meters were sufficiently accurate for the intended measurements, though this difference indicates that at least one of the meters is not meeting the manufacturer's specified accuracy. There is also the possibility that both the meters' measurements are either higher or lower than the true values.

3.6.2 Air Flowrate Measurements

Most fans are selected based on their full load working status, but in practice they are not working at the full load state most of the time. To control the flow and air volume of the fans, a variable frequency drive (VFD) is usually adopted in a range of variable load applications. The air velocity changes as the VFD speed changes, as well as along the radius of the fan.

Figure 3.8 shows the exterior of the target fan at the Connally Building. There are two sets of chillers and cooling towers, including fans. A schematic of the fan is shown in Figure 3.9 to explain its dimensions. As shown in Figure 3.9, the fans have a

disc with a diameter (OA) of 79cm (d=2.6ft) in the center so that the airflow is obstructed within the central area. The diameter (OC) for the fan is 232cm (D=7.6ft).

The measurements were implemented using a TSI model 9555P0905005 air flow meter to obtain the relationship for the air velocity versus the VFD speed and fan radius. To exclude the impact of the meshes on the air velocity, the sampled points are located within the region M shown in Figures 3.8 and 3.9. The impact of the meshes will be discussed later. It is hard to measure the exact edge of the central disc, thus the airflow at point B with a radius of 46 cm (r'=1.5 ft) is measured instead of that at point A. The test points 1-5 and 46-50 are uniformly distributed on the segment BC with different radii for one direction. Repeat this for different directions, and then we have 50 samples for a given VFD speed.

(a)

Figure 3.8 Photos of Fan at the Connally Building

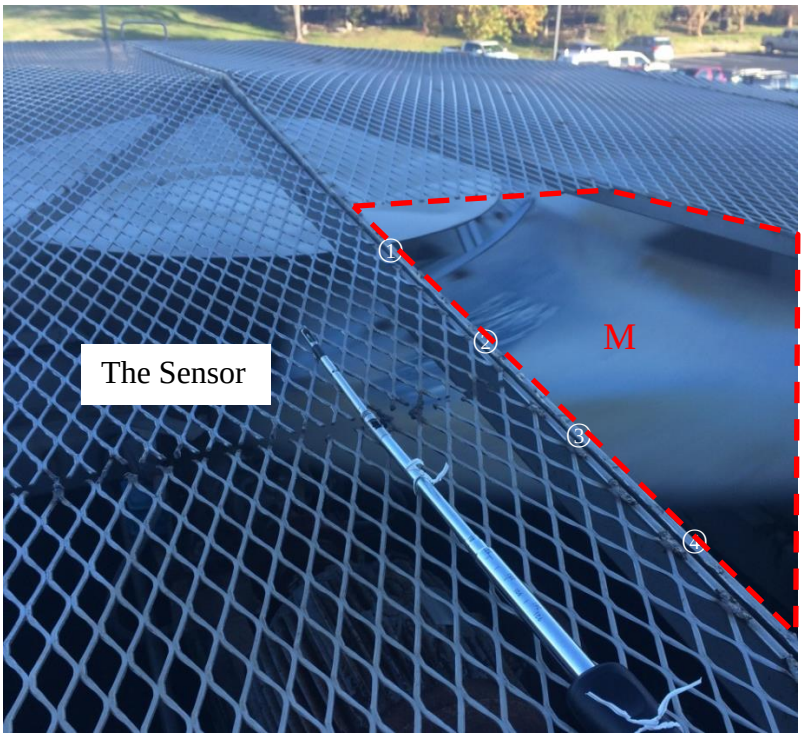

(b)

Figure 3.8 Continued

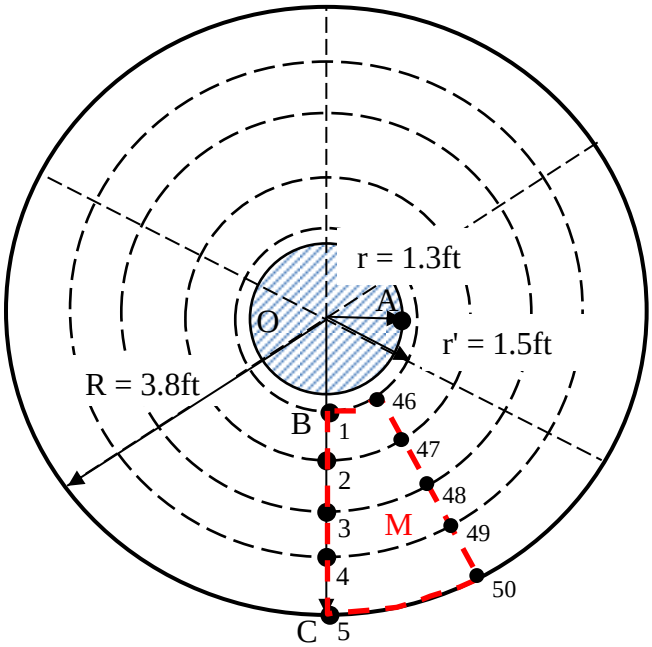

Figure 3.9 Schematic Diagram of the Fan

In the following measurements, the fan was operated at 20%, 40%, 60%, 80% and 100% of the full VFD speed. Figure 3.10 plots the air velocity versus the radius at different VFD speeds. With the measurements, an R^2 value and a quadratic curve showing the relationship between the air velocity and the radius can be obtained at the given VFD speed. These relationships are utilized to integrate to obtain the total air flowrate. The R^2 value indicates the degree of match between the regression curves and the measured samples. Overall, the air velocity reaches its peak almost at the center radius of the circular ring, and the velocity is low at the points A and B in Figure 3.9 because of the holdback.

When the fan is operated at 20% VFD speed, the equation for the curve is:

$$\text{Air Velocity} = -110.3*R^2 + 559.23*R - 441.25 \tag{3.39}$$

and the coefficient of variance $R^2 = 0.9149$. The air flowrate (cfm) after integration becomes:

$$\text{Air Flowrate} = \int_{1.3\,ft}^{3.8\,ft}[(-110.3 * R^2 + 559.23 * R - 441.25) * 2\pi R * dR$$

$$= 8388\,cfm \tag{3.40}$$

Repeat the integration for other VFD speeds, and then we have Table 3.3:

Table 3.3 Air Flowrate at Different VFD Speeds

VFD Speed (%)	20	40	60	80	100
R^2	0.8188	0.9058	0.8952	0.8993	0.9423
Air Flowrate (cfm)	8388	27487	45060	62691	79098

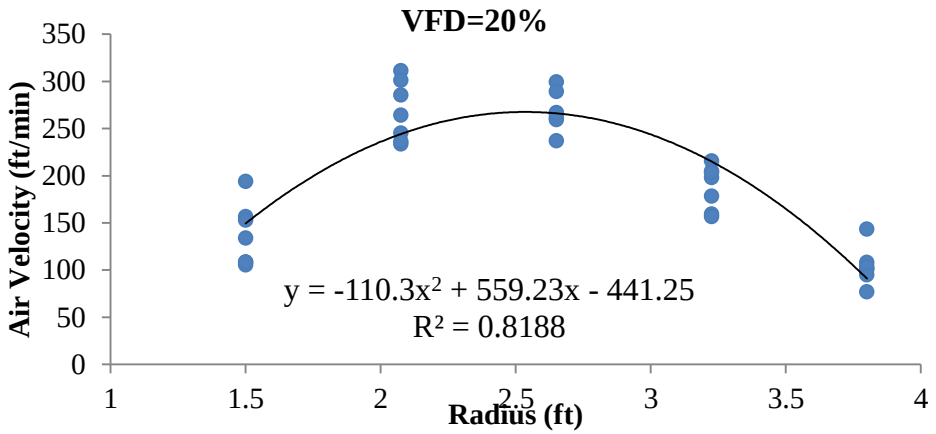

(a)

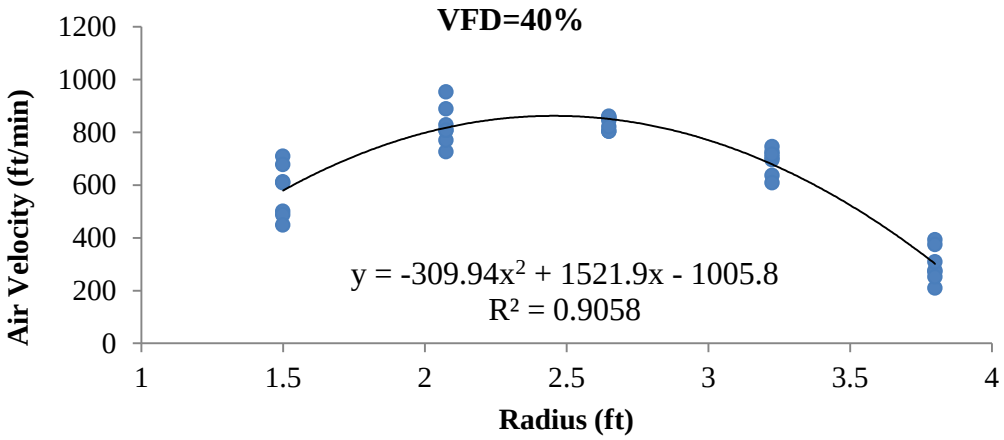

(b)

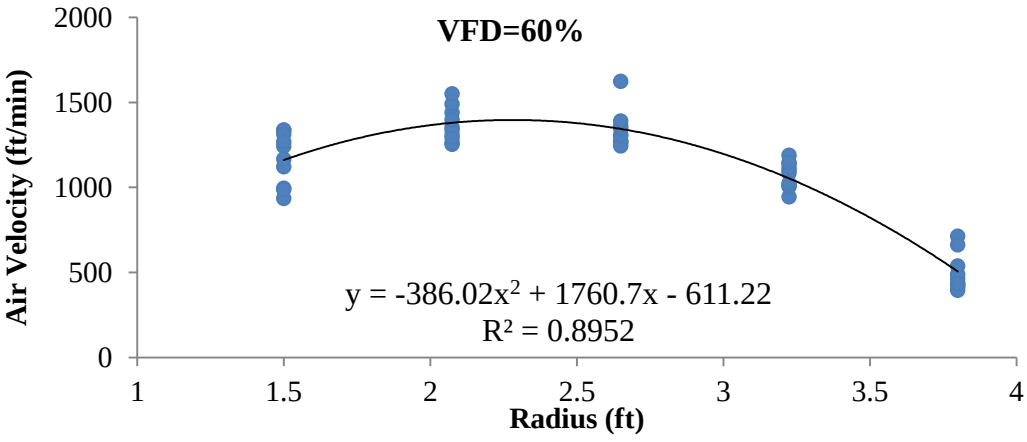

(c)

Figure 3.10 Air Velocity vs. Fan Radius at the Given VFD Speed (a)-(e)

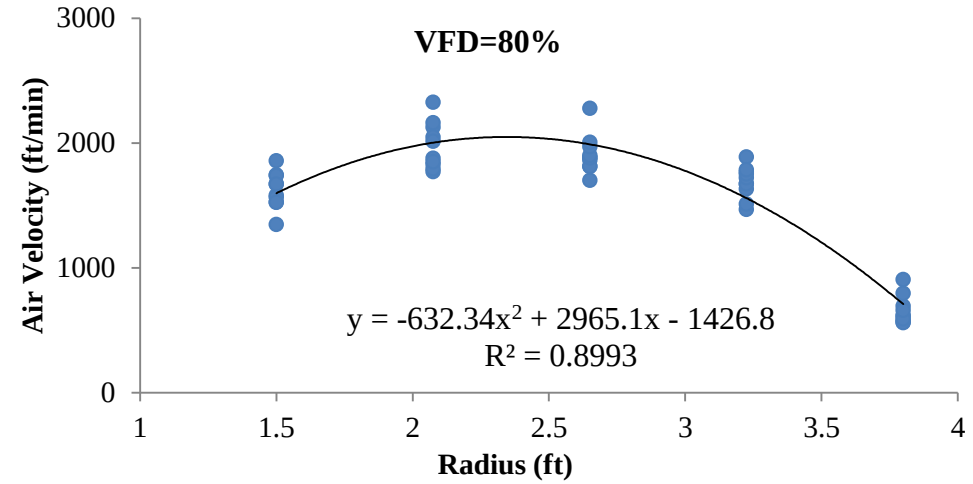

(d)

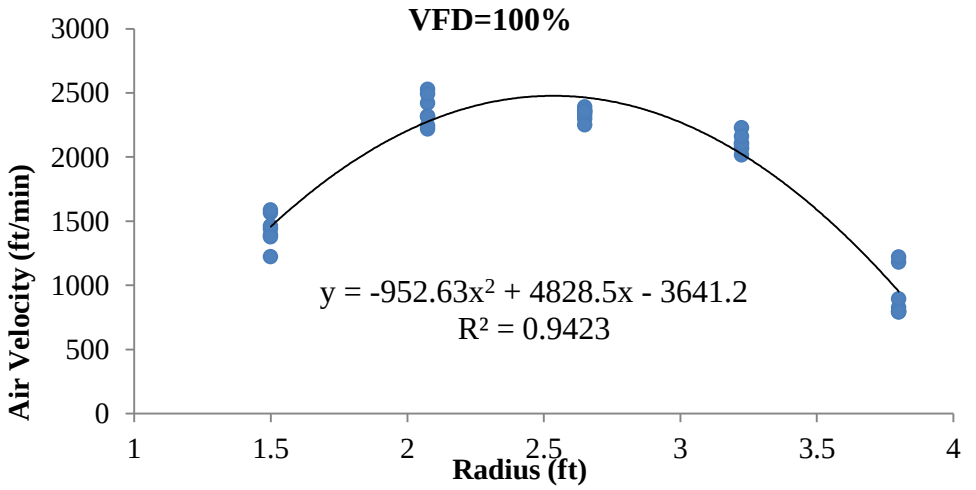

(e)

Figure 3.10 Continued

Another set of figures in Figure 3.11 is plotted with the same samples. It helps analyze another aspect of fan performance by showing the air velocity versus VFD speed for different radii. Linear relationships are applied for the regression with the measurements. The overall values of R^2 in Figure 3.11 help verify that the linear trendlines describe the data well. Thus, the air velocity at a fixed radius increases with VFD speed linearly. It may be noted that these lines intercept zero well above zero fan

speed. Hence there would be significant deviations from these linear relationships at very low fan speeds.

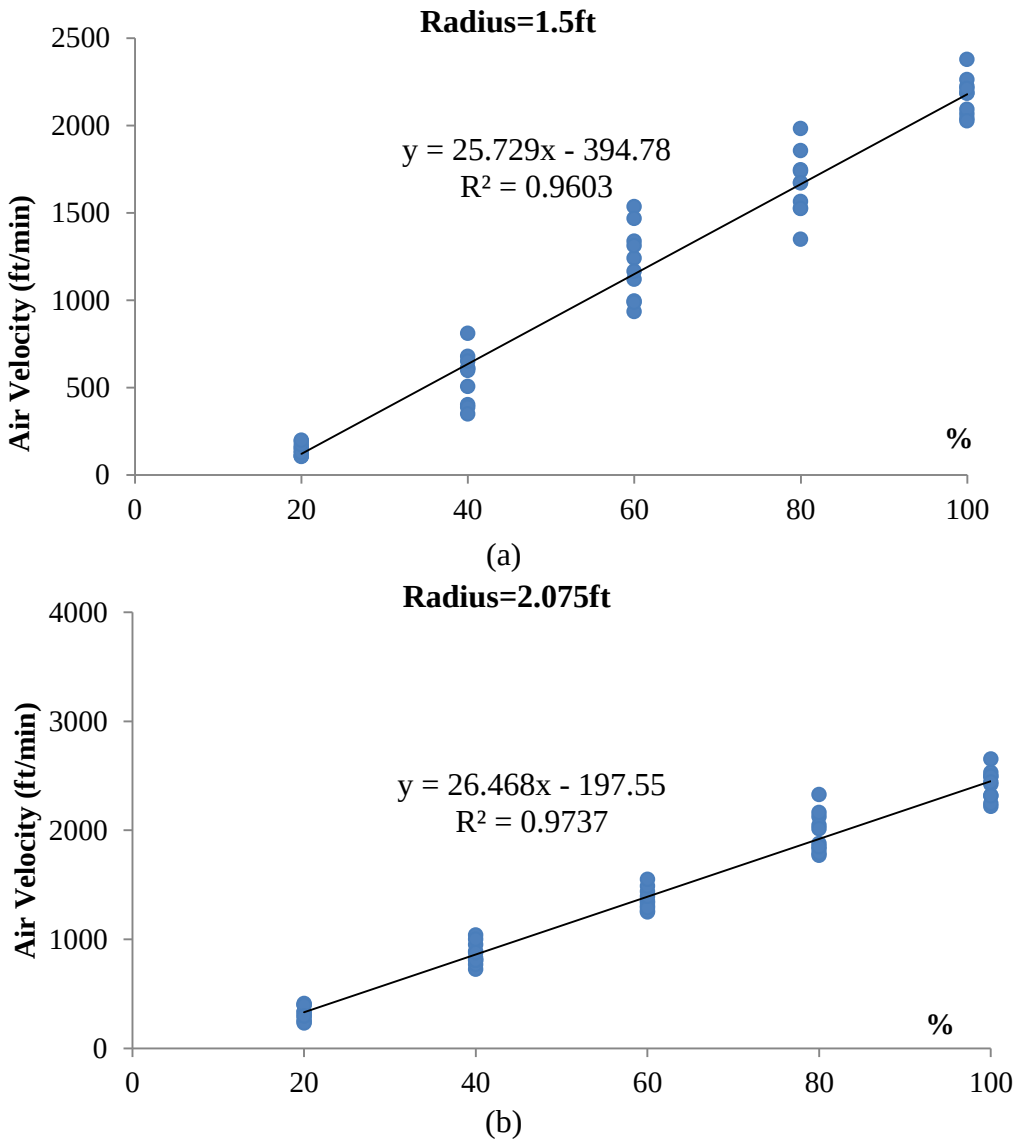

Figure 3.11 Air Velocity vs. VFD Speed w/o Meshes at the Given Radius (a)-(e)

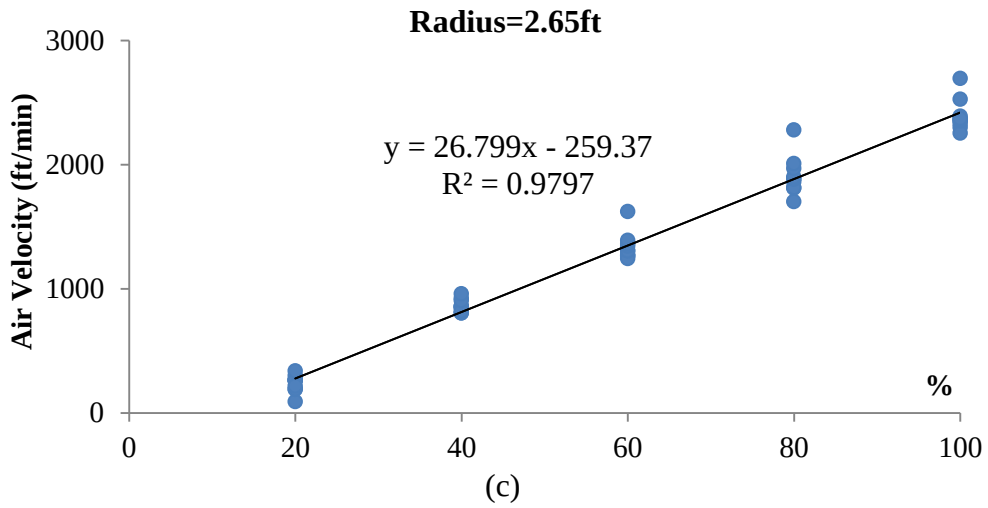

(c)

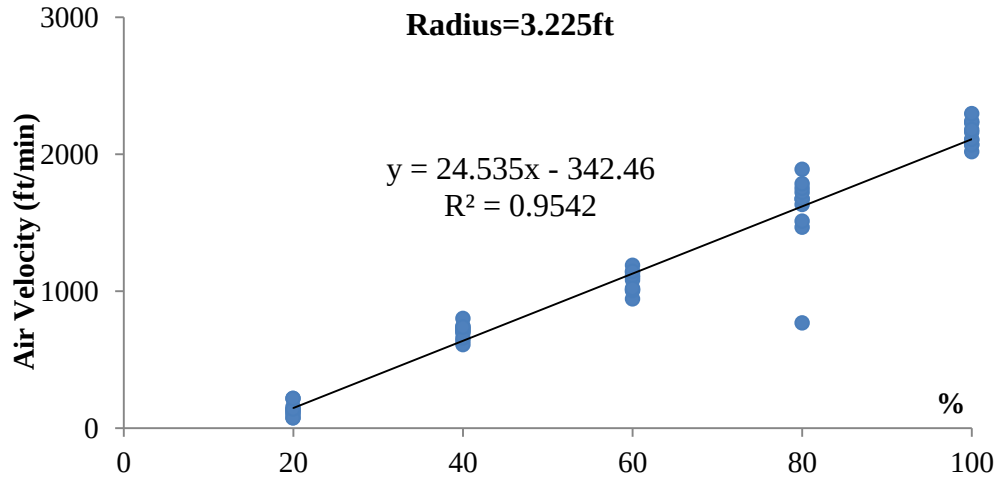

(d)

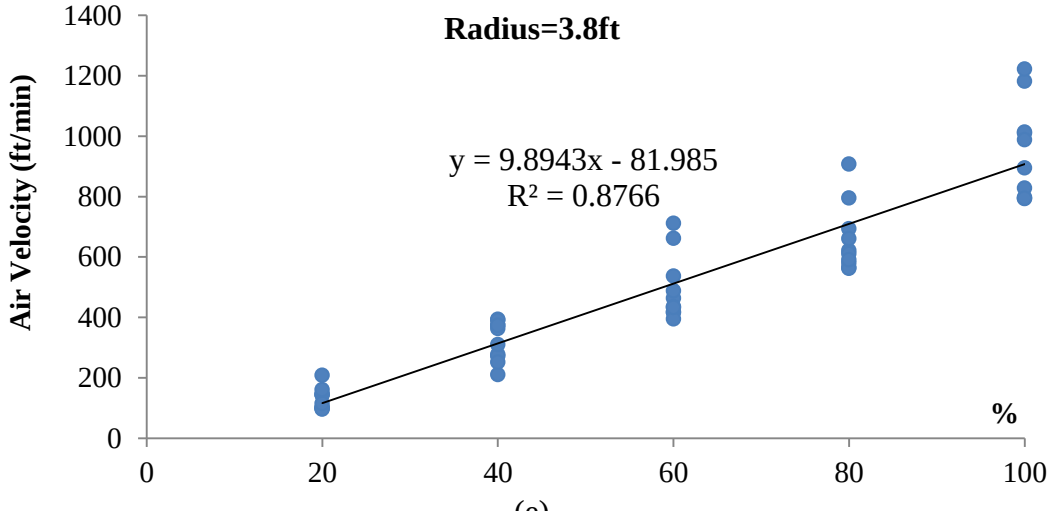

(e)

Figure 3.11 Continued

The linear relationship between the air velocity and VFD speed also verifies the linearity of the fans performance. Based on Table 3.2, Figure 3.12 shows the linear relationship between the air flowrate (CFM) and the VFD speed. The R^2 of 0.9993 suggests that the linear equation describes the change of air flowrate change with VFD speed very well, explaining 99.9% of the variation observed for the target fan. The modeling equation is:

$$\text{Air Flowrate (CFM)} = 883.12*(\text{VFD \%}) - 8442.4 \quad (3.41)$$

In theory, this equation can help determine the air flowrate for any given VFD speed. However, because of the possible error in the measurements, and the fact that the fan measurements were taken without water flow, this equation won't be utilized to describe the actual cooling tower performance practically. Instead, Figure 3.12 will be used as a reference to evaluate the performance of the Braun model developed in EES by comparing the measured and simulated air flowrate. Overall, the method and process used to analyze the air flow for the fan in this section may be applied for field measurements to investigate the performance of other fans. But further study, especially with water flow present, may give improved results. The figures and equations above verify again that the air flowrate changes approximately linearly with the VFD operation. This linearity will also be seen and used in later sections and chapters.

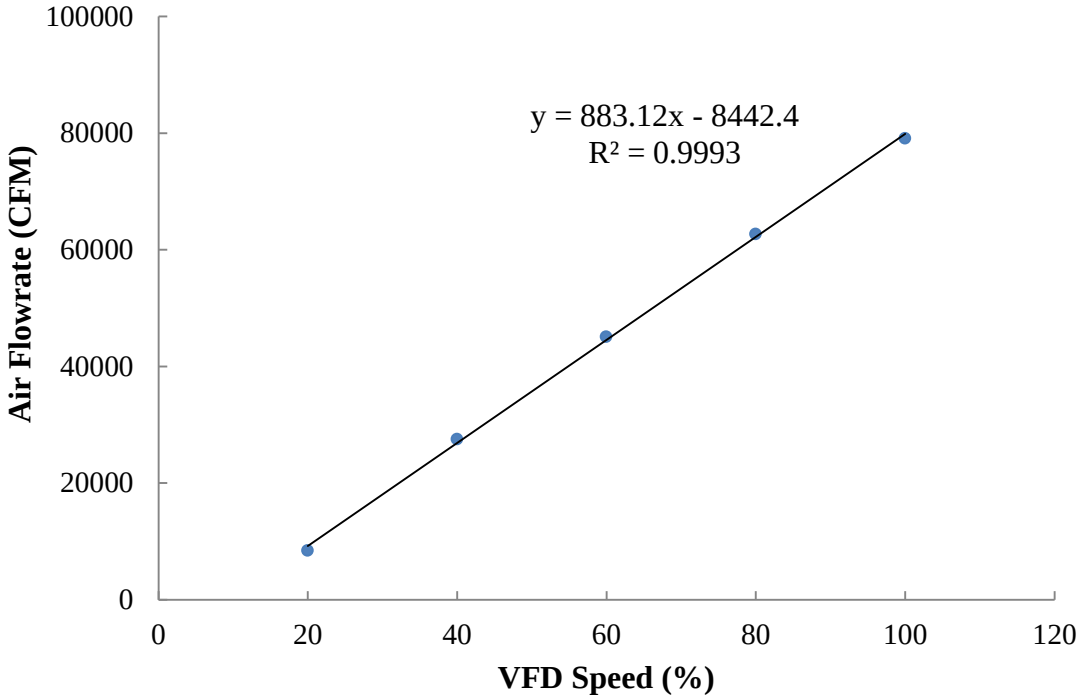

Figure 3.12 Change of Air Flowrate with VFD Speed w/o Meshes

To verify that the above measurement applies to the whole fan area, not only to the region M, one more test is conducted by using the same TSI model 9555P0905005. In this measurement, to minimize the possible error caused by the meshes, the TSI sensor is put 6 inches above the meshes for different radii and orientations, which are equally distributed on the whole fan as shown in Figure 3.13. Figure 3.14 plots the air velocity versus the radius at different VFD speeds when measured above the meshes.

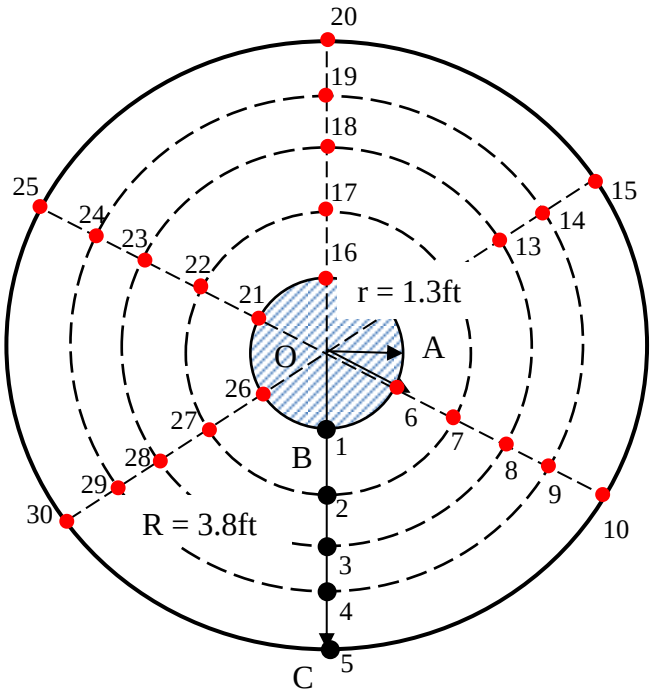

Figure 3.13 Diagram Showing the Locations of the Sampled Points

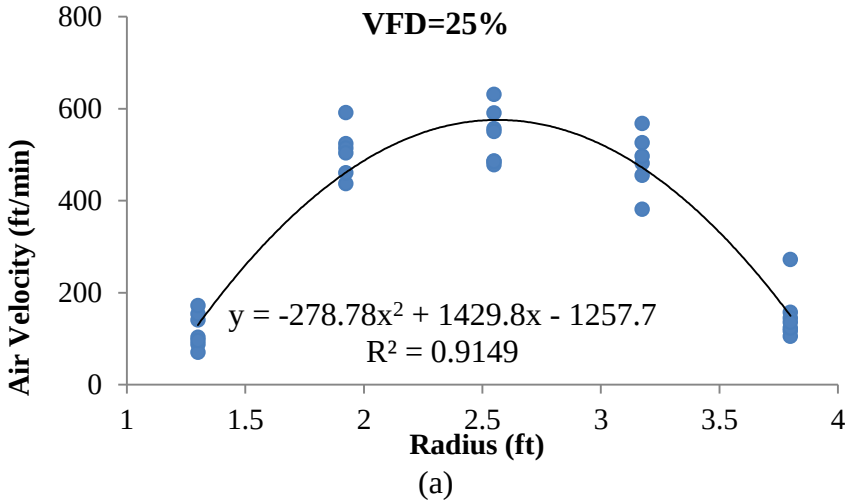

(a)

Figure 3.14 Air Velocity vs. Fan Radius w/ Meshes (a)-(d)

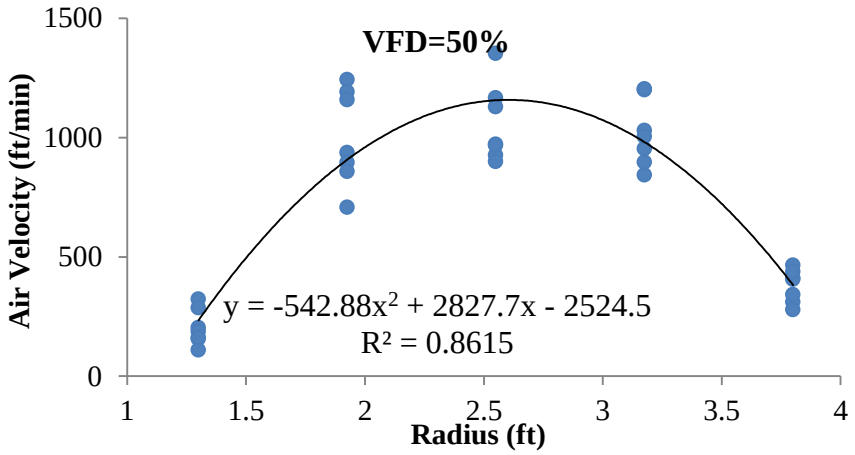

(b)

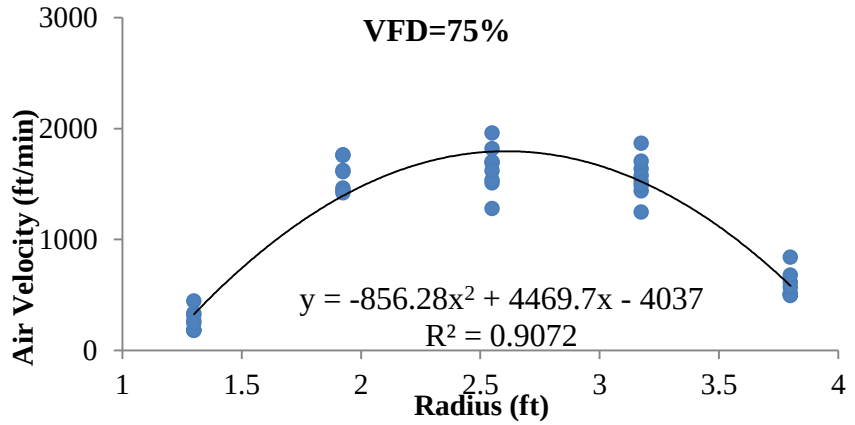

(c)

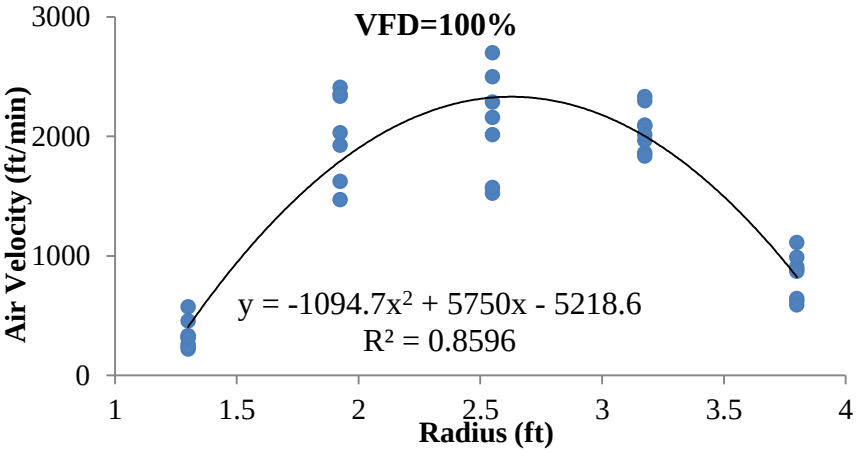

(d)

Figure 3.14 Continued

The integration of the above air velocities (ft/min) gives Figure 3.15, which plots the air flowrate versus the VFD speed and includes their corresponding equations. The cooling towers in this study were operated at VFD speeds higher than 30% for 94% of the time throughout the year 2015, and the two measurements differ by no more than 17% when the VFD speed is higher than 30%. The deviation at high fan speed may be partially due to edge losses since no practical way was found to guarantee that there is no flow outside the diameter of the fan once we are 6 inches above the mesh. Overall, we can conclude that these two air flowrate measurements are basically consistent and both the field measurements can be considered to be useable at VFD speeds higher than 30%.

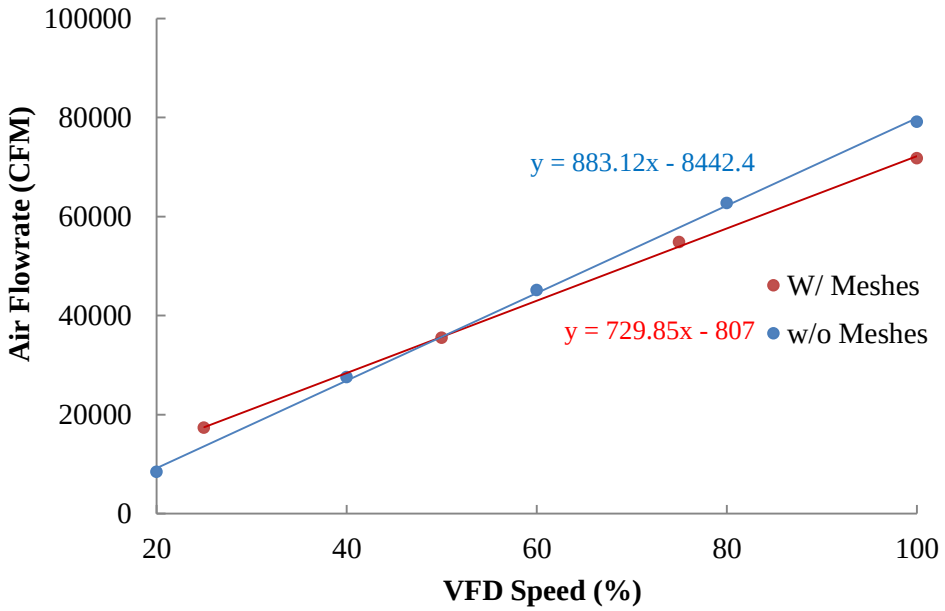

Figure 3.15 Change of Air Flowrate with VFD Speed

3.7 Verification of Temperature Sensors

The accuracy of the sensors used in the water side measurements is very important. Determining the energy balance for the tower described in Equation (3.42) between water and air side particularly requires that the sensors used to determine enthalpy and temperature differences give consistent readings at the same conditions, or the energy balance determinations will be inaccurate.

$$\dot{m}_a(h_{ao} - h_{ai}) = \dot{m}_w(T_{wi} - T_{wo}) \tag{3.42}$$

To investigate the consistency of the water temperature sensors used, a calibration was performed utilizing two new HOBO air/water temperature sensors TMC20-HD with a measurement range of (-40° to 122°F) in water and (-40° to 212°F) in air. When used with HOBO logger U12-013, the specified accuracy is ±0.45°F from 32° to 122°F and the drift is less than 0.2°F per year.

To determine whether these two sensors give credible temperature differences, both the sensors were put in the same stainless steel water sink with a dimension of 4 in*5 in*3 in for half an hour. The water was heated by adding hot water to the sink slowly. The temperature readings were taken every 5 seconds. The comparison of observed values exported from the HOBO logger U12-013 is plotted in Figure 3.16.

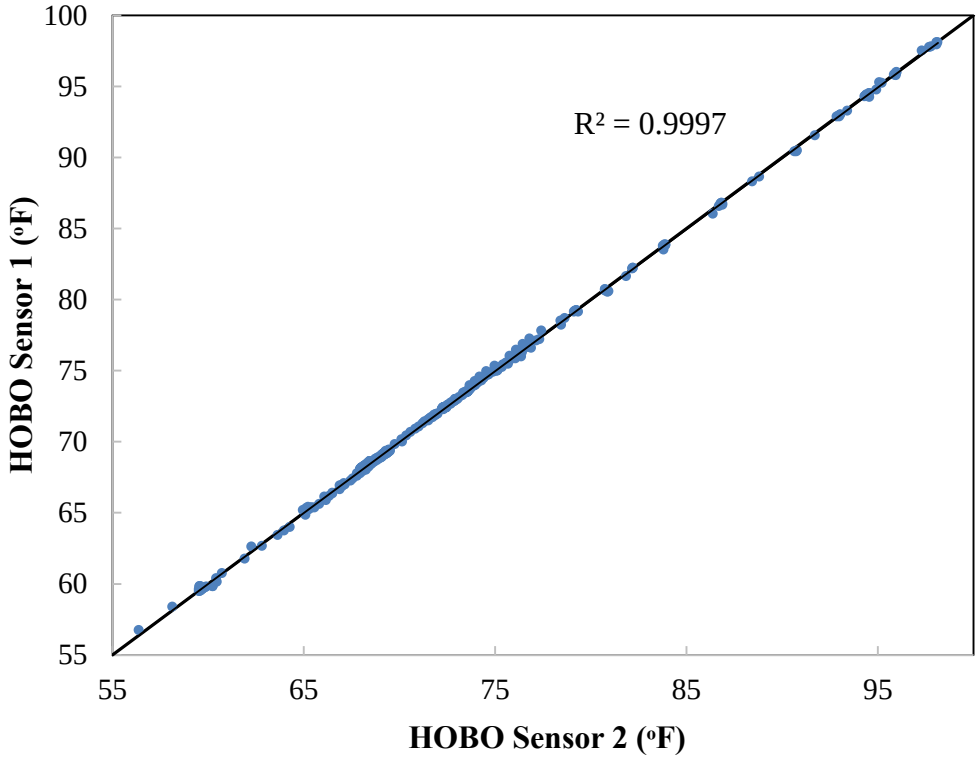

Figure 3.16 Comparison of Two Sensors for Calibration

The residual here is defined as the temperature difference between the two sensors, and then all the residuals are shown in the Figure 3.17. The maximum absolute value of the residuals shown is 0.436 °F with a mean difference of 0.021°F. Over 98% of the residuals are lower than the possible error stated in its accuracy.

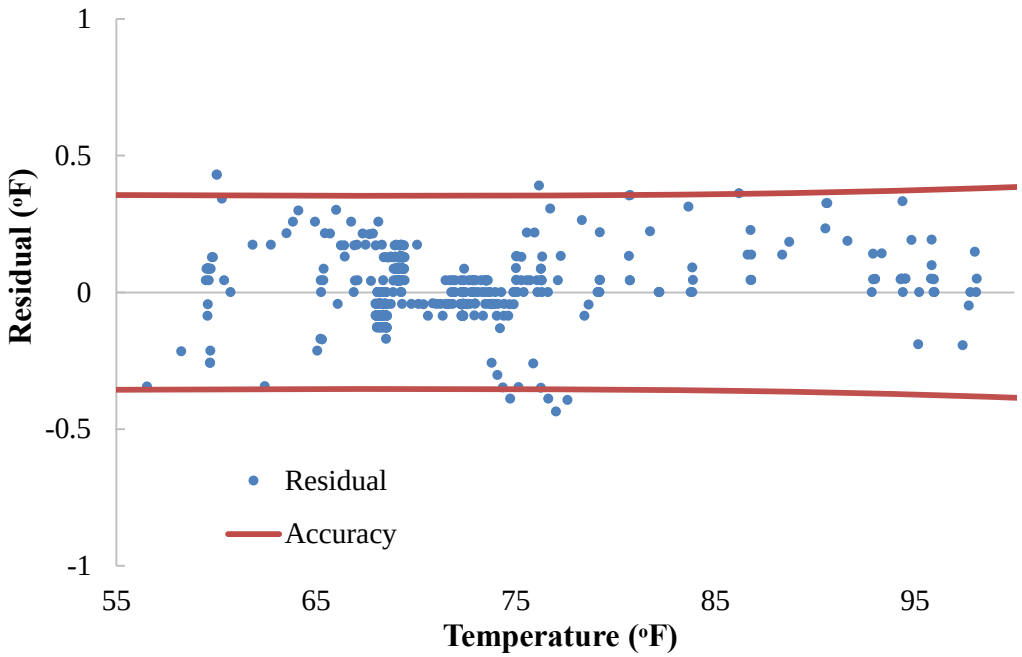

Figure 3.17 Comparison of the Accuracy and Residuals for the HOBO Sensors

Table 3.4 shows the calibration analysis with the values of the statistical metrics for the two HOBO sensors.

Table 3.4 Calibration Analysis of the HOBO Sensors

Max Temperature Residual (°F)	MBE (°F)	$(RMSE)^2$ $(°F)^2$	RMSE (°F)	$ERROR_{TOT}$(°F)
0.436	0.021	0.014	0.119	0.121

The R^2 value in Figure 3.16 is 0.9997, indicating that the two sensors agree on 99.97% of the temperature variation that they measure. Furthermore, the $ERROR_{TOT}$ of

0.121°F, compared with the water temperature range (55°F, 100°F), can be judged to indicate that the two HOBO sensors are reliable in practical use.

The two HOBO sensors were installed and logged to simultaneously measure the real-time water inlet and outlet temperatures. The measurements lasted for two weeks during January 2016. The comparisons between the HOBO sensor and the EMCS sensor measurements can be seen in Figures 3.18 and 3.19 below. Further analysis of the measurements is done by plotting the difference between measurements by HOBO and EMCS sensors for inlet and outlet temperatures in Figures 3.20 and 3.21 respectively. Almost all the inlet temperature residuals, defined as the temperature difference between the HOBO and EMCS simultaneous measurements, are within the range of ±2°F and have a maximum of 3.14°F. For the outlet temperature residuals, the main range is within ±1°F and the maximum is 1.37°F. The EMCS sensors and HOBO sensors are installed at slightly different places, which may contribute some of the differences observed. If we were aware only that the mean difference between the inlet and outlet temperatures during the period analyzed is only 1.2°F, we might conclude that the EMCS readings could not be used.

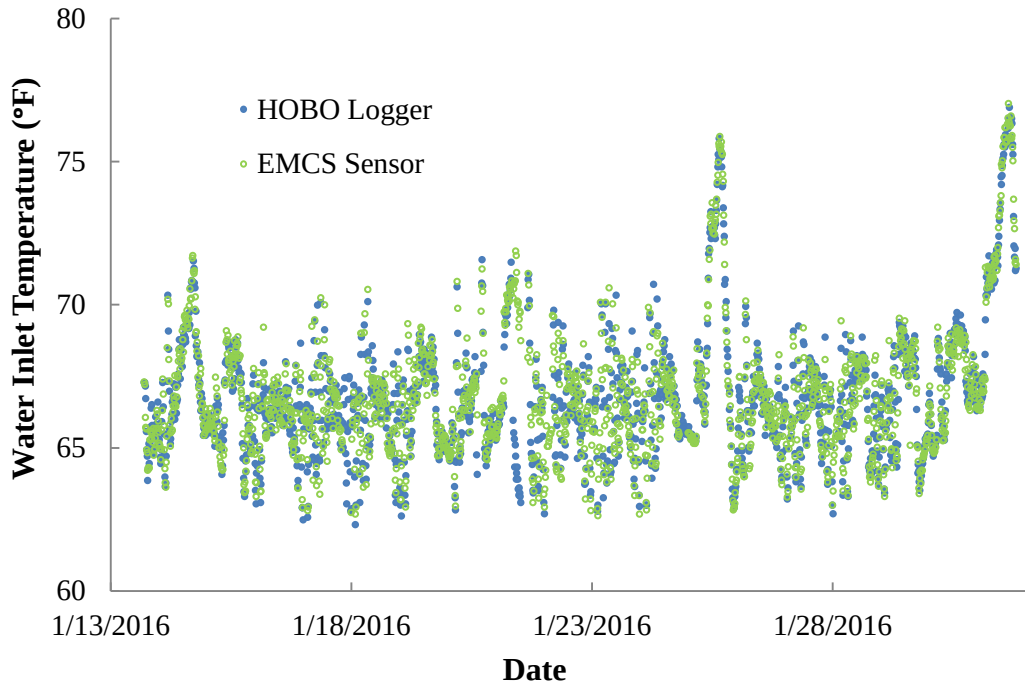

Figure 3.18 Data Comparison for Water Inlet Temperatures for January 2016

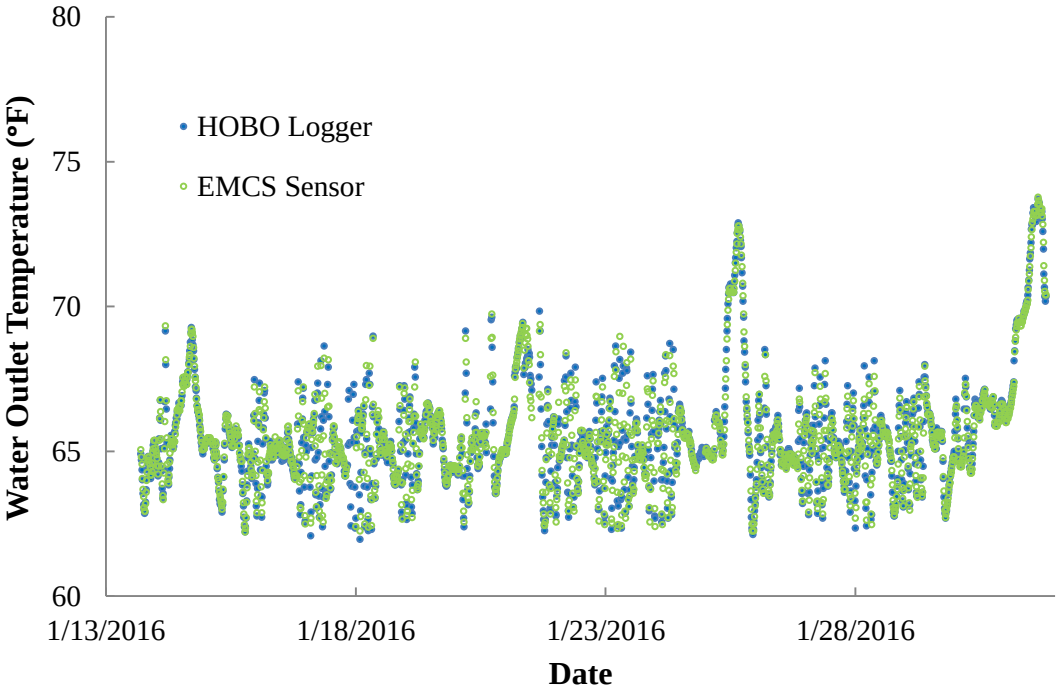

Figure 3.19 Data Comparison for Water Outlet Temperatures for January 2016

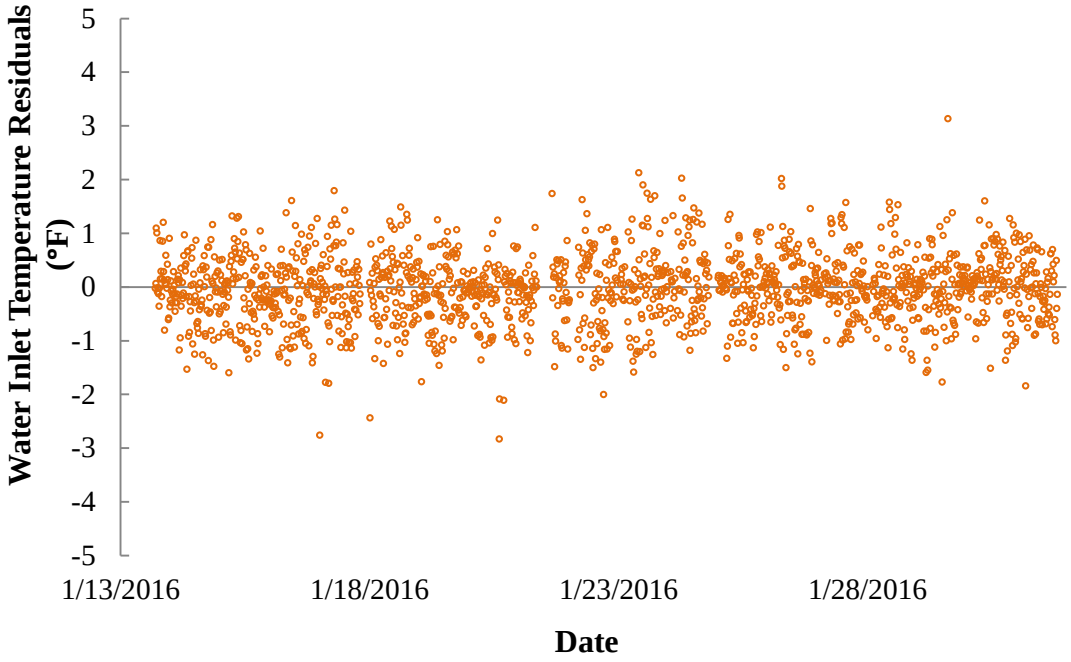

Figure 3.20 Inlet Temperature Residuals with HOBO and EMCS Sensors

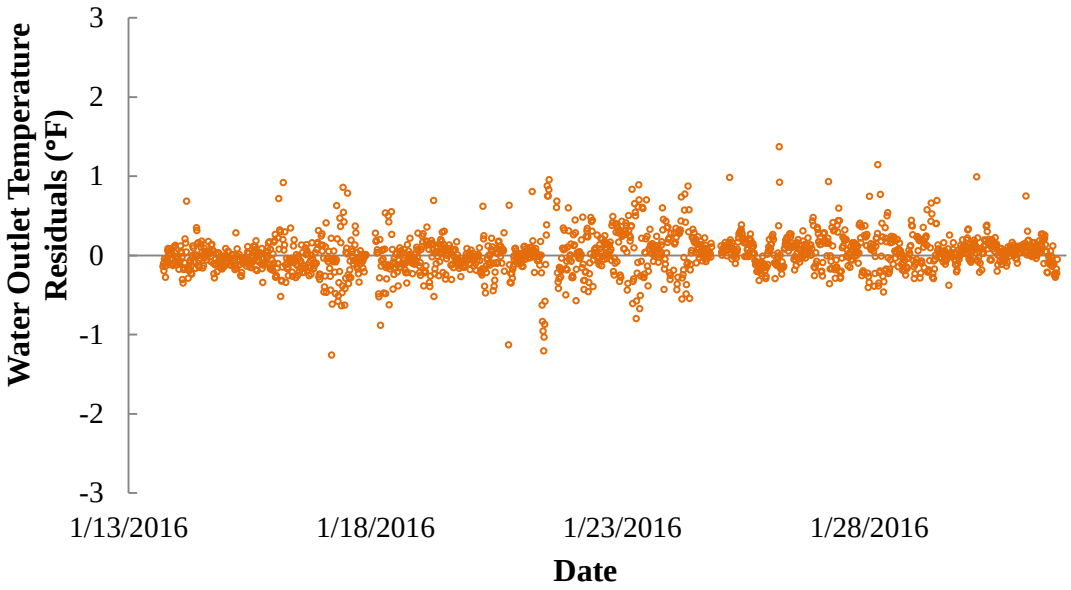

Figure 3.21 Outlet Temperature Residuals with HOBO and EMCS Sensors

Table 3.5 shows the maximum value, the MBE, the RMSE and the $ERROR_{TOT}$ of temperature residuals between HOBO and EMCS measurements. If the MBE is positive, the readings from the HOBO sensors are higher than those from the EMCS sensors.

Table 3.5 Analysis of Temperature Residuals between HOBO and EMCS Sensors

	Max Temperature Residuals (°F)	MBE (°F)	$(RMSE)^2$ $(°F)^2$	RMSE (°F)	$ERROR_{TOT}$ (°F)
Inlet	3.14	-0.030	0.420	0.648	0.649
Outlet	1.37	0.016	0.057	0.239	0.239

The MBE of -0.030°F and 0.016°F for inlet and outlet temperature residuals respectively recorded by the HOBO and EMCS sensors are very close to zero. However, further analysis, which will be presented, is required to determine whether the EMCS measurements are sufficiently reliable to be used. It may be noted that compared with the inlet temperature measurements, the outlet temperature measurements by the HOBO and EMCS sensors give much lower $ERROR_{TOT}$.

The cooling range, defined as the temperature difference between the hot entering water and the relatively cold leaving water of the tower, is an important indicator of the performance of the EMCS sensors. Figures 3.22 and 3.23 show the cooling range recorded by HOBO and EMCS sensors respectively, and based on this data, the figure showing the cooling range residuals of these two records is plotted in Figure 3.24.

To evaluate consistency of the cooling temperature ranges from the two measurements, a new non-dimensional parameter ε, defined as the temperature range differences over the average value of the HOBO cooling range ($\frac{\text{Range}_{(\text{HOBO})}-\text{Range}_{(\text{EMCS})}}{\text{Ave Range}_{(\text{HOBO})}}$) is introduced for the metric calculation. This non-dimensional ε keeps the scatter from being inflated by measurements at very low range. Table 3.6 shows the maximum value, the MBE, the RMSE, and the $\text{ERROR}_{\text{TOT}}$ of cooling range residuals between HOBO and EMCS measurements. Particularly, positive MBE means the HOBO sensors give a higher cooling range for the cooling tower than the EMCS sensors.

Table 3.6 Analysis of Cooling Range Residuals with HOBO and EMCS Measurements

Cooling Range Residuals	Max	MBE	$(\text{RMSE})^2$	RMSE	$\text{ERROR}_{\text{TOT}}$
$\varepsilon = \frac{\text{Range}_{(\text{HOBO})} - \text{Range}_{(\text{EMCS})}}{\text{Ave Range}_{(\text{HOBO})}}$	247%	-1.59%	0.256	0.506	0.506

The cooling tower modeled in this thesis has a low cooling range for the load conditions during the measurement period. It varies from 0 °F to 3.5 °F during January with an average value of only 1.3°F.

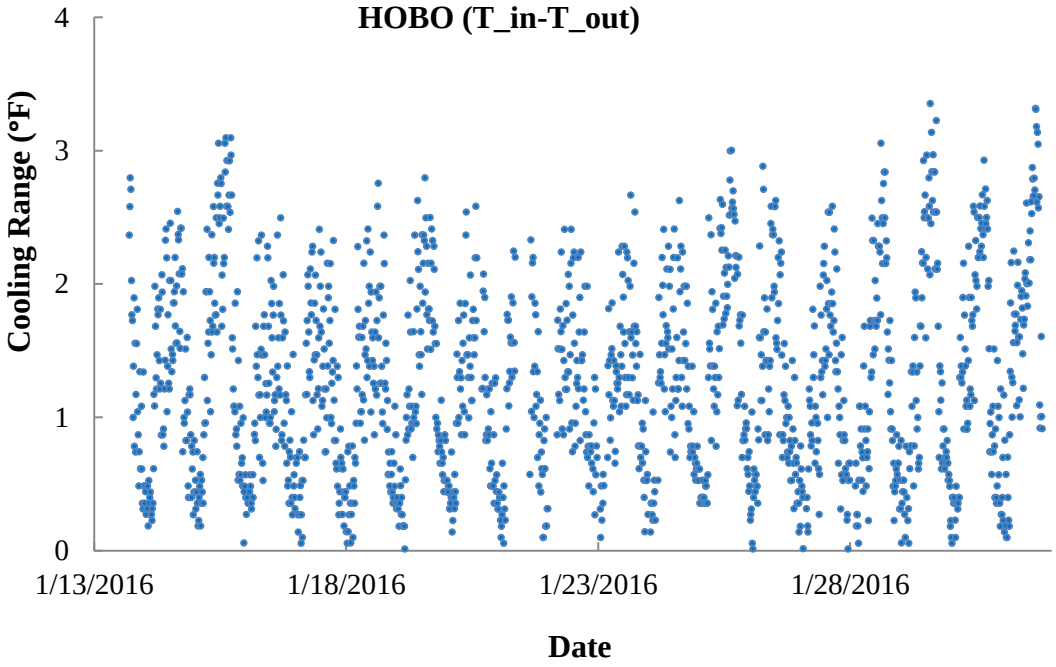

Figure 3.22 Cooling Tower Range Measurements with HOBO Logger

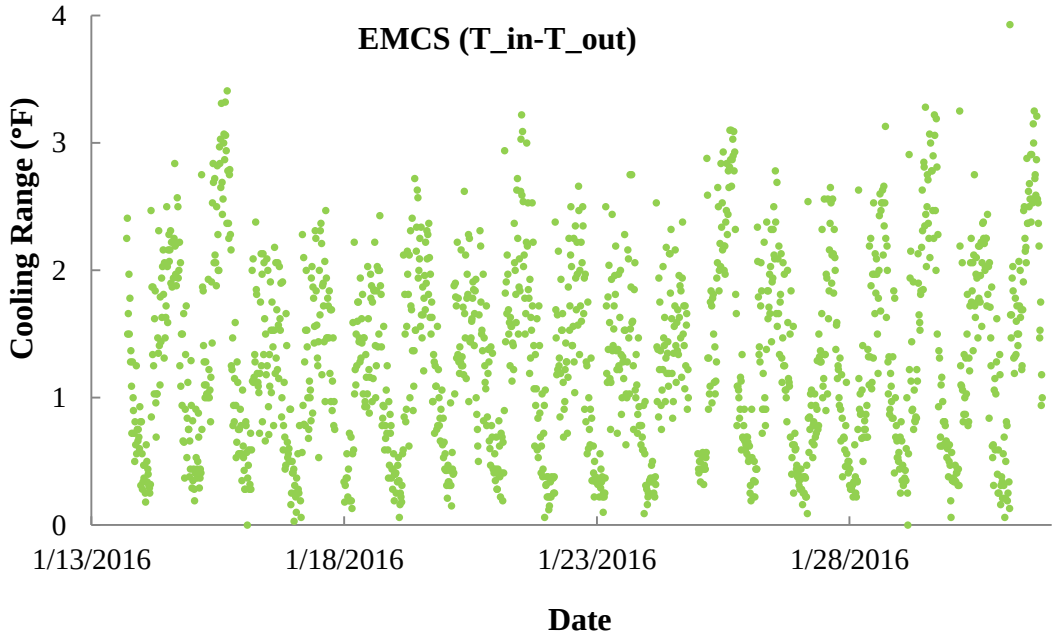

Figure 3.23 Cooling Tower Range Measurements with EMCS Sensors

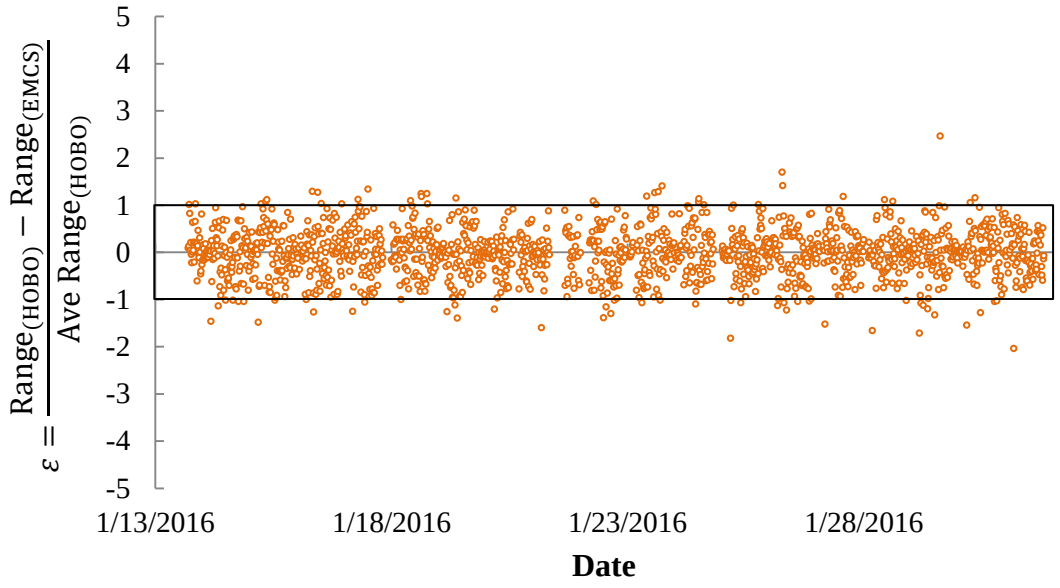

Figure 3.24 Differences between HOBO and EMCS Temperature Ranges

Based on the analysis of the inlet temperatures, outlet temperatures and cooling ranges recorded by EMCS sensors and by HOBO sensors, the measurements by the EMCS sensors are considered acceptable for use in this study since they give overall energy balance results that are within 1.59% for the low tower ranges where the comparisons were made. Comparisons for measurements made at higher tower ranges should agree even more closely.

3.8 Regression for NTU

Braun (1988) uses the number of transfer units (NTU), as a vital indicator for cooling tower performance in his model. The higher the value of the NTU, the closer the temperature of the water leaving the cooling tower will come to the ambient wet-bulb temperature. One of the key problems faced in the development of an optimization

procedure, however, is that the NTU is not given in tower specifications and is seldom known for existing cooling towers. Thus, before utilizing the Braun model for a specific cooling tower, data must be measured for that tower to determine the NTU.

The measurements taken, including water and air flowrates, ambient dry-bulb and wet-bulb temperatures, and water inlet and outlet temperatures, for the year 2015 will be utilized to determine the NTU value for the case-study tower using a regression procedure that will now be defined.

3.8.1 Energy Balance on Cooling Tower and Chiller Sides

In a cooling system, there are several energy balance requirements, and they are important indicators to verify the accuracy of the plant measurements. One of the energy balances is that in theory, the summation of the heat removed from the chilled water and the input electric energy for the chiller should equal the heat rejection of the condensed water in the cooling system, which is expressed in Equation (3.43).

$$Q_{Chiller} + P_{Chiller} = Q_{CoolingTower} \tag{3.43}$$

The Energy Balance Error is defined as:

$$EBError = (Q_{Chiller} + P_{Chiller} - Q_{CoolingTower})/Q_{CoolingTower} * 100\% \tag{3.44}$$

Figure 3.25 below shows the original tonnage measurements from the EMCS, which were taken every 15 minutes, of the cooling tower and chiller side for sampled weeks during summer (8/17-8/24), winter (12/21-12/28), and the transition period (3/30-4/6) throughout the year 2015. If possible data missing is not considered, the entire year 2015 has 365*24*4 points for each parameter. It would take a great deal of time to

analyze all of this data. Hence, to provide reasonable coverage of weather conditions throughout the year, about one week of data for each month was selected for the energy balance analysis and subsequent modeling. In addition to the plots shown in Figure 3.25, more figures and the table for corresponding data for other weeks can be found in Appendix G. The 98 days of data in Appendix G are utilized in Chapter IV for chiller modeling and Chapter V for estimating energy savings.

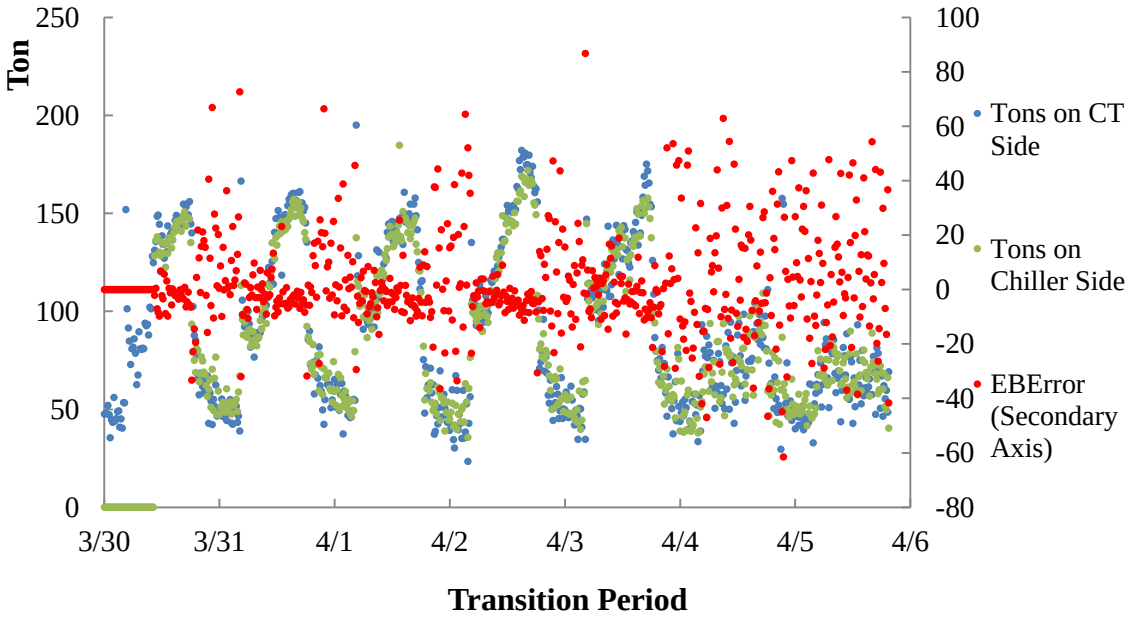

(a)

Figure 3.25 Original Plant Data of Cooling Tower and Chiller Side for Summer, Winter and the Transition Time (a)-(c)

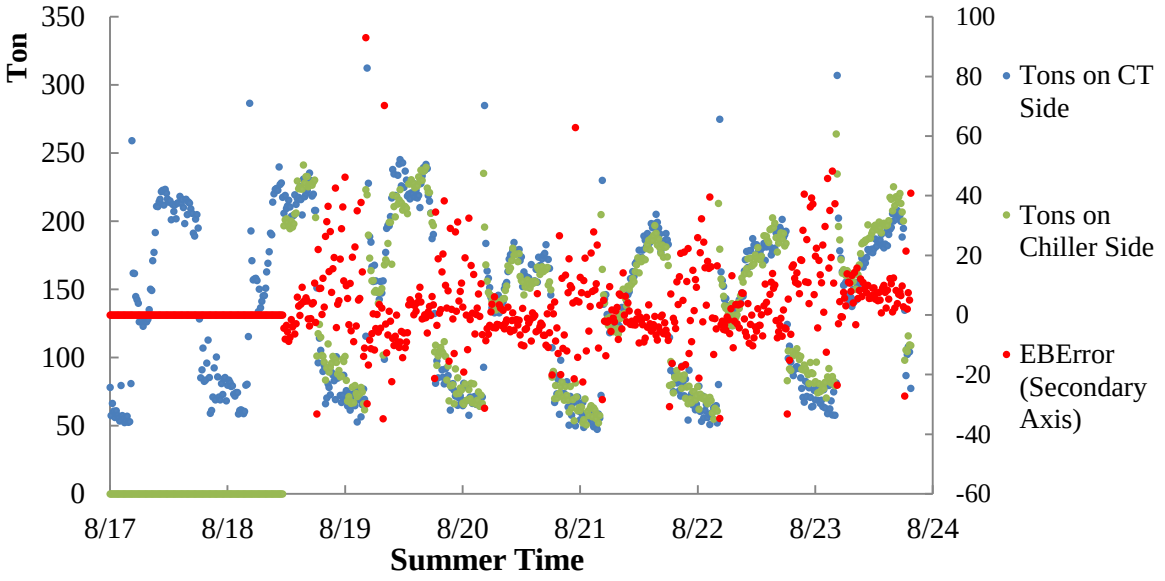

(b)

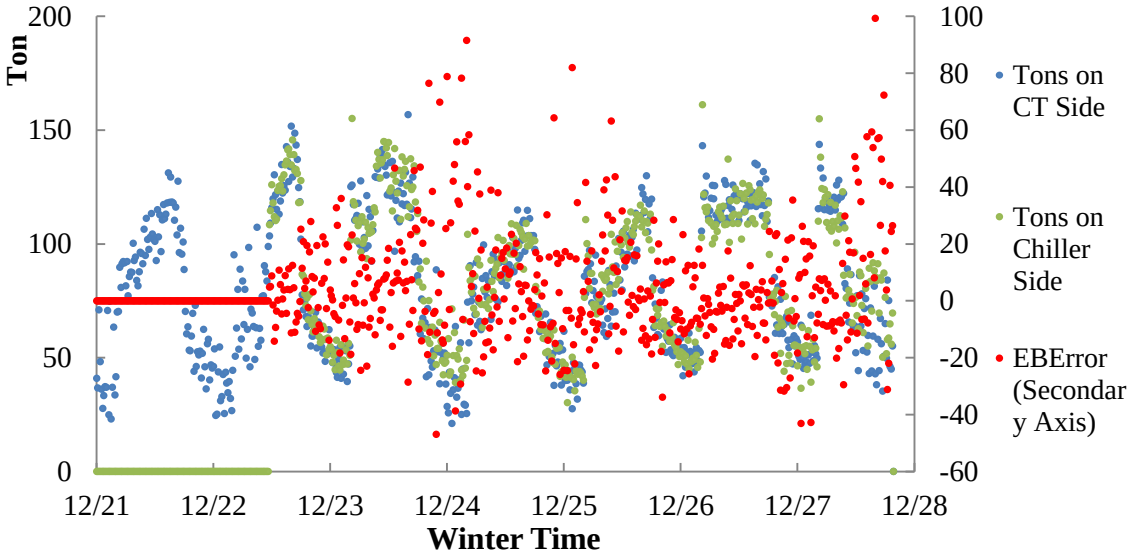

(c)

Figure 3.25 Continued

From Figure 3.25, it can be seen that the error is greater than 10% from 12/22-12/28. Generally, the error for low temperature weather is higher and more scattered

than that for high temperature weather. To simplify the analysis, daily average data is used instead of the original 15-minute interval data to perform the energy balance comparisons and analyze the cooling tower performance. Figure 3.26 below compares the average tonnage of the cooling tower and the chiller side for the 98 days analyzed. Since the performance is much more stable over a longer period of time, the daily data shows much less scatter.

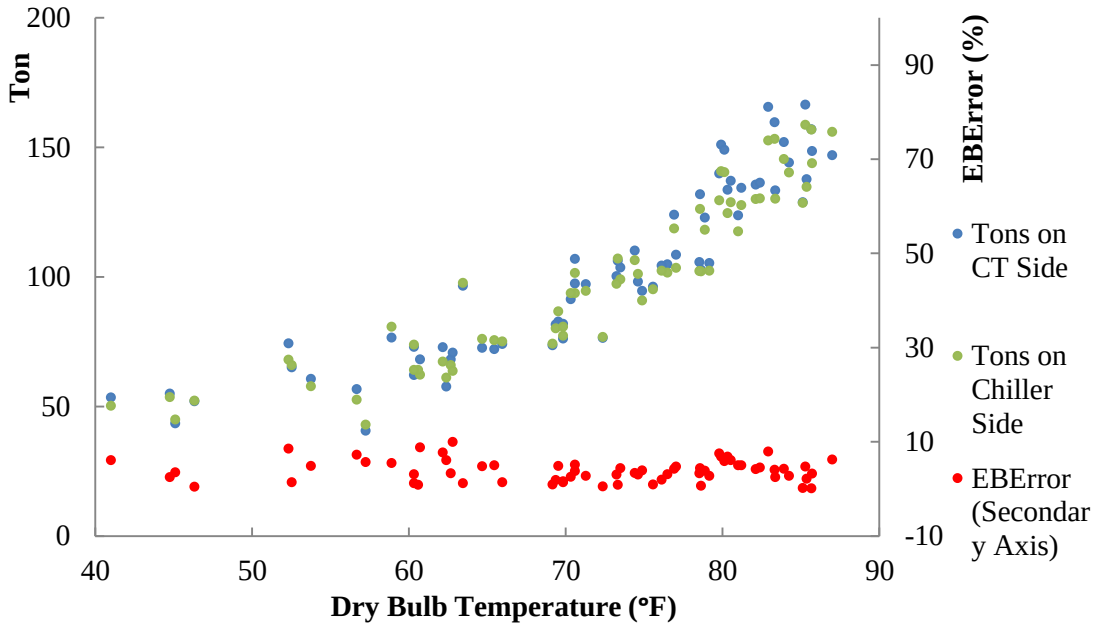

Figure 3.26 Comparison between Cooling Tower and Chiller Side Energy Flows

The metrics of the *EBError* are listed in Table 3.7. Particularly, a positive MBE means that the cooling provided on the cooling tower side is higher than the cooling plus compressor power on the chiller side. Since the two sides give overall energy balance

results that are within 2.55% and the $ERROR_{TOT}$ is 0.0548, the whole cooling plant is considered energy balanced.

Table 3.7 Analysis of Energy Balance Error between Cooling Tower and Chiller Sides

	Max	MBE	$(RMSE)^2$	RMSE	$ERROR_{TOT}$
EB_{Error}	12.8%	2.55%	0.00235	0.0485	0.0548

3.8.2 Regression Analysis

In Section 3.8.1, the energy balance for these selected days has already been verified for the cooling plant in this work, thus the measurements of these days are suitable to be used in the regression. Each set of daily measurements can produce one value of the NTU by using the programmed Braun model in the Engineering Equation Solver (EES). The calculation flowchart diagram in Figure 3.24 shows the main calculation steps of the Braun model. After applying all the measurement sets to the Braun model, all the corresponding NTU values can be obtained. Figure 3.25 is a scatterplot showing all the NTU values versus dry-bulb temperatures from programming.

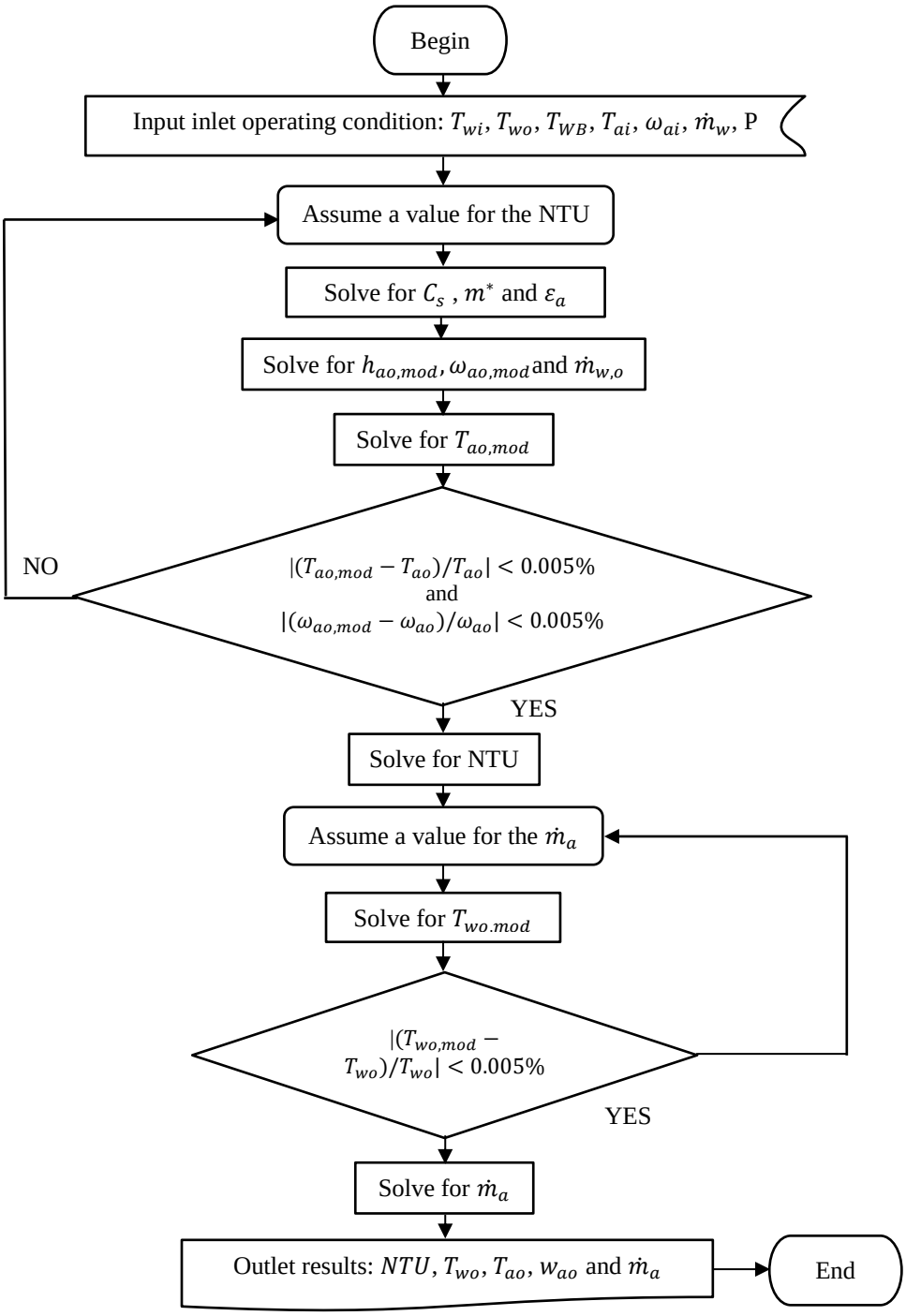

Figure 3.27 Flowchart Diagram Showing the Main Calculation Steps

The average of all NTU values calculated is 1.42. Thus the NTU for the cooling tower at the Connally Building will be considered to be 1.42 for all simulations subsequently performed in this thesis.

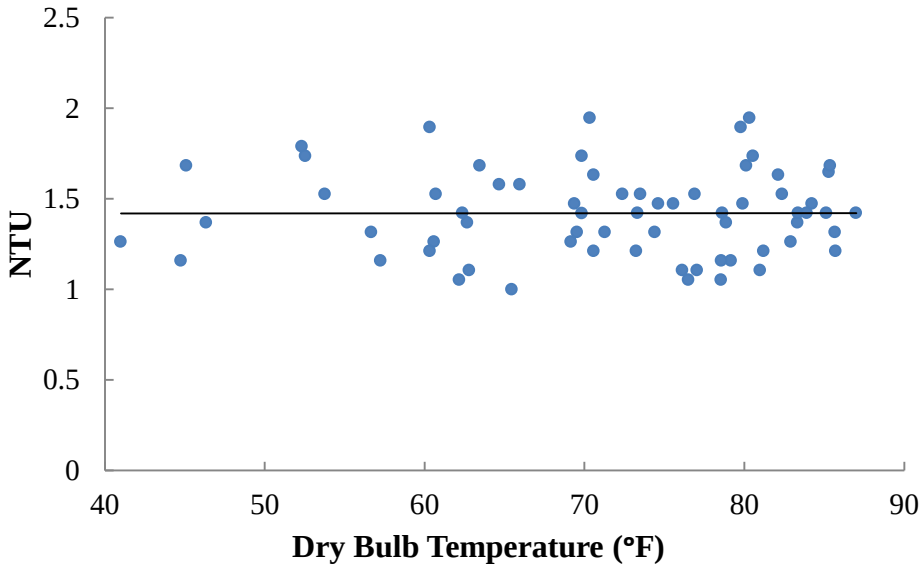

Figure 3.28 NTU at Different Dry-Bulb Temperatures

The air flowrates were also obtained from the regression. As shown in Figure 3.29, the air flowrate generally has a linear relationship with VFD speed as expected; there are still some scattered points. In addition, the simulated and measured air flowrates show very similar slope in Figure 3.29, but the simulated flow is consistently about 5000 cfm larger than the measured flow. It is also noted that the regressed flow relationships reach zero with VFD speeds well above zero. The relationship for the simulated air flowrate after regression is expressed in the following equations.

$$\text{Air Flowrate (lb/min)} = 67.369*VFD(\%)-1092.6 \quad (3.45)$$

$$\text{Air Flowrate (cfm)} = 898.25*VFD(\%)-14567 \quad (3.46)$$

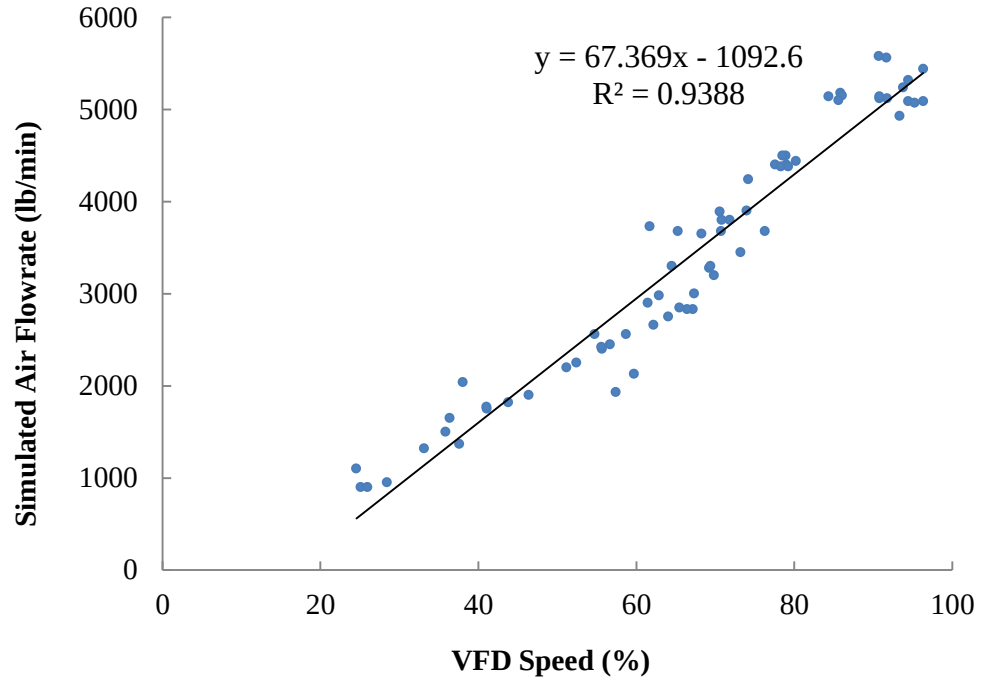

(a)

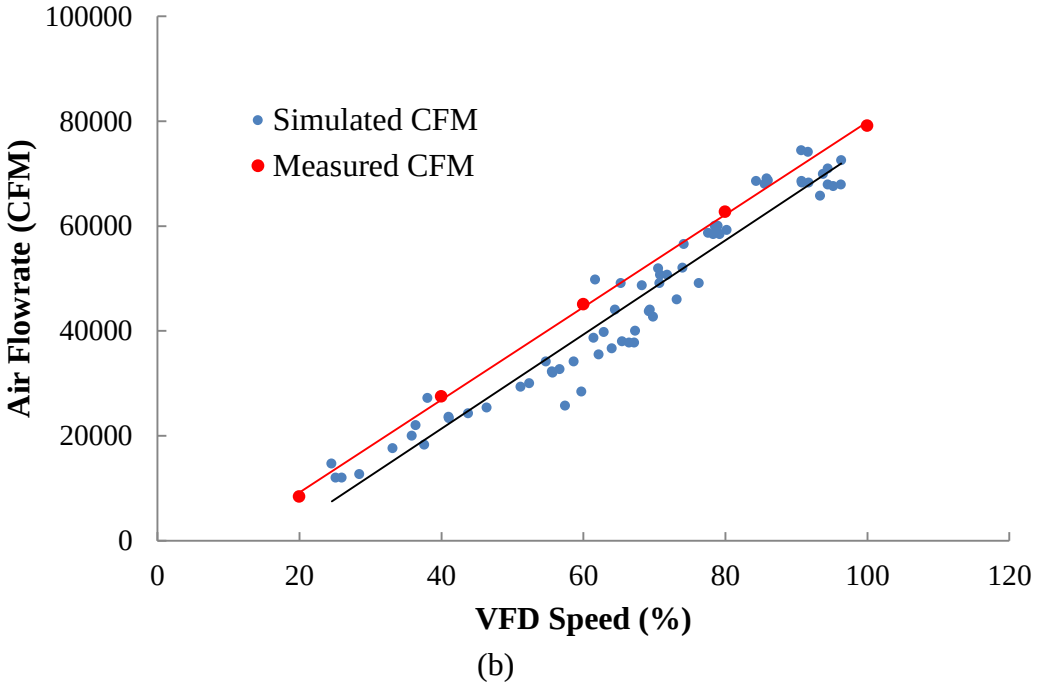

(b)

Figure 3.29 Linear Relationship between Air Flowrate and VFD Speed

3.9 Simulation Outcomes with the Braun Model

When the NTU value of 1.42 is applied to the Braun model, the predicted exiting water and air temperatures compared with actual measurements are plotted in Figure 3.30 and Figure 3.31. Overall, the predicted values match with the actual ones very well with R^2 values of 0.9976 and 0.9948 for the water and air respectively. Thus 1.42 can be considered as a reasonable value of NTU for the cooling tower modeled in this thesis.

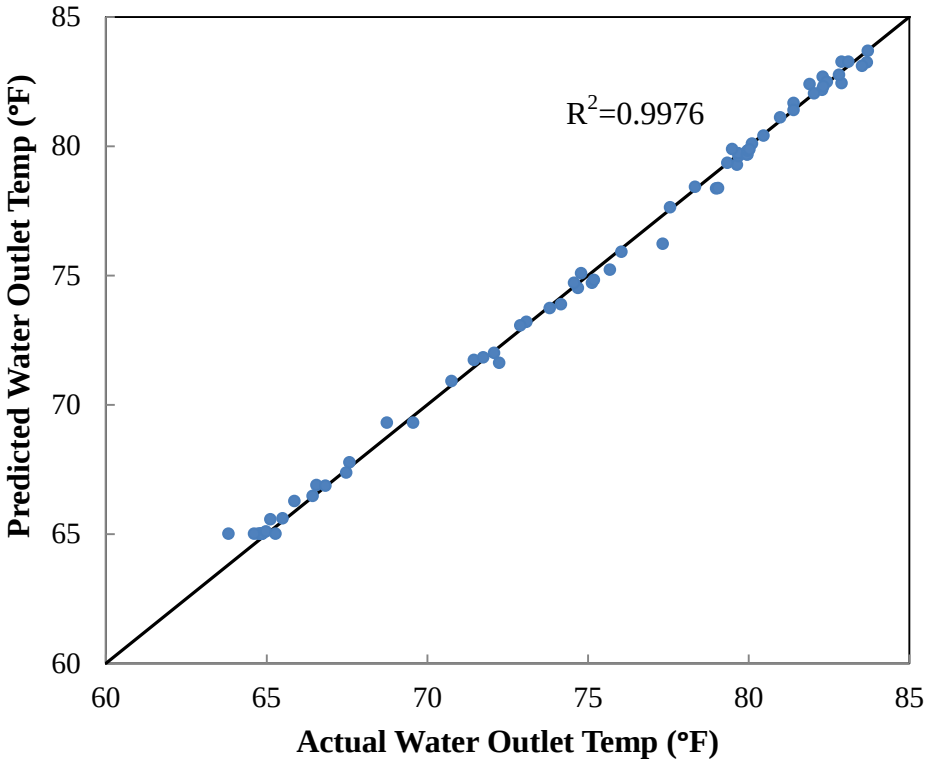

Figure 3.30 Comparisons between Predicted and Measured Outlet Temperatures of Water at NTU=1.42

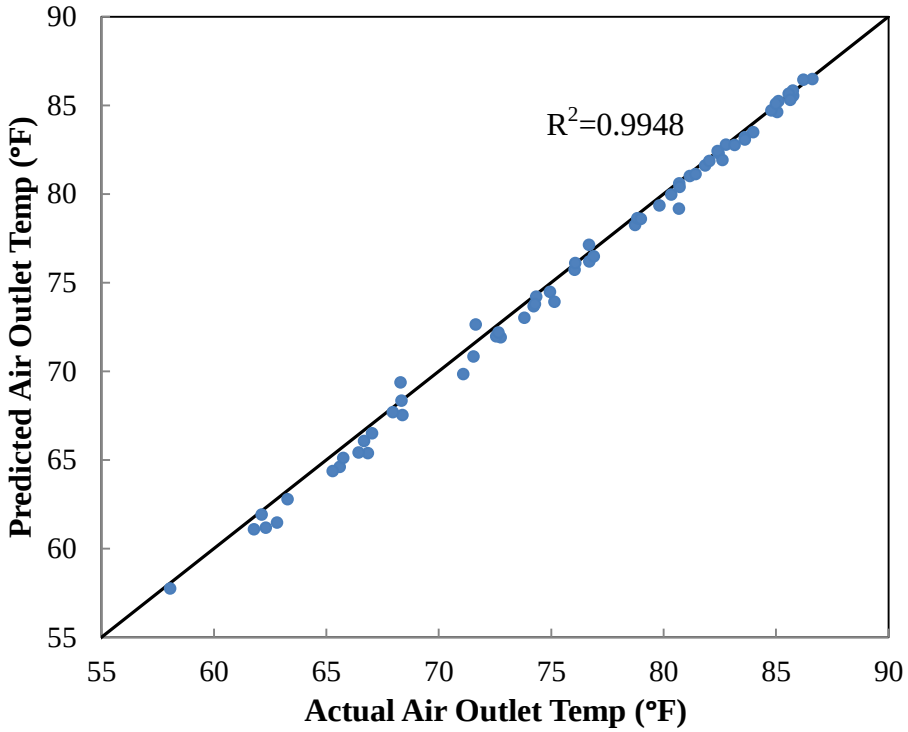

Figure 3.31 Comparisons between Predicted and Measured Outlet Temperatures of Air at NTU=1.42

The Braun model gives a good prediction for water outlet conditions. Figure 3.32 plots the predicted and measured exiting water temperatures versus dry-bulb temperature. In addition, as mentioned in Section 3.6, the cooling tower's design approach temperature is 6 °F and the minimum exiting water temperature is set to 65 °F because of the by-pass operation. The corresponding wet-bulb temperatures and the design condensing water supply temperatures are also plotted in Figure 3.32. Although the measured exiting water temperatures are generally somewhat higher than the design values, the cooling tower exit temperatures are almost all less than 3.5°F above the design points. When the dry-bulb temperature is lower than 60 °F, the exiting water

temperatures are relatively constant at 65 °F because of the by-pass setting for the cooling tower.

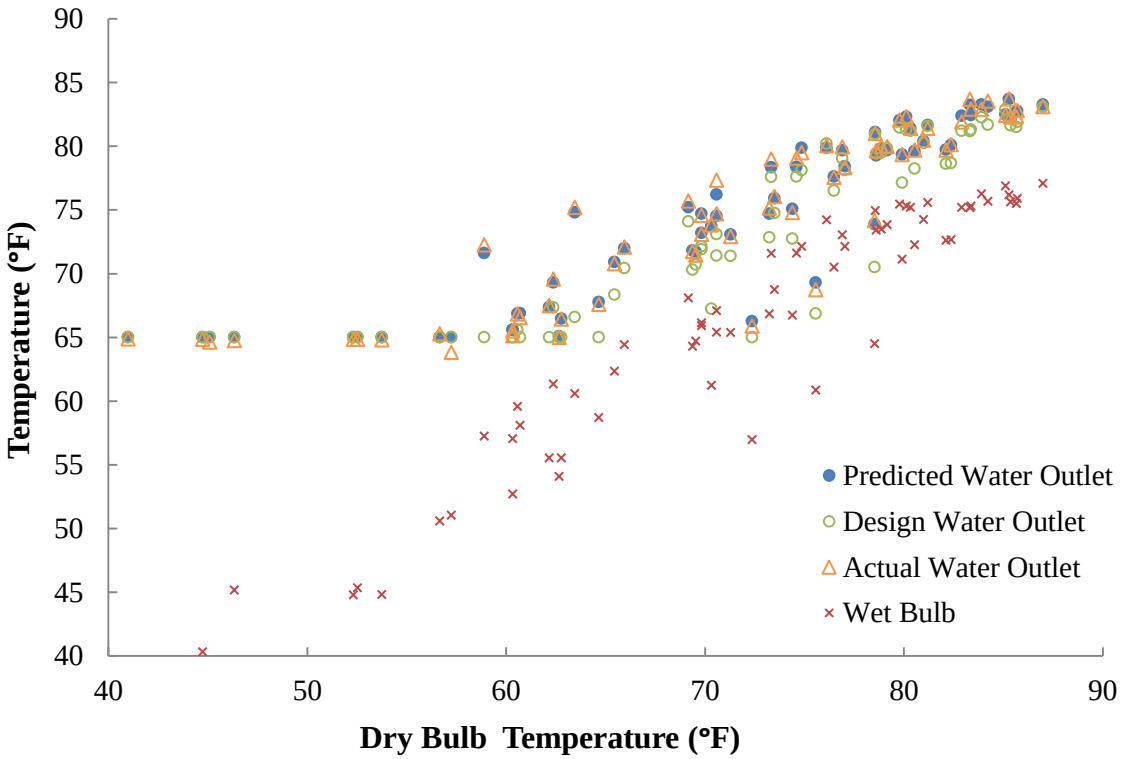

Figure 3.32 Comparison between Predicted, Design and Measured Water Outlet and Wet-Bulb Temperatures

Zhang et.al (2011) pointed out in their work that the optimal cooling tower approach setpoint reset schedule can be approximated with a 4-parameter change-point model. This kind of schedule can help achieve significant energy savings compared with the scenario with a constant cooling tower condenser water leaving temperature (CWLT). Their further simulations show that chiller part load ratio (PLR), defined as the actual cooling effect produced by the chiller divided by the maximum cooling effect available, chilled water leaving temperature, and the climate have minor effects on the coefficients

of the optimal condenser water leaving temperature reset schedule. The approach setpoint reset schedule with two straight lines is also applicative for the cooling tower in this work as plotted in Figure 3.33. Thus, when the chiller PLR is 80%, and the chilled water leaving temperature is about 42.0 °F, if the slight changes of PLR and the chilled water leaving temperature are neglected, the reset schedule of the cooling tower CWLT can be expressed as the following equations instead of operating the cooling tower with a constant approach temperature (T_{app}) at 6°F.

$$T_{app} = -0.93T_{wb}+62.2 \text{ if } T_{wb} \leq 57°F \quad (3.47)$$

$$T_{app} = -0.12\ T_{wb}\ +15.95 \text{ if } T_{wb} > 57°F \quad (3.48)$$

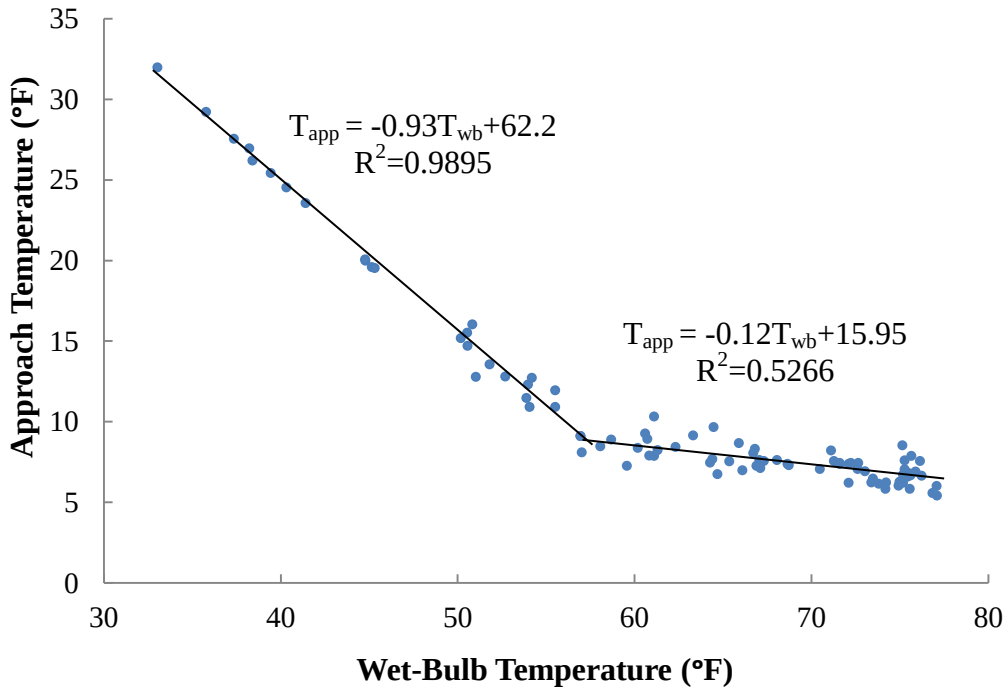

Figure 3.33 CT Approach Temperatures versus Ambient Wet-Bulb Temperatures

3.10 Performance Curve for the Cooling Tower Fan

The fan consumes electric energy to draw or force air through the tower and then to lower the water temperature. As more electricity is consumed, a lower approach temperature can be achieved. The nominal power of the target fan is 15hp. Based on the relationship of air flowrate vs. VFD speed (Figure 3.29) and the fan power consumption curve to be given in Section 3.10.1, the Braun model helps to obtain the power consumption curve for a range of operating condition. More details for the process will be included in later sections.

3.10.1 Regression for Fan Power Consumption Curve

Measurements were conducted to obtain results of the fan power consumption at different VFD speeds. Table 3.8 lists the values of the measurements.

Table 3.8 Fan Power Consumption Measurements

VFD Speed (%)	25	50	60	70	80	90	100
Power (kW)	1.058	2.352	3.046	3.782	4.768	5.692	6.726

The regression of the above measurements yields the following equation for the fan power consumption as a function of the VFD speed:

$$\text{Fan Power (kW)} = -0.0000014*(\text{VFD Speed})^3+0.00073*(\text{VFD Speed})^2 +0.0021*(\text{VFD Speed})+0.57 \quad (3.49)$$

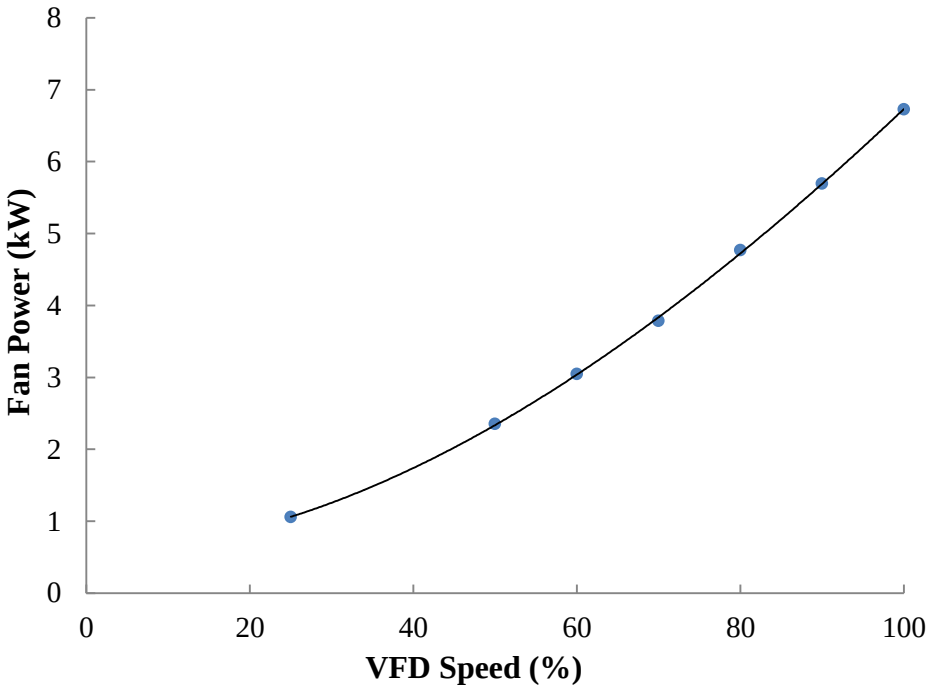

Figure 3.34 Fan Power Consumption Curve

3.10.2 kW and kW/Ton Curves for the Fan

Equation (3.46) and Equation (3.49) give the relationships between the air flowrate (CFM) and the fan power consumption (kW) and VFD speed. When the inlet and ambient conditions are fixed at a given set of values, the air flowrate can be varied in the Braun model to match the measured cooling tower water exiting temperature. Once the air flowrate is known, the corresponding VFD speed can be obtained by Equation (3.46), and then the fan power consumption can be predicted by Equation (3.49). To estimate the fan power in kW/Ton, the design condition and the NTU obtained from Section 3.8 are applied. All the input values for the Braun model are listed in Table 3.9.

Table 3.9 Inputs for Fan Power Calculation

Inputs	Water Flowrate (lb/min)	Dry-Bulb (°F)	Wet-Bulb (°F)	Water Inlet Temp (°F)	NTU
Value	6317	85	75	87	1.42

In Section 3.4, the Braun model has already been verified to be able to predict the water outlet temperatures (T_{wo}) with high accuracy. Equation (3.50) presents the relationship between T_{wo} and other parameters in the Braun model. More detailed equations and explanations about the T_{wo} calculation can be found in Section 3.3 and appendix A. Furthermore, the fan power (kW) and the efficiency (kW/ton) can be obtained using the Equations (3.50)-(3.56) developed in the Braun model.

$$T_{wo} = \frac{\dot{m}_{w,i}(T_{w,i}-T_{ref})c_{pw}-\dot{m}_a(h_{a,o}-h_{a,i})}{\dot{m}_{w,o}c_{pw}} = g(\dot{m}_w, \dot{m}_a, T_{wi}T_{ai}, T_{WB}, NTU) \quad (3.50)$$

$$T_{app} = T_{wo} - T_{WB} \quad (3.51)$$

The relationship between T_{app} and $\dot{m}_a$ can be built when other parameters are given:

$$T_{app} = f(\dot{m}_w, \dot{m}_a, T_{wi}T_{ai}, T_{WB}, NTU) \quad (3.52)$$

$$\dot{m}_a = f(\dot{m}_w, T_{app}, T_{wi}T_{ai}, T_{WB}, NTU) \quad (3.53)$$

Insert Equations (3.46), (3.53) to Equation (3.49), and then the relationship between fan power and VFD speed becomes:

$$P_{fan} = -0.0000014 * (VFD\%)^3 + 0.00073 * (VFD\%)^2 + 0.0021 * (\text{VFD}\%) + 0.57$$

$$= -0.0000014 * \left(\frac{\dot{m}_a + 1092.6}{67.369}\right)^3 + 0.00073 * \left(\frac{\dot{m}_a + 1092.6}{67.369}\right)^2 + 0.0021 * \left(\frac{\dot{m}_a + 1092.6}{67.369}\right) + 0.57$$

$$= f_1(\dot{m}_w, T_{app}, T_{wi}T_{ai}, T_{WB}, NTU) \quad (3.54)$$

The cooling capacity $Q = \dot{m}_w * (T_{wi} - T_{wo})$ (3.55)

$$\varepsilon_{fan} = \frac{P_{fan}}{Q}$$

$$= \frac{\left[-0.0000014 * \left(\frac{\dot{m}_a + 1092.6}{67.369}\right)^3 + 0.00073 * \left(\frac{\dot{m}_a + 1092.6}{67.369}\right)^2 + 0.0021 * \left(\frac{\dot{m}_a + 1092.6}{67.369}\right) + 0.57\right]}{[\dot{m}_w * (T_{wi} - T_{wo})]}$$

$$= f_2(\dot{m}_w, T_{app}, T_{wi}T_{ai}, T_{WB}, NTU) \quad (3.56)$$

If the input values of $\dot{m}_w, T_{wi}T_{ai}, T_{WB}$ and NTU are used in Equations (3.50)-(3.56), this equation set can be solved and the functions that relate the approach temperature to the fan power (kW) and efficiency (kW/ton) can be obtained. The Braun model developed in EES makes it easier to gain the functions (f_1 and f_2). Equations (3.57)-(3.62) were obtained after applying the inputs in Table 3.9 to the model.

Figure 3.35 plots curves of the fan power consumption, as total kW and as kW/ton, versus the approach temperature for air flowrates varying from 1000 lb/min to 6000 lb/min as suggested in Section 3.8. The fan power consumptions at three different wet-bulb temperatures are also shown.

Following are equations for these curves. They are mainly applied at approach temperatures lower than 20 °F:

When the wet-bulb temperature is 70 °F,

$$Fan\ Power\ (kW)=-0.004*(T_{app})^3+0.207*(T_{app})^2-3.971*(T_{app})+27.336 \quad (3.57)$$

$$Fan\ Power\ (kW/ton)=-0.00004*(T_{app})^3-0.0009*(T_{app})^2+0.0057*(T_{app})+0.0181 \quad (3.58)$$

When the wet-bulb temperature is 75 °F,

$$Fan\ Power\ (kW)=-0.011*(T_{app})^3+0.399*(T_{app})^2-5.256*(T_{app})+25.210 \quad (3.59)$$

$$Fan\ Power\ (kW/ton)=-0.0001*(T_{app})^3-0.0019*(T_{app})^2+0.0065*(T_{app})+0.0336 \quad (3.60)$$

When the wet-bulb temperature is 80 °F,

$$Fan\ Power\ (kW)=-0.055*(T_{app})^3+1.127*(T_{app})^2-8.408*(T_{app})+23.201 \quad (3.61)$$

$$Fan\ Power\ (kW/ton)=-0.0008*(T_{app})^3-0.0065*(T_{app})^2+0.0081*(T_{app})+0.0664 \quad (3.62)$$

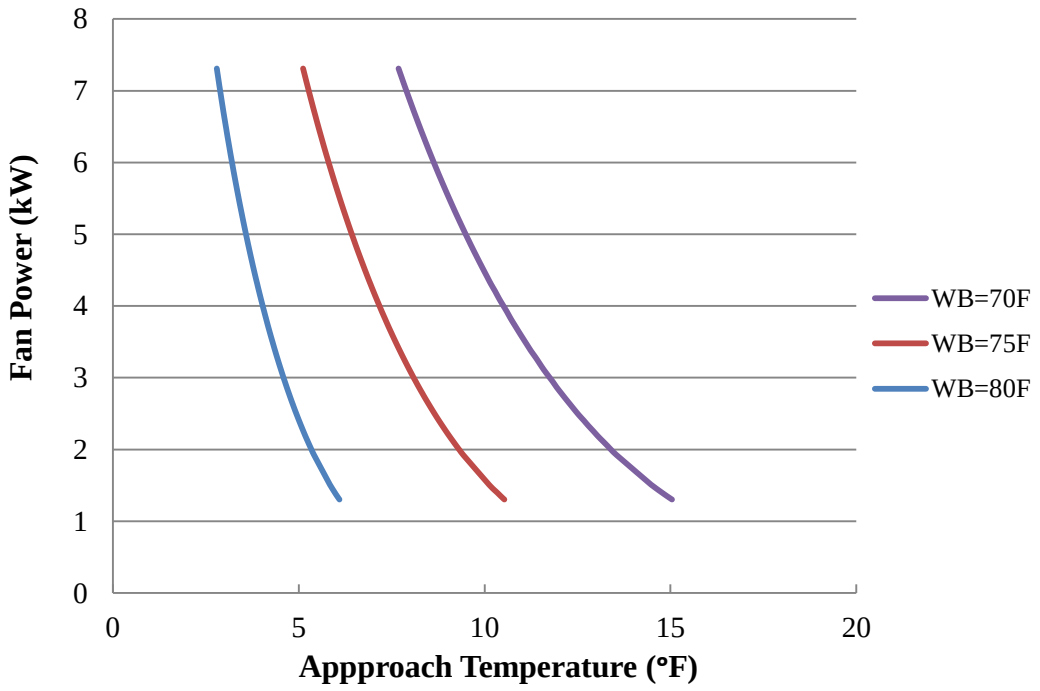

(a)

Figure 3.35 Fan Power Consumption vs. Approach Temperature

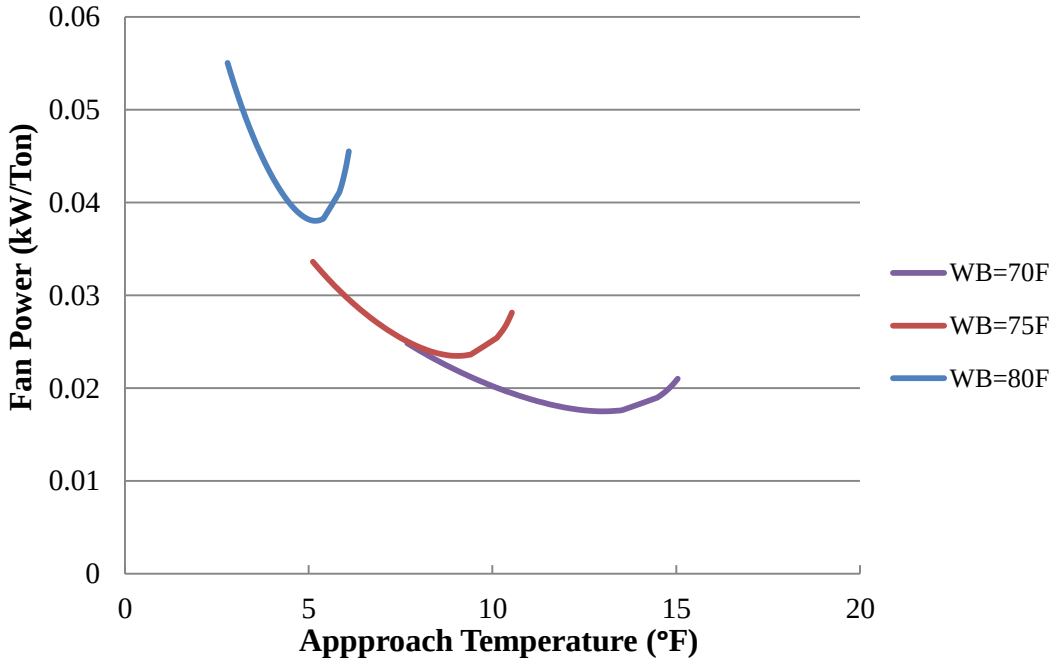

(b)

Figure 3.35 Continued

3.10.3 Comparison between Measured and Simulated Fan Power Consumption

Equations (3.57) to (3.62) give examples of cooling tower fan power calculation using the approach temperature as the only variable, under the operation condition specified in Table 3.9. At off-design operating conditions, the fan power can be also calculated using the same method. Figure 3.36 below plots the comparison of measured and simulated fan power consumption data.

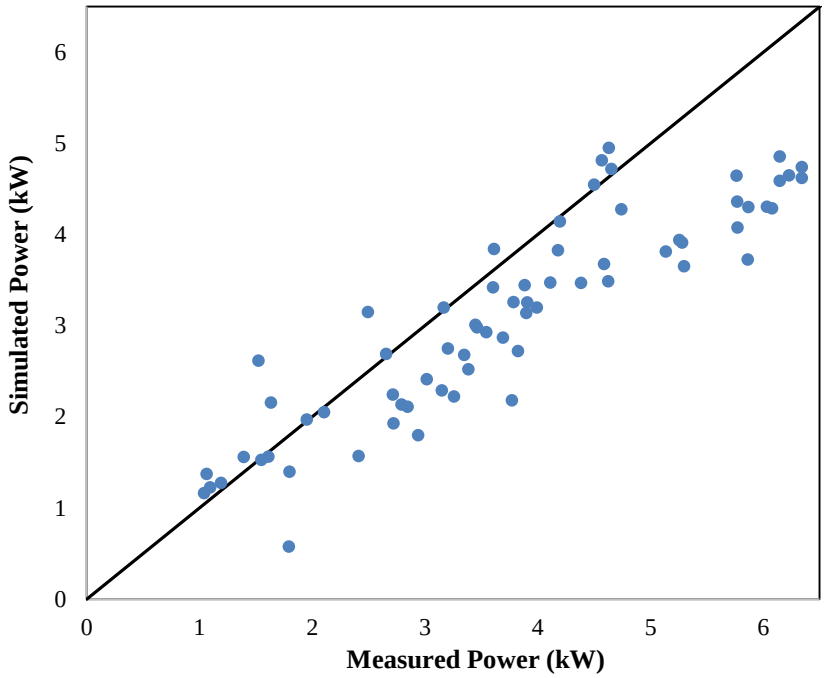

Figure 3.36 Comparisons between Measured and Simulated Fan Power

The simulated power is lower than the measured power in general, especially in the power range from 5kW to 6kW. To further illustrate the simulation results, Figure 3.37 shows the power consumption data versus the dry-bulb temperatures. The main separation occurs at dry-bulb temperatures around 80 °F and higher. The cooling tower model doesn't consider the possible fan efficiency decrease at high VFD speed; this may be one of the reasons for the deviation.

The impact of the simulated fan power deviation on the whole system will be analyzed further in Chapters IV and V.

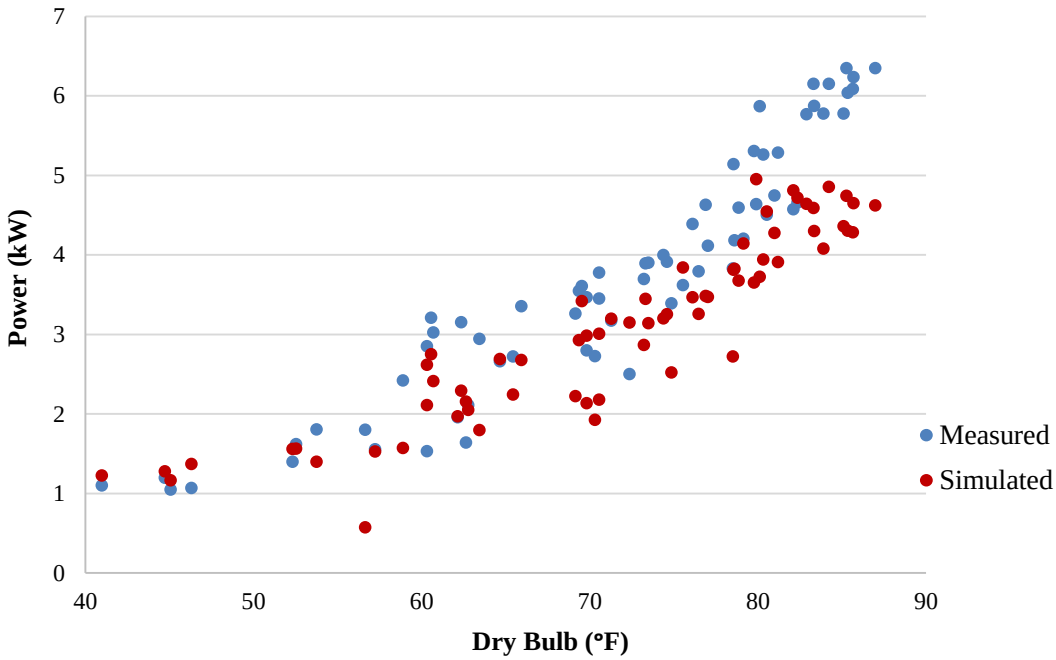

Figure 3.37 Measured and Simulated Fan Power vs. Dry-Bulb Temperatures

CHAPTER IV

CHILLER MODEL DEVELOPMENT

The chiller is another essential component of the cooling system. Consisting of an evaporater, a compressor, a condenser, and valves and pipes, it is used to remove heat from a liquid via a refrigeration cycle. Figure 4.1 shows the energy balance within the chiller control volume. The heat is transferred from the evaporator side to the condenser side. There are also heat leaks from the compressor, condenser and evaporator, which are neglected in this study.

This chapter describes the modeling development of the chiller. An electric chiller model based on condenser entering temperature is utilized. The measurements of the chiller side are employed to adjust the coefficients to match the actual performance curves for the target chiller.

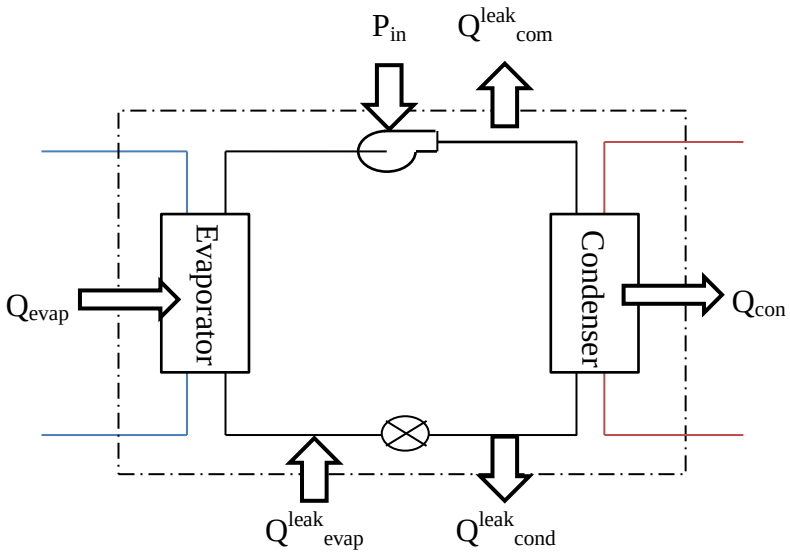

Figure 4.1 Chiller Energy Balance Diagram within A Control Volume

The chillers modeled in this thesis are York® Codepak™ Liquid Chilling Systems with a unit model number of *YT E1 E3 C1-CK F S* and serial number of *YCYM 688122*. These chillers were installed in 1990. They have been and are serving well with motors of 270 hp and with reference capacities of 220 tons. The rated kW/TON is about 0.70 at full load and full output. The picture below shows a general view of the chiller system.

Figure 4.2 A View of the Chiller System

4.1 EnergyPlus Chiller Model

EnergyPlus includes an electric chiller model based on the condenser entering temperature, which is also the cooling tower exiting water temperature. This model is based on the compression chiller model in the DOE-2.1 building energy simulation

program. A reference condition should be defined for the specific cooling tower. The chiller model uses three performance curves for cooling capacity and efficiency to determine the chiller operation in off-reference conditions. The three curves are:

- Cooling Capacity Function of Temperature Curve
- Energy Input to Cooling Output Ratio Function of Temperature Curve
- Energy Input to Cooling Output Ratio Function of Part Load Ratio Curve

These curves are important indicators of the chiller system performance. Meanwhile, they make the dominant variables clearer when the system curves are analyzed under different operating conditions. This model helps to avoid the analysis of unnecessary parameters.

Theoretically, these three curves should be defined for each chiller model in the design phase and provided by manufacturer. However, all the information relevant to the performance curves was lost because the chillers in this thesis are so old that they are no longer produced or sold. As a result, the default chiller models in EnergyPlus are referred as the baseline models to obtain the performance curves used in this thesis.

EnergyPlus includes 162 chiller models, with reference conditions provided. They are the empirical models from the DOE-2 building energy simulation program. Chiller performance at off-reference conditions can be modeled using the above mentioned curves. These three performance curves will be introduced in detail in Sections 4.2 to 4.4.

Based on the reference capacity (220 tons) and reference kW/ton (0.7) of the chillers in this work, the *ElectricEIRChiller York YT 1051kW/5.05COP/Vanes* model

was selected to model the chillers at the Connally Building. Table 4.1 lists the reference conditions of the selected chiller model.

Table 4.1 Reference Conditions of the Chiller Model

Field	Units	Object
Name		ElectricEIRChiller York YT 1051kW/5.05COP/Vanes
Reference Capacity	W	1051400
Reference COP	W/W	5.05
Reference Leaving Chilled Water Temperature	°C	6.67
Reference Entering Condenser Fluid Temperature	°C	29.44
Reference Chilled Water Flow rate	m^3/s	0.04527
Reference Condenser Fluid Flow Rate	m^3/s	0.05659
Minimum Part Load Ratio		0.2
Maximum Part Load Ratio		1.01
Optimum Part Load Ratio		1
Minimum Unloading Ratio		0.2
Condenser Type		Water-Cooled

4.2 Cooling Capacity Ratio as a Function of Temperature Curve

The cooling capacity function of temperature curve is biquadratic and describes the cooling capacity performance with two independent variables: the leaving chilled water temperature and the entering condenser fluid temperature. The output of this curve can be multiplied by the reference capacity to give the full-load cooling capacity at specific temperature operating conditions. When the temperature equals the reference temperature, the output should have a value of 1.0.

$$ChillerCapFTemp = a + b(T_{cw,l}) + c(T_{cw,l})^2 + d(T_{cond,e}) + e(T_{cond,e})^2 + f(T_{cw,l})(T_{cond,e}) \quad (4.1)$$

where $ChillerCapFTemp$ is the cooling capacity factor, defined as the actual cooling capacity divided by the full-load cooling capacity, $T_{cw,l}$ is the leaving chilled water temperature and $T_{cond,e}$ is the entering condenser fluid temperature (also cooling tower exiting temperature).

The cooling capacity curve as a function of temperature for the selected chiller model is defined as shown in Table 4.2. The corresponding curve is plotted in Figure 4.3. In the EnergyPlus manual, the minimum value of the condenser entering water ($T_{cond,e}$) was 52°F (11.11°C). However, 52°F seems too low for these old chillers. York has been contacted for the minimum $T_{cond,e}$ and has not responded yet. In additional, the towers are operated with minimum tower water leaving temperature (also $T_{cond,e}$) of 65 °F. Hence, to describe the actual operation of the chiller system, 65°F, instead of 52 °F given

by the EnergyPlus manual, will be utilized for subsequent simulation and optimization calculations.

Table 4.2 Cooling Capacity Ratio Curve Coefficients

Coefficient a – Constant	0.9482157
Coefficient b – $T_{cw,l}$	0.03306737
Coefficient c – $T_{cw,l}^2$	-6.45007E-05
Coefficient d – $T_{cond,e}$	-0.003756522
Coefficient e – $T_{cond,e}^2$	-6.50167E-05
Coefficient f – $T_{cw,l} * T_{cond,e}$	-2.518E-15
Minimum Value of $T_{cw,l}$ (°C)	4.44
Maximum Value of $T_{cw,l}$ (°C)	8.89
Minimum Value of $T_{cond,e}$ (°C)	18.33
Maximum Value of $T_{cond,e}$ (°C)	35

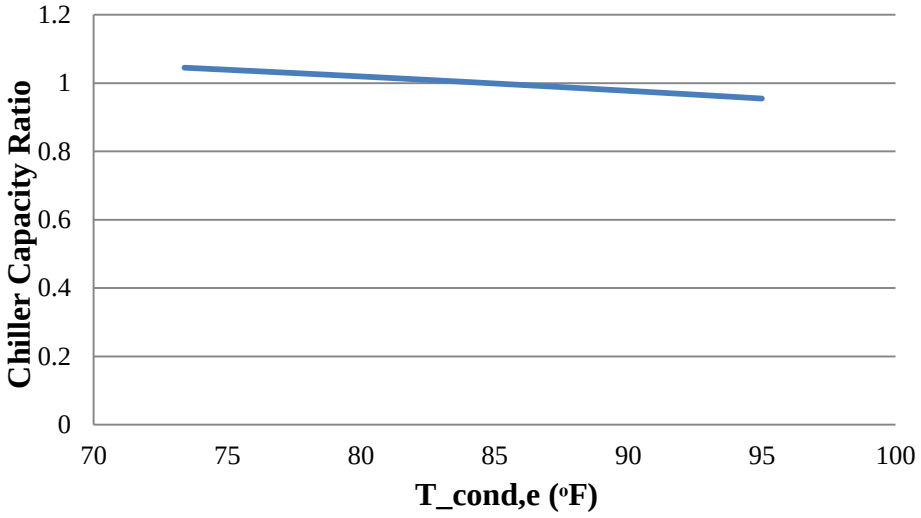

Figure 4.3 Chiller Capacity Ratio Curve

4.3 Energy Input to Cooling Output Ratio as a Function of Temperature Curve

This curve is also a biquadratic performance curve, which describes the energy input to cooling output ratio (EIR), calculated as the energy input power divided by the chiller's cooling capacity, as a function of the leaving chilled water temperature and the entering condenser fluid temperature. The output of this curve can be multiplied by the reference EIR to give the full-load EIR at specific temperature operating conditions. Similarly, the output should have a value of 1.0 at the reference temperature and flowrate specified by the user.

$$ChillerEIRFTemp = a + b(T_{cw,l}) + c(T_{cw,l})^2 + d(T_{cond,e}) + e(T_{cond,e})^2 + f(T_{cw,l})(T_{cond,e}) \quad (4.2)$$

where the $ChillerEIRFTemp$ is energy input to cooling output factor.

Table 4.3 below defines the coefficients of Equation (4.2).

Table 4.3 Energy Input to Cooling Output Ratio Curve Coefficients

Coefficient a – Constant	0.2574181
Coefficient b – $T_{cw,l}$	-0.005530317
Coefficient c – $T_{cw,l}^2$	0.001209907
Coefficient d – $T_{cond,e}$	0.009122333
Coefficient e – $T_{cond,e}^2$	0.00109237
Coefficient f – $T_{cw,l} * T_{cond,e}$	-0.001469958
Minimum Value of $T_{cw,l}$ (°C)	4.44
Maximum Value of $T_{cw,l}$ (°C)	8.89
Minimum Value of $T_{cond,e}$ (°C)	18.33
Maximum Value of $T_{cond,e}$ (°C)	35

The corresponding curve is plotted in Figure 4.4.

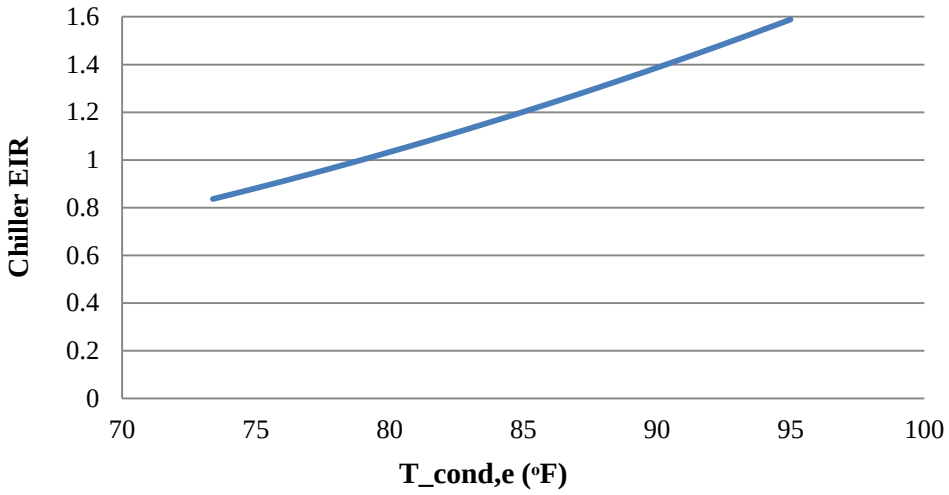

Figure 4.4 Energy Input to Cooling Output Ratio Curve as a Function of Temperature

4.4 Energy Input to Cooling Output Ratio as a Function of Part Load Ratio Curve

The energy input to cooling output ratio as a function of part-load curve is a quadratic performance curve that shows the factor dependent on the part-load ratio. The part-load ratio is the actual cooling load divided by the chiller's available cooling capacity. The output of the curve is multiplied by the reference EIR and $ChillerEIRFTemp$ to give the EIR at the specific temperature and part-load ratio at which the chiller is operating.

$$ChillerEIRFPLR = a + b(PLR) + c(PLR)^2$$

$$= P_{Chiller}/[P_{ref}(ChillerCapFTemp)(ChillerEIRFTemp) \quad (4.3)$$

$$PLR = \frac{Actual\ Cooling\ Load}{Chiller's\ Available\ Cooling\ Capacity} \quad (4.4)$$

where $ChillerEIRFPLR$ is the energy input to cooling output factor, PLR is part-load ratio, defined by Equation (4.4), $P_{Chiller}$ is the chiller power at specific PLR, and P_{ref} is the reference chiller power, which is defined as $\dot{Q}_{ref}/COP_{ref}$.

Table 4.4 below defines the coefficients of Equation (4.3). The corresponding curve is plotted in Figure 4.5.

Table 4.4 Energy Input to Cooling Output Ratio Curve Coefficients

Coefficient a – Constant	0.4904181
Coefficient b – PLR	-0.005530317
Coefficient c – PLR^2	0.001209907
Minimum Value of PLR	0.2
Maximum Value of PLR	1.01

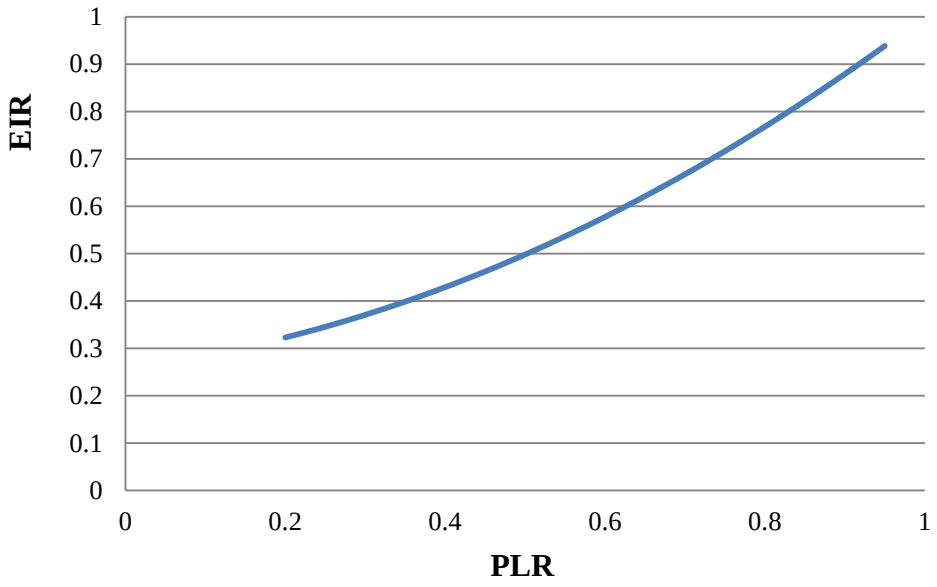

Figure 4.5 Energy Input to Cooling Output Ratio Curve as a Function of PLR

4.5 The Input Power Curves for the Chiller

The input power of the chiller is generally the most significant energy use by a cooling system. The input power curves of the chillers can be generated based on the figures and curve formulas in Sections 4.2 to 4.4.

The following Equation (4.5) is utilized as a guiding formula for the chiller input power modeling:

$$P_{Chiller} = \frac{\dot{Q}_{ref}}{COP_{ref}}(ChillerCapFTemp)(ChillerEIRFTemp)(ChillerEIRFPLR) = \frac{\dot{Q}_{ref}}{COP_{ref}}\Big[a + b(T_{cw,l}) + c(T_{cw,l})^2 + d(T_{cond,e}) + e(T_{cond,e})^2 + f(T_{cw,l})(T_{cond,e})\Big]_{ChillerCapFTemp} * \Big[a + b(T_{cw,l}) + c(T_{cw,l})^2 + d(T_{cond,e}) + e(T_{cond,e})^2 + f(T_{cw,l})(T_{cond,e})\Big]_{ChillerEIRFTemp} * [a + b(PLR) + c(PLR)^2]_{ChillerEIRFPLR} \quad (4.5)$$

In Equation (4.5) above, $\dot{Q}_{ref} = 220\ tons$ and $COP_{ref} = 1.43\ tons/kW$. Utilizing the equations and curves in former sections, when the $T_{cw,l}$ is 42 °F and the PLR is at 80%, the chiller input power is:

$$P_{Chiller} = \frac{\dot{Q}_{ref}}{COP_{ref}}(ChillerCapFTemp)(ChillerEIRFTemp)(ChillerEIRFPLR)$$

$$= \frac{220\ ton}{1.43\ ton/kW} * \Big[-0.00006501672 * (T_{cond,e})^2 - 0.003756522 * (T_{cond,e}) + 1.1659\Big]|_{Tcw,l=42F} * \Big[0.0005923591 * (T_{cond,e})^2 - 0.000682287 * (T_{cond,e}) + 0.507358317\Big]|_{Tcw,l=42F} * 0.767928|_{PLR=80\%} \quad (4.6)$$

The chiller power consumption can be plotted versus entering condenser water temperature as shown in Figure 4.6.

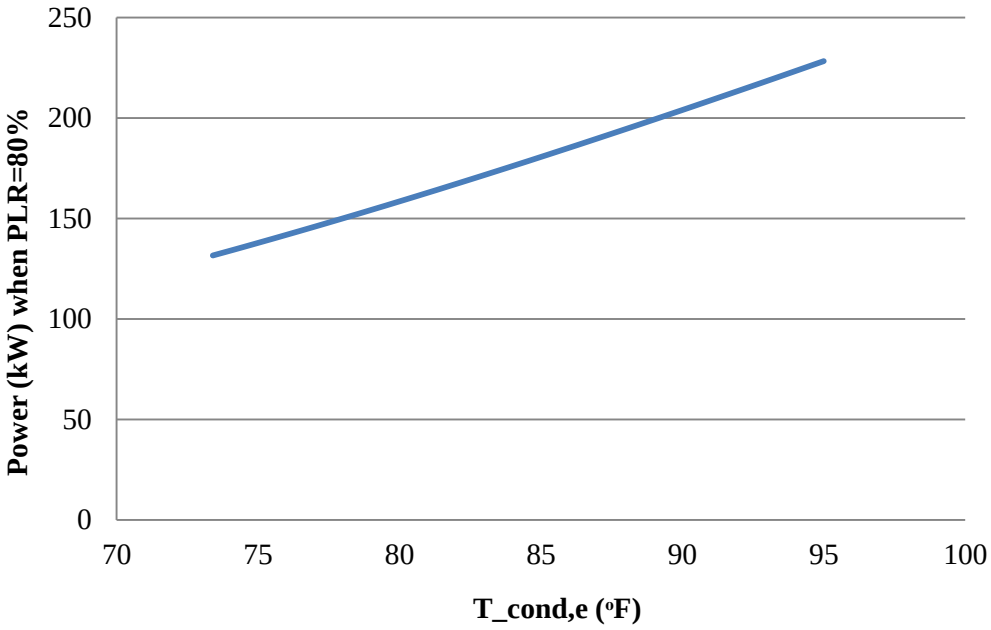

Figure 4.6 Chiller Power Curve as a Function of $T_{cond,e}$

The measurements of average daily data used in Section 3.8 (Figure 3.26) for the energy balance calculation are still utilized to evaluate the coefficients in Equations (4.1) – (4.3) and to further calibrate the above mentioned performance curves. The detailed data for these 98 days are attached in Appendix I. Figure 4.7 includes the measurements for the year 2015 without any subdivision.

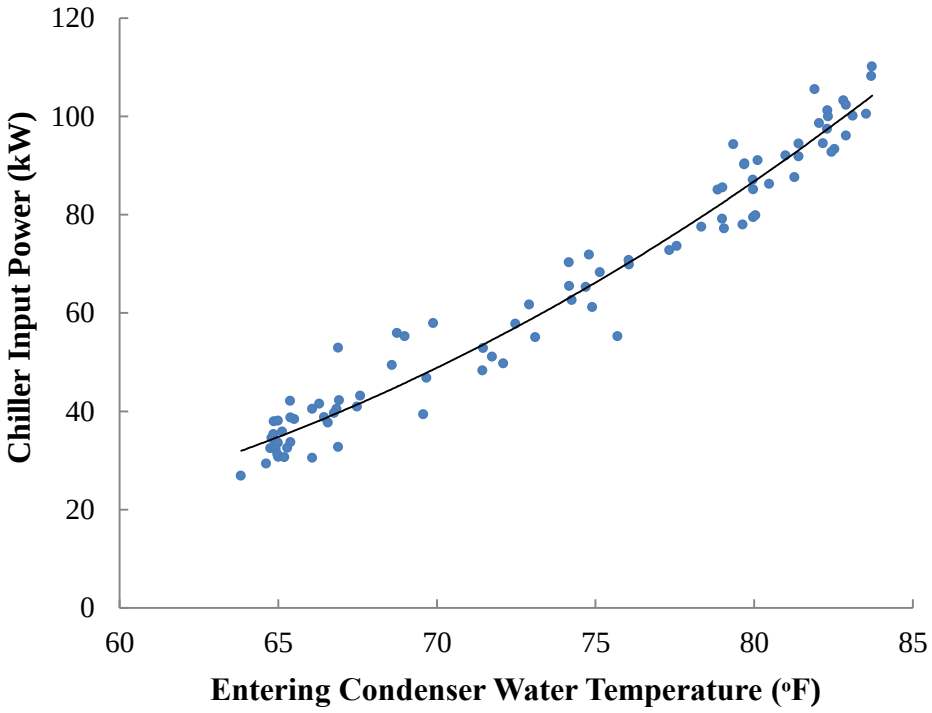

Figure 4.7 Chiller Input Power Measurements for Year 2015

To calculate the simulated chiller input power using the performance curves in a real case, measurements of $T_{ch,l}$, $T_{cond,e}$ and Q_{evap} are utilized, where $T_{ch,l}$ is the chiller leaving water temperature and Q_{evap} is the chiller load.

Take the measurements on 01/22/2015 for example; the inputs and some of the results are listed in Table 4.5. Substitute the values of $T_{ch,l}$ and $T_{cond,e}$ in Equations (4.1) and (4.2), and then the $ChillerCapFTemp$ and $ChillerEIRFTemp$ can be easily obtained (see Table 4.5).

Table 4.5 Measurements on 01/22/2015 for Chiller Power Calculation

Parameters	Value
$T_{ch,l}$ (°F)	42.65
$T_{cond,e}$ (°F)	64.75
Q_{evap} (ton)	42.87
$ChillerCapFTemp$	1.051699
$ChillerEIRFTemp$	0.6364773

The calculation of $ChillerEIRFPLR$ requires the actual value of PLR first. If the chiller's available cooling capacity Q_{avail} is defined as the full-load capacity at the given operating condition, then Q_{avail} can be calculated by following equation:

$$Q_{avail} = Q_{ref} * \ ChillerCapFTemp = 220\ tons * 1.051699 = 231.3739 \text{ tons} \quad (4.7)$$

Further,

$$PLR = \frac{Actual\ Cooling\ Load}{Chiller's\ Available\ Cooling\ Capacity} = \frac{42.871 \text{ tons}}{231.3739 \text{ tons}} = 0.18529 \quad (4.8)$$

$$ChillerEIRFPLR = a + b(PLR) + c(PLR)^2 = 0.4904181 - 0.005530317 * 0.18529 + 0.001209907 * 0.18529^2 = 0.316941 \quad (4.9)$$

The chiller's simulated power should be:

$$P_{Chiller} = \frac{\dot{Q}_{ref}}{COP_{ref}}(ChillerCapFTemp)(ChillerEIRFTemp)(ChillerEIRFPLR)$$

$$= \frac{220\ tons}{1.43\ ton/kW} * 1.051699 * 0.6364773 * 0.316941 = 32.67185\ kW \quad (4.10)$$

Equations (4.7)-(4.10) illustrate the detailed calculation process for the chiller power. Repeat this procedure for all the other measurements, and then all the

simulated chiller power values can be obtained. Figures 4.8 and 4.9 plot the comparison of the simulated and measured chiller power for the sampled days. The R^2 value in Figure 4.8 is 0.987, which suggests that the simulated power values will provide a good prediction of the chillers' performance.

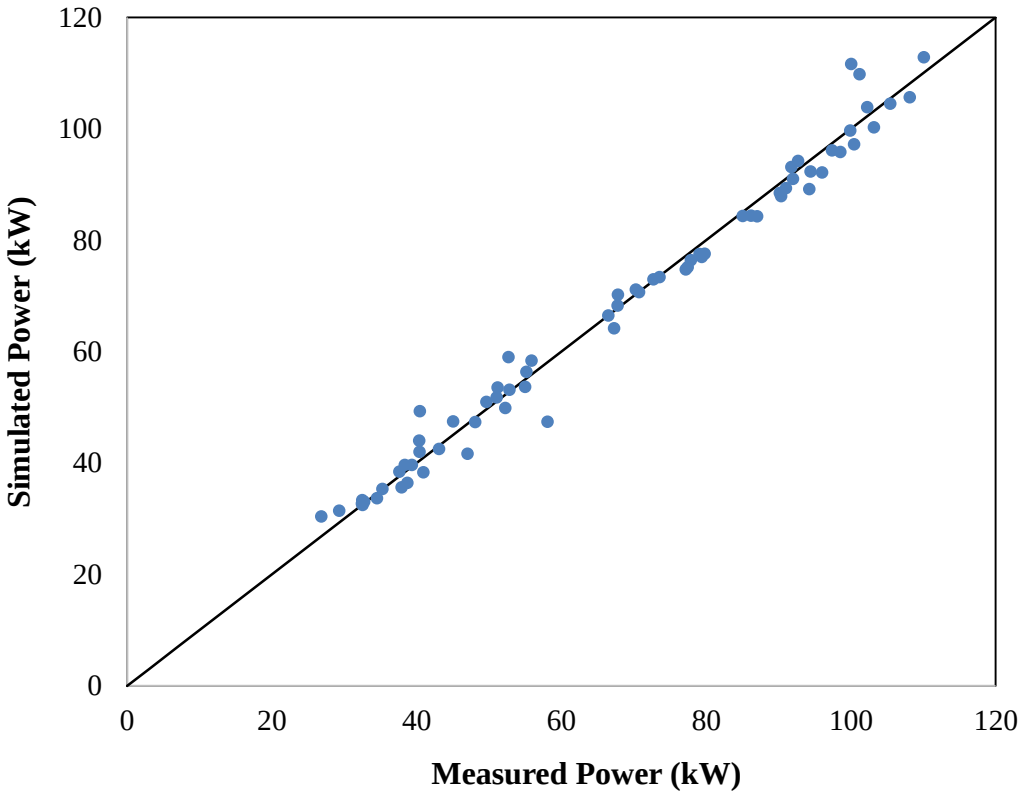

Figure 4.8 Comparison of Simulated and Measured Chiller Input Power

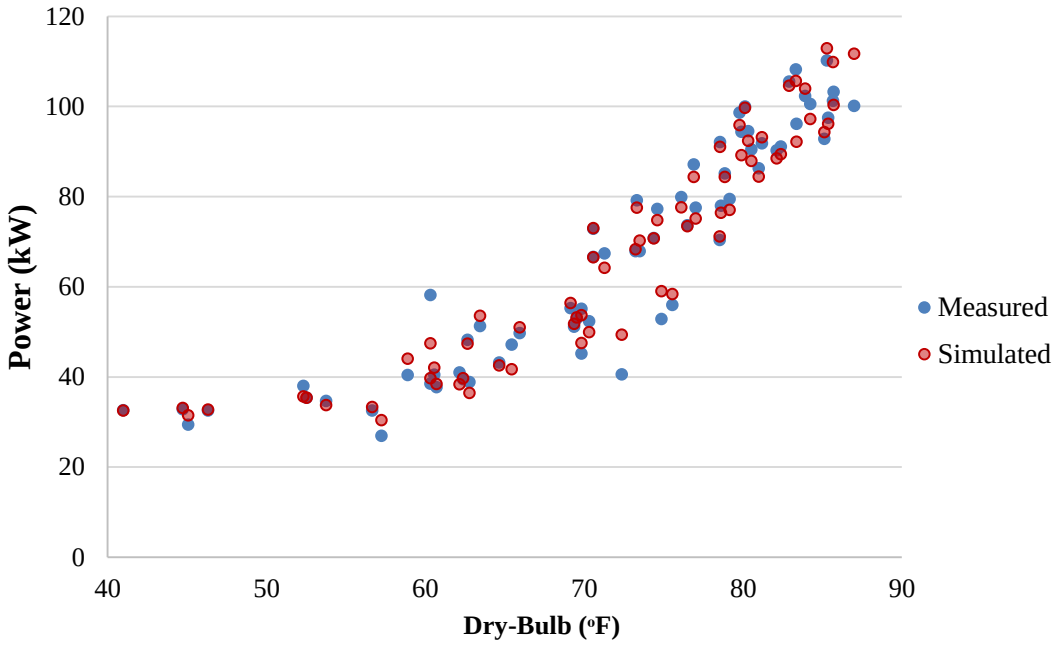

Figure 4.9 Comparison of Simulated and Measured Chiller Input Power vs. Dry-Bulb Temperature

4.6 Chiller Water Pump Power

The sum of the water pump power, the chiller input electric power, and the cooling tower fan power gives the total power consumption of the cooling system. Figure 4.10 shows the water pump power consumption throughout year 2015. The pump power consumption is relatively constant with an average consumption of 7.19 kW. The maximum and minimum power consumption is 7.50 kW and 7.05 kW respectively, which results in a maximum deviation from the average value of 4.31%. All the deviations for year 2015, with an average value of 0.011, are plotted in Figure 4.11.

The relatively constant consumption under diverse ambient conditions indicates that the water pump power can be laid aside and neglected when optimizing the total

power consumption of the cooling system. Thus, only the cooling tower fan power and the chiller input electric power will be considered in subsequent work.

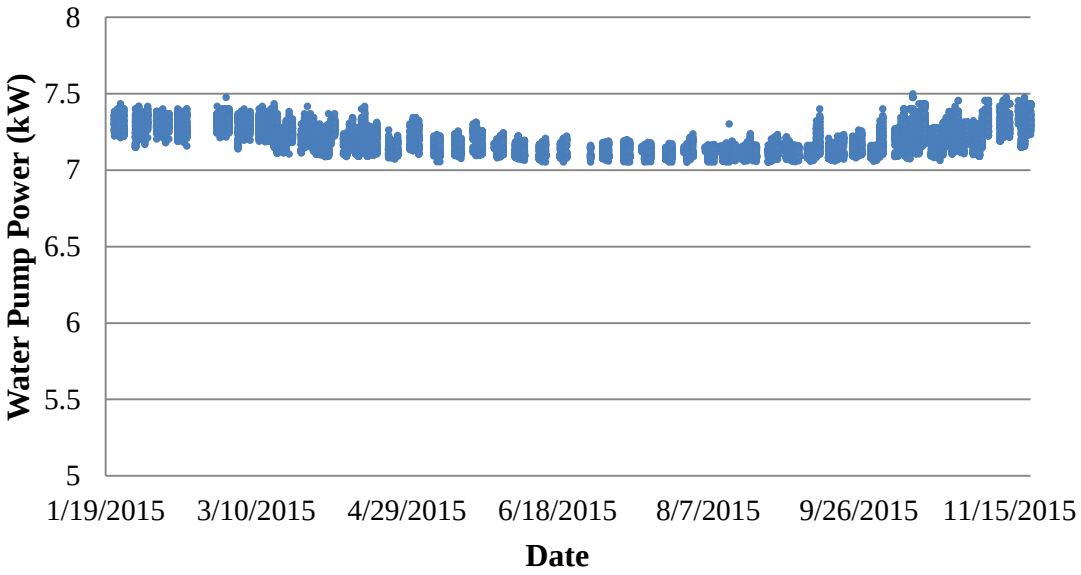

Figure 4.10 Water Pump Power Consumption for Year 2015

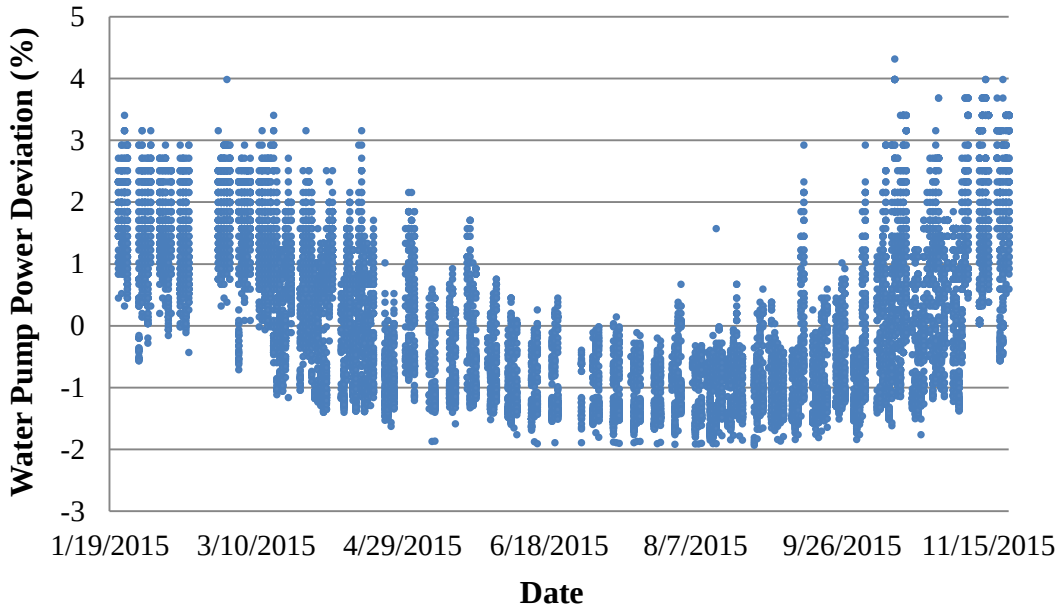

Figure 4.11 Water Pump Power Deviations for Year 2015

CHAPTER V

METHODOLOGIES FOR OPTIMAL CONTROL

The trade-off of the cooling system should consider both the chiller power and cooling tower fan power. Chapter III and Chapter IV have developed the performance curves of the chiller and the cooling tower fan respectively. This chapter integrates the individual models for each component and analyzes the combined model and curves. The sum of the chiller power and the cooling tower fan power can be minimized by using the Braun model and the performance curves described in previous chapters.

By adding the performance curves of the chiller and the cooling tower fan, the dependence of the total energy consumption on the condenser leaving water temperature and the approach temperature can be obtained. The lowest total energy consumption reveals the optimal operation point.

5.1 Baseline for Total Power Optimization

Chapters III and IV have elaborated the models and consequent figures for the simulated power consumption of the fans and the chillers under the stated conditions. By following the steps illustrated in Chapters III and IV, the power consumption (kW) for the individual components can be obtained. Overall, the modeling and simulation process for the whole system in this chapter also follow the same rules used in the previous chapters. However, when the cooling system is considered as a cohesive whole, more variables and relevant calculations should be taken into account.

To show the total power calculation more clearly, again, the day 01/22/2015 is used as an example. The operating condition and the measurements are listed in Table 5.1.

Table 5.1 Operating Condition and Measurements on 01/22/2015

Parameters	Value
Dry-Bulb - T_{db}(°F)	46.33
Wet-Bulb - T_{wb} (°F)	45.17
Chilled Water Leaving Temp - $T_{ch,l}$ (°F)	42.65
Condenser Water Entering Temp - $T_{cond,e}$ (°F)	64.75
Approach Temp - T_{app} (°F)	19.59
Chiller Load - Q_{evap} (ton)	42.87
Water Flowrate - $\dot{m}_w$ (lb/min)	6690

Based on the energy balance equation:

$$Q_{evap} + P_{Chiller} = Q_{CoolingTower} = \left(T_{cond,l} - T_{cond,e}\right) * \dot{m}_w * c_{pw} \tag{5.1}$$

$$T_{cond,l} = \frac{Q_{evap}+P_{Chiller}}{\dot{m}_w * c_{pw}} + T_{cond,e}$$

$$= \frac{(32.67185+42.871)tons}{6690\ lb/min * 1Btu/(lbF)} * \frac{200Btu/min}{ton} = 66.321\ °F \tag{5.2}$$

When modeling the cooling tower using the Braun model, the value of $T_{cond,l}$ obtained from Equation (5.2), instead of the measured data, should be used as the input

for $T_{w,i}$. For all the other inputs, use the measurements in Table 5.1. Then the Braun model will give the corresponding fan power. In this case, the fan power is 1.3684 kW.

The total power is:

$$P_{tot} = P_{Chiller} + P_{fan} = 32.6719\ tons + 1.3684\ tons = 34.0403\ tons \quad (5.2)$$

To reduce the calculation burden, 68 days was selected out from the 98 sampled days used in Chapter IV for optimization calculation. After repeating the calculation for all the 68 sampled days, the simulated total power for these days can be plotted and compared with the measured power consumption data as shown in Figure 5.2 and 5.3.

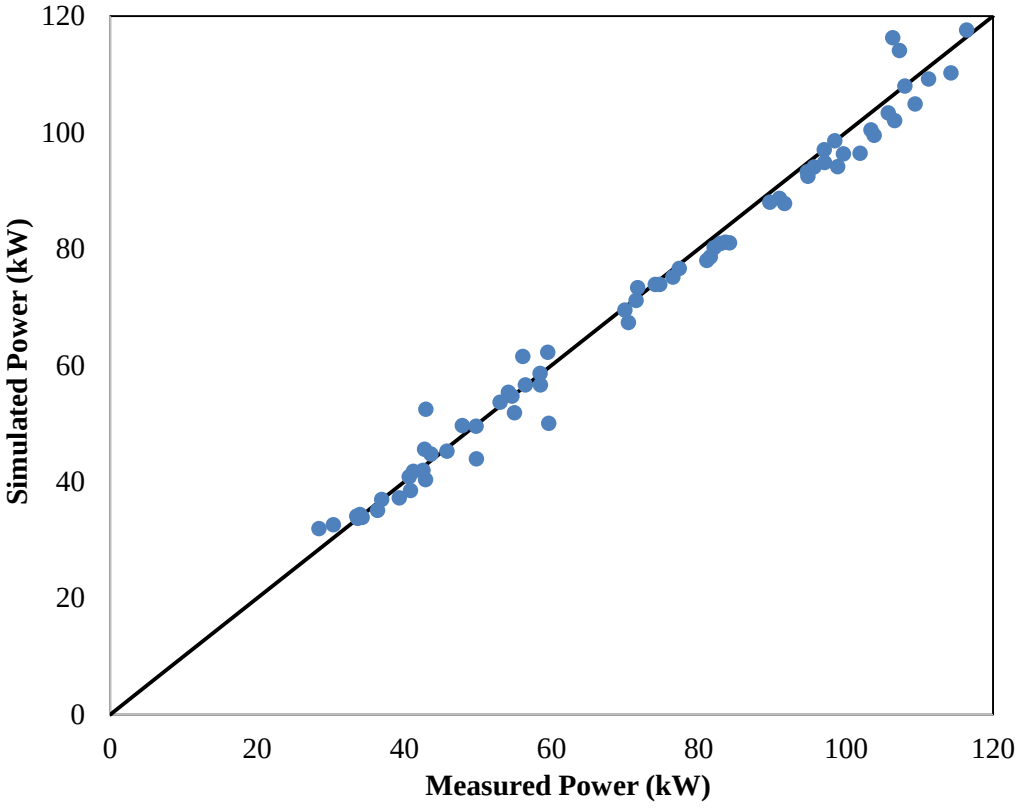

Figure 5.1 Comparison of Simulated and Measured Total Power Consumption

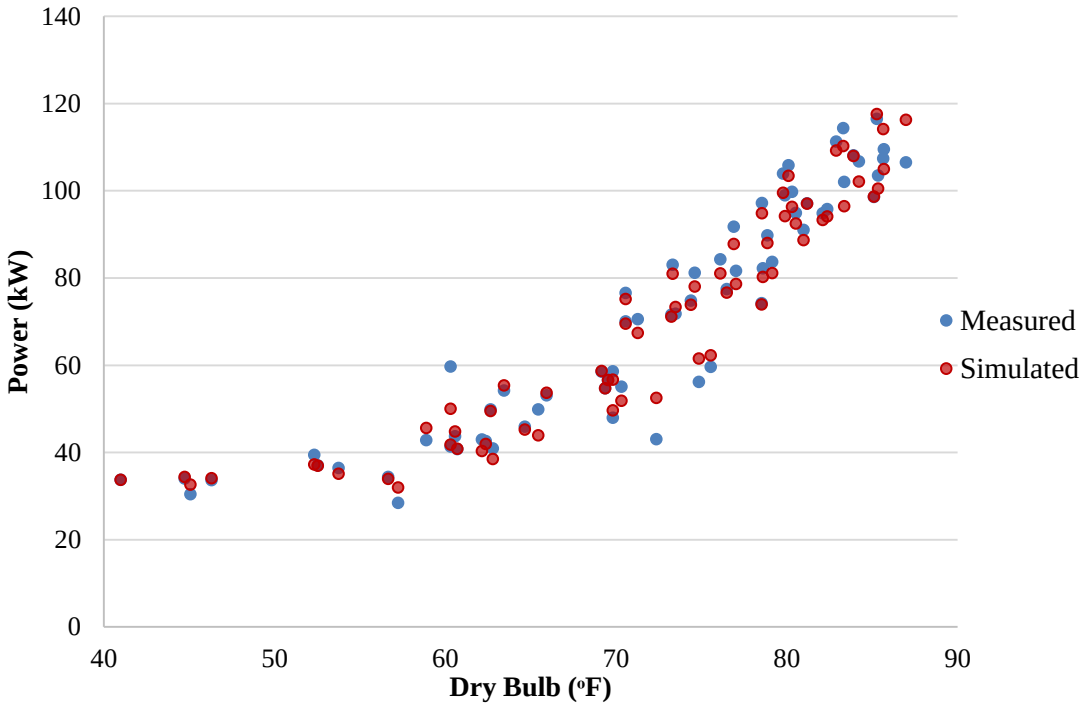

Figure 5.2 Comparison of Simulated and Measured Total Power vs. Dry-Bulb Temperature

5.2 Optimization Calculation

Instead of improving the equipment itself, this thesis focuses on determining the savings potential of the existing plant, using simple operating strategies. The most important variable stated in this work is wet-bulb temperature. By varying the desired wet-bulb temperatures, a series of corresponding total power values can be obtained.

The approach temperature with an increment of 0.25°F is set as the input variable to calculate the total power. Repeat the procedure introduced in Section 5.1. Take the day 01/22/2015 as an example; the results are given in Table 5.4 under the operating conditions listed in Table 5.1.

Table 5.2 Part of the Results on 01/22/2015

T_{app} (°F)	$T_{cond,e}$ (°F)	$T_{cond,l}$ (°F)	$P_{Chiller}$ (kW)	VFD Speed	P_{fan} (kW)	P_{tot} (kW)
3.5	48.667	50.113	19.391	96.81%	6.396	25.786
4	49.167	50.616	19.681	88.40%	5.535	25.216
5	50.167	51.621	20.286	75.88%	4.350	24.637
5.5	50.667	52.123	20.601	71.05%	3.928	24.529
5.75	50.917	52.375	20.762	68.92%	3.748	24.510
6	51.167	52.626	20.925	66.97%	3.587	24.511
6.25	51.417	52.878	21.089	65.14%	3.439	24.528
*19.88	65.000	66.561	32.936	32.08%	1.348	*34.284

*The optimal approach temperature and the corresponding power

According to Table 5.4, the approach temperature around 5.75°F gives the minimum total power consumption if the chiller could operate with a condenser entering water temperature this low. However, since the minimum condenser entering water temperature for the chiller is 65°F, the $T_{cond,e}$ of 50.92°F can't be used. In this case, the non-optimal approach temperature of 19.88°F must be used, instead of 5.75°F, to provide the $T_{cond,e}$ of 65°F. For all the other days, if the minimum total power occurs at the $T_{cond,e}$ lower than 65°F, the approach temperature corresponding to the $T_{cond,e}$ of 65°F will be used as the approach temperature to estimate the actual savings. The simulated power consumption in Chapters III and IV will be used as the baseline for the savings estimation.

To illustrate the optimizing process when the $T_{cond,e}$ is higher than 65°F, another sample day 06/06/2015 is also used to explain the optimal control. Table 5.3 includes the

relevant measurement data for 06/06/2015. Similarly, the chiller's input power can be calculated using the values of $T_{ch,l}$, $T_{cond,e}$, Q_{evap} (see Section 4.5). The other computational procedures are also the same as stated in previous chapters and sections. Based on the data listed in Table 5.3, the simulated results can be obtained as shown in Table 5.4.

Table 5.3 Measured Data for 06/06/2015

Parameters	Value
Dry-Bulb - T_{db}(°F)	82.13
Wet-Bulb - T_{wb} (°F)	72.63
Chilled Water Leaving Temp - $T_{ch,l}$ (°F)	41.49
Condenser Water Entering Temp - $T_{cond,e}$ (°F)	79.43
Approach Temp - T_{app} (°F)	6.37
Chiller Load - Q_{evap} (ton)	104.3
Water Flowrate - $\dot{m}_w$ (lb/min)	6292

Table 5.4 Simulated Results for Day 06/06/2015

$ChillerCapFTemp$	0.978358
$ChillerEIRFTemp$	1.042404
$ChillerCapFPLR$	0.486642
$P_{chiller}$ (kW)	88.43
P_{fan} (kW)	4.81
P_{total} (kW)	93.24

Again, the approach temperature with an increment of 0.25°F is set as the input variable to calculate for the total power. Repeat the procedure introduced in Section 5.1. The results are given in Table 5.5 under the operating conditions listed in Table 5.3.

Table 5.5 Part of the Results on 06/06/2015

T_{app} (°F)	$T_{cond,e}$ (°F)	$T_{cond,l}$ (°F)	$P_{Chiller}$ (kW)	VFD Speed	P_{fan} (kW)	P_{tot} (kW)
3.5	76.125	80.072	80.025	103.8%	7.147	87.172
*3.75	76.375	80.327	80.568	99.79%	6.712	87.280
4	76.625	80.581	81.114	96.13%	6.324	87.438
*6.37	78.997	83.002	88.430	80.89%	4.809	93.239

*3.75 is the optimal approach temperature with minimum total power
*6.37 is the measured average daily approach temperature

Since the $T_{cond,e}$ for sample day 06/06/2015 is always above 65°F, the minimum value of $T_{cond,e}$ doesn't not have to be considered any more. The approach temperature corresponding to the minimum total power is the optimum value, which is 3.75°F for day 06/06.This result suggests that when the dry-bulb temperature is high enough, the cooling tower fan should be operated at full VFD speed to cool the water, in order to achieve the minimum total power consumption.

Now the measured, simulated and optimal power consumptions for both 01/22 and 06/06/2015 are obtained and compared in Table 5.6. The savings are defined as the power differences between the simulated and the optimal power. The negative saving for day 01/22 is because of the error between the measured and simulated power values and indicates that no savings can be achieved on cold winter days, due to the minimum

condenser water entering temperature set point for the chillers. In comparison, 06/06 achieves the savings as expected when running the fan at full VFD speed.

Table 5.6 Power (kW) Comparisons

		01/22	06/06
Measured Power	Fan	1.065	90.200
	Chiller	32.500	4.572
	Total	33.565	94.772
Simulated Power	Fan	1.368	88.430
	Chiller	32.672	4.809
	Total	34.040	93.239
Optimal Power	Fan	1.348	6.712
	Chiller	32.936	70.568
	Total	34.284	77.280
	*Savings (Total)	-0.244	15.959

*Savings = Simulated Power – Optimal Power

5.3 Optimization Results

After repeating the calculation in Table 5.2 for all the other sampled days, Figure 5.3 is obtained. Figure 5.4 here helps to show the kW/ton comparison. Table 5.7 shows the daily power consumption of the sampled days. The overall savings are estimated to be 15.6%. Especially, the winter days, due to the minimum setting for the $T_{cond,e}$, give only a little or no savings, while the savings on higher temperature days are more stable and obvious if the cooling tower fan is fully open as recommended.

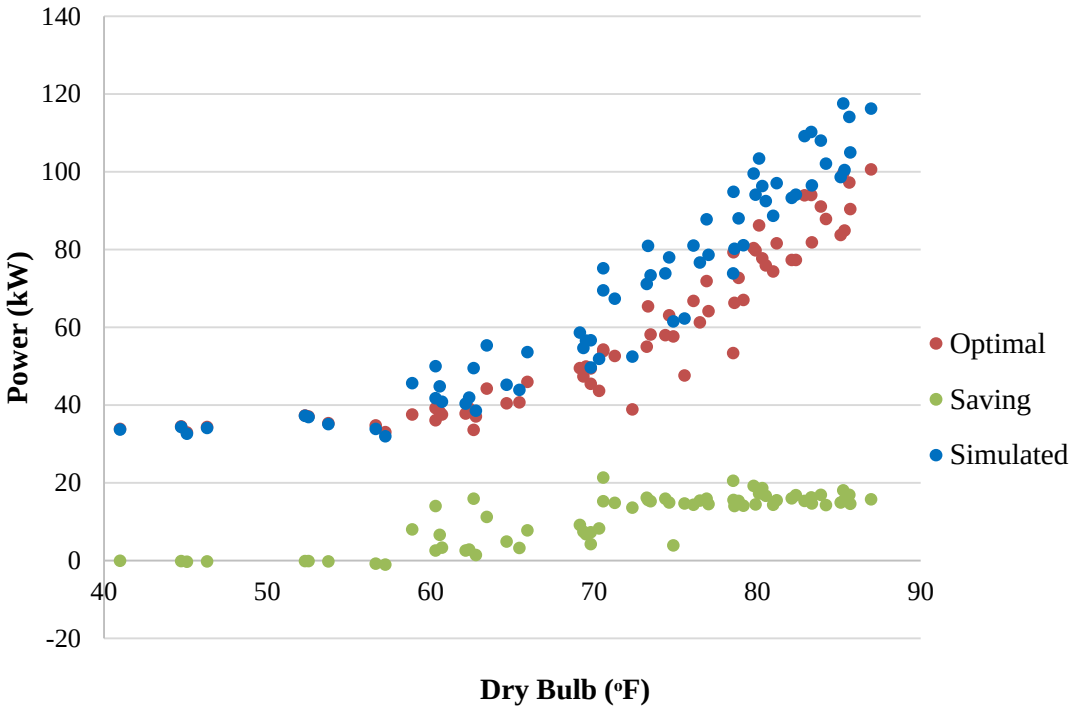

Figure 5.3 Total Power Savings for 68 Sampled Days

Table 5.7 Average Daily Total Power Comparison and Saving for 68 Sampled Days

Measured (kW)	Simulated (kW)	Optimal (kW)	*Savings (%)
71.03	70.16	59.2	15.6

*Saving = (Simulated-Optimal)/Simulated×100%

The kW/ton Figure 5.4 follows the similar pattern with the kW figure. The set of simulated and optimal data here correspond to the same chiller load.

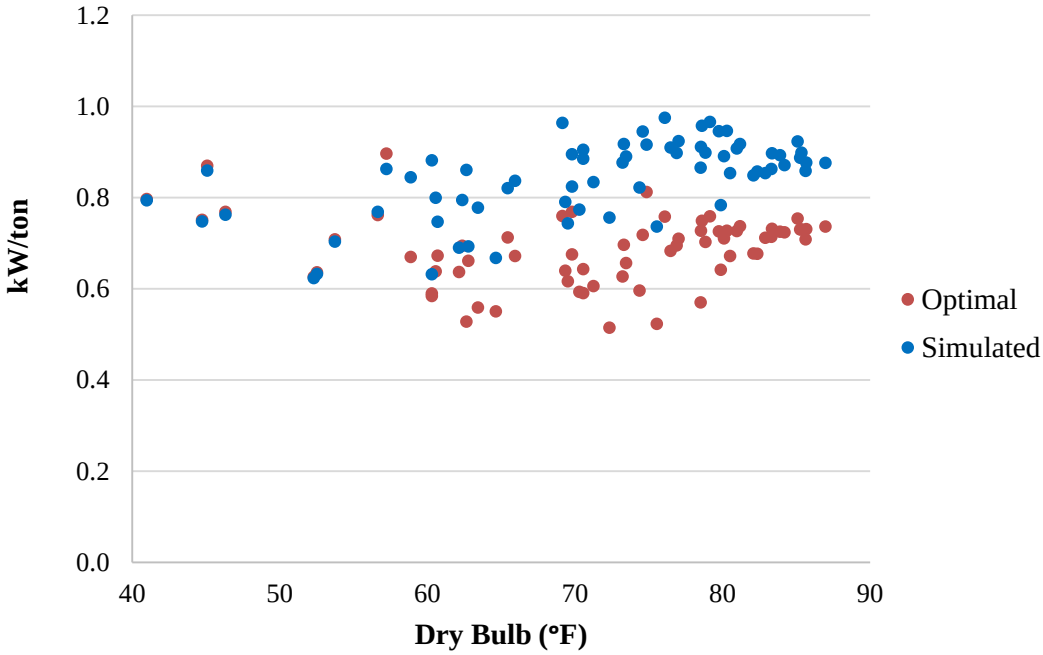

Figure 5.4 kW/ton Comparison

Figures 5.5 and 5.6 show the power of the cooling tower fan and the chiller respectively. The fan power is very low compared with the chiller input power at the same dry-bulb temperature. Thus, overall, to achieve the optimal power consumption, the cooling tower fan power is increased while the chiller power is decreased. This is also the “trade-off” for the whole cooling system.

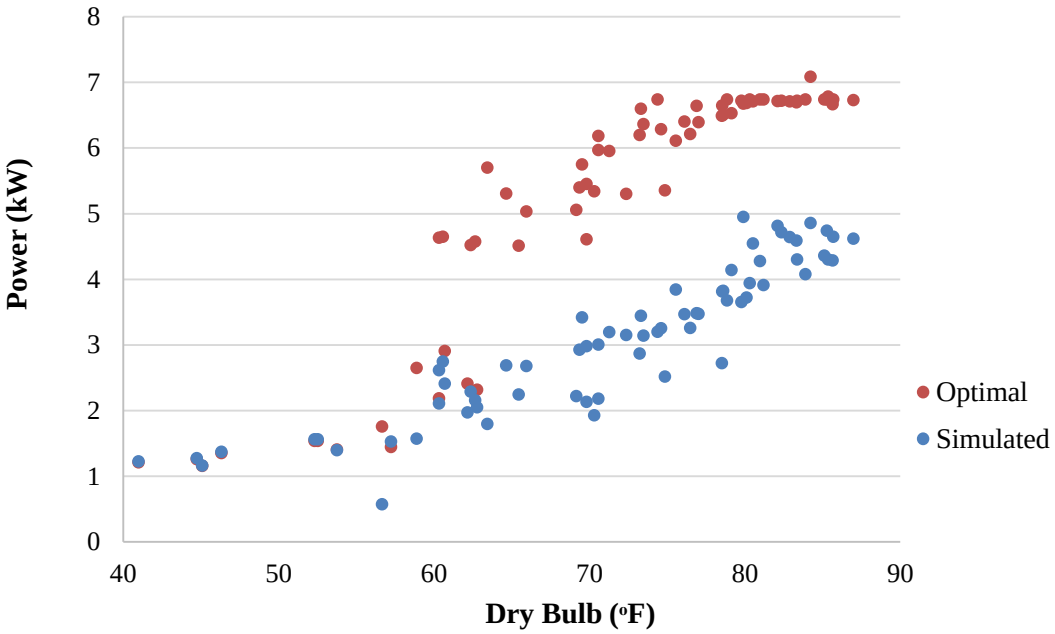

Figure 5.5 Comparison of Simulated and Optimal Fan Power

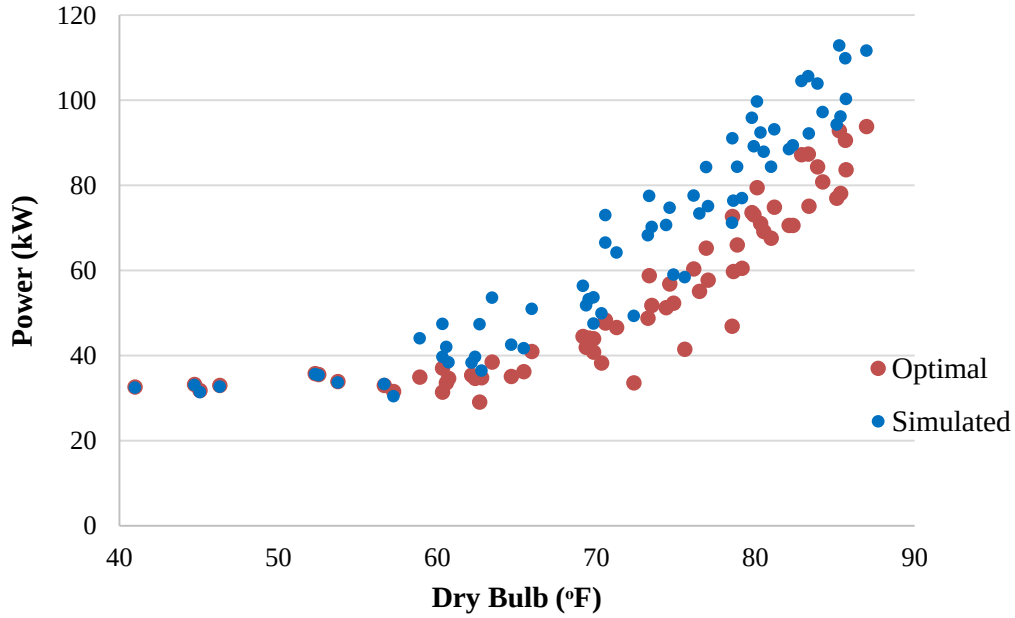

Figure 5.6 Comparison of Simulated and Optimal Chiller Power

CHAPTER VI

CONCLUSIONS AND DISCUSSION

This thesis focuses on combining the whole process of optimizing the cooling system's performance when the exiting air is not necessarily saturated. The development of classical and subsequent modified models for the cooling towers and the chillers provides opportunities to explore complex cooling systems in a simple but reliable way. Traditional models for the cooling towers, such as the Merkel model, assume saturated outlet air condition, which results in significant deviation from the real world performance. To better describe its performance, the effectiveness model developed by Braun (1988) is used in this thesis. This model doesn't assume the saturated outlet condition and can be applied to a wide operation range. It satisfies the need for simplistic representation of the relationships between operating parameters, which in turn offers an insight into the effects of various parameters on the behavior of cooling towers. It can bridge the gap between the Merkel and Poppe models by combining the simplicity of the rating procedure with a high degree of accuracy.

The Braun model requires the NTU value of the cooling tower, so field measurements were conducted to determine the NTU value for the tower as well as the fan power as a function of air flow. The measurement of the air velocity verifies the linear relationship between the air flowrate and the VFD speed. Verification of water temperatures and the energy balance suggests that the EMCS measurements are adequately accurate for model development in this case. With the measurements and the

ambient weather data, the Braun model gives a good prediction of the performance for the cooling tower under a variety of operating conditions.

The performance curves for the cooling tower and chiller together indicated the optimal operation point for the cooling system. An optimized approach temperature was determined for a wide range operating condition. When the cooling system operates using the optimized approach temperature, the sum of the chiller power and the cooling tower fan power is minimized. About 15.6% of the total measured power chiller and tower fan power can be saved for the 68 sampled days with the optimization methodology in this study applied.

6.1 Future Work

The trade-offs between power consumption of the chillers and cooling tower fans can be used as part of a more comprehensive enhancement of cooling plant system performance. This thesis did not consider variation in the flow of water to the cooling towers as part of the optimization, and this is an important addition to overall plant optimization that should be investigated in the future.

One particular weakness of this work is that more extensive data is required to achieve an accurate estimate for the overall performance and for the NTU regression. The data used in this thesis are verified to be usable, but more calibration and verification of the temperature and flowrate meters should have been done under different weather conditions. There is always space for the improvement of the accuracy

of the data, especially for this thesis, in which data is the major concern to generate reliable models for the cooling tower and the chiller.

Another area that deserves more attention is the chiller's model. This thesis focuses more on the development of the cooling tower models. To simplify the chiller side, a simple electric chiller model based on the condenser entering temperature is utilized. Some vital variables such as the chiller capacity, EIR, and condenser entering temperature are analyzed and used to predict chiller performance at different chiller leaving water temperatures and PLR values. It is desirable to have a procedure that can "calibrate" the chiller model to the performance of the chiller in the field. The work presented here used an old chiller that was not designed for variable condenser water flow. The overall optimization procedure needs to be expanded to include variable condenser water flow. Then the cooling system can be better defined and the optimized operation should be more practicable and reliable.

A third concern is that the methodology for optimize the cooling system lacks practical data support. The methodology expounded in this thesis is based on theoretical models and field measurements. However, the optimized approach temperatures and temperature ranges are not put into practice for the target cooling tower system due to the lack of time and access. The optimized operation should becarried out for the cooling system of the Connally Building, so the models can be adjusted and improved to better describe the actual system and to validate the approach proposed here.

Overall, the selection of models for the cooling towers and chillers system, the subsequent analysis, and trade-off considerations in this study can be regarded as a

starting point for other researchers to use in developing a practical procedure for field optimization of chiller plants in the future.

REFERENCES

Bourillot, C., 1983. *TEFERI, Numerical Model for Calculating the Performance of an Evaporative Cooling Towers*. EPRI Report CS-3212-SR, Electric Power Research Institute, Palo Alto, CA, UAS

Braun, J.E., 1988. *Methodologies for the Design and Control of Central Cooling Plants*, University of Wisconsin-Madison, Madsion, WI, USA

Braun, J.E. and G.T. Diderrich, 1990. *Near-optimal Control of Cooling Towers for Chilled-Water Systems.* ASHRAE Transactions 96(2):806-813.

Chua, H.T., K.C. Ng and J.M. Gordon, 1996. *Experimental Study of the Fundamental Properties of Reciprocating Chillers and Their Relation to Thermodynamic Modeling and Chiller Design*. International Journal of Heat and Mass Transfer 39(11):2195-2204.

Cortinovis, Giorgia F., José L. Paiva, Tah W. Song and José M. Printo, 2009. *A System Approach for Optimal Cooling Tower Operation*. University of São Paulo, São Paulo, SP Brazil. Polytechnic University, Brooklyn, NY, USA

Dijk, H. Van, 1985. *Investment in Cooling Tower Control Pays Big Dividends*. Process Engineering 66(10):57, 59-60.

EnergyPlus Engineering Reference: The Reference to EnergyPlus Calculations, October 1, 2013

Gordon, J.M., K.C. Ng, H.T. Chua, 1995. *Centrifugal Chillers: Thermodynamic Modeling and a Diagnostic Case Study*. International Journal of Refrigeration 18(4):253-257.

Grange, J.L., 1994. *Calculating the Evaporated Water Flow in a Wet Cooling Tower*. 9th IAHR Cooling Tower and Spraying Pond Symposium, von Karman Institute, Brussels, Belgium

Graves, Rhett David, 2003. *Thermodynamic Modeling and Optimization of A Screw Compressor Chiller and Cooling Tower*. Texas A&M University, College Station, TX, USA

Halasz, Boris, 1998. *A General Mathematical Model of Evaporative Cooling Devices*. University of Zagreb, Ulica I. Lucica 5, 10000 Zagreb, Croatia

Halasz, Boriz, 1998. *Application of a General Non-Dimensional Mathematical Model to Cooling Towers*. University of Zagreb, Ulica I. Lucica 5, HR-10000 Zagreb, Croatia

Kloppers, J.C., D.G. Kröger, 2004. *A Critical Investigation into the Heat and Mass Transfer Analysis of Counterflow Wet-Cooling Towers*. Int. J. Heat Mass Transfer 48 (2005) 765-777

Kloppers, J.C., D.G. Kröger, 2005. *Cooling Tower Performance Evaluation: Merkel, Poppe, and e-NTU Methods of Analysis*. University of Stellenbosch, Stellenbosch, South Africa

Schwedler, M. and B. Bradley, 2001. *Uncover the Hidden Assets in your Condenser Water* System. HPAC Engineering 73(11):68,75.

Threlkeld, J.L., 1970. *Thermal Environmental Engineering*, Prentice-Hall, New York, Second Edition

Whillier, Austin, 1976. *A Fresh Look at the Calculation of Performance of Cooling Towers*. ASHRAE Transactions 82(1):269-282.

Zhang, Zhiqin, Hui Li, William D. Turner and Sone Deng, 2011. *Optimization of the Cooling Tower Condenser Water Leaving Temperature Using a Component-Based Model*. ASHRAE Transactions LV-11-027.

Zheng, Wei-Ye, Dong-Sheng Zhu, Guo-Yan Zhou, Jia-Fei Wu, Yun-Yi Shi, 2012. *Thermal Performance Analysis of Closed Wet Cooling Tower under both Unsaturated and Supersaturated Conditions*. Key Laboratory of Pressure System and Safety (MOE), East China University of Science and Technology, Shanghai

APPENDIX A

EES PROGRAMMING FOR THE HALASZ AND THE BRAUN MODEL

The Halasz Model is programmed as follows:

```
Function WaterOutletTemp(n,q_mw,q_ma,T_wi,T_ai,B_WB,X_o
$Arrays ON
        T_wi=32[C],
        T_ai=35[C]
        B_WB=20[C],
        q_mw=9888
        q_ma=9370}
        P=14.7,
        w_ai=humRat(AIRH2O, P=P,B=B_WB,T=T_ai)
        w_WB=humRat(AIRH2O, P=P,B=B_WB,R=1)
        c_pw=1 {why doesn't specheat(H2O,T=T) work}
        c_pa=specheat(AIR,T=T_ai)
        W=q_mw*c_pw/q_ma/c_pa
{       X_o=1.7375*(q_ma/q_mw)^(-0.7345)}
        X_o=4

A[1]=80
i:=1
repeat
        T_w[i]=(T_wi-A[i])/Ln(T_wi/A[i])
        w_Sat[i]=humRat(AIRH2O, P=P,T=T_w[i],R=1)
        b[i]=(w_Sat[i]-w_WB)/(T_w[i]-B_WB)
        B_s[i]=b[i]*2454.1/specheat(AIR,T=T_ai)
        z[i]=(1+B_s[i])/W
```

```
        e_w[i]=z[i]*(1-exp((z[i]-1)*X_o))/(1-z[i]*exp((z[i]-1)*X_o))
        A[i+1]=T_wi-e_w[i]*(T_wi-B_WB)
        A[i]=A[i+1]
        i:=i+1
    until(abs((A[i-1]-A[i])/A[i-1])<0.0005)
    n=i-1,
    duplicate j=1,n
    WaterOutletTemp[j]=A[j]
    end
WaterOutletTemp=A[n]
end

n=5,
    T_wo=WaterOutletTemp(n,q_mw,q_ma,T_wi,T_ai,B_WB,X_o)}
    T_ai=70
    T_wi=90
    B_WB=60
    P=14.7
    w_ai=humRat(AIRH2O, P=P,B=B_WB,T=T_ai)
    h_ai=enthalpy(airh2o,P=P,T=T_ai,B=B_WB)
    w_WB=humRat(AIRH2O, P=P,B=B_WB,R=1)
    c_pw=1
    c_pa=specheat(AIR,T=T_ai)
    q_ma=4000
    q_mw=8000
    W=q_mw*c_pw/q_ma/c_pa
{       X_o=1.7375*(q_ma/q_mw)^(-0.7345)}
        X_o=4
```

```
    B_s=2.8
    z=(1+B_s)/W
    e_T=z*(1-exp((z-1)*X_o))/(1-z*exp((z-1)*X_o))
    T_wo_final=T_wi-e_T*(T_wi-B_WB)
    T_w=((T_wi-32)/1.8-(T_wo_final-32)/1.8)/Ln((T_wi-32)/1.8)/((T_wo_final-32)/1.8)
    w_Sat=humRat(AIRH2O, P=P,T=T_w,R=1)
    T_approach=T_wo_final-B_WB
    T_ao=B_WB+((T_wi-T_wo_final)/z+(T_ai-B_WB)*exp(-X_o))
    w_ao=w_WB+(w_WB-w_ai)*(B_s*(T_wi-T_wo_final)/(T_ai-B_WB)/z-exp(-X_o))
    h_ao=enthalpy(airh2o,P=P,T=T_ao,w=w_ao)
    Q_water=c_pw*q_mw*(T_wi-T_wo_final)
    Q_air=q_ma*(h_ao-h_ai)
    e_a=(h_ao-h_ai)/(enthalpy(airh2o,P=P,T=T_wi,R=1)-h_ai)
    q_mwo=q_mw-q_ma*(w_ao-w_ai)
    Loss_water=(q_mw-q_mwo)/q_mw*100

$Arrays off
$ShowWindow Arrays
```

The Braun Model is programmed as follows:

```
Function WaterOutletTemp(n,q_mw,q_ma,T_wi,T_ai,B_WB,NTU)
$Arrays ON

P=14.7,
w_ai=humRat(AIRH2O, P=P,B=B_WB,T=T_ai)
h_ai=enthalpy(AIRH2O,T=T_ai,P=P,w=w_ai)
w_WB=humRat(AIRH2O, P=P,B=B_WB,R=1)
c_pw=1
```

```
c_pa=specheat(AIR,T=T_ai)
NTU=1.428

A[1]=70[F]
i:=1
repeat
        c_s[i]=(enthalpy(AIRH2O,T=T_wi,P=P,R=1)-
        enthalpy(AIRH2O,T=A[i],P=P,R=1))/(T_wi-A[i])
        q_star[i]=q_ma*c_s[i]/q_mw/c_pw
        e_a[i]=(1-exp(-NTU*(1-q_star[i])))/(1-q_star[i]*exp(-NTU*(1-q_star[i])))
        h_ao[i]=h_ai+e_a[i]*(enthalpy(AIRH2O,T=T_wi,P=P,R=1)-h_ai)
        h_swe[i]=h_ai+(h_ao[i]-h_ai)/(1-exp(-NTU))
        w_swe[i]=humRat(AIRH2O,P=P,h=h_swe[i],R=1)
        w_ao[i]=w_swe[i]+(w_ai-w_swe[i])*exp(-NTU)
        q_mwo[i]=q_mw-q_ma*(w_ao[i]-w_ai)
        A[i+1]=(q_mw*(T_wi-32)*c_pw-q_ma*(h_ao[i]-h_ai))/q_mwo[i]/c_pw+32
        A[i]=A[i+1]
        i:=i+1
        until(abs((A[i-1]-A[i])/A[i-1])<0.000005)
                n=i-1,
                duplicate j=1,n
                WaterOutletTemp[j]=A[j]
                end
        WaterOutletTemp=A[n]
        end

        n=5,
        {       T_wi=90[F],
                T_ai=95[F],}
```

```
{       B_WB=68[F],}
        P=14.7,
   w_ai=humRat(AIRH2O, P=P,B=B_WB,T=T_ai)
   h_ai=enthalpy(AIRH2O,T=T_ai,P=P,w=w_ai)
{       q_mw=8000
        q_ma=4000}
        c_pw=1
        c_pa=specheat(AIR,T=T_ai)
        NTU=1.428

T_wo=WaterOutletTemp(n,q_mw,q_ma,T_wi,T_ai,B_WB,NTU)
h_swi=enthalpy(AIRH2O,T=T_wi,P=P,R=1)
h_swo=enthalpy(AIRH2O,T=T_wo,P=P,R=1)
c_s=(h_swi-h_swo)/(T_wi-T_wo)
q_star=q_ma*c_s/q_mw/c_pw
e_a=(1-exp(-NTU*(1-q_star)))/(1-q_star*exp(-NTU*(1-q_star)))
h_ao=h_ai+e_a*(enthalpy(AIRH2O,T=T_wi,P=P,R=1)-h_ai)
h_swe=h_ai+(h_ao-h_ai)/(1-exp(-NTU))
w_swe=humRat(AIRH2O,P=P,h=h_swe,R=1)
w_ao=w_swe+(w_ai-w_swe)*exp(-NTU)
T_ao=temperature(AIRH2O,h=h_ao,P=P,w=w_ao)
q_mwo=q_mw-q_ma*(w_ao-w_ai)
T_wo_final=(q_mw*(T_wi-32)*c_pw-q_ma*(h_ao-h_ai))/q_mwo/c_pw+32
T_approach=T_wo_final-B_WB
Q_heat=e_a*q_ma*(enthalpy(AIRH2O,T=T_wi,P=P,R=1)-h_ai)
Q_water=c_pw*q_mw*(T_wi-T_wo_final)
Q_air=q_ma*(h_ao-h_ai)
w=q_ma/q_mw
Loss_water=(q_mw-q_mwo)/q_mw*100
```

e_w=(T_wi-T_wo_final)/(T_wi-B_WB)

$Arrays off
$ShowWindow Arrays

Note for both models: The number of equations programmed above is less than the number of variables. To solve the equations, a parametric table including all the missing input variables should be created in EES and then solve for the equation system. By doing so, modification of these variables can be made easily and their effects on the final results are clearer.

APPENDIX B

CALIBRATION MEASUREMENTS FOR TSI METERS

Table B.1 Calibration Measurements for TSI Meters

# of Points	TSI 1	TSI 2
1	1176	1255
2	1282	1210
3	1105	1116
4	1228	1050
5	1267	1316
6	1348	1303
7	1193	1293
8	1374	1273
9	1201	1275
10	1186	1251
11	1296	1271
12	1390	1291
13	1429	1290
14	1320	1300
15	1309	1323
16	1321	1237
17	1328	1207
18	1331	1258
19	1304	1246
20	1228	1255
21	1188	1093
22	1267	1176
23	1250	1254
24	1249	1279
25	1301	1296
26	1234	1451
27	1337	1266

28	1320	1282
29	1295	1310
30	1276	1272
31	1322	1272
32	1318	1298
33	1324	1320
34	1342	1295
35	1379	1347
36	1338	1282
37	1266	1133
38	1202	1136
39	1269	1179
40	1308	1252
41	1307	1291
42	1244	1253
43	1299	1268
44	1206	1260
45	1299	1289
46	1273	1286
47	1294	1288
48	1329	1304
49	1293	1291
50	1286	1282
51	1294	1240
52	1292	1234
53	1317	1271
54	1302	1241

APPENDIX C

AIR VELOCITY MEASUREMENTS

The air velocities in Tables C.1 to C.5 were measured at different VFD speeds: 20%, 40%, 60%, 80% and 100% without meshes. Figure 3.9 shows the dimensions of the fan and the location for the sensors at different radii and directions.

Table C.1 Air Velocity Measurements at VFD Speed = 20%

Radius (cm) / ft/min	46	63.5	81	98.5	116
Set 1	157	411	299	216	208
Set 2	108	264	261	77	98
Set 3	194	245	267	135	102
Set 4	105	335	89	128	101
Set 5	134	234	259	104	143
Set 6	153	301	187	109	95
Set 7	108	336	266	157	143
Set 8	127	400	193	75	146
Set 9	173	396	216	140	115
Set 10	199	296	339	218	161

Table C.2 Air Velocity Measurements at VFD Speed = 40%

Radius (cm) / ft/min	46	63.5	81	98.5	116
Set 1	809	726	846	727	393
Set 2	401	770	804	637	374
Set 3	388	808	854	609	276

Set 4	349	889	804	746	272
Set 5	612	828	857	696	210
Set 6	609	953	861	704	252
Set 7	678	808	821	717	310
Set 8	598	879	923	657	390
Set 9	651	1039	905	802	363
Set 10	505	1001	960	738	373

Table C.3 Air Velocity Measurements at VFD Speed = 60%

Radius (cm) / ft/min	46	63.5	81	98.5	116
Set 1	1535	1251	1265	1188	712
Set 2	995	1351	1273	1139	416
Set 3	1120	1260	1263	1100	416
Set 4	934	1307	1242	943	394
Set 5	987	1336	1307	1004	464
Set 6	1240	1290	1304	1011	434
Set 7	1337	1438	1343	1082	487
Set 8	1311	1397	1360	1113	432
Set 9	1166	1490	1389	1021	536
Set 10	1467	1549	1623	1144	661

Table C.4 Air Velocity Measurements at VFD Speed = 80%

Radius (cm) / ft/min	46	63.5	81	98.5	116
Set 1	1982	1879	1701	1769	907
Set 2	1673	1830	1811	1467	694
Set 3	1526	1770	1862	1889	621

Set 4	1745	1793	1886	1673	611
Set 5	1739	1851	1815	1632	565
Set 6	1670	2127	1881	1674	580
Set 7	1565	2047	1900	1721	561
Set 8	1348	2013	1969	1752	590
Set 9	1856	2163	2007	1785	660
Set 10	1524	2328	2279	1511	795

Table C.5 Air Velocity Measurements at VFD Speed = 100%

Radius (cm) / ft/min	46	63.5	81	98.5	116
Set 1	2066	2530	2391	2017	1182
Set 2	2041	2423	2300	2070	1222
Set 3	2093	2319	2328	2102	797
Set 4	2225	2219	2252	2069	793
Set 5	2263	2245	2365	2229	827
Set 6	2378	2316	2351	2110	794
Set 7	2187	2495	2356	2161	895
Set 8	2026	2495	2373	2240	1010
Set 9	2183	2443	2526	2296	1013
Set 10	2212	2654	2694	2178	988

The air velocities in Tables C.6 to C.9 were measured at different VFD speeds: 25%, 50%, 75% and 100%, Figure 3.13 shows the dimensions of the fan and the location for the sensors at different radius and directions.

Table C.6 Air Velocity Measurements at VFD Speed = 25%

Radius (cm) / ft/min	40	59	78	97	116
Set 1	141	524	556	472	157
Set 2	154	591	631	526	144
Set 3	87	514	591	568	117
Set 4	172	437	478	454	272
Set 5	103	461	486	381	105
Set 6	70	462	485	481	123
Set 7	96	503	550	496	135

Table C.7 Air Velocity Measurements at VFD Speed = 50%

Radius (cm) / ft/min	40	59	78	97	116
Set 1	323	1243	1167	1200	311
Set 2	204	1192	1353	1204	342
Set 3	157	1158	1129	1030	412
Set 4	109	938	972	953	465
Set 5	287	895	926	843	406
Set 6	188	858	900	898	279
Set 7	163	708	967	1005	439

Table C.8 Air Velocity Measurements at VFD Speed = 75%

Radius (cm) / ft/min	40	59	78	97	116
Set 1	334	1463	1961	1868	501
Set 2	265	1622	1820	1637	616
Set 3	183	1759	1693	1578	511
Set 4	182	1441	1510	1439	840
Set 5	315	1420	1537	1521	506
Set 6	446	1394	1278	1246	493
Set 7	181	1612	1701	1487	568
Set 8	246	1765	1621	1707	680

Table C.9 Air Velocity Measurements at VFD Speed = 100%

Radius (cm) / ft/min	40	59	78	97	116
Set 1	259	2410	2697	2332	624
Set 2	331	1470	2326	2094	885
Set 3	220	2334	1523	2085	908
Set 4	323	1924	2287	1860	1110
Set 5	456	2030	2014	1966	642
Set 6	574	1794	1570	1833	589
Set 7	241	1623	2497	2012	871
Set 8	311	2350	2158	2298	987

APPENDIX D

INTEGRATION OF FAN AIR FLOWRATE

Chapter III introduces the integration for the air flowrate. When the VFD speed is 20%, the formula for air velocity is

$$\text{Air Velocity} = -110.3*(R)^2 + 559.23*(R) - 441.25 \quad \text{(D.1)}$$

$$\text{Air Flowrate} = \int \text{Air Velocity} * dA$$

$$= \int_{1.3\ ft}^{3.8\ ft} [(-110.3 * R^2 + 559.23 * R - 441.25) * 2\pi R * dR$$

$$= 2\pi \int_{1.3\ ft}^{3.8\ ft} [(-110.3 * R^3 + 559.23 * R^2 - 441.25 * R) * dR]$$

$$= 2\pi * [(\frac{-110.3}{4} * R^4 + \frac{559.23}{3} * R^3 - \frac{441.25}{2} * R^2)|_{1.3\ ft}^{3.8\ ft}]$$

$$= 2\pi * [\frac{-110.3}{4} * (3.8^4 - 1.3^4) + \frac{559.23}{3} * (3.8^3 - 1.3^3) - \frac{441.25}{2}$$

$$* (3.8^2 - 1.3^2)] = 8388\ cfm$$

(D.2)

When the VFD speed is 40%, the formula for air velocity is:

$$\text{Air Velocity} = -309.94*(R)^2 + 1521.9*(R) - 1005.8 \quad \text{(D.3)}$$

$$\text{Air Flowrate} = \int \text{Air Velocity} * dA$$

$$= \int_{1.3\ ft}^{3.8\ ft} [(-309.94 * R^2 + 1521.9 * R - 1005.8) * 2\pi R * dR$$

$$= 2\pi \int_{1.3\ ft}^{3.8\ ft} [(-309.94 * R^3 + 1521.9 * R^2 - 1005.8 * R) * dR]$$

$$= 2\pi * [(\frac{-309.94}{4} * R^4 + \frac{1521.9}{3} * R^3 - \frac{1005.8}{2} * R^2)|_{1.3\ ft}^{3.8\ ft}]$$

$$= 2\pi * [\frac{-309.94}{4} * (3.8^4 - 1.3^4) + \frac{1521.9}{3} * (3.8^3 - 1.3^3) - \frac{1005.8}{2}$$

$$* (3.8^2 - 1.3^2)] = 27487\ cfm$$

(D.4)

When the VFD speed is 60%, the formula for air velocity is:

$$\text{Air Velocity} = -386.02*(R)^2 + 1760.7*(R) - 611.22 \quad \text{(D.5)}$$

$$\text{Air Flowrate} = \int \text{Air Velocity} * dA$$

$$= \int_{1.3\ ft}^{3.8\ ft} [(-386.02 * R^2 + 1760.7 * R - 611.22) * 2\pi R * dR$$

$$= 2\pi \int_{1.3\ ft}^{3.8\ ft} [(-386.02 * R^3 + 1760.7 * R^2 - 611.22 * R) * dR]$$

$$= 2\pi * \left[\left(\frac{-386.02}{4} * R^4 + \frac{1760.7}{3} * R^3 - \frac{611.22}{2} * R^2\right)|_{1.3\ ft}^{3.8\ ft}\right]$$

$$= 2\pi * \left[\frac{-386.02}{4} * (3.8^4 - 1.3^4) + \frac{1760.7}{3} * (3.8^3 - 1.3^3) - \frac{611.22}{2} * (3.8^2 - 1.3^2)\right]$$

$$= 45060\ cfm \quad \text{(D.6)}$$

When the VFD speed is 80%, the formula for air velocity is:

$$\text{Air Velocity} = -632.34*(R)^2 + 2965.1*(R) - 1426.8 \quad \text{(D.7)}$$

$$\text{Air Flowrate} = \int \text{Air Velocity} * dA$$

$$= \int_{1.3\ ft}^{3.8\ ft} [(-632.34 * R^2 + 2965.1 * R - 1426.8) * 2\pi R * dR$$

$$= 2\pi \int_{1.3\ ft}^{3.8\ ft} [(-632.34 * R^3 + 2965.1 * R^2 - 1426.8 * R) * dR]$$

$$= 2\pi * [(\frac{-632.34}{4} * R^4 + \frac{2965.1}{3} * R^3 - \frac{1426.8}{2} * R^2)|_{1.3\ ft}^{3.8\ ft}]$$

$$= 2\pi * [\frac{-632.34}{4} * (3.8^4 - 1.3^4) + \frac{2965.1}{3} * (3.8^3 - 1.3^3) - \frac{1426.8}{2}$$

$$* (3.8^2 - 1.3^2)] = 62691\ cfm$$

(D.8)

When the VFD speed is 100%, the formula for air velocity is:

$$\text{Air Velocity} = -952.63*(R)^2 + 4828.5*(R) - 3641.2 \quad \text{(D.9)}$$

$$\text{Air Flowrate} = \int \text{Air Velocity} * dA$$

$$= \int_{1.3\ ft}^{3.8\ ft} [(-952.63 * R^2 + 4828.5 * R - 3641.2) * 2\pi R * dR$$

$$= 2\pi \int_{1.3\ ft}^{3.8\ ft} [(-952.63 * R^3 + 4828.5 * R^2 - 3641.2 * R) * dR]$$

$$= 2\pi * [(\frac{-952.63}{4} * R^4 + \frac{4828.5}{3} * R^3 - \frac{3641.2}{2} * R^2)|_{1.3\ ft}^{3.8\ ft}]$$

$$= 2\pi * [\frac{-952.63}{4} * (3.8^4 - 1.3^4) + \frac{4828.5}{3} * (3.8^3 - 1.3^3) - \frac{3641.2}{2}$$

$$* (3.8^2 - 1.3^2)] = 79098\ cfm$$

(D.10)

APPENDIX E

WATER TEMPERATURE MEASUREMENTS

Table E.1 Water Temperature Measurements

°F	HOBO Sensor			EMCS Sensor		
Date	Inlet Temp	Outlet Temp	Cooling Range	Inlet Temp	Outlet Temp	Cooling Range
1/13/2016	67.285	64.918	2.367	67.31	65.06	2.25
1/13/2016	67.285	64.704	2.581	67.22	64.81	2.41
1/13/2016	67.158	64.362	2.796	66.06	64.56	1.5
1/13/2016	66.729	64.018	2.711	65.72	64.06	1.66
1/13/2016	65.574	63.548	2.026	65.66	63.69	1.97
1/13/2016	64.931	63.161	1.77	64.94	63.44	1.5
1/13/2016	64.717	62.99	1.727	64.84	63.06	1.78
1/13/2016	63.862	62.862	1	64.22	62.94	1.28
1/13/2016	64.288	62.906	1.382	64.31	62.94	1.37
1/13/2016	65.145	63.248	1.897	64.28	63.19	1.09
1/13/2016	64.459	63.676	0.783	64.31	63.59	0.72
1/13/2016	65.574	64.018	1.556	65.28	64	1.28
1/13/2016	65.102	64.362	0.74	65.28	64.28	1
1/13/2016	65.745	64.574	1.171	65.59	64.69	0.9
1/13/2016	66.385	64.832	1.553	65.53	64.81	0.72
1/13/2016	66.515	64.704	1.811	65.31	64.81	0.5
1/13/2016	65.788	64.747	1.041	65.5	64.69	0.81
1/13/2016	65.316	64.446	0.87	65.19	64.56	0.63
1/13/2016	64.888	64.403	0.485	65.69	64.44	1.25
1/13/2016	64.803	64.061	0.742	64.75	64.19	0.56
1/13/2016	65.53	64.189	1.341	64.94	64.19	0.75
1/13/2016	65.017	64.403	0.614	64.97	64.31	0.66
1/13/2016	65.316	64.704	0.612	65.34	64.59	0.75
1/13/2016	66.087	65.003	1.084	65.66	64.97	0.69

1/13/2016	65.829	65.217	0.612	65.69	65.09	0.6
1/13/2016	65.701	65.345	0.356	66.31	65.38	0.93
1/13/2016	65.615	65.303	0.312	66.19	65.38	0.81
1/13/2016	66.6	65.26	1.34	65.69	65.38	0.31
1/13/2016	65.574	65.089	0.485	65.94	65.13	0.81
1/14/2016	65.316	64.959	0.357	65.56	65	0.56
1/14/2016	65.273	64.788	0.485	65.16	64.88	0.28
1/14/2016	65.017	64.574	0.443	65.09	64.75	0.34
1/14/2016	64.674	64.403	0.271	64.97	64.5	0.47
1/14/2016	64.459	64.148	0.311	64.59	64.22	0.37
1/14/2016	64.931	64.617	0.314	64.97	64.5	0.47
1/14/2016	65.916	65.431	0.485	65.63	65.38	0.25
1/14/2016	66.344	66.158	0.186	66.31	66.13	0.18
1/14/2016	67.285	66.758	0.527	67.41	66.78	0.63
1/14/2016	66.429	66.074	0.355	66.88	66.38	0.5
1/14/2016	65.487	65.089	0.398	65.78	65.44	0.34
1/14/2016	64.76	64.319	0.441	64.94	64.5	0.44
1/14/2016	63.99	63.719	0.271	64.28	63.88	0.4
1/14/2016	63.648	63.375	0.273	63.78	63.47	0.31
1/14/2016	63.775	63.548	0.227	63.63	63.34	0.29
1/14/2016	64.717	64.403	0.314	64.5	64.25	0.25
1/14/2016	65.487	65.132	0.355	65.41	65.09	0.32
1/14/2016	67.329	66.714	0.615	68.5	66.03	2.47
1/14/2016	70.329	69.157	1.172	70.19	69.34	0.85
1/14/2016	69.085	68	1.085	70.03	68.16	1.87
1/14/2016	68.443	66.459	1.984	68.09	66.75	1.34
1/14/2016	66.985	65.303	1.682	67.34	65.47	1.87
1/14/2016	65.658	64.362	1.296	65.81	64.56	1.25
1/14/2016	65.145	63.933	1.212	65.06	64.03	1.03
1/14/2016	65.316	63.847	1.469	65.53	63.91	1.62
1/14/2016	65.916	64.104	1.812	66.03	64.19	1.84
1/14/2016	66.173	64.403	1.77	65.59	64.63	0.96
1/14/2016	66.6	64.704	1.896	65.63	64.94	0.69

1/14/2016	66.643	65.217	1.426	66.25	65.22	1.03
1/14/2016	66.772	65.559	1.213	66.47	65.44	1.03
1/14/2016	67.242	65.431	1.811	66.81	65.34	1.47
1/14/2016	66.515	65.26	1.255	66.69	65.34	1.35
1/14/2016	66	65.132	0.868	67.53	65.22	2.31
1/14/2016	67.158	65.089	2.069	66.5	65.09	1.41
1/14/2016	67.114	65.174	1.94	66.44	65.34	1.1
1/14/2016	66.214	65.345	0.869	67.13	65.34	1.79
1/14/2016	66.6	65.688	0.912	66.78	65.34	1.44
1/14/2016	66.686	65.903	0.783	67.53	65.59	1.94
1/14/2016	67.199	65.987	1.212	67.47	65.84	1.63
1/14/2016	67.586	66.158	1.428	68.03	66	2.03
1/14/2016	68.443	66.115	2.328	68.41	66.25	2.16
1/14/2016	68.785	66.372	2.413	68.25	66.44	1.81
1/14/2016	68.484	66.288	2.196	67.75	66.44	1.31
1/14/2016	67.413	66.372	1.041	68.47	66.41	2.06
1/14/2016	68.056	66.673	1.383	68	66.53	1.47
1/14/2016	68.4	66.63	1.77	68.16	66.53	1.63
1/14/2016	67.842	66.587	1.255	68.13	66.41	1.72
1/14/2016	67.842	66.63	1.212	69.09	66.59	2.5
1/14/2016	68.614	66.587	2.027	68.78	66.75	2.03
1/14/2016	69.213	66.758	2.455	68.34	66.75	1.59
1/14/2016	68.956	66.929	2.027	69.22	67.06	2.16
1/14/2016	68.913	67.4	1.513	69.59	67.31	2.28
1/14/2016	68.871	67.528	1.343	69.63	67.56	2.07
1/14/2016	68.828	67.357	1.471	69.47	67.31	2.16
1/14/2016	68.698	67.272	1.426	69.56	67.25	2.31
1/14/2016	69.3	67.443	1.857	69.34	67.44	1.9
1/14/2016	69.386	67.528	1.858	69.81	67.59	2.22
1/14/2016	69.386	67.443	1.943	69.31	67.44	1.87
1/14/2016	69.514	67.314	2.2	69.19	67.31	1.88
1/14/2016	69.17	67.485	1.685	69.53	67.31	2.22
1/14/2016	69.17	67.614	1.556	69.5	67.56	1.94

1/14/2016	69.728	67.742	1.986	69.97	67.72	2.25
1/14/2016	69.3	67.742	1.558	70.56	67.72	2.84
1/14/2016	70.587	68.043	2.544	70.19	68	2.19
1/14/2016	70.543	68.171	2.372	70.22	68.25	1.97
1/14/2016	70.803	68.471	2.332	70.22	68.34	1.88
1/14/2016	70.846	68.77	2.076	70.84	68.63	2.21
1/14/2016	70.759	69.114	1.645	71.63	69.06	2.57
1/14/2016	70.803	69.285	1.518	71.72	69.22	2.5
1/14/2016	71.533	69.114	2.419	71.16	69.22	1.94
1/14/2016	71.274	68.856	2.418	71.09	69.09	2
1/14/2016	70.759	68.685	2.074	71.19	68.97	2.22
1/14/2016	70.587	68.471	2.116	69.84	68.59	1.25
1/14/2016	68.913	68.171	0.742	70.28	68.22	2.06
1/14/2016	69.771	67.829	1.942	69.03	67.94	1.09
1/14/2016	68.571	67.571	1	69.06	67.56	1.5
1/14/2016	68.185	67.229	0.956	68.38	67.44	0.94
1/14/2016	68.227	67.1	1.127	68.69	67.19	1.5
1/14/2016	68.356	66.844	1.512	67.47	66.81	0.66
1/14/2016	67.413	66.587	0.826	68.22	66.56	1.66
1/14/2016	67.199	66.372	0.827	67.09	66.44	0.65
1/14/2016	67.971	66.372	1.599	66.81	66.44	0.37
1/14/2016	67.285	66.245	1.04	67.22	66.31	0.91
1/14/2016	66.6	66.115	0.485	67.59	66.25	1.34
1/14/2016	66.301	65.903	0.398	67.78	66.06	1.72
1/14/2016	66.9	65.73	1.17	66.34	65.81	0.53
1/14/2016	66.729	65.517	1.212	66.53	65.69	0.84
1/14/2016	66.472	65.303	1.169	66.56	65.44	1.12
1/14/2016	66.043	65.174	0.869	66.06	65.31	0.75
1/14/2016	65.444	65.046	0.398	65.81	65.06	0.75
1/14/2016	65.701	64.918	0.783	65.44	65.06	0.38
1/14/2016	65.658	65.046	0.612	65.75	65.09	0.66
1/14/2016	65.829	65.089	0.74	65.53	65.09	0.44
1/14/2016	65.444	65.174	0.27	66.38	65.09	1.29

1/14/2016	65.658	65.217	0.441	66.16	65.22	0.94
1/14/2016	66.13	65.303	0.827	65.63	65.34	0.29
1/15/2016	65.701	65.26	0.441	66.16	65.34	0.82
1/15/2016	65.916	65.388	0.528	65.69	65.34	0.35
1/15/2016	65.701	65.388	0.313	65.78	65.34	0.44
1/15/2016	65.872	65.431	0.441	65.75	65.47	0.28
1/15/2016	66.173	65.431	0.742	65.66	65.47	0.19
1/15/2016	65.745	65.388	0.357	65.88	65.47	0.41
1/15/2016	65.53	65.345	0.185	66.38	65.47	0.91
1/15/2016	65.658	65.431	0.227	66	65.47	0.53
1/15/2016	65.745	65.345	0.4	65.84	65.47	0.37
1/15/2016	65.829	65.345	0.484	65.78	65.34	0.44
1/15/2016	65.916	65.345	0.571	65.84	65.34	0.5
1/15/2016	65.53	65.345	0.185	66.22	65.34	0.88
1/15/2016	65.658	65.303	0.355	66.03	65.34	0.69
1/15/2016	65.745	65.217	0.528	65.63	65.34	0.29
1/15/2016	65.53	65.089	0.441	65.59	65.22	0.37
1/15/2016	65.487	64.788	0.699	65.41	64.97	0.44
1/15/2016	65.059	64.704	0.355	65.25	64.84	0.41
1/15/2016	65.872	65.003	0.869	67.47	64.72	2.75
1/15/2016	66.472	65.174	1.298	66.09	65.34	0.75
1/15/2016	66.258	65.303	0.955	67.09	65.22	1.87
1/15/2016	65.916	64.959	0.957	66.81	64.97	1.84
1/15/2016	66.729	64.788	1.941	66.25	64.84	1.41
1/15/2016	66.344	64.403	1.941	65.75	64.47	1.28
1/15/2016	66.515	64.104	2.411	65.19	64.09	1.1
1/15/2016	65.059	63.933	1.126	65	64	1
1/15/2016	65.188	63.633	1.555	65.03	63.75	1.28
1/15/2016	64.974	63.334	1.64	64.69	63.59	1.1
1/15/2016	65.403	63.204	2.199	64.5	63.47	1.03
1/15/2016	65.102	63.161	1.941	64.38	63.38	1
1/15/2016	64.931	63.204	1.727	64.28	63.25	1.03
1/15/2016	64.074	63.033	1.041	65.06	63.13	1.93

1/15/2016	64.375	62.906	1.469	64.22	63	1.22
1/15/2016	65.53	63.161	2.369	64.25	63.25	1
1/15/2016	65.273	63.633	1.64	64.75	63.69	1.06
1/15/2016	65.788	64.104	1.684	64.94	64.13	0.81
1/15/2016	67.285	64.704	2.581	65.97	64.81	1.16
1/15/2016	67.372	65.217	2.155	67.19	65.28	1.91
1/15/2016	67.971	65.773	2.198	67.34	65.91	1.43
1/15/2016	67.971	66.115	1.856	68.69	66.16	2.53
1/15/2016	68.056	66.288	1.768	69.09	66.25	2.84
1/15/2016	67.971	66.201	1.77	68.78	66.09	2.69
1/15/2016	68.742	66.245	2.497	68.28	66.22	2.06
1/15/2016	67.885	66.245	1.64	68.94	66.22	2.72
1/15/2016	68.571	65.816	2.755	68.06	65.94	2.12
1/15/2016	68.484	65.816	2.668	67.97	65.91	2.06
1/15/2016	68.657	65.602	3.055	67.63	65.75	1.88
1/15/2016	67.928	65.474	2.454	68.13	65.63	2.5
1/15/2016	67.971	65.474	2.497	68.38	65.56	2.82
1/15/2016	67.928	65.345	2.583	67.72	65.44	2.28
1/15/2016	68.227	65.431	2.796	67.44	65.44	2
1/15/2016	67.885	65.132	2.753	67.19	65.19	2
1/15/2016	66.985	65.303	1.682	68.16	65.19	2.97
1/15/2016	67.285	65.217	2.068	68.03	65.19	2.84
1/15/2016	67.071	65.26	1.811	68.22	65.19	3.03
1/15/2016	67.798	65.303	2.495	67.84	65.19	2.65
1/15/2016	67.413	65.26	2.153	68.75	65.44	3.31
1/15/2016	67.971	65.773	2.198	68.28	65.59	2.69
1/15/2016	68.785	65.73	3.055	68.16	65.72	2.44
1/15/2016	68.527	65.688	2.839	68.44	65.88	2.56
1/15/2016	68.614	65.517	3.097	68.59	65.59	3
1/15/2016	68.185	65.602	2.583	68.66	65.59	3.07
1/15/2016	68.657	65.73	2.927	68.59	65.72	2.87
1/15/2016	68.056	65.474	2.582	68.88	65.56	3.32
1/15/2016	67.798	65.217	2.581	68.25	65.19	3.06

1/15/2016	67.627	65.217	2.41	68.13	65.19	2.94
1/15/2016	67.627	64.959	2.668	67.31	64.94	2.37
1/15/2016	67.627	64.704	2.923	68.22	64.81	3.41
1/15/2016	67.285	64.747	2.538	67.44	64.66	2.78
1/15/2016	67.586	64.49	3.096	67.03	64.66	2.37
1/15/2016	67.285	64.319	2.966	66.91	64.66	2.25
1/15/2016	66.515	63.847	2.668	66.72	63.97	2.75
1/15/2016	65.145	63.548	1.597	66.38	63.59	2.79
1/15/2016	64.632	63.12	1.512	65.5	63.22	2.28
1/15/2016	63.946	62.733	1.213	65	62.84	2.16
1/15/2016	63.475	62.391	1.084	63.72	62.47	1.25
1/15/2016	63.304	62.22	1.084	63.44	62.22	1.22
1/15/2016	63.433	62.391	1.042	63.81	62.34	1.47
1/15/2016	64.546	62.691	1.855	63.5	62.72	0.78
1/15/2016	64.161	63.291	0.87	64.19	63.25	0.94
1/15/2016	64.76	63.847	0.913	64.56	63.75	0.81
1/15/2016	65.102	64.319	0.783	65.31	64.16	1.15
1/15/2016	66.729	64.788	1.941	66.5	64.91	1.59
1/15/2016	65.788	65.26	0.528	66.03	65.09	0.94
1/15/2016	66.385	64.959	1.426	65.66	65.13	0.53
1/15/2016	65.53	64.959	0.571	65.53	64.88	0.65
1/15/2016	65.788	64.704	1.084	66.16	64.88	1.28
1/15/2016	65.017	64.49	0.527	65.75	64.63	1.12
1/15/2016	64.888	64.319	0.569	65.13	64.38	0.75
1/15/2016	65.017	64.061	0.956	64.81	64.25	0.56
1/15/2016	64.803	64.148	0.655	64.88	64.13	0.75
1/15/2016	64.845	64.148	0.697	64.81	64.25	0.56
1/15/2016	65.403	64.918	0.485	65.66	64.75	0.91
1/15/2016	67.242	66.245	0.997	66.84	66.06	0.78
1/15/2016	67.543	67.485	0.058	67.78	67.22	0.56
1/15/2016	66.472	66.03	0.442	66.66	66.31	0.35
1/15/2016	65.23	64.747	0.483	66.06	65	1.06
1/16/2016	64.459	63.89	0.569	64.78	64.16	0.62

1/16/2016	63.518	63.12	0.398	63.81	63.28	0.53
1/16/2016	63.048	62.776	0.272	63.31	62.88	0.43
1/16/2016	64.117	63.719	0.398	63.78	63.5	0.28
1/16/2016	64.375	65.345	-0.97	64.91	64.63	0.28
1/16/2016	66.344	65.987	0.357	66.72	65.91	0.81
1/16/2016	66.643	66.758	-0.115	67.22	66.44	0.78
1/16/2016	67.242	67.357	-0.115	67.63	67.06	0.57
1/16/2016	66.301	65.859	0.442	66.38	66.38	0
1/16/2016	64.931	64.362	0.569	65.06	64.69	0.37
1/16/2016	63.946	63.462	0.484	64.25	63.78	0.47
1/16/2016	63.09	62.733	0.357	63.47	62.88	0.59
1/16/2016	63.732	63.419	0.313	63.5	63.22	0.28
1/16/2016	64.546	65.26	-0.714	64.66	64.34	0.32
1/16/2016	66.385	65.816	0.569	66.47	65.75	0.72
1/16/2016	66.686	66.288	0.398	66.44	66.16	0.28
1/16/2016	66.857	67.015	-0.158	67.31	66.72	0.59
1/16/2016	67.971	67.1	0.871	69.22	67.22	2
1/16/2016	67.114	66.158	0.956	67.63	66.5	1.13
1/16/2016	66.258	65.431	0.827	67.56	65.47	2.09
1/16/2016	66.173	64.49	1.683	65.78	64.66	1.12
1/16/2016	65.53	64.148	1.382	65.41	64.25	1.16
1/16/2016	66.043	63.847	2.196	65.34	64	1.34
1/16/2016	65.403	63.933	1.47	65.47	64.19	1.28
1/16/2016	65.53	64.232	1.298	66.66	64.28	2.38
1/16/2016	67.028	64.704	2.324	66.63	64.78	1.85
1/16/2016	66	64.832	1.168	66.69	64.88	1.81
1/16/2016	66.043	65.345	0.698	66.19	65	1.19
1/16/2016	66.301	65.132	1.169	66.34	65.22	1.12
1/16/2016	66.087	65.089	0.998	66.22	65.13	1.09
1/16/2016	66.385	64.875	1.51	66.13	65.09	1.04
1/16/2016	67.071	64.704	2.367	65.69	64.97	0.72
1/16/2016	66.214	64.747	1.467	66.03	64.84	1.19
1/16/2016	65.745	65.089	0.656	66.72	64.97	1.75

1/16/2016	65.53	65.003	0.527	66.94	64.81	2.13
1/16/2016	66.686	65.003	1.683	66.34	65.09	1.25
1/16/2016	66.943	65.174	1.769	67.19	65.22	1.97
1/16/2016	66.686	65.217	1.469	66.31	65.5	0.81
1/16/2016	66.258	65.26	0.998	67.38	65.25	2.13
1/16/2016	66.385	65.132	1.253	66.59	65.25	1.34
1/16/2016	66.043	65.003	1.04	67.19	65.13	2.06
1/16/2016	66.043	64.875	1.168	66.75	65.13	1.62
1/16/2016	67.242	64.959	2.283	65.63	64.97	0.66
1/16/2016	67.242	65.046	2.196	66.59	65.09	1.5
1/16/2016	66.857	65.174	1.683	66.56	65.38	1.18
1/16/2016	66.558	65.303	1.255	67.47	65.38	2.09
1/16/2016	66.173	65.217	0.956	66.63	65.38	1.25
1/16/2016	66.13	65.174	0.956	67.25	65.25	2
1/16/2016	66.258	65.26	0.998	66.06	65.13	0.93
1/16/2016	66.985	64.959	2.026	65.84	65.13	0.71
1/16/2016	66.515	64.661	1.854	66.22	64.88	1.34
1/16/2016	66.515	64.918	1.597	65.97	64.88	1.09
1/16/2016	66.214	64.875	1.339	66.91	65	1.91
1/16/2016	66.686	64.918	1.768	66.66	65.13	1.53
1/16/2016	66.686	64.704	1.982	65.88	64.84	1.04
1/16/2016	65.788	64.747	1.041	66.66	64.91	1.75
1/16/2016	66.13	65.003	1.127	66.44	64.91	1.53
1/16/2016	66.087	64.918	1.169	66.31	64.91	1.4
1/16/2016	65.916	65.132	0.784	65.78	65	0.78
1/16/2016	66	65.089	0.911	66.56	65.03	1.53
1/16/2016	66.729	65.431	1.298	67.59	65.41	2.18
1/16/2016	68.013	65.645	2.368	67.03	65.84	1.19
1/16/2016	67.114	65.73	1.384	67.94	65.88	2.06
1/16/2016	67.028	65.431	1.597	67	65.69	1.31
1/16/2016	66.429	65.217	1.212	67	65.31	1.69
1/16/2016	66.857	65.003	1.854	66.38	65.16	1.22
1/16/2016	66.043	64.875	1.168	67	64.94	2.06

1/16/2016	67.071	64.574	2.497	66.38	64.81	1.57
1/16/2016	66.429	64.661	1.768	65.81	64.66	1.15
1/16/2016	65.615	64.788	0.827	66.66	64.63	2.03
1/16/2016	65.487	64.617	0.87	66.28	64.66	1.62
1/16/2016	65.959	64.362	1.597	66.06	64.53	1.53
1/16/2016	66.344	64.275	2.069	66.34	64.44	1.9
1/16/2016	65.872	64.148	1.724	65.13	64.28	0.85
1/16/2016	65.017	64.061	0.956	65.16	64.16	1
1/16/2016	64.845	64.061	0.784	65.94	64.03	1.91
1/16/2016	65.701	64.061	1.64	64.75	64.16	0.59
1/16/2016	65.23	64.061	1.169	64.94	64.16	0.78
1/16/2016	65.359	64.232	1.127	65.28	64.16	1.12
1/16/2016	65.273	64.617	0.656	65.16	64.47	0.69
1/16/2016	67.329	65.944	1.385	66.22	65.78	0.44
1/16/2016	67.885	67.4	0.485	67.56	67.09	0.47
1/16/2016	66.472	65.944	0.528	67.88	66.22	1.66
1/16/2016	64.931	64.574	0.357	66.22	64.81	1.41
1/16/2016	64.375	63.633	0.742	64.59	63.94	0.65
1/16/2016	63.648	62.819	0.829	63.59	63.06	0.53
1/16/2016	63.862	63.161	0.701	63.59	63.03	0.56
1/16/2016	64.632	64.275	0.357	64.63	64.03	0.6
1/16/2016	66.344	65.303	1.041	65.53	65.03	0.5
1/16/2016	66.515	66.115	0.4	66.97	66.06	0.91
1/16/2016	67.114	66.844	0.27	67.63	66.72	0.91
1/16/2016	68.657	67.186	1.471	67.38	67.22	0.16
1/16/2016	65.959	65.474	0.485	66.19	65.94	0.25
1/16/2016	64.332	63.762	0.57	64.66	64.16	0.5
1/16/2016	62.919	62.519	0.4	63.19	62.78	0.41
1/16/2016	62.919	62.605	0.314	62.91	62.5	0.41
1/17/2016	62.49	65.217	-2.727	65.25	64.81	0.44
1/17/2016	65.658	65.003	0.655	65.5	65.47	0.03
1/17/2016	66.344	65.645	0.699	66	65.69	0.31
1/17/2016	66.344	65.645	0.699	65.94	65.69	0.25

1/17/2016	66	65.73	0.27	66.03	65.81	0.22
1/17/2016	66	65.859	0.141	65.91	65.81	0.1
1/17/2016	66.173	65.903	0.27	66.31	65.94	0.37
1/17/2016	66.515	65.773	0.742	65.91	65.94	-0.03
1/17/2016	64.161	63.762	0.399	64.59	64.03	0.56
1/17/2016	62.577	62.09	0.487	62.81	62.53	0.28
1/17/2016	62.962	62.906	0.056	62.94	62.69	0.25
1/17/2016	64.418	64.148	0.27	66.19	65.41	0.78
1/17/2016	65.658	65.132	0.526	65.72	65.75	-0.03
1/17/2016	65.745	65.645	0.1	65.88	65.69	0.19
1/17/2016	66.385	65.859	0.526	66	65.94	0.06
1/17/2016	66.943	66.115	0.828	66	66.06	-0.06
1/17/2016	66.214	66.245	-0.031	66.88	66.31	0.57
1/17/2016	67.456	66.758	0.698	69.25	66.97	2.28
1/17/2016	65.403	64.704	0.699	66.13	65.19	0.94
1/17/2016	64.674	63.505	1.169	65.69	63.59	2.1
1/17/2016	64.589	63.033	1.556	63.88	63.09	0.79
1/17/2016	65.959	64.788	1.171	65.44	64.16	1.28
1/17/2016	68.742	67.015	1.727	67.59	66.81	0.78
1/17/2016	69.427	67.357	2.07	69.47	67.94	1.53
1/17/2016	66.943	64.959	1.984	67.47	65.47	2
1/17/2016	65.102	63.462	1.64	65.34	63.81	1.53
1/17/2016	64.074	62.733	1.341	64.34	62.94	1.4
1/17/2016	64.459	63.161	1.298	63.69	62.69	1
1/17/2016	67.885	65.773	2.112	66.09	65.41	0.68
1/17/2016	69.985	68.127	1.858	68.72	67.97	0.75
1/17/2016	67.971	66.201	1.77	67.97	66.84	1.13
1/17/2016	65.959	63.719	2.24	65.19	64.19	1
1/17/2016	64.674	62.391	2.283	63.84	62.78	1.06
1/17/2016	64.546	63.419	1.127	63.38	62.56	0.82
1/17/2016	66.943	66.074	0.869	67.47	65.53	1.94
1/17/2016	70.072	68.642	1.43	70.25	68.22	2.03
1/17/2016	68.227	66.372	1.855	67.88	67	0.88

1/17/2016	65.959	64.49	1.469	66.78	64.91	1.87
1/17/2016	65.658	63.59	2.068	65.66	63.88	1.78
1/17/2016	65.145	63.419	1.726	64.81	63.38	1.43
1/17/2016	65.059	63.59	1.469	65.06	63.5	1.56
1/17/2016	65.188	64.018	1.17	66.31	64	2.31
1/17/2016	68.227	67.314	0.913	68.78	66.53	2.25
1/17/2016	69.129	67.913	1.216	70	68.16	1.84
1/17/2016	67.798	66.201	1.597	68.13	66.56	1.57
1/17/2016	67.071	64.661	2.41	66.25	64.94	1.31
1/17/2016	65.658	63.975	1.683	65.41	64.16	1.25
1/17/2016	65.658	63.676	1.982	65.19	63.75	1.44
1/17/2016	65.959	63.719	2.24	64.53	64	0.53
1/17/2016	65.829	64.189	1.64	66	64	2
1/17/2016	66.043	64.959	1.084	66.53	64.88	1.65
1/17/2016	66.558	65.431	1.127	67.69	65.38	2.31
1/17/2016	66.985	65.602	1.383	68	65.63	2.37
1/17/2016	67.586	65.773	1.813	68.09	65.88	2.21
1/17/2016	67.329	65.816	1.513	67.06	65.88	1.18
1/17/2016	66.643	65.431	1.212	67.38	65.5	1.88
1/17/2016	66	65.26	0.74	67.03	65.13	1.9
1/17/2016	65.701	64.959	0.742	66.31	64.59	1.72
1/17/2016	66.087	64.875	1.212	66.03	64.59	1.44
1/17/2016	65.872	64.875	0.997	66.91	64.84	2.07
1/17/2016	66.729	64.574	2.155	65.69	64.72	0.97
1/17/2016	66.173	64.788	1.385	67.31	64.84	2.47
1/17/2016	66.814	64.918	1.896	67.03	65.09	1.94
1/17/2016	67.028	65.046	1.982	66.75	65.28	1.47
1/17/2016	66.558	65.003	1.555	66.81	65.34	1.47
1/17/2016	66.814	65.089	1.725	66.94	65.16	1.78
1/17/2016	67.199	65.046	2.153	66.88	65.16	1.72
1/17/2016	66.087	65.089	0.998	66.5	65.03	1.47
1/17/2016	65.829	64.875	0.954	66.75	64.91	1.84
1/17/2016	66.043	64.788	1.255	65.97	64.78	1.19

1/17/2016	66.043	64.704	1.339	66.47	64.78	1.69
1/17/2016	66.13	64.704	1.426	65.75	64.78	0.97
1/17/2016	66.943	64.617	2.326	66.47	64.78	1.69
1/17/2016	65.745	64.617	1.128	65.56	64.66	0.9
1/17/2016	65.145	64.319	0.826	65.66	64.53	1.13
1/17/2016	65.959	64.148	1.811	65.63	64.16	1.47
1/17/2016	64.974	64.148	0.826	64.94	64.16	0.78
1/17/2016	64.974	64.319	0.655	65.28	64.31	0.97
1/17/2016	65.059	64.446	0.613	65.19	64.44	0.75
1/18/2016	62.834	62.691	0.143	62.75	62.41	0.34
1/18/2016	62.875	65.303	-2.428	65.31	65.13	0.18
1/18/2016	65.745	65.688	0.057	65.81	65.5	0.31
1/18/2016	66.772	66.03	0.742	65.97	66	-0.03
1/18/2016	66.344	66.201	0.143	66.5	66.13	0.37
1/18/2016	67.199	66.416	0.783	66.94	66.38	0.56
1/18/2016	66	65.73	0.27	66.59	66.22	0.37
1/18/2016	63.99	63.505	0.485	64.25	64.03	0.22
1/18/2016	62.319	61.962	0.357	62.69	62.25	0.44
1/18/2016	63.005	62.947	0.058	62.94	62.75	0.19
1/18/2016	64.546	64.275	0.271	65.88	65.16	0.72
1/18/2016	66	65.645	0.355	65.63	65.78	-0.15
1/18/2016	66.558	65.773	0.785	66.03	65.84	0.19
1/18/2016	66.13	66.03	0.1	66.66	65.97	0.69
1/18/2016	66.814	66.288	0.526	66.41	66.22	0.19
1/18/2016	67.028	66.543	0.485	66.72	66.59	0.13
1/18/2016	64.161	63.804	0.357	64.84	64.28	0.56
1/18/2016	63.09	62.391	0.699	64.09	62.5	1.59
1/18/2016	65.615	64.959	0.656	65.47	64.88	0.59
1/18/2016	68.27	67.314	0.956	69	66.78	2.22
1/18/2016	68.871	67.485	1.386	69	67.97	1.03
1/18/2016	66.643	65.431	1.212	66.81	65.59	1.22
1/18/2016	66.043	63.762	2.281	65.16	64.06	1.1
1/18/2016	64.459	62.648	1.811	64.28	62.78	1.5

1/18/2016	63.862	62.261	1.601	63.63	62.38	1.25
1/18/2016	66.772	65.089	1.683	66.19	64.59	1.6
1/18/2016	69.3	67.699	1.601	69.03	67.28	1.75
1/18/2016	68.27	67.314	0.956	69.69	67.94	1.75
1/18/2016	65.959	64.918	1.041	66.53	65.09	1.44
1/18/2016	64.375	63.334	1.041	64.94	63.47	1.47
1/18/2016	63.903	62.304	1.599	63.72	62.44	1.28
1/18/2016	65.059	63.89	1.169	65.28	63.34	1.94
1/18/2016	68.227	66.543	1.684	67.59	66.28	1.31
1/18/2016	70.115	68.984	1.131	70.53	68.91	1.62
1/18/2016	68.356	66.201	2.155	68.06	66.63	1.43
1/18/2016	65.403	64.574	0.829	66.47	64.66	1.81
1/18/2016	64.888	63.419	1.469	64.69	63.66	1.03
1/18/2016	65.102	63.375	1.727	64.88	63.41	1.47
1/18/2016	65.316	63.804	1.512	65.38	63.91	1.47
1/18/2016	67.071	64.747	2.324	65.84	64.91	0.93
1/18/2016	66.9	65.602	1.298	66.56	65.59	0.97
1/18/2016	67.456	66.03	1.426	67.34	66	1.34
1/18/2016	68.571	66.158	2.413	67.44	66.28	1.16
1/18/2016	68.056	66.201	1.855	67.34	66.41	0.93
1/18/2016	67.757	65.773	1.984	67.19	66.16	1.03
1/18/2016	66.729	65.345	1.384	67.44	65.41	2.03
1/18/2016	67.242	65.003	2.239	66.78	65.16	1.62
1/18/2016	66.043	65.003	1.04	66.13	64.91	1.22
1/18/2016	66.985	65.046	1.939	65.91	65.03	0.88
1/18/2016	66.515	64.875	1.64	66.19	65.03	1.16
1/18/2016	66.515	65.089	1.426	67	65.03	1.97
1/18/2016	66.9	65.303	1.597	67.19	65.41	1.78
1/18/2016	66.686	65.431	1.255	67.41	65.53	1.88
1/18/2016	67.071	65.688	1.383	66.63	65.66	0.97
1/18/2016	66.429	65.559	0.87	67.41	65.66	1.75
1/18/2016	66.985	65.345	1.64	66.56	65.41	1.15
1/18/2016	66.344	65.132	1.212	66.91	65.06	1.85

1/18/2016	66.772	64.832	1.94	66.78	64.94	1.84
1/18/2016	66.043	64.875	1.168	67.28	65.06	2.22
1/18/2016	66.472	64.747	1.725	66.38	64.97	1.41
1/18/2016	67.329	64.747	2.582	65.84	64.84	1
1/18/2016	67.372	64.617	2.755	66.22	64.97	1.25
1/18/2016	66.729	65.132	1.597	66.84	65	1.84
1/18/2016	66.9	65.003	1.897	67.25	65.22	2.03
1/18/2016	67.114	65.132	1.982	66.53	65.13	1.4
1/18/2016	66.558	65.303	1.255	67.25	65.25	2
1/18/2016	67.158	65.174	1.984	66.75	65.25	1.5
1/18/2016	66.6	65.345	1.255	67.13	65.13	2
1/18/2016	66.558	65.174	1.384	67.59	65.16	2.43
1/18/2016	66.043	65.003	1.04	66.91	65.03	1.88
1/18/2016	65.701	64.747	0.954	66.56	64.75	1.81
1/18/2016	66.301	64.533	1.768	66.03	64.63	1.4
1/18/2016	66.515	64.148	2.367	65.16	64.38	0.78
1/18/2016	66.214	64.061	2.153	64.97	64.13	0.84
1/18/2016	65.145	63.89	1.255	64.94	64	0.94
1/18/2016	65.059	63.847	1.212	65.44	63.88	1.56
1/18/2016	65.403	63.847	1.556	64.81	63.88	0.93
1/18/2016	65.444	64.018	1.426	64.72	64.13	0.59
1/18/2016	65.059	64.148	0.911	64.91	64.13	0.78
1/18/2016	65.188	64.061	1.127	64.81	64.13	0.68
1/18/2016	64.803	64.232	0.571	65.19	64.13	1.06
1/18/2016	65.059	64.319	0.74	64.97	64.25	0.72
1/18/2016	64.931	64.362	0.569	65.63	64.38	1.25
1/18/2016	66.515	66.03	0.485	66.34	65.75	0.59
1/18/2016	67.928	67.272	0.656	67.59	67.22	0.37
1/18/2016	66.9	66.459	0.441	67.56	66.59	0.97
1/18/2016	65.574	65.003	0.571	65.69	65.22	0.47
1/18/2016	64.589	63.847	0.742	64.81	63.94	0.87
1/18/2016	63.347	62.906	0.441	63.88	63.16	0.72
1/18/2016	63.09	62.733	0.357	63.44	62.66	0.78

1/18/2016	64.418	64.018	0.4	64.28	63.91	0.37
1/18/2016	65.959	65.303	0.656	65.5	65.06	0.44
1/18/2016	66.9	66.416	0.484	66.53	66.25	0.28
1/18/2016	68.356	67.272	1.084	67.44	67	0.44
1/18/2016	67.158	66.801	0.357	67.75	67.19	0.56
1/18/2016	66.258	65.388	0.87	65.78	65.59	0.19
1/19/2016	64.503	64.189	0.314	64.81	64.41	0.4
1/19/2016	63.604	63.204	0.4	63.81	63.41	0.4
1/19/2016	63.005	62.648	0.357	63.19	62.78	0.41
1/19/2016	63.433	63.12	0.313	63.19	62.94	0.25
1/19/2016	62.62	64.918	-2.298	64.38	64.56	-0.18
1/19/2016	65.829	65.645	0.184	65.81	65.47	0.34
1/19/2016	66.515	66.158	0.357	66.5	66.03	0.47
1/19/2016	67.199	66.587	0.612	66.97	66.44	0.53
1/19/2016	67.372	66.885	0.487	67.16	66.81	0.35
1/19/2016	65.959	65.688	0.271	66.09	66.03	0.06
1/19/2016	64.503	64.104	0.399	64.66	64.5	0.16
1/19/2016	63.347	63.077	0.27	63.59	63.34	0.25
1/19/2016	63.048	62.862	0.186	62.94	62.72	0.22
1/19/2016	64.033	63.847	0.186	63.84	63.66	0.18
1/19/2016	65.444	65.26	0.184	65.59	65.28	0.31
1/19/2016	66	65.816	0.184	66.22	65.66	0.56
1/19/2016	66.301	66.288	0.013	66.81	66.22	0.59
1/19/2016	68.443	67.913	0.53	69.34	67.22	2.12
1/19/2016	68.4	67.571	0.829	68.94	68.09	0.85
1/19/2016	66.985	65.987	0.998	68.03	66.22	1.81
1/19/2016	66.087	64.918	1.169	66.59	65.09	1.5
1/19/2016	65.102	64.232	0.87	65	64.19	0.81
1/19/2016	65.444	63.676	1.768	64.69	63.78	0.91
1/19/2016	64.717	63.804	0.913	65.25	63.69	1.56
1/19/2016	65.188	63.975	1.213	66.03	63.88	2.15
1/19/2016	65.574	64.49	1.084	66.47	64.5	1.97
1/19/2016	66.985	64.959	2.026	66.72	64.91	1.81

1/19/2016	67.071	65.431	1.64	66.31	65.69	0.62
1/19/2016	66.686	65.773	0.913	67.75	65.63	2.12
1/19/2016	66.814	65.859	0.955	66.94	65.94	1
1/19/2016	66.9	65.816	1.084	68.09	65.78	2.31
1/19/2016	66.558	65.859	0.699	67.38	65.66	1.72
1/19/2016	67.158	65.517	1.641	67.19	65.5	1.69
1/19/2016	66.643	65.645	0.998	67.88	65.47	2.41
1/19/2016	66.686	65.73	0.956	66.81	65.44	1.37
1/19/2016	67.842	65.474	2.368	66.59	65.69	0.9
1/19/2016	66.857	65.816	1.041	66.84	65.75	1.09
1/19/2016	67.158	66.074	1.084	67.31	65.94	1.37
1/19/2016	67.199	66.245	0.954	68.66	65.94	2.72
1/19/2016	68.185	66.372	1.813	67.81	66.28	1.53
1/19/2016	68.956	66.329	2.627	68.16	66.63	1.53
1/19/2016	68.657	66.416	2.241	68.81	66.66	2.15
1/19/2016	68.698	66.587	2.111	68.97	66.63	2.34
1/19/2016	68.142	66.673	1.469	69.22	66.59	2.63
1/19/2016	67.971	66.587	1.384	69.16	66.59	2.57
1/19/2016	68.443	66.459	1.984	68.38	66.44	1.94
1/19/2016	68.142	66.5	1.642	68.44	66.44	2
1/19/2016	67.714	66.245	1.469	68.28	66.19	2.09
1/19/2016	67.329	66.158	1.171	68.28	66.03	2.25
1/19/2016	68.443	66.074	2.369	67.59	66.03	1.56
1/19/2016	67.885	66.03	1.855	68.28	65.94	2.34
1/19/2016	67.971	65.816	2.155	67.59	65.94	1.65
1/19/2016	67.842	65.474	2.368	67.25	65.78	1.47
1/19/2016	67.586	65.26	2.326	67.25	65.38	1.87
1/19/2016	68.313	65.517	2.796	67.28	65.63	1.65
1/19/2016	67.627	65.688	1.939	66.84	65.63	1.21
1/19/2016	67.971	65.474	2.497	67.41	65.63	1.78
1/19/2016	68.142	65.859	2.283	67.84	65.88	1.96
1/19/2016	67.586	65.816	1.77	67.44	65.75	1.69
1/19/2016	67.586	66.074	1.512	68.22	66	2.22

1/19/2016	68.27	66.115	2.155	68.06	66.16	1.9
1/19/2016	68.013	66.201	1.812	68.59	66.28	2.31
1/19/2016	68.142	66.329	1.813	68.25	66.16	2.09
1/19/2016	68.013	66.288	1.725	68.56	66.28	2.28
1/19/2016	68.871	66.372	2.499	68.22	66.41	1.81
1/19/2016	67.798	66.288	1.51	68.78	66.41	2.37
1/19/2016	68.356	66.201	2.155	68.38	66.28	2.1
1/19/2016	68.527	66.115	2.412	67.91	66.28	1.63
1/19/2016	67.627	65.903	1.724	68	66.03	1.97
1/19/2016	68.099	65.773	2.326	67.41	65.91	1.5
1/19/2016	67.028	65.388	1.64	67.41	65.66	1.75
1/19/2016	67.456	65.174	2.282	66.91	65.28	1.63
1/19/2016	67.199	65.089	2.11	66.13	65.16	0.97
1/19/2016	66.344	64.661	1.683	65.72	64.75	0.97
1/19/2016	65.916	64.362	1.554	65.84	64.5	1.34
1/19/2016	65.102	64.104	0.998	65.53	64.25	1.28
1/19/2016	65.487	63.933	1.554	64.72	64	0.72
1/19/2016	64.76	63.847	0.913	65.25	64	1.25
1/19/2016	64.76	63.804	0.956	64.97	63.88	1.09
1/19/2016	64.589	63.847	0.742	64.97	63.88	1.09
1/19/2016	64.845	63.975	0.87	64.75	64	0.75
1/19/2016	64.974	64.148	0.826	65.69	64.13	1.56
1/19/2016	65.059	64.275	0.784	64.97	64.19	0.78
1/19/2016	65.102	64.446	0.656	65.72	64.5	1.22
1/19/2016	65.316	64.49	0.826	65.5	64.5	1
1/19/2016	65.574	64.446	1.128	65.28	64.5	0.78
1/19/2016	65.273	64.533	0.74	65.34	64.5	0.84
1/19/2016	65.102	64.446	0.656	65.16	64.5	0.66
1/19/2016	64.888	64.319	0.569	65.41	64.5	0.91
1/19/2016	64.974	64.275	0.699	65.03	64.38	0.65
1/19/2016	64.888	64.446	0.442	65.44	64.38	1.06
1/19/2016	65.017	64.49	0.527	65.13	64.5	0.63
1/19/2016	65.359	64.49	0.869	65.34	64.5	0.84

1/19/2016	65.273	64.446	0.827	65.03	64.5	0.53
1/19/2016	64.931	64.403	0.528	65.03	64.38	0.65
1/19/2016	64.888	64.362	0.526	64.94	64.5	0.44
1/20/2016	64.888	64.362	0.526	64.94	64.38	0.56
1/20/2016	64.803	64.362	0.441	64.81	64.38	0.43
1/20/2016	64.803	64.362	0.441	64.81	64.38	0.43
1/20/2016	64.76	64.275	0.485	64.69	64.38	0.31
1/20/2016	64.674	64.189	0.485	64.59	64.38	0.21
1/20/2016	64.546	64.232	0.314	64.72	64.25	0.47
1/20/2016	64.632	64.319	0.313	64.72	64.38	0.34
1/20/2016	64.845	64.49	0.355	64.84	64.5	0.34
1/20/2016	65.188	64.788	0.4	65.09	64.78	0.31
1/20/2016	65.872	65.132	0.74	65.56	65.13	0.43
1/20/2016	65.615	65.474	0.141	66.34	65.38	0.96
1/20/2016	65.658	65.431	0.227	65.81	65.5	0.31
1/20/2016	65.359	64.918	0.441	65.28	65.13	0.15
1/20/2016	64.546	64.148	0.398	64.91	64.34	0.57
1/20/2016	63.648	63.334	0.314	64	63.56	0.44
1/20/2016	63.262	62.691	0.571	63.34	62.94	0.4
1/20/2016	62.834	62.391	0.443	62.97	62.56	0.41
1/20/2016	64.503	64.148	0.355	65.41	63.53	1.88
1/20/2016	67.971	67.015	0.956	67.84	66.81	1.03
1/20/2016	70.63	69.157	1.473	70.81	68.91	1.9
1/20/2016	68.999	67.699	1.3	69.88	68.09	1.79
1/20/2016	66.943	65.987	0.956	67.88	66.16	1.72
1/20/2016	66.13	64.403	1.727	66.19	64.88	1.31
1/20/2016	64.674	63.676	0.998	66.03	63.81	2.22
1/20/2016	64.503	63.161	1.342	64.72	63.38	1.34
1/20/2016	65.059	63.204	1.855	65.03	63.25	1.78
1/20/2016	64.803	63.59	1.213	64.91	63.63	1.28
1/20/2016	65.444	64.148	1.296	65.22	64.03	1.19
1/20/2016	65.53	64.661	0.869	66.06	64.66	1.4
1/20/2016	66.385	64.959	1.426	66.34	65.06	1.28

1/20/2016	66.385	65.303	1.082	67.47	65.31	2.16
1/20/2016	66.9	65.345	1.555	66.72	65.47	1.25
1/20/2016	66.985	65.217	1.768	66.63	65.31	1.32
1/20/2016	66.173	65.132	1.041	66.31	65.06	1.25
1/20/2016	66.214	65.345	0.869	66.84	65.13	1.71
1/20/2016	67.028	65.174	1.854	66.31	65.13	1.18
1/20/2016	67.885	65.517	2.368	68.03	65.41	2.62
1/20/2016	68.313	65.773	2.54	67.88	66.22	1.66
1/20/2016	67.028	65.559	1.469	67.13	65.66	1.47
1/20/2016	67.798	66.329	1.469	68.84	66.72	2.12
1/20/2016	66.814	65.345	1.469	66.81	65.66	1.15
1/20/2016	66.087	64.788	1.299	66.78	65	1.78
1/20/2016	65.53	64.533	0.997	66.47	64.5	1.97
1/20/2016	66	64.403	1.597	66.31	64.5	1.81
1/20/2016	65.916	64.533	1.383	66.91	64.63	2.28
1/20/2016	66.558	64.49	2.068	65.56	64.59	0.97
1/20/2016	66.13	64.832	1.298	67.06	64.81	2.25
1/20/2016	66.385	65.26	1.125	66.53	65.09	1.44
1/20/2016	66.643	65.517	1.126	66.78	65.34	1.44
1/20/2016	67.372	65.645	1.727	67	65.53	1.47
1/20/2016	67.413	65.602	1.811	67.13	65.53	1.6
1/20/2016	67.242	65.645	1.597	67.28	65.66	1.62
1/20/2016	67.114	65.645	1.469	67.31	65.53	1.78
1/20/2016	67.199	65.602	1.597	67.44	65.53	1.91
1/20/2016	67.627	65.431	2.196	67.38	65.53	1.85
1/20/2016	68.185	65.602	2.583	66.94	65.53	1.41
1/20/2016	67.329	65.602	1.727	67.19	65.53	1.66
1/20/2016	67.5	65.303	2.197	67.09	65.25	1.84
1/20/2016	64.76	65.944	-1.184	67.59	65.66	1.93
1/20/2016	64.074	64.959	-0.885	66.16	65.16	1
1/20/2016	67.671	66.459	1.212	69.78	67.59	2.19
1/20/2016	70.759	69.542	1.217	70.66	68.91	1.75
1/20/2016	71.577	69.629	1.948	71.25	69.75	1.5

1/20/2016	70.673	68.599	2.074	70.47	68.94	1.53
1/20/2016	69.042	67.4	1.642	69	67.63	1.37
1/20/2016	67.885	65.987	1.898	68.31	66.34	1.97
1/20/2016	66.13	64.832	1.298	65.88	65.06	0.82
1/20/2016	64.974	64.148	0.826	65.91	64.44	1.47
1/20/2016	64.632	63.762	0.87	65.19	63.94	1.25
1/20/2016	64.717	63.548	1.169	64.81	63.69	1.12
1/20/2016	64.375	63.548	0.827	64.63	63.56	1.07
1/20/2016	64.845	63.633	1.212	65.41	63.69	1.72
1/20/2016	64.803	63.89	0.913	64.59	63.81	0.78
1/20/2016	65.017	64.148	0.869	64.91	64.06	0.85
1/20/2016	65.574	64.362	1.212	65.5	64.31	1.19
1/20/2016	65.188	64.574	0.614	65.94	64.56	1.38
1/20/2016	65.102	64.617	0.485	65.97	64.69	1.28
1/20/2016	65.745	64.704	1.041	65.47	64.81	0.66
1/20/2016	65.487	64.832	0.655	65.41	64.81	0.6
1/20/2016	66.043	64.788	1.255	65.28	64.81	0.47
1/20/2016	65.359	64.875	0.484	66.34	64.94	1.4
1/20/2016	65.444	64.959	0.485	65.72	64.94	0.78
1/20/2016	65.829	64.959	0.87	65.75	65.06	0.69
1/20/2016	65.359	65.003	0.356	66.41	65.06	1.35
1/20/2016	66.214	64.959	1.255	65.5	65.06	0.44
1/20/2016	65.53	65.003	0.527	65.5	65.06	0.44
1/20/2016	66.214	64.918	1.296	65.47	65.06	0.41
1/20/2016	65.403	64.959	0.444	65.5	64.94	0.56
1/20/2016	65.487	64.918	0.569	65.41	65.06	0.35
1/21/2016	65.273	64.918	0.355	65.38	64.94	0.44
1/21/2016	65.359	65.046	0.313	65.63	64.94	0.69
1/21/2016	65.487	65.174	0.313	65.34	65.06	0.28
1/21/2016	65.701	65.26	0.441	65.59	65.31	0.28
1/21/2016	65.788	65.388	0.4	65.75	65.31	0.44
1/21/2016	65.872	65.474	0.398	65.84	65.44	0.4
1/21/2016	65.788	65.559	0.229	66.38	65.56	0.82

1/21/2016	65.829	65.73	0.099	66.31	65.69	0.62
1/21/2016	66.043	65.859	0.184	66.19	65.81	0.38
1/21/2016	66.173	65.903	0.27	66.16	65.94	0.22
1/21/2016	66.643	65.987	0.656	66.66	65.94	0.72
1/21/2016	66.472	66.074	0.398	66.47	66.06	0.41
1/21/2016	66.214	66.158	0.056	66.75	66.06	0.69
1/21/2016	66.643	66.158	0.485	66.38	66.19	0.19
1/21/2016	66.558	66.245	0.313	66.84	66.19	0.65
1/21/2016	66.558	66.329	0.229	66.72	66.31	0.41
1/21/2016	66.429	66.543	-0.114	67.34	66.44	0.9
1/21/2016	68.527	67.614	0.913	69.75	66.81	2.94
1/21/2016	68.956	67.742	1.214	69.38	67.56	1.82
1/21/2016	69.685	67.913	1.772	69.28	67.84	1.44
1/21/2016	69.685	67.956	1.729	69.88	67.97	1.91
1/21/2016	69.6	67.872	1.728	69.75	68.09	1.66
1/21/2016	69.343	68.257	1.086	70.34	68.22	2.12
1/21/2016	69.643	68.385	1.258	70.31	68.34	1.97
1/21/2016	69.901	68.556	1.345	70.16	68.47	1.69
1/21/2016	70.201	68.599	1.602	70.09	68.59	1.5
1/21/2016	70.329	68.77	1.559	70.34	68.75	1.59
1/21/2016	70.716	68.813	1.903	70.13	68.88	1.25
1/21/2016	70.286	68.984	1.302	70.63	69	1.63
1/21/2016	70.502	68.943	1.559	70.56	69	1.56
1/21/2016	70.93	69.071	1.859	70.69	69.13	1.56
1/21/2016	71.49	69.242	2.248	70.38	69.25	1.13
1/21/2016	70.846	69.285	1.561	70.84	69.41	1.43
1/21/2016	70.803	69.456	1.347	70.69	69.28	1.41
1/21/2016	69.901	67.571	2.33	68.16	66.97	1.19
1/21/2016	70.887	69.843	1.044	71.09	69.16	1.93
1/21/2016	71.06	69.157	1.903	70.69	69.38	1.31
1/21/2016	70.158	68	2.158	69.97	68.34	1.63
1/21/2016	68.657	66.459	2.198	68.41	66.88	1.53
1/21/2016	66.515	65.174	1.341	68	65.47	2.53

1/21/2016	65.188	64.189	0.999	66.06	64.34	1.72
1/21/2016	64.803	63.419	1.384	65.81	63.59	2.22
1/21/2016	64.803	62.947	1.856	64.63	63.22	1.41
1/21/2016	64.418	62.648	1.77	63.91	62.84	1.07
1/21/2016	63.518	62.434	1.084	63.09	62.47	0.62
1/21/2016	63.433	62.261	1.172	63.78	62.44	1.34
1/21/2016	63.99	62.648	1.342	63.5	62.56	0.94
1/21/2016	64.632	63.933	0.699	64.66	63.59	1.07
1/21/2016	66.429	64.788	1.641	66.34	64.72	1.62
1/21/2016	66.429	65.944	0.485	66.22	65.63	0.59
1/21/2016	67.456	66.587	0.869	67.34	66.5	0.84
1/21/2016	68.099	67.143	0.956	67.59	67.06	0.53
1/21/2016	67.158	66.03	1.128	68.25	66.53	1.72
1/21/2016	65.273	64.832	0.441	66.41	65	1.41
1/21/2016	64.503	63.762	0.741	64.72	63.84	0.88
1/21/2016	63.648	63.033	0.615	63.91	63.22	0.69
1/21/2016	63.518	62.947	0.571	63.25	62.84	0.41
1/21/2016	64.418	64.319	0.099	64.34	63.72	0.62
1/21/2016	65.316	65.217	0.099	65.94	64.91	1.03
1/21/2016	66.301	65.474	0.827	65.91	65.53	0.38
1/21/2016	66.686	65.773	0.913	66.22	65.78	0.44
1/21/2016	66.558	65.944	0.614	66.66	65.94	0.72
1/21/2016	66.385	66.201	0.184	67	66.06	0.94
1/21/2016	67.114	66.115	0.999	66.25	66.19	0.06
1/21/2016	65.403	65.217	0.186	66.56	65.5	1.06
1/21/2016	64.247	63.933	0.314	64.5	64.19	0.31
1/22/2016	63.09	62.776	0.314	63.38	63.06	0.32
1/22/2016	62.704	62.819	-0.115	62.94	62.56	0.38
1/22/2016	66.772	65.903	0.869	67.75	66.06	1.69
1/22/2016	69.3	67.571	1.729	68.56	67.09	1.47
1/22/2016	69.814	68.298	1.516	69.59	68.41	1.18
1/22/2016	67.543	66.372	1.171	68.34	66.69	1.65
1/22/2016	66.301	64.788	1.513	66.44	65.22	1.22

1/22/2016	64.717	63.59	1.127	66.06	63.91	2.15
1/22/2016	64.76	62.947	1.813	64.41	63.16	1.25
1/22/2016	64.375	62.733	1.642	64.25	62.94	1.31
1/22/2016	65.788	63.548	2.24	64.16	63.31	0.85
1/22/2016	66.6	65.089	1.511	65.97	64.78	1.19
1/22/2016	67.413	66.5	0.913	68.09	66.16	1.93
1/22/2016	69.386	67.699	1.687	69	67.47	1.53
1/22/2016	67.627	66.758	0.869	68.75	67.22	1.53
1/22/2016	66.643	65.217	1.426	67.22	65.56	1.66
1/22/2016	66.558	64.148	2.41	65.5	64.38	1.12
1/22/2016	64.76	63.462	1.298	64.25	63.56	0.69
1/22/2016	64.288	63.077	1.211	63.97	63.06	0.91
1/22/2016	65.273	63.419	1.854	63.91	62.94	0.97
1/22/2016	66.385	65.174	1.211	65.97	64.75	1.22
1/22/2016	68.443	66.714	1.729	67.84	66.41	1.43
1/22/2016	69.256	67.913	1.343	68.75	67.47	1.28
1/22/2016	68.614	66.543	2.071	68.22	66.94	1.28
1/22/2016	66.472	65.132	1.34	65.91	65.19	0.72
1/22/2016	66.043	64.061	1.982	65.22	64.06	1.16
1/22/2016	64.674	63.762	0.912	65.56	63.69	1.87
1/22/2016	65.102	63.633	1.469	65.81	63.56	2.25
1/22/2016	66.13	63.975	2.155	65.47	63.94	1.53
1/22/2016	66.943	64.533	2.41	66.16	64.44	1.72
1/22/2016	65.916	64.959	0.957	67.06	64.94	2.12
1/22/2016	66.087	65.345	0.742	67.59	65.09	2.5
1/22/2016	67.456	65.688	1.768	67.75	65.72	2.03
1/22/2016	67.842	65.645	2.197	67.13	65.72	1.41
1/22/2016	67.928	65.688	2.24	67.13	65.72	1.41
1/22/2016	67.158	65.602	1.556	67.28	65.72	1.56
1/22/2016	66.258	65.474	0.784	67.59	65.34	2.25
1/22/2016	66.258	65.303	0.955	66.5	65.22	1.28
1/22/2016	66.385	65.303	1.082	66.13	65.09	1.04
1/22/2016	66.385	65.132	1.253	67.44	65.09	2.35

1/22/2016	66.385	64.959	1.426	67.03	65.09	1.94
1/22/2016	66.344	65.046	1.298	66.53	64.84	1.69
1/22/2016	67.158	64.959	2.199	67.19	64.97	2.22
1/22/2016	66.173	64.959	1.214	66.94	64.97	1.97
1/22/2016	66.643	65.003	1.64	66.41	64.84	1.57
1/22/2016	66.686	64.788	1.898	67.5	64.84	2.66
1/22/2016	66.043	65.217	0.826	67.44	64.97	2.47
1/22/2016	67.627	65.388	2.239	66.56	65.22	1.34
1/22/2016	67.028	65.602	1.426	67.47	65.47	2
1/22/2016	67.114	65.688	1.426	67.31	65.59	1.72
1/22/2016	66.9	65.431	1.469	67.69	65.47	2.22
1/22/2016	64.632	65.174	-0.542	66.63	65.03	1.6
1/22/2016	65.916	64.788	1.128	66.84	64.78	2.06
1/22/2016	66	64.788	1.212	67.16	64.66	2.5
1/22/2016	66.214	64.574	1.64	66.88	64.53	2.35
1/22/2016	66.643	64.661	1.982	66.19	64.53	1.66
1/22/2016	65.615	64.574	1.041	66.47	64.53	1.94
1/22/2016	65.316	64.446	0.87	65.19	64.28	0.91
1/22/2016	64.845	64.104	0.741	66	64.03	1.97
1/22/2016	65.829	63.847	1.982	64.72	63.91	0.81
1/22/2016	65.487	64.788	0.699	65.69	64.41	1.28
1/22/2016	66.857	66.074	0.783	66.91	65.66	1.25
1/22/2016	67.885	67.4	0.485	67.47	66.91	0.56
1/22/2016	67.543	66.673	0.87	68.63	66.88	1.75
1/22/2016	65.829	65.089	0.74	65.94	65.34	0.6
1/22/2016	64.717	63.933	0.784	64.97	63.97	1
1/22/2016	63.732	62.99	0.742	63.84	63.09	0.75
1/22/2016	63.775	62.99	0.785	63.22	62.59	0.63
1/22/2016	64.288	63.633	0.655	64.25	63.34	0.91
1/22/2016		65.345		66.28	64.97	1.31
1/22/2016	66	65.388	0.612	66.31	65.47	0.84
1/22/2016	66.13	65.688	0.442	65.69	65.34	0.35
1/22/2016	67.329	66.372	0.957	66.44	66.09	0.35

1/22/2016	68.185	66.885	1.3	67.34	66.72	0.62
1/22/2016	67.798	67.528	0.27	67.63	67.22	0.41
1/22/2016	66.6	65.388	1.212	65.94	65.72	0.22
1/22/2016	64.288	63.719	0.569	64.47	63.97	0.5
1/22/2016	63.347	62.562	0.785	63.22	62.84	0.38
1/22/2016	63.475	62.776	0.699	62.81	62.47	0.34
1/23/2016	65.615	65.303	0.312	65.56	65.22	0.34
1/23/2016	65.701	65.602	0.099	65.56	65.34	0.22
1/23/2016	66.515	66.03	0.485	66.28	65.72	0.56
1/23/2016	66.729	66.5	0.229	66.38	66.09	0.29
1/23/2016	66.686	66.844	-0.158	66.91	66.47	0.44
1/23/2016	67.114	66.758	0.356	67.06	66.72	0.34
1/23/2016	64.632	64.061	0.571	64.88	64.5	0.38
1/23/2016	62.791	62.304	0.487	62.88	62.66	0.22
1/23/2016	63.005	63.033	-0.028	62.63	62.53	0.1
1/23/2016	67.071	66.372	0.699	67.72	66	1.72
1/23/2016	70.029	68.642	1.387	69	67.81	1.19
1/23/2016	69.643	67.829	1.814	69.56	68.44	1.12
1/23/2016	66.429	65.26	1.169	67.38	65.59	1.79
1/23/2016	64.717	63.291	1.426	64.97	63.59	1.38
1/23/2016	63.262	62.434	0.828	64.38	62.34	2.04
1/23/2016	64.117	63.12	0.997	64.06	62.47	1.59
1/23/2016	66.643	65.174	1.469	65.78	64.63	1.15
1/23/2016	69.042	67.528	1.514	67.78	67.03	0.75
1/23/2016	70.029	68.171	1.858	70.09	68.97	1.12
1/23/2016	66.429	65.303	1.126	67.81	65.88	1.93
1/23/2016	64.418	63.334	1.084	66	63.56	2.44
1/23/2016	63.775	62.348	1.427	63.81	62.44	1.37
1/23/2016	64.546	63.419	1.127	64.22	62.81	1.41
1/23/2016	66.385	65.73	0.655	66.38	64.84	1.54
1/23/2016	68.443	67.699	0.744	68.72	67	1.72
1/23/2016	69.343	67.956	1.387	70.59	68.63	1.96
1/23/2016	66.772	65.431	1.341	67.75	65.94	1.81

1/23/2016	64.931	63.676	1.255	66.13	63.94	2.19
1/23/2016	64.074	62.862	1.212	64.31	62.94	1.37
1/23/2016	64.161	62.906	1.255	63.91	62.69	1.22
1/23/2016	67.627	65.388	2.239	65.5	64.78	0.72
1/23/2016	69.17	67.872	1.298	68.66	67.28	1.38
1/23/2016	68.828	67.785	1.043	70.03	68.06	1.97
1/23/2016	67.242	65.559	1.683	67.09	65.84	1.25
1/23/2016	65.574	64.104	1.47	65.56	64.34	1.22
1/23/2016	64.459	63.375	1.084	64.97	63.34	1.63
1/23/2016	64.503	63.12	1.383	65.09	63.09	2
1/23/2016	65.959	63.676	2.283	64.81	63.47	1.34
1/23/2016	68.4	66.329	2.071	66.5	65.63	0.87
1/23/2016	70.329	68.428	1.901	69.19	68.19	1
1/23/2016	68.313	66.673	1.64	68.13	66.81	1.32
1/23/2016	67.456	65.174	2.282	66.84	65.56	1.28
1/23/2016	66.043	64.49	1.553	65.84	64.69	1.15
1/23/2016	65.188	63.89	1.298	65.34	63.81	1.53
1/23/2016	64.717	63.633	1.084	65.84	63.56	2.28
1/23/2016	65.188	64.018	1.17	65.22	63.69	1.53
1/23/2016	66.686	64.446	2.24	64.94	64.31	0.63
1/23/2016	67.028	64.832	2.196	65.75	64.72	1.03
1/23/2016	67.842	65.816	2.026	66.72	65.72	1
1/23/2016	67.285	65.987	1.298	67.25	65.97	1.28
1/23/2016	67.285	66.115	1.17	68.13	65.97	2.16
1/23/2016	67.671	66.03	1.641	68.06	65.97	2.09
1/23/2016	67.627	65.645	1.982	67.19	65.72	1.47
1/23/2016	67.885	65.217	2.668	66.25	65.22	1.03
1/23/2016	66.686	65.089	1.597	67.72	64.97	2.75
1/23/2016	66.558	64.918	1.64	66.38	64.84	1.54
1/23/2016	66.043	64.747	1.296	66.59	64.72	1.87
1/23/2016	66.214	64.747	1.467	67.47	64.72	2.75
1/23/2016	66.087	64.959	1.128	66.31	64.72	1.59
1/23/2016	67.114	64.959	2.155	66.44	64.84	1.6

1/23/2016	66.772	65.089	1.683	66.22	64.97	1.25
1/23/2016	67.671	65.132	2.539	65.97	65.22	0.75
1/23/2016	66.814	65.132	1.682	66.91	65.06	1.85
1/23/2016	66.472	64.918	1.554	67	64.94	2.06
1/23/2016	66.087	64.704	1.383	65.75	64.69	1.06
1/23/2016	66.087	64.446	1.641	65.44	64.44	1
1/23/2016	65.359	64.232	1.127	65.53	64.19	1.34
1/23/2016	65.359	64.189	1.17	65.16	64.06	1.1
1/23/2016	65.017	64.232	0.785	64.78	64.06	0.72
1/23/2016	65.403	64.788	0.615	65.06	64.19	0.87
1/23/2016	66.943	66.158	0.785	67.31	65.84	1.47
1/23/2016	69.085	67.614	1.471	68.09	67.16	0.93
1/23/2016	67.329	66.63	0.699	67.84	67.06	0.78
1/23/2016	65.829	65.046	0.783	66	65.22	0.78
1/23/2016	64.546	63.762	0.784	64.59	63.81	0.78
1/23/2016	63.903	62.947	0.956	63.69	63.06	0.63
1/23/2016	63.648	62.99	0.658	63.34	62.56	0.78
1/23/2016	64.632	63.719	0.913	64.38	63.69	0.69
1/23/2016	65.316	64.788	0.528	65.03	64.44	0.59
1/23/2016	66	65.602	0.398	66.03	65.44	0.59
1/23/2016	66.558	66.416	0.142	67	66.06	0.94
1/23/2016	68.27	67.143	1.127	67.03	66.94	0.09
1/23/2016	68.4	67.658	0.742	68	67.44	0.56
1/23/2016	66.214	65.688	0.526	66.88	65.91	0.97
1/23/2016	64.503	63.975	0.528	64.59	64.28	0.31
1/23/2016	63.347	62.776	0.571	63.34	63.03	0.31
1/23/2016	62.962	62.691	0.271	62.69	62.41	0.28
1/24/2016	65.23	65.089	0.141	65.63	65.28	0.35
1/24/2016	65.916	65.559	0.357	65.63	65.28	0.35
1/24/2016	66.13	65.773	0.357	66	65.63	0.37
1/24/2016	66.344	66.074	0.27	66.25	65.91	0.34
1/24/2016	66.6	66.372	0.228	66.5	66.03	0.47
1/24/2016	67.798	66.758	1.04	66.47	66.53	-0.06

1/24/2016	66.301	65.944	0.357	66.88	66.38	0.5
1/24/2016	64.546	64.018	0.528	64.75	64.38	0.37
1/24/2016	63.005	62.562	0.443	63.09	62.84	0.25
1/24/2016	63.005	62.776	0.229	62.84	62.47	0.37
1/24/2016	66.9	66.372	0.528	67.34	65.94	1.4
1/24/2016	69.557	68.298	1.259	68.53	67.56	0.97
1/24/2016	69.685	67.785	1.9	69.72	68.34	1.38
1/24/2016	67.242	65.773	1.469	66.91	66.06	0.85
1/24/2016	65.273	63.975	1.298	66.16	64.22	1.94
1/24/2016	64.375	63.033	1.342	64.44	63.22	1.22
1/24/2016	63.946	62.691	1.255	64.47	62.72	1.75
1/24/2016	65.788	64.232	1.556	65.03	63.66	1.37
1/24/2016	68.999	66.801	2.198	66.97	66.03	0.94
1/24/2016	70.716	68.727	1.989	69.06	68.31	0.75
1/24/2016	67.971	66.201	1.77	67.75	66.69	1.06
1/24/2016	66.729	64.319	2.41	65.91	64.69	1.22
1/24/2016	64.632	63.419	1.213	65.56	63.53	2.03
1/24/2016	64.288	62.819	1.469	64.38	62.91	1.47
1/24/2016	64.974	63.933	1.041	64.47	63.06	1.41
1/24/2016	67.627	66.074	1.553	67.41	65.78	1.63
1/24/2016	70.201	68.513	1.688	68.91	67.94	0.97
1/24/2016	69.256	67.143	2.113	69	67.69	1.31
1/24/2016	67.586	65.944	1.642	68.31	66.13	2.18
1/24/2016	66.729	65.132	1.597	66.44	65.25	1.19
1/24/2016	66.9	64.617	2.283	65.94	64.59	1.35
1/24/2016	65.916	64.403	1.513	65.78	64.34	1.44
1/24/2016	66.429	64.446	1.983	65.31	64.22	1.09
1/24/2016	67.028	64.918	2.11	65.78	64.59	1.19
1/24/2016	66.043	65.303	0.74	67.22	65.09	2.13
1/24/2016	66.857	65.773	1.084	67.72	65.59	2.13
1/24/2016	67.372	66.372	1	67.91	66.09	1.82
1/24/2016	68.013	66.5	1.513	68.66	66.34	2.32
1/24/2016	67.842	66.63	1.212	68.09	66.47	1.62

1/24/2016	68.356	66.543	1.813	67.53	66.34	1.19
1/24/2016	68.571	66.372	2.199	67.31	66.47	0.84
1/24/2016	68.785	66.372	2.413	67.31	66.34	0.97
1/24/2016	67.028	66.158	0.87	67.44	66.09	1.35
1/24/2016	66.686	65.987	0.699	67.31	65.75	1.56
1/24/2016	66.943	65.816	1.127	67.44	65.72	1.72
1/24/2016	66.9	65.602	1.298	67.75	65.59	2.16
1/24/2016	67.158	65.559	1.599	67	65.59	1.41
1/24/2016	67.798	65.602	2.196	66.59	65.47	1.12
1/24/2016	66.814	65.602	1.212	67.06	65.47	1.59
1/24/2016	66.857	65.645	1.212	66.84	65.47	1.37
1/24/2016	66.943	65.517	1.426	67.16	65.47	1.69
1/24/2016	68.185	65.559	2.626	66.81	65.47	1.34
1/24/2016	67.5	65.559	1.941	67.59	65.63	1.96
1/24/2016	67.714	65.602	2.112	67.22	65.59	1.63
1/24/2016	67.928	65.645	2.283	67.47	65.59	1.88
1/24/2016	66.857	65.559	1.298	67.06	65.59	1.47
1/24/2016	66.772	65.688	1.084	67.31	65.47	1.84
1/24/2016	67.671	65.431	2.24	66.5	65.34	1.16
1/24/2016	66.772	65.345	1.427	67.16	65.22	1.94
1/24/2016	66.9	65.26	1.64	67.72	65.34	2.38
1/24/2016	67.158	65.174	1.984	66.72	65.22	1.5
1/24/2016	66.472	65.046	1.426	66.69	64.97	1.72
1/24/2016	66.857	64.875	1.982	66.25	64.84	1.41
1/24/2016	66.385	64.832	1.553	65.91	64.84	1.07
1/24/2016	66.686	64.704	1.982	66.44	64.72	1.72
1/24/2016	65.829	64.617	1.212	65.84	64.59	1.25
1/24/2016	66.472	64.617	1.855	66.16	64.59	1.57
1/24/2016	65.444	64.49	0.954	66.13	64.47	1.66
1/24/2016	65.829	64.446	1.383	65.38	64.47	0.91
1/24/2016	65.403	64.49	0.913	65.56	64.34	1.22
1/24/2016	65.658	64.574	1.084	65.47	64.47	1
1/25/2016	65.701	65.089	0.612	65.53	64.97	0.56

1/25/2016	65.745	65.132	0.613	65.53	65.09	0.44
1/25/2016	65.444	65.089	0.355	65.5	65.09	0.41
1/25/2016	65.403	65.046	0.357	65.47	64.97	0.5
1/25/2016	65.403	65.003	0.4	65.47	64.97	0.5
1/25/2016	65.403	65.003	0.4	65.31	64.97	0.34
1/25/2016	65.359	64.959	0.4	65.28	64.84	0.44
1/25/2016	65.487	64.959	0.528	65.28	64.84	0.44
1/25/2016	65.403	65.003	0.4	65.38	64.84	0.54
1/25/2016	65.316	64.959	0.357	65.41	64.84	0.57
1/25/2016	65.316	64.918	0.398	65.28	64.84	0.44
1/25/2016	65.188	64.832	0.356	65.16	64.84	0.32
1/25/2016	65.359	64.832	0.527	65.19	64.72	0.47
1/25/2016	65.316	64.832	0.484	65.16	64.72	0.44
1/25/2016	65.273	64.788	0.485	65.16	64.72	0.44
1/25/2016	65.23	64.875	0.355	65.25	64.72	0.53
1/25/2016	65.359	65.003	0.356	65.41	64.84	0.57
1/25/2016	66.643	66.074	0.569	67.97	65.09	2.88
1/25/2016	67.372	66.074	1.298	68.47	65.88	2.59
1/25/2016	68.698	66.201	2.497	67.44	66.13	1.31
1/25/2016	67.928	66.372	1.556	67.16	66.25	0.91
1/25/2016	67.714	66.201	1.513	67.56	66.25	1.31
1/25/2016	67.543	66.158	1.385	67.03	66	1.03
1/25/2016	68.443	66.074	2.369	67.09	66	1.09
1/25/2016	66.814	65.987	0.827	67.75	66	1.75
1/25/2016	67.928	65.987	1.941	67.84	66	1.84
1/25/2016	67.798	65.987	1.811	67.72	66	1.72
1/25/2016	67.329	65.944	1.385	66.84	65.88	0.96
1/25/2016	66.857	65.645	1.212	67.53	65.75	1.78
1/25/2016	66.515	65.431	1.084	67.19	65.38	1.81
1/25/2016	66.6	65.217	1.383	66.75	65.25	1.5
1/25/2016	66.472	65.174	1.298	66.25	65.13	1.12
1/25/2016	66.814	64.959	1.855	66.28	64.88	1.4
1/25/2016	65.829	65.046	0.783	65.91	64.88	1.03

1/25/2016	66.258	65.217	1.041	66.13	65	1.13
1/25/2016	67.158	65.517	1.641	66.53	65.25	1.28
1/25/2016	67.199	66.03	1.169	67.69	65.75	1.94
1/25/2016	68.227	66.543	1.684	68.31	66.25	2.06
1/25/2016	68.484	67.186	1.298	69.53	66.88	2.65
1/25/2016	69.343	67.829	1.514	70	67.5	2.5
1/25/2016	70.93	68.513	2.417	69.97	68.13	1.84
1/25/2016	71.791	69.157	2.634	70.88	68.88	2
1/25/2016	71.964	69.585	2.379	71.59	69.38	2.21
1/25/2016	72.523	70.1	2.423	71.91	69.88	2.03
1/25/2016	72.696	70.442	2.254	73.09	70.25	2.84
1/25/2016	73.256	70.658	2.598	72.84	70.5	2.34
1/25/2016	72.307	70.615	1.692	73.16	70.63	2.53
1/25/2016	72.61	70.701	1.909	72.66	70.5	2.16
1/25/2016	72.523	70.786	1.737	73.56	70.63	2.93
1/25/2016	72.739	70.658	2.081	72.69	70.5	2.19
1/25/2016	72.739	70.485	2.254	72.5	70.5	2
1/25/2016	72.351	70.572	1.779	72.69	70.5	2.19
1/25/2016	72.696	70.572	2.124	72.47	70.5	1.97
1/25/2016	72.437	70.529	1.908	72.88	70.5	2.38
1/25/2016	72.307	70.485	1.822	72.97	70.5	2.47
1/25/2016	72.826	70.829	1.997	73.47	70.63	2.84
1/25/2016	73.299	71.087	2.212	73.16	70.88	2.28
1/25/2016	73.645	71.517	2.128	73.69	71.25	2.44
1/25/2016	74.206	71.69	2.516	74.28	71.5	2.78
1/25/2016	74.813	72.033	2.78	74.53	71.88	2.65
1/25/2016	75.247	72.248	2.999	74.97	72.16	2.81
1/25/2016	75.074	72.55	2.524	75.63	72.53	3.1
1/25/2016	75.81	72.807	3.003	75.53	72.66	2.87
1/25/2016	75.463	72.894	2.569	75.88	72.78	3.1
1/25/2016	75.42	72.807	2.613	75.44	72.78	2.66
1/25/2016	75.376	72.678	2.698	75.53	72.66	2.87
1/25/2016	75.16	72.593	2.567	75.69	72.66	3.03

1/25/2016	74.813	72.291	2.522	75.31	72.41	2.9
1/25/2016	74.12	72.077	2.043	75.25	72.16	3.09
1/25/2016	74.163	71.69	2.473	74.56	71.78	2.78
1/25/2016	73.386	71.173	2.213	74.31	71.38	2.93
1/25/2016	72.826	70.701	2.125	73.13	70.81	2.32
1/25/2016	72.394	70.185	2.209	72.19	70.38	1.81
1/25/2016	70.716	69.629	1.087	71.41	69.75	1.66
1/25/2016	70.887	68.813	2.074	69.91	69.13	0.78
1/25/2016	69.557	68.428	1.129	69.72	68.63	1.09
1/25/2016	70.115	67.913	2.202	69.09	68	1.09
1/25/2016	69.085	67.4	1.685	68.69	67.63	1.06
1/25/2016	68.443	66.714	1.729	67.88	66.88	1
1/25/2016	68.185	66.416	1.769	67.34	66.5	0.84
1/25/2016	67.671	66.115	1.556	67.16	66.25	0.91
1/25/2016	67.158	65.987	1.171	67.16	66	1.16
1/25/2016	66.344	65.645	0.699	66.88	65.75	1.13
1/25/2016	66.985	65.217	1.768	65.97	65.38	0.59
1/25/2016	65.829	65.003	0.826	66.47	65.13	1.34
1/25/2016	65.701	64.875	0.826	65.69	65	0.69
1/25/2016	65.059	64.189	0.87	65.06	64.38	0.68
1/25/2016	64.418	63.334	1.084	64.41	63.63	0.78
1/25/2016	63.561	62.733	0.828	63.91	63	0.91
1/25/2016	63.262	62.348	0.914	63.16	62.5	0.66
1/25/2016	63.219	62.261	0.958	62.84	62.25	0.59
1/25/2016	63.048	62.133	0.915	62.88	62.25	0.63
1/25/2016	62.919	62.304	0.615	62.94	62.25	0.69
1/25/2016	63.304	62.605	0.699	63.06	62.5	0.56
1/25/2016	63.518	62.947	0.571	63.44	62.75	0.69
1/25/2016	63.648	63.204	0.444	63.78	63.13	0.65
1/26/2016	64.204	63.462	0.742	63.88	63.38	0.5
1/26/2016	64.247	63.762	0.485	64.16	63.63	0.53
1/26/2016	64.247	64.018	0.229	64.5	63.88	0.62
1/26/2016	64.888	64.617	0.271	64.63	64.38	0.25

1/26/2016	65.701	65.388	0.313	65.47	65.16	0.31
1/26/2016	67.114	66.074	1.04	66	65.81	0.19
1/26/2016	66.814	66.758	0.056	67.47	66.56	0.91
1/26/2016	66.985	66.972	0.013	67.5	66.97	0.53
1/26/2016	66.643	66.245	0.398	66.25	66.34	-0.09
1/26/2016	66.13	65.517	0.613	66.03	65.81	0.22
1/26/2016	65.487	64.959	0.528	65.41	65.06	0.35
1/26/2016	64.888	64.446	0.442	65.06	64.56	0.5
1/26/2016	64.632	64.061	0.571	64.41	64.19	0.22
1/26/2016	64.418	63.847	0.571	64.28	63.94	0.34
1/26/2016	64.161	63.676	0.485	64.13	63.69	0.44
1/26/2016	64.074	63.59	0.484	64	63.56	0.44
1/26/2016	64.288	63.933	0.355	64	63.56	0.44
1/26/2016	67.413	66.5	0.913	67.47	65.13	2.34
1/26/2016	69.343	68.513	0.83	69.66	67.59	2.07
1/26/2016	69.942	68.342	1.6	70.13	68.34	1.79
1/26/2016	69.557	67.272	2.285	68.78	67.44	1.34
1/26/2016	67.885	66.288	1.597	67.84	66.44	1.4
1/26/2016	66.301	65.174	1.127	66.69	65.41	1.28
1/26/2016	65.916	64.446	1.47	66.25	64.53	1.72
1/26/2016	65.017	63.89	1.127	66.09	64.03	2.06
1/26/2016	64.888	63.505	1.383	65.5	63.66	1.84
1/26/2016	66.301	63.419	2.882	64.28	63.56	0.72
1/26/2016	66.258	63.548	2.71	64.38	63.47	0.91
1/26/2016	65.574	63.933	1.641	65.03	63.84	1.19
1/26/2016	66.258	64.362	1.896	65.13	64.22	0.91
1/26/2016	65.53	64.661	0.869	66.69	64.47	2.22
1/26/2016	66.643	65.003	1.64	65.88	64.88	1
1/26/2016	66.814	65.388	1.426	65.94	65.16	0.78
1/26/2016	66.943	65.517	1.426	66.22	65.31	0.91
1/26/2016	67.5	65.688	1.812	66.94	65.56	1.38
1/26/2016	66.472	65.645	0.827	67.97	65.59	2.38
1/26/2016	66.472	65.602	0.87	67.34	65.5	1.84

1/26/2016	66.857	65.645	1.212	67	65.38	1.62
1/26/2016	66.814	65.773	1.041	67.34	65.5	1.84
1/26/2016	67.242	65.859	1.383	67.34	65.63	1.71
1/26/2016	67.285	65.859	1.426	67.56	65.59	1.97
1/26/2016	68.27	65.816	2.454	67.38	65.72	1.66
1/26/2016	68.657	66.074	2.583	68	65.97	2.03
1/26/2016	68.142	66.245	1.897	68.41	66.09	2.32
1/26/2016	68.313	65.944	2.369	67.28	65.84	1.44
1/26/2016	68.099	65.688	2.411	67.47	65.56	1.91
1/26/2016	67.757	65.388	2.369	67.38	65.44	1.94
1/26/2016	66.857	64.875	1.982	67.38	65.06	2.32
1/26/2016	66.985	65.046	1.939	67.56	65.06	2.5
1/26/2016	67.456	64.875	2.581	67.06	64.94	2.12
1/26/2016	67.158	64.533	2.625	66.75	64.66	2.09
1/26/2016	66.214	64.617	1.597	67.28	64.5	2.78
1/26/2016	66.173	64.617	1.556	66.97	64.59	2.38
1/26/2016	66.258	64.747	1.511	66.25	64.59	1.66
1/26/2016	66.515	64.788	1.727	67.28	64.59	2.69
1/26/2016	67.158	64.959	2.199	66.44	64.88	1.56
1/26/2016	66.686	64.832	1.854	66.97	64.88	2.09
1/26/2016	66.985	64.661	2.324	66.41	64.75	1.66
1/26/2016	65.444	64.574	0.87	66.69	64.5	2.19
1/26/2016	66.515	64.446	2.069	65.72	64.38	1.34
1/26/2016	66.729	64.574	2.155	66.25	64.5	1.75
1/26/2016	66.9	64.661	2.239	66.44	64.63	1.81
1/26/2016	66.214	64.747	1.467	66.91	64.78	2.13
1/26/2016	65.788	65.089	0.699	66.09	64.78	1.31
1/26/2016	65.959	65.089	0.87	66.03	64.91	1.12
1/26/2016	65.829	65.003	0.826	66.38	64.91	1.47
1/26/2016	66.087	64.918	1.169	66.97	64.91	2.06
1/26/2016	66.472	64.918	1.554	66.03	64.78	1.25
1/26/2016	66	64.875	1.125	66.88	64.91	1.97
1/26/2016	66.301	64.918	1.383	66.16	64.91	1.25

1/26/2016	65.829	64.875	0.954	65.84	64.78	1.06
1/26/2016	65.788	64.788	1	65.72	64.66	1.06
1/26/2016	65.444	64.747	0.697	65.66	64.66	1
1/26/2016	65.487	64.747	0.74	65.34	64.53	0.81
1/26/2016	65.658	64.574	1.084	66.53	64.53	2
1/26/2016	65.359	64.704	0.655	66.25	64.66	1.59
1/26/2016	65.745	64.747	0.998	65.81	64.66	1.15
1/26/2016	65.53	64.788	0.742	65.78	64.66	1.12
1/26/2016	65.487	64.661	0.826	65.75	64.66	1.09
1/26/2016	65.188	64.661	0.527	66.03	64.53	1.5
1/26/2016	65.316	64.533	0.783	65.22	64.53	0.69
1/26/2016	65.017	64.49	0.527	66.25	64.41	1.84
1/26/2016	66.772	65.345	1.427	65.31	64.91	0.4
1/26/2016	67.329	66.416	0.913	66.47	65.94	0.53
1/26/2016	67.842	67.186	0.656	67.44	66.81	0.63
1/26/2016	66.857	66.543	0.314	68.25	66.69	1.56
1/26/2016	66.729	65.431	1.298	65.94	65.69	0.25
1/26/2016	65.444	64.617	0.827	65.41	64.78	0.63
1/26/2016	64.632	64.061	0.571	64.75	64.03	0.72
1/26/2016	64.247	63.548	0.699	64.25	63.66	0.59
1/26/2016	63.862	63.204	0.658	63.88	63.28	0.6
1/26/2016	63.99	63.633	0.357	63.72	63.28	0.44
1/26/2016	64.845	64.49	0.355	64.63	64.16	0.47
1/26/2016	65.745	65.303	0.442	65.41	65.03	0.38
1/26/2016	66.087	65.73	0.357	65.97	65.56	0.41
1/26/2016	66	65.859	0.141	66.13	65.69	0.44
1/27/2016	66.6	66.074	0.526	66.25	65.94	0.31
1/27/2016	66.472	66.288	0.184	66.41	66.06	0.35
1/27/2016	67.114	66.329	0.785	66.47	66.19	0.28
1/27/2016	66.214	65.602	0.612	66.19	65.81	0.38
1/27/2016	64.974	64.49	0.484	65.13	64.69	0.44
1/27/2016	63.99	63.548	0.442	64.09	63.81	0.28
1/27/2016	63.219	62.819	0.4	63.28	62.91	0.37

1/27/2016	63.604	63.59	0.014	63.47	63.31	0.16
1/27/2016	65.403	65.089	0.314	65.16	64.94	0.22
1/27/2016	65.701	65.303	0.398	65.53	65.31	0.22
1/27/2016	65.788	65.602	0.186	65.91	65.44	0.47
1/27/2016	66.043	65.903	0.14	65.78	65.69	0.09
1/27/2016	67.885	67.272	0.613	68.88	66.34	2.54
1/27/2016	69.085	67.872	1.213	68.56	67.72	0.84
1/27/2016	67.329	66.201	1.128	67.13	66.56	0.57
1/27/2016	66	64.918	1.082	65.94	65.09	0.85
1/27/2016	64.803	63.933	0.87	64.69	63.94	0.75
1/27/2016	63.99	63.204	0.786	64.31	63.28	1.03
1/27/2016	63.819	62.862	0.957	63.97	63.03	0.94
1/27/2016	64.459	63.633	0.826	64.34	63.28	1.06
1/27/2016	66.558	64.747	1.811	65.28	64.63	0.65
1/27/2016	67.242	65.944	1.298	66.06	65.53	0.53
1/27/2016	68.056	66.587	1.469	67.06	66.28	0.78
1/27/2016	69.256	67.571	1.685	68.06	67.25	0.81
1/27/2016	67.285	66.63	0.655	67.44	66.81	0.63
1/27/2016	66.173	65.089	1.084	66.41	65.38	1.03
1/27/2016	64.931	63.933	0.998	64.78	64.09	0.69
1/27/2016	63.903	63.161	0.742	64.16	63.22	0.94
1/27/2016	63.648	62.691	0.957	63.56	62.84	0.72
1/27/2016	64.674	63.719	0.955	64.25	63.34	0.91
1/27/2016	65.959	65.132	0.827	66.13	64.84	1.29
1/27/2016	66.772	66.158	0.614	66.47	65.72	0.75
1/27/2016	67.586	67.314	0.272	67.5	66.72	0.78
1/27/2016	68.698	68.127	0.571	69.19	67.69	1.5
1/27/2016	68.614	66.63	1.984	68.16	66.84	1.32
1/27/2016	66.729	65.431	1.298	67	65.72	1.28
1/27/2016	66.214	64.446	1.768	66.09	64.72	1.37
1/27/2016	65.359	64.018	1.341	65.5	64.22	1.28
1/27/2016	65.23	63.804	1.426	65.5	63.84	1.66
1/27/2016	65.102	63.933	1.169	66.16	63.84	2.32

1/27/2016	66.385	64.319	2.066	65.09	64.09	1
1/27/2016	66.9	64.747	2.153	65.72	64.63	1.09
1/27/2016	67.627	65.345	2.282	66.28	65.13	1.15
1/27/2016	67.071	65.688	1.383	68.06	65.5	2.56
1/27/2016	67.627	66.201	1.426	67.22	65.88	1.34
1/27/2016	67.842	66.329	1.513	67.47	66.13	1.34
1/27/2016	68.142	66.329	1.813	67.03	66.13	0.9
1/27/2016	68.013	65.987	2.026	67.97	66	1.97
1/27/2016	66.729	65.73	0.999	67.69	65.75	1.94
1/27/2016	68.013	65.474	2.539	66.44	65.41	1.03
1/27/2016	66.943	65.089	1.854	67.78	65.22	2.56
1/27/2016	66.429	64.959	1.47	66.56	64.94	1.62
1/27/2016	67.456	64.918	2.538	66.78	64.94	1.84
1/27/2016	66.6	64.832	1.768	66.97	64.81	2.16
1/27/2016	66.472	64.788	1.684	67.31	64.94	2.37
1/27/2016	66.9	65.046	1.854	67.59	64.94	2.65
1/27/2016	67.071	65.132	1.939	67.72	65.19	2.53
1/27/2016	67.842	65.26	2.582	67.09	65.19	1.9
1/27/2016	67.199	65.345	1.854	67.31	65.19	2.12
1/27/2016	66.772	65.132	1.64	67.75	65.19	2.56
1/27/2016	66.943	65.217	1.726	67.19	65.06	2.13
1/27/2016	67.586	65.174	2.412	66.88	65.06	1.82
1/27/2016	67.456	65.217	2.239	67.38	65.06	2.32
1/27/2016	66.472	65.046	1.426	67.16	65.06	2.1
1/27/2016	66.173	64.832	1.341	66.69	64.69	2
1/27/2016	66.173	64.617	1.556	65.94	64.56	1.38
1/27/2016	66.515	64.403	2.112	65.88	64.31	1.57
1/27/2016	65.53	64.189	1.341	65.78	64.19	1.59
1/27/2016	65.188	63.975	1.213	65.09	63.94	1.15
1/27/2016	64.459	63.804	0.655	64.94	63.69	1.25
1/27/2016	64.674	63.59	1.084	64.91	63.69	1.22
1/27/2016	64.717	63.719	0.998	64.69	63.69	1
1/27/2016	65.188	64.319	0.869	64.88	63.94	0.94

1/27/2016	65.658	65.345	0.313	66.25	64.94	1.31
1/27/2016	67.5	66.03	1.47	66.72	65.81	0.91
1/27/2016	67.199	66.63	0.569	67.13	66.47	0.66
1/27/2016	68.871	67.272	1.599	68.09	66.91	1.18
1/27/2016	66.429	65.903	0.526	67	66.16	0.84
1/27/2016	65.615	64.788	0.827	65.38	65	0.38
1/27/2016	65.059	63.933	1.126	64.81	64.13	0.68
1/27/2016	64.161	63.291	0.87	64.19	63.5	0.69
1/27/2016	63.732	62.906	0.826	63.81	63.13	0.68
1/27/2016	64.247	63.633	0.614	63.97	63.38	0.59
1/27/2016	65.574	65.003	0.571	65.09	64.63	0.46
1/27/2016	66.301	65.73	0.571	66.28	65.5	0.78
1/27/2016	66.344	66.115	0.229	67	65.88	1.12
1/27/2016	66.772	66.5	0.272	66.94	66.38	0.56
1/27/2016	67.028	67.015	0.013	67.22	66.75	0.47
1/27/2016	66.429	65.903	0.526	66.63	66.13	0.5
1/27/2016	65.059	64.403	0.656	65.22	64.81	0.41
1/27/2016	63.819	63.291	0.528	64.06	63.56	0.5
1/28/2016	63.005	62.348	0.657	63	62.69	0.31
1/28/2016	62.704	63.804	-1.1	63.5	63.06	0.44
1/28/2016	65.403	64.918	0.485	65.94	65.31	0.63
1/28/2016	65.487	64.832	0.655	65.44	65.06	0.38
1/28/2016	65.359	65.174	0.185	65.44	65.19	0.25
1/28/2016	65.574	65.303	0.271	65.41	65.19	0.22
1/28/2016	66.043	65.773	0.27	65.91	65.56	0.35
1/28/2016	66.344	66.158	0.186	66.28	65.94	0.34
1/28/2016	66.643	66.587	0.056	67.06	66.31	0.75
1/28/2016	68.484	67.956	0.528	69.44	66.81	2.63
1/28/2016	66.857	65.773	1.084	67.31	66.16	1.15
1/28/2016	65.23	64.148	1.082	65.41	64.5	0.91
1/28/2016	63.819	63.033	0.786	64.28	63.25	1.03
1/28/2016	63.347	62.434	0.913	63.5	62.63	0.87
1/28/2016	64.546	64.018	0.528	64.13	63.25	0.88

1/28/2016	65.829	65.089	0.74	65.59	64.91	0.68
1/28/2016	66.214	65.517	0.697	66.59	65.53	1.06
1/28/2016	67.158	66.714	0.444	67.72	66.31	1.41
1/28/2016	68.956	67.571	1.385	67.84	67.34	0.5
1/28/2016	68.356	66.673	1.683	67.63	66.94	0.69
1/28/2016	65.788	64.875	0.913	66.09	65.34	0.75
1/28/2016	64.589	63.505	1.084	64.66	63.84	0.82
1/28/2016	63.475	62.648	0.827	63.59	62.84	0.75
1/28/2016	63.304	62.819	0.485	63.34	62.47	0.87
1/28/2016	64.974	64.275	0.699	64.75	64.06	0.69
1/28/2016	65.788	65.046	0.742	66.16	65.22	0.94
1/28/2016	66.643	65.73	0.913	66.25	65.56	0.69
1/28/2016	67.285	67.058	0.227	67.94	66.56	1.38
1/28/2016	68.742	68.127	0.615	68.91	67.59	1.32
1/28/2016	68.099	67.058	1.041	68.19	67.09	1.1
1/28/2016	67.543	65.859	1.684	68.28	66.09	2.19
1/28/2016	66.857	65.132	1.725	66.66	65.34	1.32
1/28/2016	65.959	64.661	1.298	67.09	64.84	2.25
1/28/2016	65.872	64.533	1.339	66.47	64.59	1.88
1/28/2016	67.242	64.747	2.495	65.66	64.59	1.07
1/28/2016	67.285	64.959	2.326	65.84	64.72	1.12
1/28/2016	66.643	65.174	1.469	66.94	64.97	1.97
1/28/2016	67.714	65.388	2.326	66.53	65.22	1.31
1/28/2016	67.413	65.688	1.725	68	65.47	2.53
1/28/2016	67.372	65.859	1.513	67.94	65.97	1.97
1/28/2016	68.227	66.201	2.026	67.63	65.97	1.66
1/28/2016	67.971	66.245	1.726	68.19	66.06	2.13
1/28/2016	67.798	66.115	1.683	67.88	66.06	1.82
1/28/2016	67.798	65.903	1.895	68.03	65.94	2.09
1/28/2016	67.586	65.859	1.727	67.78	65.81	1.97
1/28/2016	68.142	65.688	2.454	67.16	65.66	1.5
1/28/2016	68.013	65.73	2.283	66.72	65.53	1.19
1/28/2016	68.013	65.73	2.283	67.31	65.53	1.78

1/28/2016	67.885	65.602	2.283	67.53	65.53	2
1/28/2016	67.757	65.517	2.24	68.09	65.66	2.43
1/28/2016	67.372	65.602	1.77	68.13	65.53	2.6
1/28/2016	68.871	65.816	3.055	67.34	65.66	1.68
1/28/2016	68.27	65.645	2.625	68.13	65.66	2.47
1/28/2016	68.185	65.688	2.497	68.16	65.63	2.53
1/28/2016	67.798	65.645	2.153	68.16	65.63	2.53
1/28/2016	67.842	65.388	2.454	68.13	65.5	2.63
1/28/2016	68.142	65.388	2.754	67.5	65.38	2.12
1/28/2016	67.928	65.089	2.839	67.94	65.28	2.66
1/28/2016	67.5	65.003	2.497	67.44	65.09	2.35
1/28/2016	67.714	64.875	2.839	67.5	64.97	2.53
1/28/2016	66.814	64.661	2.153	67.97	64.84	3.13
1/28/2016	66.985	64.661	2.324	66.97	64.72	2.25
1/28/2016	66.344	64.148	2.196	65.97	64.34	1.63
1/28/2016	65.23	63.59	1.64	66.03	63.84	2.19
1/28/2016	64.332	63.161	1.171	65.31	63.31	2
1/28/2016	64.418	62.906	1.512	64.34	63.06	1.28
1/28/2016	64.204	62.776	1.428	63.97	62.94	1.03
1/28/2016	64.033	62.776	1.257	64.13	62.81	1.32
1/28/2016	64.632	62.906	1.726	63.81	62.94	0.87
1/28/2016	64.161	63.12	1.041	63.97	63.06	0.91
1/28/2016	64.117	63.204	0.913	64.38	63.19	1.19
1/28/2016	64.888	63.462	1.426	64.53	63.44	1.09
1/28/2016	64.717	63.804	0.913	64.66	63.69	0.97
1/28/2016	64.888	64.061	0.827	64.78	63.94	0.84
1/28/2016	65.487	65.003	0.484	65.88	64.56	1.32
1/28/2016	66.472	65.816	0.656	66.28	65.44	0.84
1/28/2016	66.814	66.587	0.227	68.06	66.22	1.84
1/28/2016	67.543	67.1	0.443	67.25	66.84	0.41
1/28/2016	66.857	66.372	0.485	68.22	66.44	1.78
1/28/2016	66.043	65.517	0.526	66.66	65.66	1
1/28/2016	65.316	64.704	0.612	65.69	65	0.69

1/28/2016	64.888	64.018	0.87	65.03	64.25	0.78
1/28/2016	64.204	63.633	0.571	64.41	63.75	0.66
1/28/2016	63.946	63.291	0.655	63.91	63.38	0.53
1/28/2016	63.732	63.077	0.655	63.66	63.13	0.53
1/28/2016	64.674	63.89	0.784	64.16	63.66	0.5
1/28/2016	65.359	65.046	0.313	65.38	64.81	0.57
1/28/2016	66.087	65.559	0.528	65.94	65.5	0.44
1/29/2016	66.301	65.987	0.314	66.47	65.78	0.69
1/29/2016	67.199	66.372	0.827	66.41	66.16	0.25
1/29/2016	66.772	66.714	0.058	67.34	66.53	0.81
1/29/2016	66.6	66.245	0.355	67.19	66.53	0.66
1/29/2016	65.745	65.303	0.442	65.88	65.53	0.35
1/29/2016	64.931	64.403	0.528	64.97	64.5	0.47
1/29/2016	64.204	63.676	0.528	64.06	63.75	0.31
1/29/2016	63.561	63.12	0.441	63.56	63.22	0.34
1/29/2016	63.433	63.161	0.272	63.31	62.97	0.34
1/29/2016	64.332	64.232	0.1	64.25	63.88	0.37
1/29/2016	65.658	64.875	0.783	65.38	65.03	0.35
1/29/2016	65.829	65.431	0.398	65.88	65.28	0.6
1/29/2016	65.872	65.903	-0.031	66.69	65.69	1
1/29/2016	66.515	66.288	0.227	66.31	66.06	0.25
1/29/2016	67.028	66.714	0.314	66.47	66.47	0
1/29/2016	66.9	66.844	0.056	67.28	66.72	0.56
1/29/2016	67.158	66.416	0.742	68.75	65.84	2.91
1/29/2016	65.959	65.345	0.614	66.78	65.56	1.22
1/29/2016	65.359	64.574	0.785	66.72	64.78	1.94
1/29/2016	64.76	63.975	0.785	66.31	64.16	2.15
1/29/2016	64.931	63.59	1.341	64.91	63.78	1.13
1/29/2016	64.546	63.462	1.084	64.97	63.53	1.44
1/29/2016	64.845	63.505	1.34	64.31	63.41	0.9
1/29/2016	66.344	64.959	1.385	65.44	64.53	0.91
1/29/2016	66.985	66.5	0.485	67.75	65.84	1.91
1/29/2016	68.185	67.4	0.785	67.63	66.88	0.75

1/29/2016	68.571	66.972	1.599	68.31	67.25	1.06
1/29/2016	67.798	65.859	1.939	66.91	66.09	0.82
1/29/2016	66.6	64.704	1.896	65.81	65	0.81
1/29/2016	65.145	64.018	1.127	64.94	64.09	0.85
1/29/2016	64.888	63.548	1.34	64.56	63.72	0.84
1/29/2016	64.332	63.419	0.913	64.69	63.47	1.22
1/29/2016	64.589	63.59	0.999	64.72	63.59	1.13
1/29/2016	65.102	64.49	0.612	66.22	64.09	2.13
1/29/2016	66.686	66.03	0.656	67.53	65.63	1.9
1/29/2016	68.27	67.571	0.699	68.53	66.88	1.65
1/29/2016	69.386	68	1.386	69.53	67.94	1.59
1/29/2016	69.256	67.571	1.685	68.97	67.44	1.53
1/29/2016	68.956	67.272	1.684	69	67.19	1.81
1/29/2016	69.17	66.929	2.241	68.75	66.91	1.84
1/29/2016	68.527	66.63	1.897	68.84	66.66	2.18
1/29/2016	68.657	66.5	2.157	69.16	66.53	2.63
1/29/2016	68.484	66.329	2.155	68.59	66.28	2.31
1/29/2016	69.256	66.329	2.927	68.13	66.28	1.85
1/29/2016	68.742	66.245	2.497	69.13	66.28	2.85
1/29/2016	68.871	66.329	2.542	69.09	66.28	2.81
1/29/2016	68.956	66.288	2.668	68.63	66.28	2.35
1/29/2016	67.671	66.074	1.597	69.44	66.16	3.28
1/29/2016	68.356	66.158	2.198	68.44	66	2.44
1/29/2016	68.871	65.903	2.968	67.91	65.88	2.03
1/29/2016	68.185	65.688	2.497	68.13	65.63	2.5
1/29/2016	67.5	65.388	2.112	68.25	65.5	2.75
1/29/2016	67.798	65.303	2.495	68.09	65.38	2.71
1/29/2016	68.013	65.217	2.796	67.59	65.22	2.37
1/29/2016	67.757	65.174	2.583	67.47	65.22	2.25
1/29/2016	67.158	65.089	2.069	68.16	65.09	3.07
1/29/2016	68.443	65.089	3.354	67.19	65.09	2.1
1/29/2016	67.757	65.303	2.454	68.22	65.22	3
1/29/2016	68.227	65.089	3.138	65.09	65.47	-0.38

1/29/2016	68.657	65.816	2.841	68.34	65.56	2.78
1/29/2016	68.27	65.645	2.625	68.44	65.66	2.78
1/29/2016	68.657	65.688	2.969	68.13	65.66	2.47
1/29/2016	68.185	65.645	2.54	68.56	65.66	2.9
1/29/2016	68.4	65.559	2.841	67.78	65.53	2.25
1/29/2016	68.356	65.517	2.839	68.75	65.53	3.22
1/29/2016	67.757	65.645	2.112	68.72	65.66	3.06
1/29/2016	68.142	65.602	2.54	68	65.53	2.47
1/29/2016	68.913	65.688	3.225	67.53	65.53	2
1/29/2016	68.099	65.559	2.54	68.72	65.53	3.19
1/29/2016	67.798	65.688	2.11	68.47	65.66	2.81
1/29/2016	67.5	65.345	2.155	66.91	65.41	1.5
1/29/2016	66.344	64.661	1.683	67.06	64.78	2.28
1/29/2016	65.102	64.061	1.041	65.06	64.13	0.93
1/29/2016	64.117	63.419	0.698	65	63.63	1.37
1/29/2016	64.418	63.033	1.385	64.53	63.22	1.31
1/29/2016	64.204	62.862	1.342	63.59	62.97	0.62
1/29/2016	63.819	62.691	1.128	63.41	62.72	0.69
1/29/2016	63.518	62.906	0.612	63.94	62.84	1.1
1/29/2016	64.204	62.947	1.257	64.16	63	1.16
1/29/2016	63.819	63.161	0.658	63.75	63.13	0.62
1/29/2016	64.033	63.248	0.785	64.22	63.25	0.97
1/29/2016	64.418	63.505	0.913	64.19	63.38	0.81
1/29/2016	64.589	63.676	0.913	64.22	63.59	0.63
1/29/2016	64.459	63.847	0.612	64.59	63.78	0.81
1/29/2016	64.632	63.933	0.699	64.72	63.91	0.81
1/29/2016	64.76	64.104	0.656	64.69	63.91	0.78
1/29/2016	65.017	64.275	0.742	64.81	64.16	0.65
1/29/2016	65.102	64.403	0.699	64.94	64.28	0.66
1/29/2016	65.316	64.49	0.826	64.94	64.41	0.53
1/29/2016	65.273	64.617	0.656	65.16	64.56	0.6
1/29/2016	65.316	64.788	0.528	65.31	64.69	0.62
1/29/2016	65.403	64.832	0.571	65.19	64.81	0.38

1/29/2016	65.444	64.918	0.526	65.31	64.81	0.5
1/29/2016	65.487	65.003	0.484	65.44	64.81	0.63
1/29/2016	65.872	65.688	0.184	65.94	65.47	0.47
1/30/2016	66.515	66.288	0.227	66.16	65.97	0.19
1/30/2016	66.9	66.801	0.099	66.53	66.47	0.06
1/30/2016	66.6	66.543	0.057	67.16	66.59	0.57
1/30/2016	66.472	66.074	0.398	66.44	66.09	0.35
1/30/2016	66.173	65.773	0.4	66.19	65.84	0.35
1/30/2016	65.788	65.431	0.357	65.84	65.47	0.37
1/30/2016	65.403	65.003	0.4	65.44	65.09	0.35
1/30/2016	65.145	64.788	0.357	65.06	64.72	0.34
1/30/2016	64.845	64.617	0.228	64.94	64.59	0.35
1/30/2016	64.717	64.617	0.1	64.94	64.47	0.47
1/30/2016	65.017	64.533	0.484	64.81	64.47	0.34
1/30/2016	64.931	64.574	0.357	64.88	64.47	0.41
1/30/2016	65.017	64.661	0.356	64.88	64.47	0.41
1/30/2016	65.059	64.747	0.312	65.03	64.59	0.44
1/30/2016	65.188	64.832	0.356	65.03	64.72	0.31
1/30/2016	65.359	64.959	0.4	65.28	64.84	0.44
1/30/2016	65.444	65.046	0.398	65.28	64.97	0.31
1/30/2016	67.757	66.459	1.298	68.72	65.47	3.25
1/30/2016	68.571	66.972	1.599	69.22	67.03	2.19
1/30/2016	68.828	67.528	1.3	68.56	67.31	1.25
1/30/2016	68.614	67.229	1.385	68.41	67.31	1.1
1/30/2016	68.142	66.885	1.257	68	66.91	1.09
1/30/2016	67.798	66.459	1.339	68.47	66.41	2.06
1/30/2016	67.714	65.816	1.898	67.09	66.03	1.06
1/30/2016	67.586	65.431	2.155	66.34	65.53	0.81
1/30/2016	66.13	65.217	0.913	66	65.13	0.87
1/30/2016	66.6	64.832	1.768	66.09	64.75	1.34
1/30/2016	65.959	64.446	1.513	65.63	64.63	1
1/30/2016	65.788	64.403	1.385	65.25	64.38	0.87
1/30/2016	65.359	64.275	1.084	65.56	64.25	1.31

1/30/2016	65.403	64.275	1.128	65.28	64.25	1.03
1/30/2016	65.273	64.362	0.911	65.75	64.25	1.5
1/30/2016	65.53	64.574	0.956	66.19	64.38	1.81
1/30/2016	66.301	64.875	1.426	65.53	64.75	0.78
1/30/2016	67.543	65.26	2.283	65.94	65.13	0.81
1/30/2016	67.586	65.688	1.898	66.81	65.5	1.31
1/30/2016	67.329	66.245	1.084	67.09	65.88	1.21
1/30/2016	67.842	66.63	1.212	67.97	66.25	1.72
1/30/2016	67.971	66.801	1.17	68.56	66.5	2.06
1/30/2016	68.571	66.673	1.898	68.84	66.59	2.25
1/30/2016	68.484	66.758	1.726	68.34	66.59	1.75
1/30/2016	68.356	66.673	1.683	68.31	66.47	1.84
1/30/2016	68.4	66.63	1.77	68.53	66.47	2.06
1/30/2016	68.999	66.416	2.583	67.84	66.47	1.37
1/30/2016	68.698	66.158	2.54	68.34	66.22	2.12
1/30/2016	67.456	66.329	1.127	68.97	66.22	2.75
1/30/2016	68.227	66.158	2.069	67.94	66.22	1.72
1/30/2016	68.614	66.288	2.326	67.72	66.09	1.63
1/30/2016	68.443	66.416	2.027	68.31	66.34	1.97
1/30/2016	68.313	66.5	1.813	68.44	66.34	2.1
1/30/2016	68.571	66.587	1.984	68.41	66.47	1.94
1/30/2016	69.129	66.63	2.499	68.22	66.47	1.75
1/30/2016	68.999	66.801	2.198	68.22	66.75	1.47
1/30/2016	69.17	66.972	2.198	68.94	66.75	2.19
1/30/2016	69.514	67.015	2.499	68.66	66.88	1.78
1/30/2016	69.343	67.1	2.243	69.19	67	2.19
1/30/2016	69.728	67.143	2.585	68.75	67	1.75
1/30/2016	69.343	66.929	2.414	69.09	67.13	1.96
1/30/2016	68.913	66.63	2.283	68.97	66.75	2.22
1/30/2016	69.085	66.63	2.455	68.19	66.63	1.56
1/30/2016	69.3	66.63	2.67	68.69	66.63	2.06
1/30/2016	69.042	66.673	2.369	69	66.63	2.37
1/30/2016	68.871	66.673	2.198	69.13	66.75	2.38

1/30/2016	69.643	66.714	2.929	68.88	66.63	2.25
1/30/2016	69.256	66.673	2.583	68.84	66.63	2.21
1/30/2016	69.129	66.714	2.415	68.63	66.63	2
1/30/2016	69.256	66.543	2.713	68.69	66.66	2.03
1/30/2016	68.913	66.459	2.454	68.78	66.53	2.25
1/30/2016	69.085	66.587	2.498	68.78	66.53	2.25
1/30/2016	69.085	66.459	2.626	68.25	66.53	1.72
1/30/2016	68.956	66.543	2.413	68.94	66.5	2.44
1/30/2016	68.657	66.673	1.984	68.56	66.75	1.81
1/30/2016	68.871	66.844	2.027	68.91	66.88	2.03
1/30/2016	68.4	66.885	1.515	67.72	66.88	0.84
1/30/2016	67.329	66.587	0.742	68.69	66.63	2.06
1/30/2016	67.199	66.245	0.954	68.09	66.38	1.71
1/30/2016	66.943	65.903	1.04	67.47	66	1.47
1/30/2016	66.643	65.903	0.74	67.13	65.88	1.25
1/30/2016	66.558	65.987	0.571	67.75	65.88	1.87
1/30/2016	66.814	65.944	0.87	66.5	65.88	0.62
1/30/2016	66.985	65.903	1.082	66.41	65.88	0.53
1/30/2016	66.729	65.987	0.742	66.63	66	0.63
1/30/2016	67.586	66.074	1.512	66.31	66	0.31
1/30/2016	66.9	66.115	0.785	67.06	66	1.06
1/30/2016	66.6	66.201	0.399	67.28	66.13	1.15
1/30/2016	67.242	66.329	0.913	66.84	66.25	0.59
1/30/2016	66.943	66.543	0.4	67.41	66.38	1.03
1/30/2016	67.028	66.673	0.355	67.91	66.63	1.28
1/30/2016	67.158	66.673	0.485	68.25	66.63	1.62
1/30/2016	68.185	66.758	1.427	67.03	66.63	0.4
1/30/2016	67.798	66.714	1.084	66.88	66.63	0.25
1/30/2016	67.199	66.63	0.569	67.22	66.63	0.59
1/30/2016	67.586	66.587	0.999	66.75	66.5	0.25
1/30/2016	66.814	66.459	0.355	67.84	66.5	1.34
1/30/2016	66.6	66.416	0.184	67.56	66.38	1.18
1/30/2016	67.413	66.201	1.212	66.41	66.25	0.16

1/31/2016	66.301	66.03	0.271	66.44	66.13	0.31
1/31/2016	66.385	66.115	0.27	66.38	66	0.38
1/31/2016	66.472	66.074	0.398	66.34	66	0.34
1/31/2016	66.857	66.158	0.699	66.34	66.13	0.21
1/31/2016	66.385	66.158	0.227	66.69	66.13	0.56
1/31/2016	67.413	66.245	1.168	66.44	66.13	0.31
1/31/2016	66.429	66.288	0.141	66.94	66.25	0.69
1/31/2016	67.158	66.329	0.829	66.31	66.25	0.06
1/31/2016	66.686	66.5	0.186	66.59	66.38	0.21
1/31/2016	67.158	66.587	0.571	67	66.5	0.5
1/31/2016	66.729	66.63	0.099	67.31	66.5	0.81
1/31/2016	66.814	66.714	0.1	67.41	66.63	0.78
1/31/2016	67.586	66.885	0.701	66.94	66.75	0.19
1/31/2016	67.413	67.015	0.398	67.13	66.88	0.25
1/31/2016	67.372	67.143	0.229	66.97	67	-0.03
1/31/2016	67.456	67.272	0.184	67.47	67.13	0.34
1/31/2016	68.27	67.4	0.87	67.38	67.25	0.13
1/31/2016	69.471	68.127	1.344	71.31	67.38	3.93
1/31/2016	70.329	68.471	1.858	70.09	68.44	1.65
1/31/2016	70.974	68.813	2.161	70.28	68.81	1.47
1/31/2016	70.543	69.242	1.301	70.59	68.94	1.65
1/31/2016	70.372	69.371	1.001	71.13	69.19	1.94
1/31/2016	70.759	69.499	1.26	71.34	69.31	2.03
1/31/2016	71.103	69.542	1.561	71.28	69.44	1.84
1/31/2016	71.704	69.456	2.248	70.75	69.44	1.31
1/31/2016	71.317	69.542	1.775	70.63	69.44	1.19
1/31/2016	71.231	69.585	1.646	70.91	69.59	1.32
1/31/2016	71.231	69.542	1.689	71.25	69.47	1.78
1/31/2016	71.231	69.456	1.775	70.81	69.47	1.34
1/31/2016	70.543	69.456	1.087	70.94	69.34	1.6
1/31/2016	71.06	69.499	1.561	71.06	69.34	1.72
1/31/2016	71.447	69.456	1.991	70.97	69.47	1.5
1/31/2016	71.661	69.499	2.162	70.88	69.47	1.41

1/31/2016	71.231	69.629	1.602	70.97	69.47	1.5
1/31/2016	70.759	69.629	1.13	71.66	69.59	2.07
1/31/2016	71.317	69.713	1.604	71.44	69.72	1.72
1/31/2016	70.846	69.843	1.003	71.72	69.72	2
1/31/2016	71.533	69.8	1.733	71.47	69.84	1.63
1/31/2016	71.791	69.886	1.905	71.53	69.84	1.69
1/31/2016	71.92	69.971	1.949	71.19	69.97	1.22
1/31/2016	71.92	70.1	1.82	71.22	69.97	1.25
1/31/2016	71.661	70.185	1.476	71.78	70.09	1.69
1/31/2016	71.361	70.143	1.218	72	70.09	1.91
1/31/2016	72.093	70.401	1.692	72.69	70.22	2.47
1/31/2016	72.394	70.658	1.736	73.09	70.59	2.5
1/31/2016	72.955	70.916	2.039	73.13	70.88	2.25
1/31/2016	73.342	71.259	2.083	73.28	71.13	2.15
1/31/2016	73.558	71.646	1.912	73.56	71.38	2.18
1/31/2016	74.467	71.861	2.606	73.81	71.75	2.06
1/31/2016	74.206	72.204	2.002	74.91	72.03	2.88
1/31/2016	74.511	72.678	1.833	74.78	72.41	2.37
1/31/2016	74.856	72.851	2.005	75.03	72.66	2.37
1/31/2016	75.117	72.807	2.31	75.53	72.91	2.62
1/31/2016	75.247	73.239	2.008	75.53	73.03	2.5
1/31/2016	75.594	73.412	2.182	75.84	73.16	2.68
1/31/2016	75.81	73.412	2.398	75.84	73.28	2.56
1/31/2016	75.508	73.326	2.182	76.19	73.28	2.91
1/31/2016	75.942	73.326	2.616	75.66	73.28	2.38
1/31/2016	75.594	73.067	2.527	76.19	73.28	2.91
1/31/2016	75.81	72.937	2.873	75.72	73.16	2.56
1/31/2016	75.853	73.067	2.786	75.69	73.16	2.53
1/31/2016	75.81	73.153	2.657	76.31	73.16	3.15
1/31/2016	76.158	73.497	2.661	76.53	73.53	3
1/31/2016	76.507	73.713	2.794	77.03	73.78	3.25
1/31/2016	76.246	73.54	2.706	76.38	73.66	2.72
1/31/2016	76.899	73.583	3.316	76.28	73.53	2.75

1/31/2016	76.464	73.153	3.311	75.84	73.25	2.59
1/31/2016	76.55	73.369	3.181	76.25	73.38	2.87
1/31/2016	75.853	73.239	2.614	76.59	73.38	3.21
1/31/2016	76.507	73.369	3.138	75.81	73.25	2.56
1/31/2016	76.332	73.283	3.049	75.91	73.38	2.53
1/31/2016	75.594	73.023	2.571	75.5	73.13	2.37
1/31/2016	75.247	72.593	2.654	75.03	72.84	2.19
1/31/2016	73.083	71.99	1.093	73.69	72.22	1.47
1/31/2016	72.05	71.13	0.92	72.94	71.41	1.53
1/31/2016	71.661	70.658	1.003	72.66	70.91	1.75
1/31/2016	71.964	70.358	1.606	71.47	70.53	0.94
1/31/2016	71.19	70.185	1.005	71.59	70.41	1.18
1/31/2016	71.274	70.358	0.916	71.41	70.41	1

APPENDIX F

COOLING TOWER WATER TEMPERATURE AND FLOW MEASUREMENTS

The Figures below show the water temperature and flow measurements for CT1 and CT2 respectively through the year 2015.

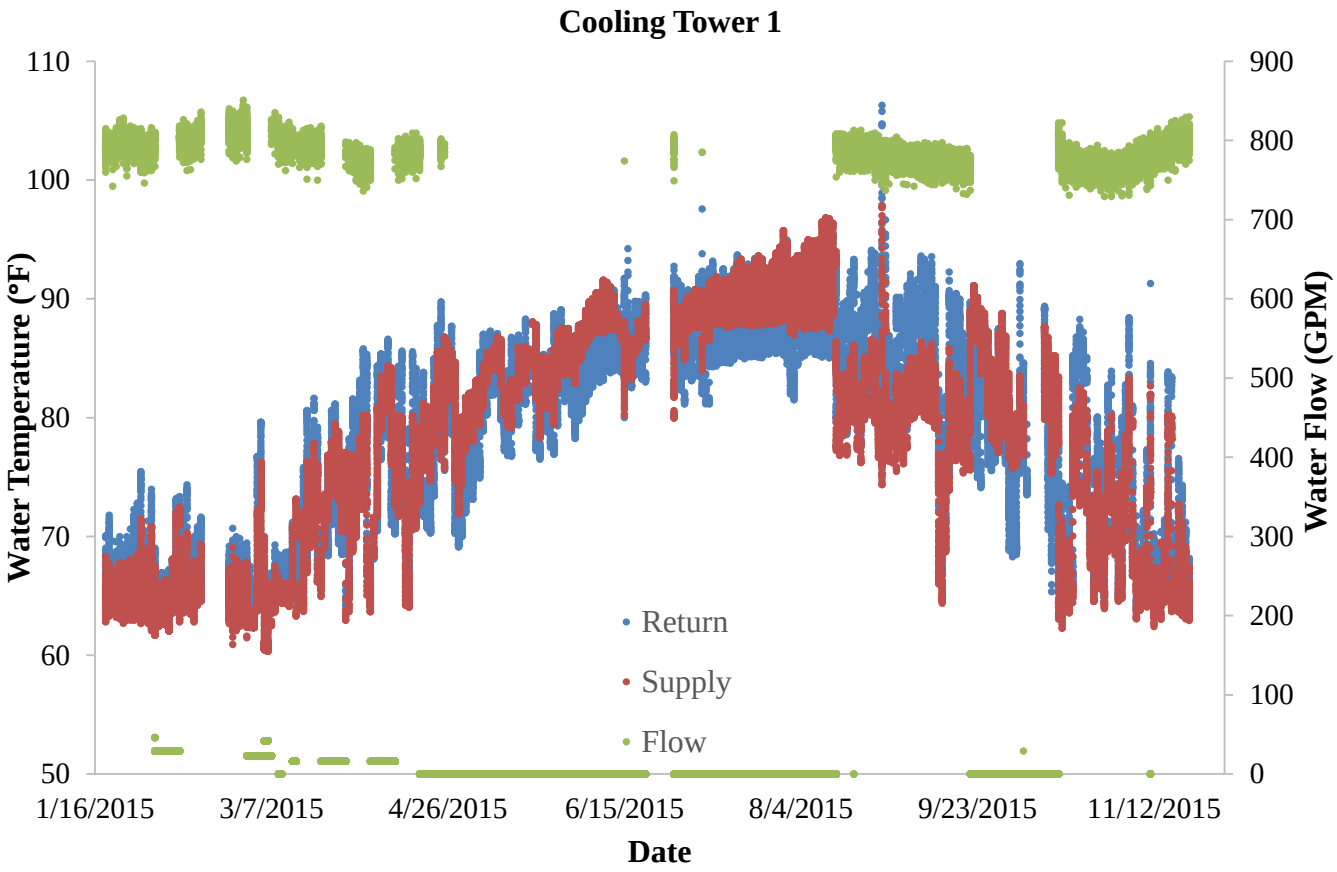

Figure F.1 Water Temperatures and Flowrate of Cooling Tower 1 for year 2015

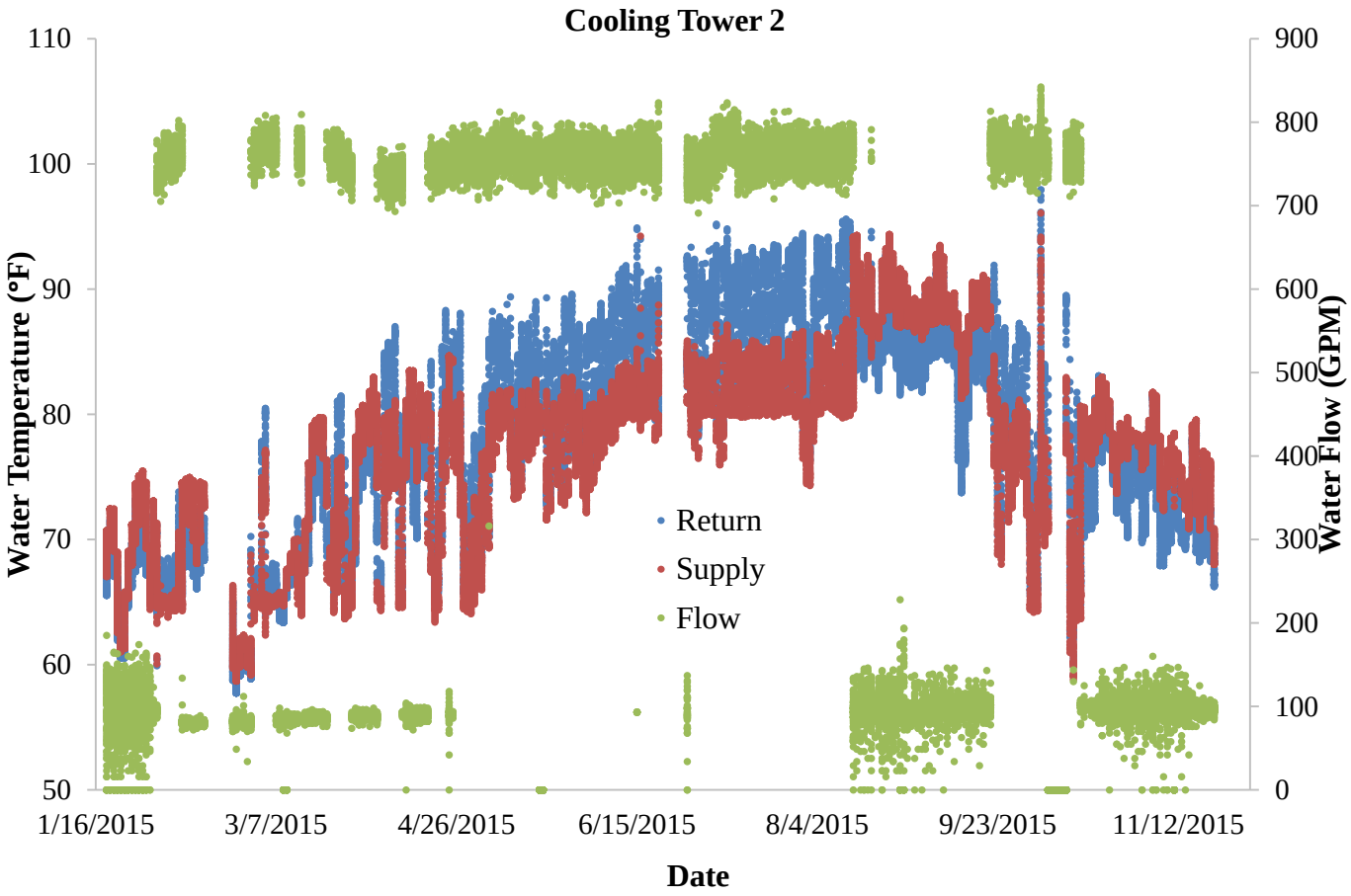

Figure F.2 Water Temperatures and Flowrate of Cooling Tower 2 for year 2015

APPENDIX G

POWER MEASUREMENTS OF COOLING TOWER AND CHILLER

1. Figures of cooling tower and chiller tonnage comparisons for sampled weeks

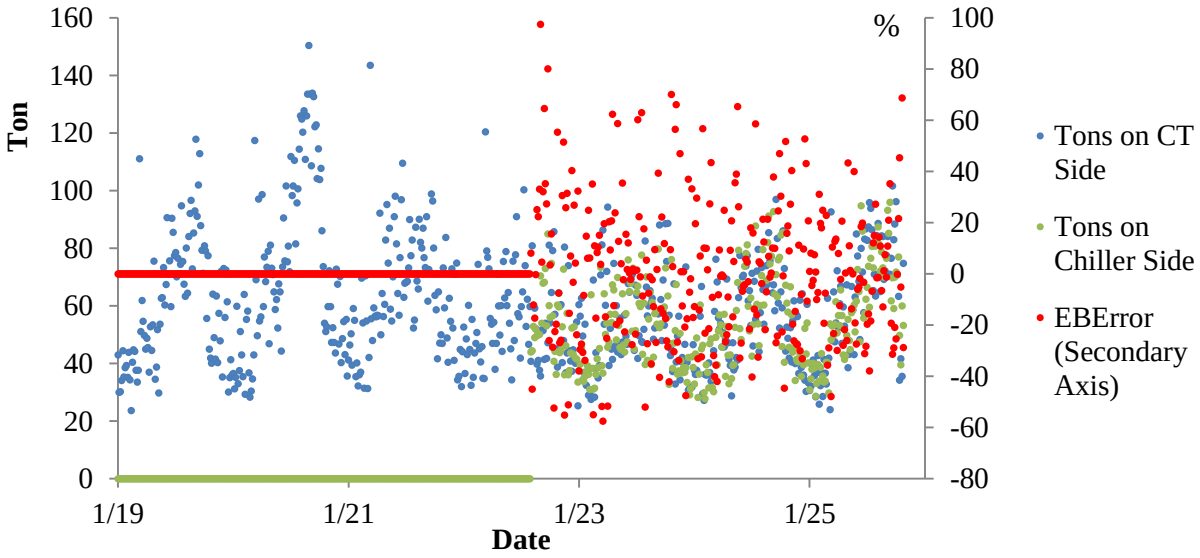

Figure G.1 Tonnage Comparisons for January (1/19-1/25)

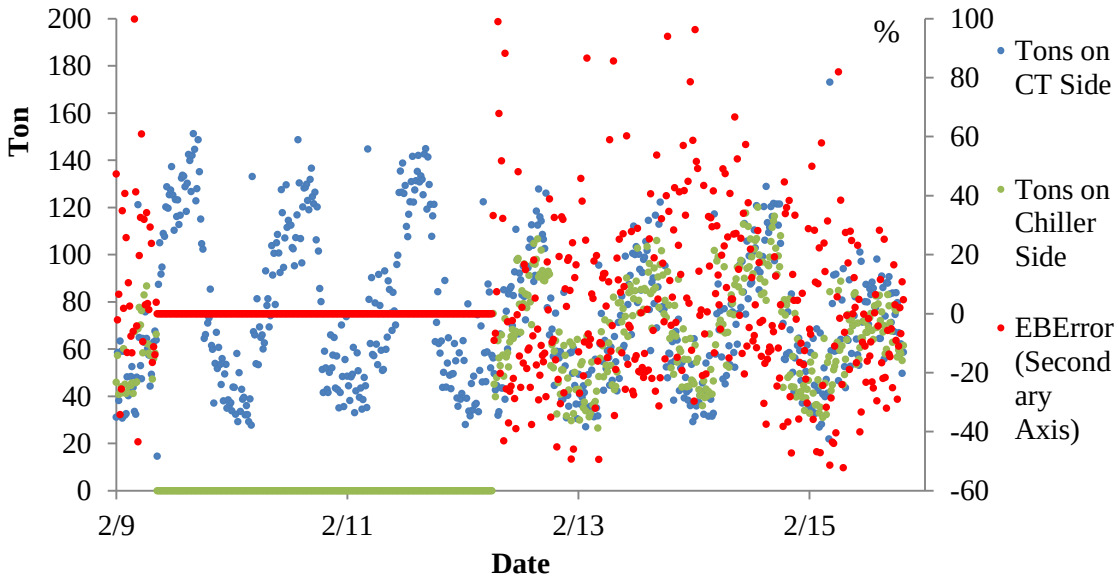

Figure G.2 Tonnage Comparisons for February (2/9-2/15)

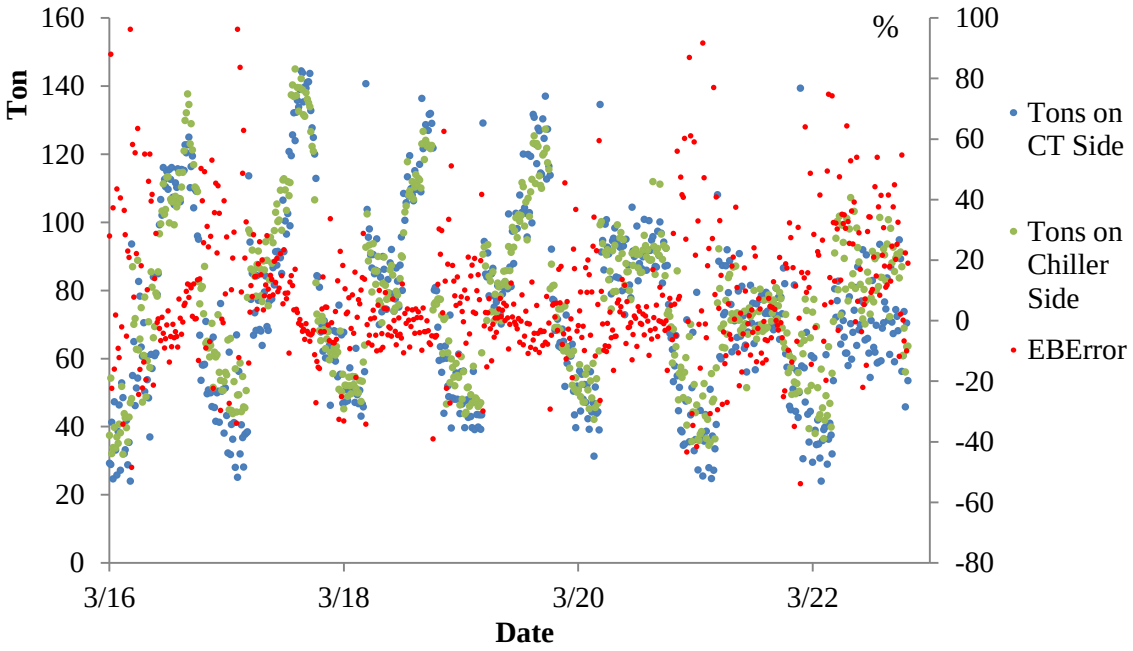

Figure G.3 Tonnage Comparisons for March (3/16-3/22)

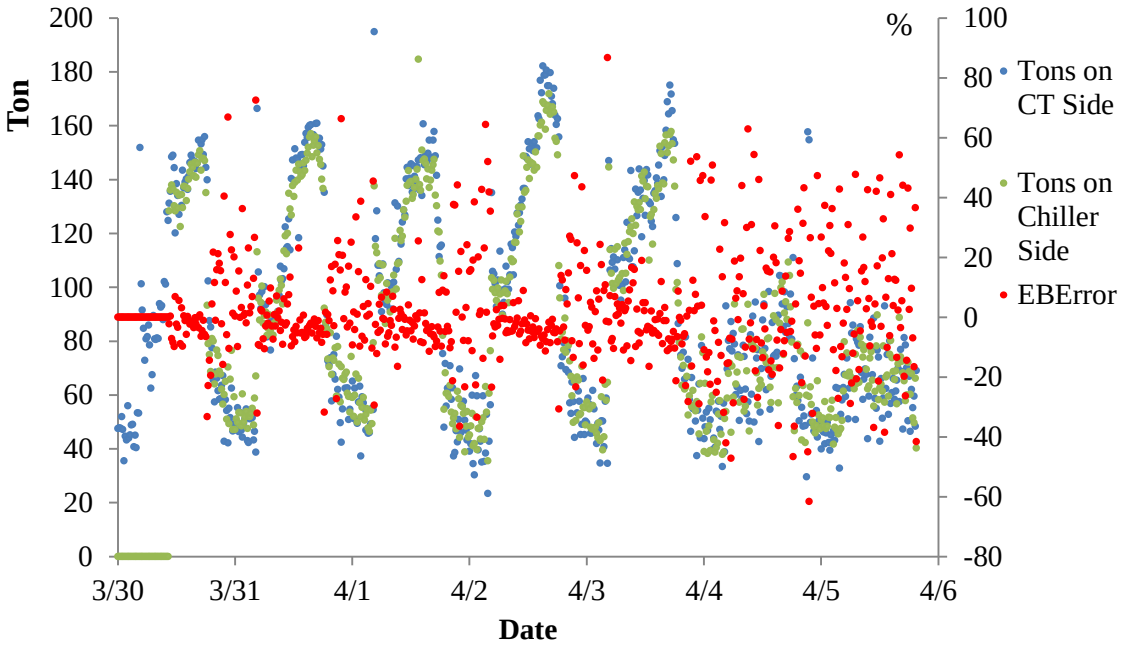

Figure G.4 Tonnage Comparisons for April (3/30-4/6)

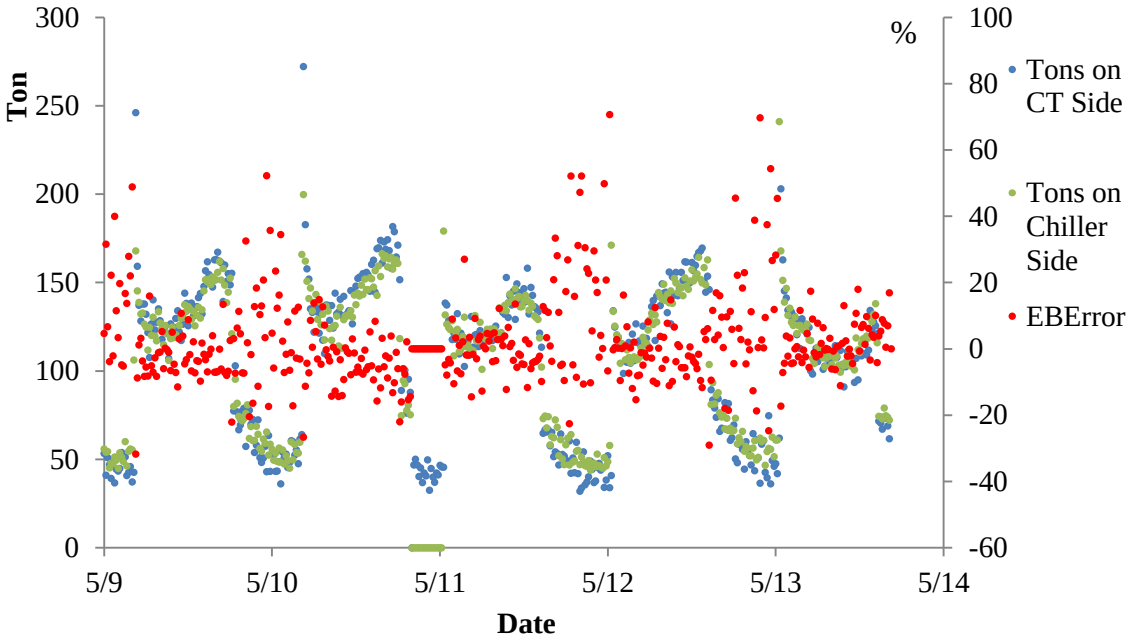

Figure G.5 Tonnage Comparisons for May (5/9-5/14)

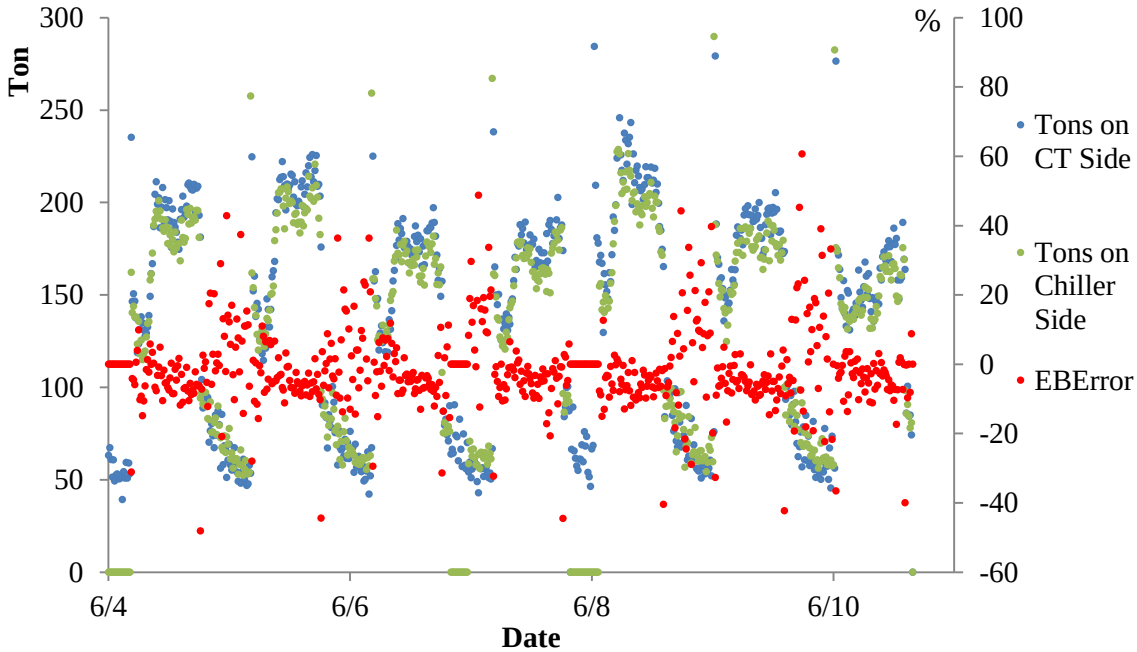

Figure G.6 Tonnage Comparisons for June (6/4-6/10)

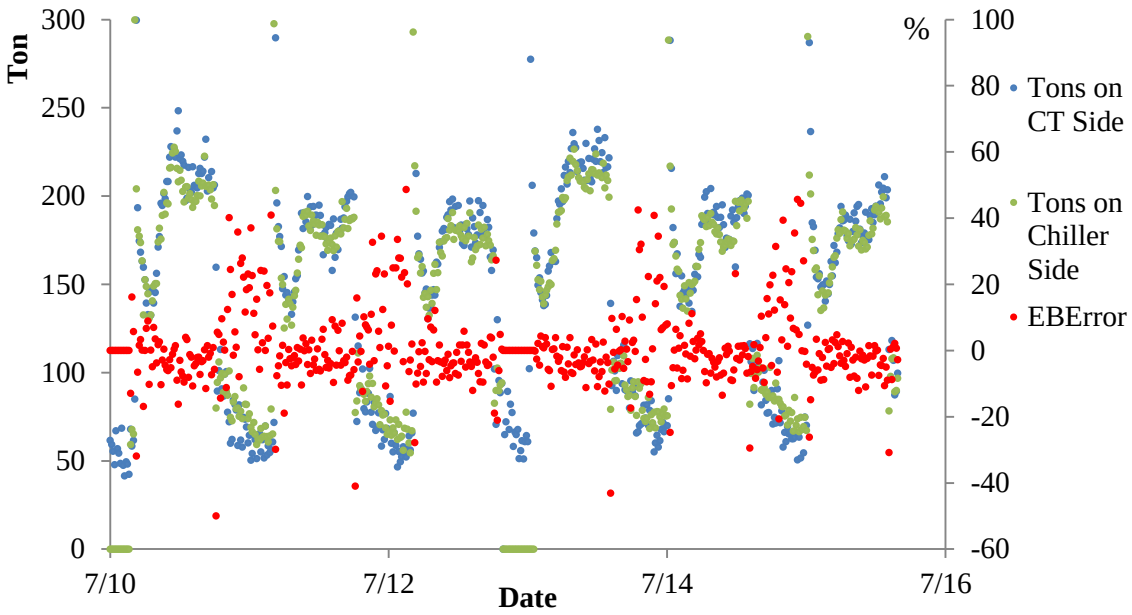

Figure G.7 Tonnage Comparisons for July (7/10-7/16)

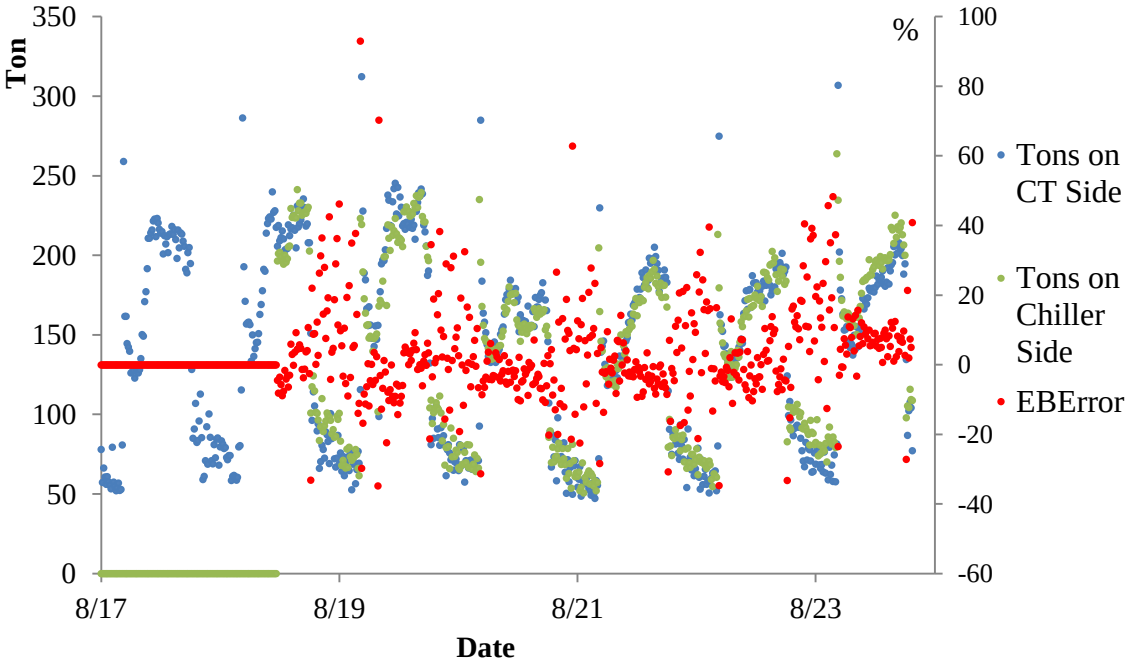

Figure G. 8 Tonnage Comparisons for August (8/17-8/23)

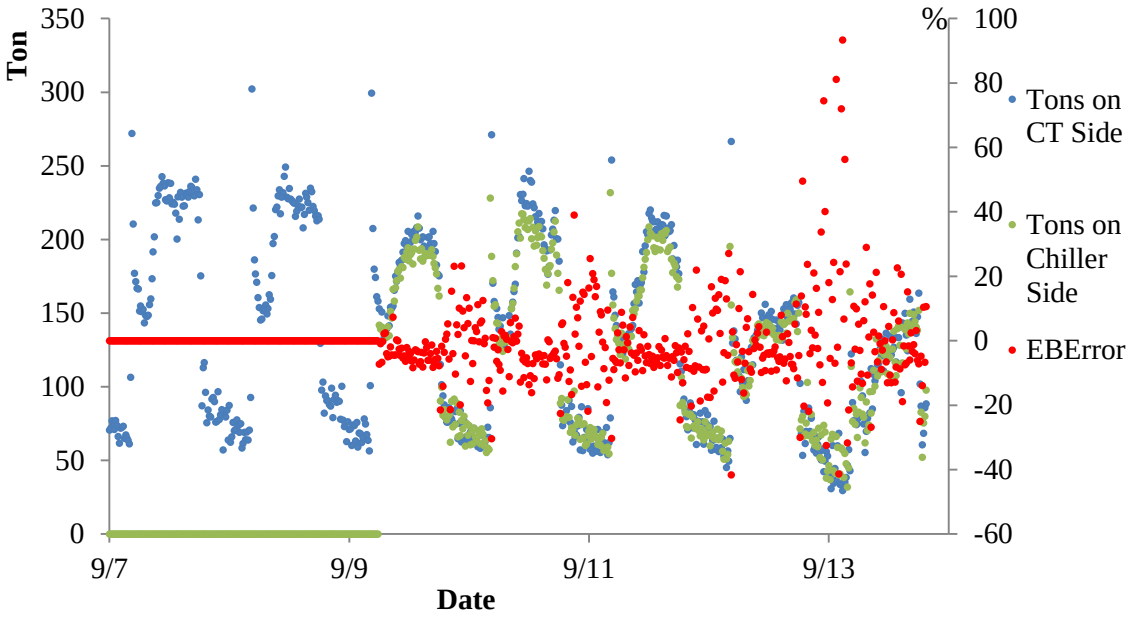

Figure G.9 Tonnage Comparisons for September (9/7-9/13)

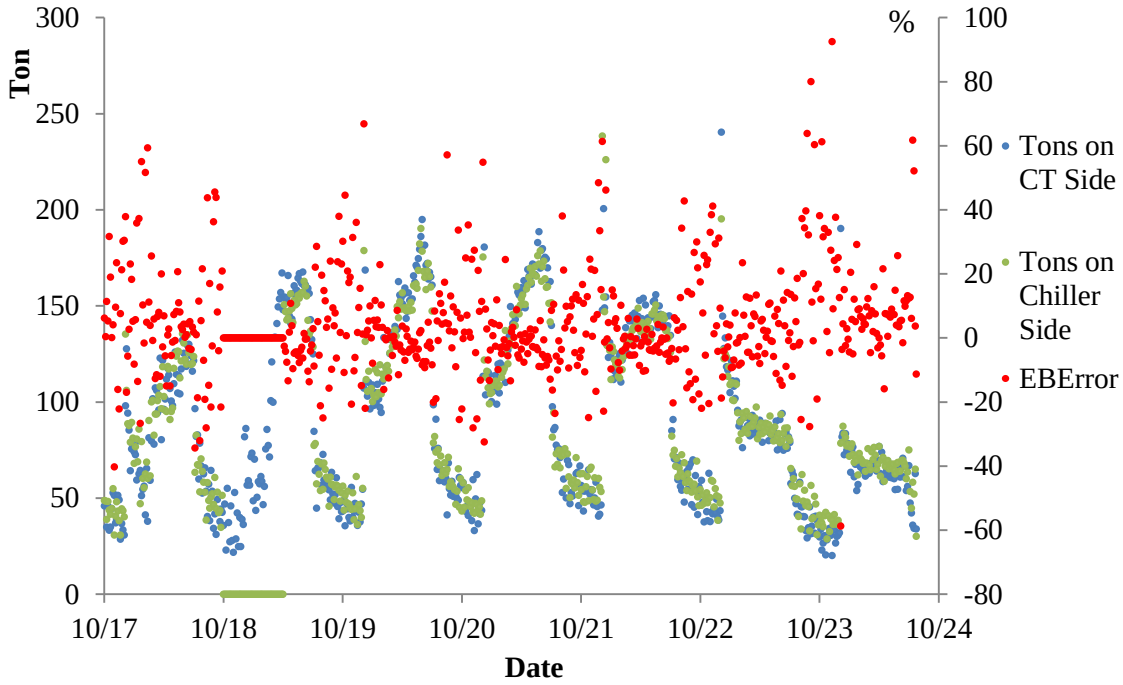

Figure G.10 Tonnage Comparisons for October (10/17-10/23)

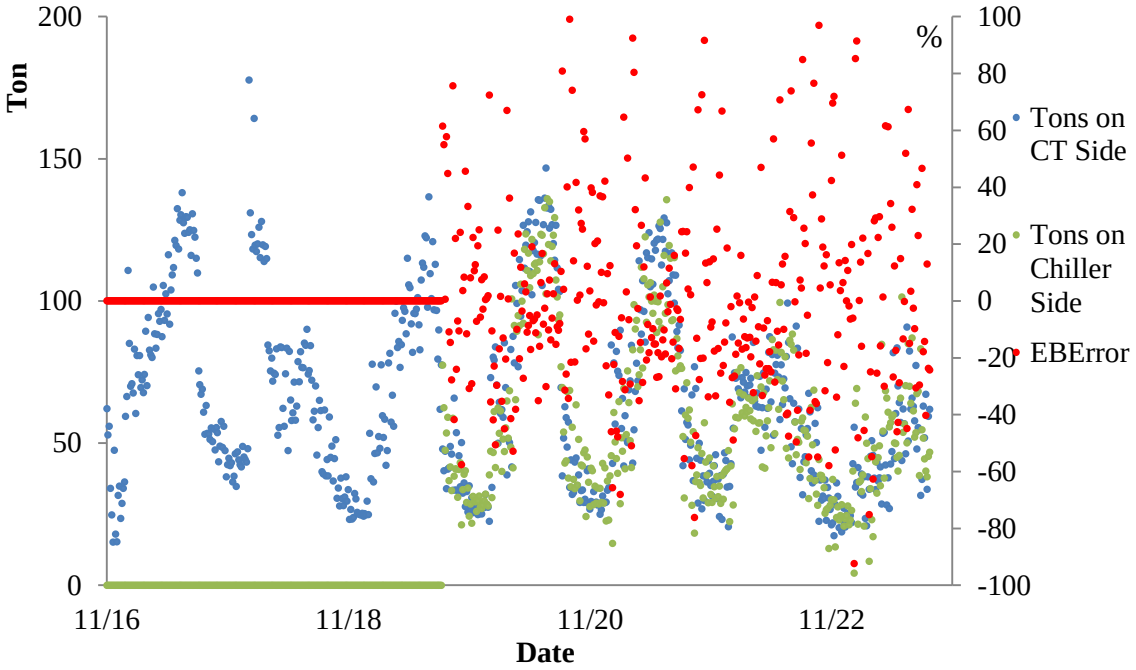

Figure G. 11 Tonnage Comparisons for November (11/16-11/22)

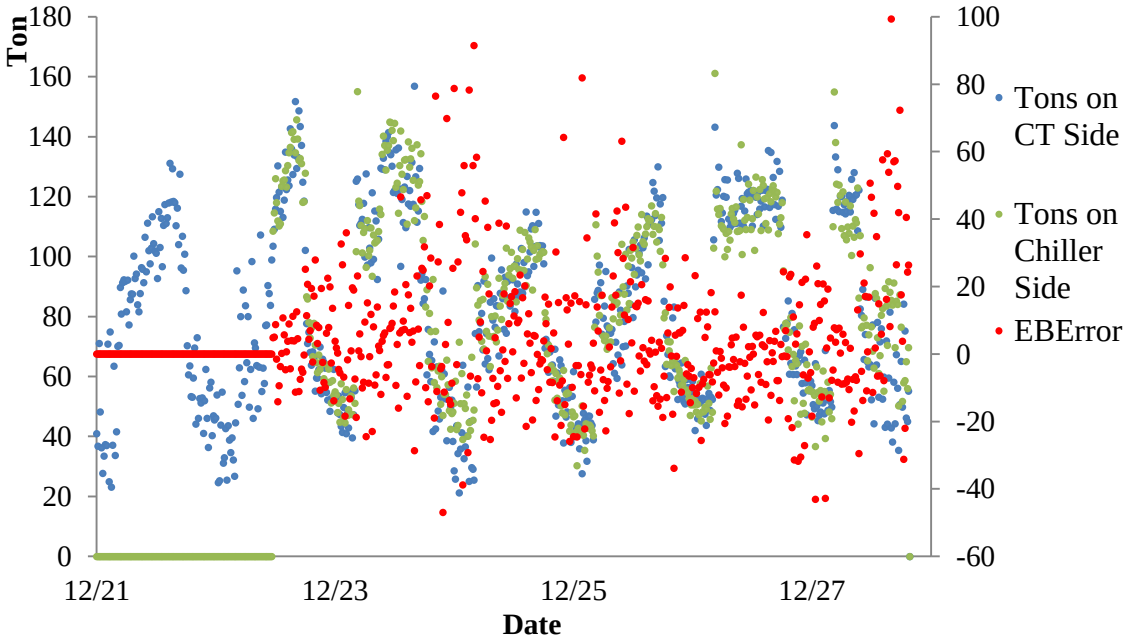

Figure G. 12 Tonnage Comparisons for December (12/21-12/27)

2. Average daily data

Table G.1 Average Daily Data for Year 2015

Date	Dry-Bulb Temp(°F)	Tons on CT Side	Tons on Chiller Side
01/22/2015	46.33	51.92	52.11
01/23/2015	41.00	53.39	50.17
01/24/2015	44.75	54.90	53.54
01/25/2015	53.76	60.60	57.69
02/12/2015	52.33	74.26	67.93
02/13/2015	52.54	65.04	65.91
02/14/2015	60.33	72.86	73.71
02/15/2015	60.71	68.11	62.13
03/16/2015	64.67	72.55	76.02
03/17/2015	69.54	82.59	86.57
03/18/2015	69.38	81.52	80.02
03/19/2015	69.83	81.83	80.73
03/20/2015	65.96	74.03	75.03
03/21/2015	60.58	63.54	64.05
03/30/2015	74.40	110.01	106.37
03/31/2015	71.29	97.14	94.47
04/01/2015	70.58	97.32	93.68
04/02/2015	73.50	103.52	98.99
04/03/2015	73.25	100.25	97.27
04/04/2015	62.67	68.03	65.82
04/05/2015	60.33	62.04	63.95
05/09/2015	79.17	105.20	102.32
05/10/2015	81.00	123.61	117.51
05/15/2015	73.33	106.08	106.98
05/16/2015	78.63	102.64	101.98

05/17/2015	74.62	98.12	101.04
06/04/2015	79.92	150.94	140.70
06/05/2015	80.54	137.00	128.69
06/06/2015	82.13	135.51	129.90
06/07/2015	82.38	136.26	130.19
06/12/2015	82.92	165.49	152.50
06/13/2015	81.21	134.31	127.64
06/14/2015	78.57	131.76	126.07
07/10/2015	83.33	159.56	153.20
07/11/2015	83.38	133.33	130.07
07/12/2015	84.24	144.08	140.19
07/24/2015	85.29	166.39	158.55
07/25/2015	85.38	137.59	134.68
07/26/2015	85.71	148.49	143.78
08/18/2015	85.67	156.83	156.70
08/19/2015	83.92	151.88	145.43
08/20/2015	76.92	123.86	118.64
08/21/2015	78.88	122.77	118.08
08/22/2015	85.13	128.67	128.50
08/23/2015	87.00	146.84	155.90
09/09/2015	80.13	148.98	140.29
09/10/2015	79.79	139.88	129.44
09/11/2015	80.33	133.56	124.49
09/12/2015	78.54	105.66	102.21
09/13/2015	75.57	96.06	95.18
10/17/2015	72.38	76.37	76.73
10/20/2015	70.58	106.81	101.38
10/21/2015	76.50	104.76	101.57

10/22/2015	77.04	108.46	103.38
10/23/2015	76.13	104.29	102.30
10/24/2015	69.17	73.54	74.19
10/25/2015	62.38	57.59	61.06
11/18/2015	57.25	40.59	42.87
11/19/2015	62.17	72.80	67.21
11/20/2015	62.79	70.61	63.59
11/21/2015	56.67	56.60	52.54
11/22/2015	45.10	43.40	44.91
12/22/2015	63.46	96.54	97.64
12/23/2015	70.33	91.33	93.61
12/24/2015	65.46	71.99	75.54
12/25/2015	69.83	76.05	77.26
12/26/2015	74.88	94.46	90.78
12/27/2015	58.90	76.52	80.67

APPENDIX H

COOLING TOWER INLET AND OUTLET CONDITION MEASUREMENTS

Table H.1 Cooling Tower Inlet and Outlet Conditions Measurements

Entering Water Temp (°F)	Exiting Water Temp (°F)	Entering Air Temp (°F)	Exiting Air Temp (°F)
66.30	64.75	46.33	54.88
66.47	64.88	41.00	51.94
66.49	64.85	44.75	54.06
66.63	64.80	53.76	62.82
67.09	64.86	52.33	63.34
66.80	64.85	52.54	62.54
67.68	65.51	60.33	65.61
68.58	66.57	60.71	66.86
69.77	67.59	64.67	67.99
73.95	71.46	69.54	72.76
74.20	71.75	69.38	72.56
75.57	73.10	69.83	73.82
74.33	72.09	65.96	71.56
68.76	66.84	60.58	66.44
78.18	74.80	74.40	76.06
75.91	72.91	71.29	73.60
77.71	74.70	70.58	74.40
79.26	76.05	73.50	76.56
78.24	75.14	73.25	75.63
67.11	64.99	62.67	65.66
67.14	65.13	60.33	65.18
83.24	79.97	79.17	80.86
84.32	80.47	81.00	82.16

82.40	79.00	73.33	78.00
82.92	79.64	78.63	80.60
82.18	79.06	74.62	78.50
84.13	79.34	79.92	81.47
84.06	79.70	80.54	81.69
84.00	79.69	82.13	82.21
84.43	80.11	82.38	82.54
87.17	81.91	82.92	84.11
85.66	81.41	81.21	82.86
85.19	80.99	78.57	81.50
88.58	83.69	83.33	85.10
86.98	82.90	83.38	84.35
87.95	83.54	84.24	85.24
88.93	83.72	85.29	86.14
86.63	82.30	85.38	84.89
87.47	82.82	85.71	85.46
87.09	82.31	85.67	85.19
87.53	82.90	83.92	84.94
83.71	79.96	76.92	80.14
83.69	79.97	78.88	81.00
86.35	82.44	85.13	84.72
87.58	83.11	87.00	85.85
86.93	82.33	80.13	83.11
86.37	82.05	79.79	82.78
85.53	81.41	80.33	82.54
77.43	74.16	78.54	76.64
71.71	68.75	75.57	71.59
68.24	65.87	72.38	68.31
80.65	77.33	70.58	76.22
80.81	77.56	76.50	78.89

81.73	78.34	77.04	79.79
83.29	80.04	76.13	80.43
77.99	75.70	69.17	74.60
71.36	69.57	62.38	67.64
65.05	63.83	57.25	62.50
69.67	67.49	62.17	67.77
68.56	66.44	62.79	67.15
66.98	65.29	56.67	63.26
65.92	64.62	45.10	58.74
78.21	75.20	63.46	72.22
76.64	73.82	70.33	74.35
72.99	70.77	65.46	70.70
76.92	74.58	69.83	74.36
82.40	79.49	74.88	79.08

APPENDIX I

DATA FOR CHILLER MODEL

Table I.1 Chiller Model Data

Date	Dry-Bulb Temp (°F)	Leaving Chilled Water Temp (°F)	Entering Condenser Water Temp (°F)	App-roach Temp (°F)	Chiller Flow (GPM)	Chiller Input Power (kW)	Chiller Load (tons)
01/22/15	46.33	42.65	64.75	19.59	395	32.50	42.87
01/23/15	41.00	42.74	64.88	25.42	395	32.58	40.90
01/24/15	44.75	42.58	64.85	24.52	395	32.78	44.22
01/25/15	53.76	42.63	64.80	19.99	402	34.58	47.86
02/12/15	52.33	42.74	64.86	20.07	401	37.96	57.14
02/13/15	52.54	42.68	64.85	19.52	381	35.86	53.75
02/14/15	60.33	42.66	65.51	12.80	415	46.79	73.21
02/15/15	60.71	42.70	66.57	8.47	422	49.39	71.34
02/25/15	39.88	42.74	64.92	27.55	439	69.80	93.39
02/26/15	39.08	42.70	64.99	29.20	435	65.48	78.88
02/27/15	37.54	42.69	65.00	31.96	423	62.63	74.19
02/28/15	42.21	42.69	65.20	26.95	416	61.16	69.18
03/01/15	41.50	41.47	64.97	23.55	393	35.31	55.87
03/16/15	64.67	42.68	67.59	8.88	401	38.41	62.79
03/17/15	69.54	42.73	71.46	6.75	390	37.65	51.43
03/18/15	69.38	42.75	71.75	7.45	398	32.32	39.38
03/19/15	69.83	42.78	73.10	6.97	397	33.55	44.34
03/20/15	65.96	42.71	72.09	7.68	391	30.70	36.05
03/21/15	60.58	42.54	66.84	7.26	400	40.46	52.54
03/26/15	60.17	41.71	66.92	12.71	402	38.05	55.00
03/27/15	60.88	41.69	65.38	15.17	370	31.29	42.51
03/28/15	66.08	41.84	66.29	12.29	411	43.16	63.74

03/29/15	68.46	42.76	71.44	10.31	416	52.85	71.54
03/30/15	74.40	42.80	74.80	8.06	413	55.04	65.07
03/31/15	71.29	42.81	72.91	7.53	405	49.69	60.90
04/01/15	70.58	42.79	74.70	7.61	435	61.69	76.93
04/02/15	73.50	42.79	76.05	7.30	443	65.27	75.12
04/03/15	73.25	42.72	75.14	8.30	445	70.72	78.88
04/04/15	62.67	42.61	64.99	10.91	433	68.27	77.86
04/05/15	60.33	41.69	65.13	8.09	386	42.24	63.92
04/13/15	73.42	42.80	76.06	7.39	390	41.52	63.90
04/14/15	63.88	42.74	69.68	8.93	413	48.29	66.67
04/15/15	66.50	42.70	68.58	8.37	384	30.67	36.89
04/16/15	70.42	42.77	74.18	7.26	413	51.08	65.50
04/17/15	70.63	42.74	74.25	7.13	452	71.81	85.95
04/18/15	70.50	42.66	74.90	7.56	393	42.07	67.06
04/19/15	69.21	41.67	72.48	9.14	399	57.79	73.55
05/09/15	79.17	41.58	79.97	5.41	409	79.44	79.73
05/10/15	81.00	41.60	80.47	5.57	423	86.25	92.99
05/15/15	73.33	41.56	79.00	6.82	407	79.11	84.49
05/16/15	78.63	41.62	79.64	5.51	404	77.95	79.82
05/17/15	74.62	41.50	79.06	6.56	404	77.21	79.09
06/04/15	79.92	41.52	79.34	6.01	452	94.29	113.89
06/05/15	80.54	41.51	79.70	6.81	446	90.39	102.99
06/06/15	82.13	41.49	79.69	6.37	435	90.20	104.25
06/07/15	82.38	41.62	80.11	6.76	433	91.06	104.30
06/12/15	82.92	41.53	81.91	5.97	470	105.49	122.51
06/13/15	81.21	41.53	81.41	6.07	430	91.79	101.54
06/14/15	78.57	41.62	80.99	6.23	424	92.01	99.90
06/20/15	79.08	41.52	81.27	6.27	418	87.58	92.51
06/21/15	82.13	41.46	82.53	5.41	424	93.31	100.37
07/10/15	83.33	41.52	83.69	6.42	470	108.18	122.44

07/11/15	83.38	41.59	82.90	5.69	437	96.07	102.75
07/12/15	84.24	41.57	83.54	5.28	442	100.49	111.62
07/24/15	85.29	41.44	83.72	6.77	472	110.12	127.23
07/25/15	85.38	41.59	82.30	6.00	439	97.42	106.98
07/26/15	85.71	41.52	82.82	5.56	446	103.20	114.44
08/18/15	85.67	42.67	82.31	6.81	494	101.22	127.92
08/19/15	83.92	42.73	82.90	6.65	482	102.29	116.35
08/20/15	76.92	42.77	79.96	6.92	462	87.09	93.88
08/21/15	78.88	42.77	79.97	6.47	464	85.10	93.88
08/22/15	85.13	42.76	82.44	5.57	466	92.75	102.13
08/23/15	87.00	42.81	83.11	6.02	485	100.08	127.44
08/28/15	81.42	42.78	82.17	11.55	478	94.50	101.24
08/29/15	80.50	42.78	78.85	7.56	465	85.05	95.70
08/30/15	80.42	42.79	79.01	7.38	470	85.53	95.63
09/09/15	80.13	42.75	82.33	7.04	484	99.93	111.88
09/10/15	79.79	42.81	82.05	6.59	478	98.59	101.40
09/11/15	80.33	42.82	81.41	6.20	471	94.45	97.64
09/12/15	78.54	42.78	74.16	9.66	451	70.31	82.22
09/13/15	75.57	42.83	68.75	7.89	443	55.91	79.28
10/13/15	79.50	41.74	69.89	9.26	440	57.93	88.14
10/15/15	74.58	41.69	68.99	7.87	438	55.26	83.27
10/16/15	74.58	42.78	66.89	5.48	450	52.89	81.88
10/17/15	72.38	43.36	66.07	7.91	414	40.47	65.22
10/18/15	68.29	43.32	65.39	13.55	406	38.71	62.75
10/20/15	70.58	43.27	77.33	11.92	442	72.77	80.69
10/21/15	76.50	43.30	77.56	7.06	438	73.61	80.64
10/22/15	77.04	43.24	78.34	6.22	440	77.48	81.35
10/23/15	76.13	43.27	80.04	5.83	449	79.82	79.60
10/24/15	69.17	43.25	75.70	7.61	416	55.22	58.49
10/25/15	62.38	43.22	69.57	8.24	407	39.40	49.86

11/12/15	68.33	43.26	66.76	5.82	431	39.63	61.91
11/13/15	60.98	43.21	66.89	16.04	406	32.71	46.54
11/14/15	60.08	43.13	66.07	15.51	399	30.54	41.46
11/15/15	62.15	43.23	65.39	11.47	402	33.71	44.10
11/18/15	57.25	43.23	63.83	12.78	386	26.86	35.23
11/19/15	62.17	43.27	67.49	11.94	423	40.96	55.57
11/20/15	62.79	43.24	66.44	10.90	420	38.77	52.57
11/21/15	56.67	43.22	65.29	14.70	403	32.51	43.29
11/22/15	45.10	43.20	64.62	26.20	398	29.33	36.57
12/22/15	63.46	41.61	75.20	14.61	400	101.22	68.86
12/23/15	70.33	41.66	73.82	12.57	396	102.29	64.52
12/24/15	65.46	41.59	70.77	8.44	382	87.09	50.78
12/25/15	69.83	41.63	74.58	8.66	383	85.10	53.06
12/26/15	74.88	41.60	79.49	7.37	392	92.75	64.41
12/27/15	58.91	41.51	72.25	15.01	383	100.38	52.13

$$PLR = \frac{Actual\ Cooling\ Load}{Chiller's\ Available\ Cooling\ Capacity} \quad \text{(I.1)}$$

$$ChillerCapFTemp = \frac{Available\ Cooling\ Capacity}{Nominal\ Rated\ Capacity\ at\ Design\ Condition}$$

$$= \frac{Available\ Cooling\ Capacity\ (ton)}{220\ tons} \quad \text{(I.2)}$$

$$ChillerEIRFTemp = \frac{Input\ Power/Output\ Cooling}{Rated\ Efficiency}$$

$$= \frac{Chiller\ Input\ Power\ (kW)/Chiller\ Output(ton)}{0.7\ kW/ton} \quad \text{(I.3)}$$